

# TECHNISCHE UNIVERSITÄT MÜNCHEN

Lehrstuhl für Entwicklungsgenetik

## Migratory neuronal precursor populations arising from the zebrafish cerebellar rhombic lip

Katrin Volkmann

Vollständiger Abdruck der von der Fakultät Wissenschaftszentrum Weihenstephan für Ernährung, Landnutzung und Umwelt der Technischen Universität München zur Erlangung des akademischen Grades eines

Doktors der Naturwissenschaften

genehmigten Dissertation.

Vorsitzender: Univ.-Prof. Dr. A. Gierl  
Prüfer der Dissertation: 1. Univ.-Prof. Dr. W. Wurst  
2. Univ.-Prof. Dr. H. Luksch

Die Dissertation wurde am 14.04.2010 bei der Technischen Universität München eingereicht und durch die Fakultät Wissenschaftszentrum Weihenstephan für Ernährung, Landnutzung und Umwelt am 14.06.2010 angenommen.



Migratory neuronal precursor populations arising from the  
zebrafish cerebellar rhombic lip

Kumulative Arbeit

Katrin Volkmann



## Abstract

The cerebellum is an evolutionarily ancient part of the brain with a function, structure and cell type composition highly conserved among vertebrate species. Here migration of neuronal precursors from sites of proliferation to their target regions during the development is essential for the functionality of the mature compartment. I have analyzed the migratory behavior, fate and integration into neuronal circuitries of descendants of the upper rhombic lip (URL) proliferation zone in the model organism zebrafish via confocal *in vivo* fluorescence microscopy. The URL of the developing mammalian cerebellum produces different neuronal cell types in a temporal sequence. The first neuronal populations include the progenitors of the parabrachial, parabigeminal and laterodorsal-pedunculopontine tegmental hindbrain nuclei. Cerebellar granule cells are a population arising late from the URL.

(I) By means of expression analysis, histology and retrograde neuronal tracing, I identified the zebrafish homologues of these nuclei - the secondary gustatory/viscerosensory nucleus (SGN/SVN), nucleus isthmi (NI) and superior reticular nucleus (SRN), respectively, in the embryonic and larval brain of a stable transgenic *wnt1:Gal4-VP16-14xUAS:GFP* zebrafish strain. Combining transgenic fluorescence labeling of specific cells with time-lapse confocal imaging for the tracking of individual cells, I characterized the migration paths, velocity and directionality of these neuronal precursor populations. In addition, I identified SGN/SVN and NI/SRN neuronal progenitors as belonging to the polysialic acid (PSA)-dependent migrating cell population in rhombomere 1. In sum, my results show that the origin of the tegmental hindbrain nuclei, NI/SRN and SGN/SVN, is in the URL, and that the temporal order of cell types produced by the URL and their developmental program as well as their connectivity are conserved among vertebrate species. To further investigate the development of early URL-derived cells, I have created a stable transgenic *atoh1a:KalTA4* activator strain expressing Gal4 under the control of the URL-specific *atoh1a* enhancer. This *atoh1a:KalTA4* strain was used in a study addressing the migration and axonogenesis of NI/SRN and SGN/SVN precursors on a subcellular level. In contrast to what was known from previous *in vitro* studies this study revealed that the centrosome is not

permanently ahead of the nucleus and that the position of the centrosome does not determine the site of axon outgrowth.

(II) With extensive co-expression studies and detailed intravital time-lapse imaging, I identified the granule cell lineage of the zebrafish cerebellum. Using the stable transgenic *gata1:GFP* zebrafish strain, I characterized granule cell migration and the time course of their differentiation. The teleost cerebellum, as in mammals, has functional compartments forming the vestibulo- and the non-vestibulocerebellum, which control balance and locomotion respectively. Software-supported tracking of individual cells, histological analysis at larval and juvenile stages and retrograde labeling of parallel fiber projections to the crista cerebellaris revealed that granule cell precursors arising from different medio-lateral positions in the URL either contribute to the granule cell population of the vestibulocerebellum or the non-vestibulocerebellum. My results show that the URL is spatially subdivided along its medio-lateral axis to simultaneously produce granule cells of different connectivity and function.

(III) To investigate which signaling molecules guide neuronal precursors from the URL to their target regions of terminal differentiation, I have performed an expression analysis of candidate factors. This revealed that the zebrafish *netrin-1* receptors *dcc* and *unc5c* are expressed by migrating URL-derived neuronal precursors whereas the ligand *netrin-1* is expressed in cells of the floorplate ventral to rhombomere 1. As a basis for future gain and loss of function studies I have cloned a full length and a dominant negative zebrafish Dcc receptor variant that can be expressed via the Gal4-UAS system in a cell type specific manner.

(IV) Finally as part of a morpholino-based study by the lab of Oliver Bandmann my transmission electron microscopically analysis revealed a novel phenotype in the trunk muscle tissue of *parkin* knockdown zebrafish larvae.

Taken together, I have identified major neuronal populations arising from the URL in zebrafish and characterized their migratory behavior in detail. Furthermore, I have compiled a marker gene expression profile and described the formation of neuronal circuitries, thereby unraveling early cerebellar development and laying the groundwork for functional studies in this model organism. My study provides new insights into how a single proliferation zone can give rise to neuronal populations and cell types with completely different morphology, connectivity and functions.

## Zusammenfassung

Das Kleinhirn ist in seiner Funktion, Struktur, zellulären Zusammensetzung und Entwicklung in allen Wirbeltieren hoch konserviert. Migration von neuronalen Vorläuferzellen von ihren Proliferationszonen in Zielregionen terminaler Differenzierung während der Entwicklung dieses Hirnkompartiments ist essentiell für dessen spätere Funktion. In meiner Doktorarbeit habe ich das Migrationsverhalten und Schicksal sowie die Intergration in neuronale Schaltkreise von Zellen der oberen Rautenlippe, einer spezifischen Proliferationszone des Kleinhirns, u.a. mittels konfokaler *in vivo* Fluoreszenzmikroskopie im Modellorganismus Zebrafisch detailliert untersucht.

Die Rautenlippe des sich entwickelnden Kleinhirns in Säugetieren erzeugt verschiedene neuronale Zelltypen in einer festgelegten zeitlichen Reihenfolge. Erste neuronale Populationen umfassen die Vorläuferzellen der parabrachialen, parabigeminalen und laterodorsal-pedunculo-pontinen Kerne des Hinterhirn-Tegmentums. Als eine späte neuronale Zellpopulation entstehen die Körnerzellen des Kleinhirns aus der oberen Rautenlippe.

(I) Mit Hilfe von Expressions-Analysen, Histologie und retrograden Anfärbungen in der stabil transgenen *wnt1:Gal4-VP16-14xUAS:GFP* Linie konnte ich die homologen Populationen der frühen aus der oberen Rautenlippe stammenden Kerne im embryonalen und larvalen Zebrafisch-Gehirn identifizieren. Diese umfassen die sekundären gustatorischen/viscerosensorischen und die nucleus isthmi und/oder superior retikulären Kerne. Die Kombination von Transgenese zur Fluoreszenzmarkierung spezifischer Zellen mit konfokaler Zeitraffer-Mikroskopie zur kontinuierlichen Beobachtung individueller Zellen ermöglichte mir die detaillierte Charakterisierung des Migrationsverhaltens dieser neuronalen Vorläuferzellen und ich konnte Informationen über ihren Migrationsweg, Migrationsgeschwindigkeit und Direktionalität gewinnen. Darüber hinaus konnte ich zeigen, daß die Vorläuferzellen dieser tegmentalen Hinterhirnkerne zu der polysialic acid (PSA) exprimierenden Zellpopulation der Kleinhirnplatte gehören, die PSA abhängig wandert. Meine Ergebnisse zeigen, daß der Ursprung der

tegmentalen Kerne des Hinterhirns, sekundärer gustatorischer/viscerosensorischer Kern bzw. nucleus isthmi und/oder superior retikulärer Kern in der Rautenlippe des Kleinhirns liegt, und daß sowohl die zeitliche Abfolge ihrer Entstehung als auch ihr Entwicklungsprogramm und ihre Verknüpfungen im Gehirn zwischen den Wirbeltieren konserviert sind.

Um die Entwicklung von URL Zellen näher zu untersuchen habe ich eine stabil transgene *atoh1a:KalTA4* Aktivator-Linie erzeugt, die Gal4 unter Kontrolle des *atoh1a* Enhancers exprimiert. Diese *atoh1a:KalTA4* Linie wurde dazu verwendet Migration und Axonogenese der URL Zellen auf subzellulärer Ebene zu untersuchen. Dabei zeigte sich im Gegensatz zu bisherigen Erkenntnissen aus *in vitro* Studien, dass das Zentrosom während der Zellmigration nicht permanent vor dem Zellkern verweilt und daß die Position des Zentrosoms nicht den Ort bestimmt, von dem das spätere Axon auswächst.

(II) Mit Hilfe von umfangreichen Koexpressions-Analysen und mikroskopischen Zeitraffer-Aufnahmen konnte ich die Körnerzell-Population des Zebrafisch-Kleinhirns in der stabil transgenen *gata1:GFP* Linie identifizieren und ihre Wanderung charakterisieren. Anhand dieser Linie wurde der zeitliche Verlauf der Körnerzell-Differenzierung *in vivo* untersucht. Mittels software-unterstützter kontinuierlicher Beobachtung von einzelnen Zellen konnte gezeigt werden, daß Körnerzell-Vorläufer von verschiedenen Positionen der Rautenlippe unterschiedlichen Wanderwegen folgen. Daraufhin durchgeführte histologische Analysen von larvalen und juvenilen Stadien, sowie retrograde Anfärbung von Parallelfaser-Projektionen zur Crista Cerebellaris ergaben, daß diese Subpopulationen entweder Teil der Körnerzell-Population des vestibulären (Eminentia Granularis) oder des nicht-vestibulären (Corpus Cerebelli) Kleinhirns ausbilden. Diese funktionellen Kompartimente sind für die Kontrolle der Balance bzw. die Koordination von Bewegungen zuständig.

Meine Ergebnisse zeigen, daß die Rautenlippe des Kleinhirns räumlich und zwar entlang ihrer medio-lateralen Achse unterteilt ist und zeitgleich Körnerzellen mit unterschiedlichen Verknüpfungen und Funktionen produziert.

(III) Um zu untersuchen, welche Signalmoleküle die Wanderungsrichtung der neuronalen Vorläuferzellen der oberen Rautenlippe, zu ihren Zielregionen terminaler Differenzierung bestimmen, habe ich ferner Expressionsanalysen von



Kandidatengeneten im Zebrafisch durchgeführt. Dabei zeigte sich, dass migrierende neuronale Vorläuferzellen aus der oberen Rautenlippe die Netrin-1 Rezeptoren *dcc* und *unc5c* exprimieren. Ferner konnte ich zeigen, dass der Ligand *netrin-1* in der Bodenplatte des Neuralrohres in Rhombomer 1 exprimiert ist. Für zukünftige „gain- und loss of function“-Studien eine funktionelle sowie eine dominant negativ wirkende Variante des Dcc Rezeptors kloniert. Diese lassen sich zelltypspezifisch mittels des Gal4-UAS Systemes exprimieren.

(IV) Zusätzlich habe ich, in Kollaboration mit dem Labor von Oliver Bandmann, im Rahmen einer Morpholino Knockdown Studie dazu beigetragen einen neuartigen Phänotyp im Muskelgewebe von *parkin*-Knockdown Zebrafisch-Larven zu identifizieren.

In meiner Doktorarbeit habe ich die wichtigsten neuronalen Populationen, die aus der oberen Rautenlippe des Zebrafisch-Kleinhirns entstehen, identifiziert und ihr Wanderverhalten im Detail charakterisiert. Außerdem habe ich ein Markerexpressionsprofil für wichtige Populationen des Kleinhirns erstellt und die Bildung ihrer neuronalen Schaltkreise beschrieben. Ich konnte so wichtige Aspekte der frühen Entwicklung des Zebrafisch-Kleinhirns aufklären und habe somit eine Grundlage für funktionelle Studien in diesem Modellorganismus geschaffen. Durch unsere *in vivo* Analysen erhielten wir neue Erkenntnisse darüber, wie aus einer einzigen Proliferationszone neuronale Zelltypen und Populationen mit völlig unterschiedlicher Morphologie, Verschaltung und Funktion entstehen können.



# Index

<b>Abstract</b> .....	<b>I</b>
<b>Zusammenfassung</b> .....	<b>III</b>
<b>Index</b> .....	<b>VII</b>
<b>1 Introduction</b> .....	<b>1</b>
1.1 The zebrafish as model organism for brain development.....	1
1.2 Cell migration.....	3
1.2.1 Neuronal migration .....	3
1.3 The Cerebellum .....	6
1.3.1 Cerebellar functions .....	6
1.3.2 Cerebellar development .....	6
1.3.3 The cell types of the cerebellum - morphology and organization .....	7
1.3.4 Cerebellar circuitries and neurotransmitters.....	8
1.3.5 Similarities and differences – brief comparison of the mammalian and teleostean cerebellum .....	10
1.3.5.1 The mammalian cerebellum .....	10
1.3.5.2 The zebrafish cerebellum .....	11
1.4 Migratory neuronal cell populations arising from the upper rhombic lip of the developing zebrafish cerebellum .....	14
1.4.1 The cerebellar rhombic lip or upper rhombic lip (URL) – a proliferation zone.....	15
1.4.1.1 The expression of the transcription factor Math1/Atonal1 defines the URL molecularly.....	15
1.4.2 Mammalian tegmental hindbrain nuclei arise from the <i>wnt1</i> -expressing URL .....	17
1.4.3 Cerebellar granule cells.....	21
1.4.4 Granule cells of the zebrafish cerebellum .....	23
1.4.5 Is the URL spatially subdivided? .....	24
1.4.6 The <i>gata1</i> :GFP transgenic strain shows GFP expression in a migratory population in the developing zebrafish cerebellum.....	24
1.5 Input for the cerebellum - the precerebellar system and mossy fiber-like projections .....	25
1.6 Adhesion factors in cerebellar development.....	26
1.7 The receptor/ligand pairs Dcc/Netrin-1 and Unc5c/Netrin-1 as candidate factors for the guidance of URL-derived migratory cell populations .....	27
1.7.1 Netrin-1 and Netrin-1 receptors in zebrafish.....	30
1.8 In vivo retrograde labeling of neurons in zebrafish larvae .....	31
1.9 Retrograde labeling as potential means to analyze <i>parkin</i> function in the posterior tuberculum .....	32

<b>2</b>	<b>Aims and Achievements .....</b>	<b>33</b>
<b>3</b>	<b>Results .....</b>	<b>36</b>
3.1	Characterization of GFP-expressing cell populations in the cerebellar anlage of the <i>wnt1</i> -GVP-UG stable transgenic zebrafish strain.....	36
3.1.1	Early cerebellar <i>wnt1</i> -expressing cells represent URL-derived cell types that migrate over long distances (Appendix 1: Figure 2 and 3) .....	36
3.1.2	Ventrally migrating <i>wnt1</i> -GVP-UG cells do not contribute to zebrafish deep cerebellar neurons or eurydendroid cells: (Appendix 1, Figure 4) .	37
3.1.3	<i>wnt1</i> -GVP-UG cells are tegmental hindbrain nuclei of rhombomere 1 (Appendix 1: Figure 5 and 6) .....	38
3.1.4	Axonal projections and adhesion factors (Appendix 1: Figure 3, 4 , 7 and 8) .....	38
3.2	Enzymatic removal of PSA results in impaired migration of NI/SRN and SGN/SVN precursors.....	40
3.3	Generation of a zebrafish <i>atona1a</i> activator strain .....	40
3.4	Characterization of the GFP-expressing cell population in the cerebellum of the <i>gata1</i> :GFP stable transgenic zebrafish strain.....	44
3.4.1	<i>gata1</i> :GFP cells represent the granule cell population of the embryonic, larval and juvenile zebrafish cerebellum (Appendix 4: Figure 1, 2, 3) ....	44
3.4.2	<i>gata1</i> :GFP cells in the cerebellum represent all cerebellar granule cell populations in teleost fish .....	46
3.4.3	The URL of the embryonic zebrafish cerebellum is spatially subdivided and simultaneously gives rise to granule cells of different fate and function (Appendix 4: Figure 4, 5, 6, 7; Movie 6) .....	47
3.4.4	Migration of cerebellar granule cell precursors continues at larval and juvenile stages and the regionalization of the URL is maintained (Appendix 4: Figure1, Movie 7 and Movie 8) .....	48
3.5	Zebrafish Netrin-1 and its receptors in URL-derived precursor populations	49
3.5.1	The guidance molecules zebrafish <i>netrin-1a</i> and <i>netrin-1b</i> are expressed at embryonic stages when migration from the URL occurs...	49
3.5.2	<i>dcc</i> -expression in the embryonic zebrafish cerebellum is confined to regions of neuronal migration .....	52
3.5.3	The Netrin-1 receptor <i>dcc</i> is expressed in URL-derived precursors in zebrafish .....	55
3.5.4	The Netrin-1 receptor <i>dcc</i> is expressed in migrating cerebellar granule cell precursors .....	55
3.5.5	Cloning of a partial cDNA of zebrafish <i>unc5c</i> .....	57
3.5.6	The Netrin-1 receptor zebrafish <i>unc5c</i> is expressed in the embryonic cerebellum and hindbrain .....	58
3.5.7	The Netrin-1 receptor <i>unc5c</i> is expressed in migrating cerebellar granule cell precursors .....	60
3.5.8	Cloning of full length zebrafish <i>dcc</i> .....	62
3.5.9	Bicistronic expression constructs for driving simultaneous expression of Dcc and the red-fluorescent Cherry protein.....	63
3.5.10	Injection of antisense MOs against <i>netrin-1a</i> , <i>netrin-1b</i> and <i>dcc</i> .....	65
3.6	TEM study of <i>parkin</i> knockdown zebrafish embryos.....	66

<b>4</b>	<b>Discussion .....</b>	<b>67</b>
4.1	Identification and characterization of tegmental hindbrain nuclei precursor populations .....	67
4.1.1	Tegmental hindbrain nuclei of the isthmic region originate in the URL... ..	67
4.1.2	Migratory behavior of tegmental hindbrain nuclei precursors .....	68
4.1.3	Tegmental nuclei of rhombomere 1 contain besides cholinergic also glutamatergic subpopulations of neurons .....	69
4.1.4	Expression of adhesion factors in the cells of the NI/SRN and SGN/SVN during distinct differentiation steps .....	70
4.1.5	Tegmental hindbrain nuclei can be discriminated by their different axonal projections in the larval brain .....	72
4.1.6	Pretectal input to the corpus cerebelli .....	73
4.1.7	Constraints of the study .....	75
4.2	PSA-NCAM regulates motility of URL-derived tegmental hindbrain precursors .....	75
4.3	New Gal4 activator strain allows transgene expression in <i>atonal1a</i> -expressing rhombic lip derived populations .....	76
4.4	Characterization of the granule cell population of the developing zebrafish cerebellum .....	77
4.4.1	<i>gata1</i> :GFP cells represent the granule cell population of the embryonic, larval and juvenile zebrafish cerebellum .....	77
4.4.2	The URL of the embryonic zebrafish cerebellum is spatially subdivided and simultaneously gives rise to granule cells of different fate and function .....	77
4.4.3	Comparison of granule cell migration in the mammalian (avian) and the zebrafish cerebellum .....	80
4.4.4	Possible molecular bases of the regionalization of the URL .....	80
4.5	Comparison of mouse and zebrafish URL-derived cell types .....	81
4.6	The function of Netrin-1/Dcc in URL-derived populations remains elusive ..	83
4.7	Zebrafish as novel vertebrate model system for early onset Parkinson's Disease .....	85
<b>5</b>	<b>Table of Figures .....</b>	<b>87</b>
<b>6</b>	<b>Movie Legends .....</b>	<b>89</b>
<b>7</b>	<b>Abbreviations .....</b>	<b>92</b>
<b>8</b>	<b>References .....</b>	<b>95</b>
<b>9</b>	<b>Appendices .....</b>	<b>103</b>
	Eidesstattliche Erklärung	
	Danksagung	



# 1 Introduction

## 1.1 The zebrafish as model organism for brain development

Over the past decades the zebrafish (*Danio rerio*) has been established as a vertebrate model organism for the characterization of various developmental processes. This small teleost species offers several advantages like the high number of offspring and the characteristics of the zebrafish embryo: the transparency of the body and the extracorporal development, which makes the zygotes accessible for manipulations such as injections of DNA, RNA and morpholinos or dye injections and for microscopic approaches.

The zebrafish embryonic development is an extremely rapid process - it takes only 5 days from the fertilized egg to a swimming, and preying larvae, that already can be used for behavior analysis (Blin et al., 2008; Neuhauss, 2003).

A large number of mutant zebrafish strains is available, and as new techniques like tilling (Moens et al., 2008) and targeted mutagenesis (Ekker, 2008; Woods and Schier, 2008) are arising, approaches to analyze vertebrate development using zebrafish are constantly growing and become more sophisticated. Furthermore as transgenic zebrafish can be generated easily, and several enhancer trap screens were performed recently an increasing number of stable transgenic zebrafish strains becomes available, allowing tissue and even cell type specific transgene expression (Bae et al., 2009; Balciunas et al., 2004; McFarland et al., 2008; Mione et al., 2008; Scott et al., 2007). Combined with the combinatorial Gal4-UAS system (Köster and Fraser, 2001b) these transgenic strains allow the expression of various transgenes (reporter, effector) (Distel et al., 2009) with a single activator strain that expresses Gal4 under a specific enhancer or the expression of a certain transgene in different specific tissues of interest by simple crossing of activator and reporter/effector strains.

Moreover due to the extracorporal development reagents can be simply added to the zebrafish embryo medium offering the possibility for high throughput drug-screens (Flinn et al., 2008; Hong, 2009). Furthermore injection of reagents into the older embryo e.g. into the heart or the ventricles of the brain is possible, allowing

electroporation of DNA or morpholinos and *in vivo* retrograde labeling of neurons (see chapter 1.8 and **Appendix 5**).

By now the zebrafish genome is sequenced to large extends and sequence information for two other fish species the pufferfish *Takifugu rubripes* and *Tetraodon nigroviridis* is available. This allows the comparison of sequences divergent among teleosts facilitating the search for conserved regions that contain regulatory elements and thus the isolation of enhancers. Furthermore, small regulatory elements of the condensed pufferfish genome are usually active in zebrafish and can be easily exchanged among teleosts.

The set of genes expressed during specific steps of development is often conserved between zebrafish and mammals (Chuang et al., 1999; McClintock et al., 2003; Schier and Talbot, 2005) which demonstrates the relevance of findings in zebrafish for the understanding of developmental processes in mammals. Thorough comparison of developmental processes among different vertebrates serves to distinguish between conserved and specific processes and mechanisms. Here zebrafish embryos contribute with non invasive *in vivo* imaging approaches covering important steps of development such as gastrulation, neurulation or somitogenesis.

In contrast to mammalian and avian model organisms the small size of the zebrafish embryo allows whole brain imaging with high resolution on the level of single cells and even subcellular structures ((Suli et al., 2006) **Appendix 3**). Moreover time-lapse imaging approaches take advantage of the temporal highly condensed brain development in zebrafish embryos.

The possibility of non invasive *in vivo* imaging combined with expression of transgenes encoding for fluorescence proteins in transient transgenic experiments or in stable transgenic strains allows the analysis of important steps of neuronal development on a cellular level directly in the living organism. Thus zebrafish embryos were used recently in studies investigating e.g. proliferation (Kosodo et al., 2008), morphogenesis (Gilmour et al., 2004; Gutzman et al., 2008; Gutzman and Sive, 2010; Harrington et al., 2010), axon growth and pathfinding (Bak and Fraser, 2003; Dynes and Ngai, 1998; Hutson and Chien, 2002), differentiation (McGraw et al., 2008; McLean and Fetcho, 2009), neuronal migration (Kirby et al.,



2006; Köster and Fraser, 2001a; 2004; Mione et al., 2008), wiring of the neuronal network (Bae et al., 2009; Bianco et al., 2008; McLean and Fetcho, 2008), dendrite formation (Suli et al., 2006) or regeneration (Köster and Fraser, 2006).

In sum these unique features make zebrafish an ideal model organism for the investigation of brain development and differentiation.

## **1.2 Cell migration**

During embryonic and postnatal development cell migration is involved in events shaping the organism and its organs like angiogenesis, neuronal migration in the brain and the spreading of neural crest cells all over the body. In the adult organism important processes like immune response, wound healing, vasculogenesis and regeneration are mediated by the directional migration of cells.

During migration cells are oriented by sets of guidance cues that determine the migration path of the cells. Some guidance cues are secreted diffusible molecules that can mediate long range guidance by chemoattraction or chemorepulsion (Sansom and Livesey, 2009), others are bound to membranes or the extracellular matrix and mediate short range guidance by contact attraction or contact repulsion. The secreted diffusible cues are thought to form a gradient that provides positional information for the migrating cell. In general the extracellular guidance cues are interpreted through receptors that are expressed in the migrating cells and activate intracellular signaling pathways. The binding of a ligand finally induces changes in the cytoskeleton - the microtubules, actin filaments and associated proteins (Kawauchi and Hoshino, 2008).

Some guidance factors are repulsive and cause a migration away from the source others act attractive and cause migration towards the source. Often the attractive or repulsive effect is determined by the kind of receptors expressed on the surface of the migrating cells.

### **1.2.1 Neuronal migration**

After the final divisions start signals initiate migration of neuronal precursors out of the proliferative neuroepithelium or a secondary germinal zone. Certain stop signals then trigger the termination of migration at the final location. Recent

evidence demonstrated that cell polarity is involved in the determination of directional migration of neurons with a potential role of the centrosome (Higginbotham and Gleeson, 2007; Metin et al., 2008).

Several families of cues are known to be involved in the guidance of neuronal migration (Figure 1): Semaphorins (He et al., 2002) (Sema6a for example regulates the tangential migration of cerebellar granule cells (Kerjan et al., 2005)) and Ephrins (Klein, 2004) (Ephrin A5 acts as a repulsive cue for olfactory cortex neurons in the developing telencephalon (Nomura et al., 2006)) both membrane-bound contact attraction/repulsion molecules whereas Slits (Piper and Little, 2003) (Slits have a role in the migration of interneurons during cortical development (Andrews et al., 2007)) and Netrins (see chapter 1.7) are diffusible cues mediating long range chemorepulsion/chemoattraction. Recently chemokines like SDF-1 have been found to act as guidance factors for neuronal precursors (Tiveron and Cremer, 2008). As a single guidance cue can often bind to several different receptors the response of a cell and thus the attractive or repulsive effect of a cue depends on the receptors expressed on the surface of the migrating cell.

Interestingly often same molecules are involved in axonal guidance and guidance of neuronal migration (e.g. Semaphorins, Netrin-1/Dcc, SDF-1). This phenomenon might be partly explained by the fact that the extension and retraction of short leading processes exploring the environment is involved in neuronal migration.

Interactions between neurons and the extracellular matrix proteins like Laminin, and Fibronectin are known to support migration. The extracellular matrix has to be permissive to enable cells to migrate through a tissue, which is regulated by the activity of metalloproteases (Luo, 2005).

Migration in cohorts involves homotypic migration of cells contacting neighboring cells of the same cell type e.g. during neuronal migration towards the olfactory bulb (Alvarez-Buylla, 1997; O'Rourke, 1996). On the other side a common mode of migration in the cerebellar and cerebral cortex is heterotypic migration along glia cells: cerebellar granule cell precursors migrate during radial migration “outward in” along Bergmann glia fibers (Edmondson and Hatten, 1987) and precursors of cortical neurons migrate along radial glial fibers when undergoing “inward out” migration during the formation of the layers of the cerebral cortex (Hatten, 1999).

The dynamic regulation of cell-cell adhesion mediated by cell adhesion molecules like Cadherins (Suzuki and Takeichi, 2008) and PSA-NCAM (Rutishauser, 2008) (see chapter 1.6 and **Appendix 2**) is important for the regulation of neuronal migration in cohorts.

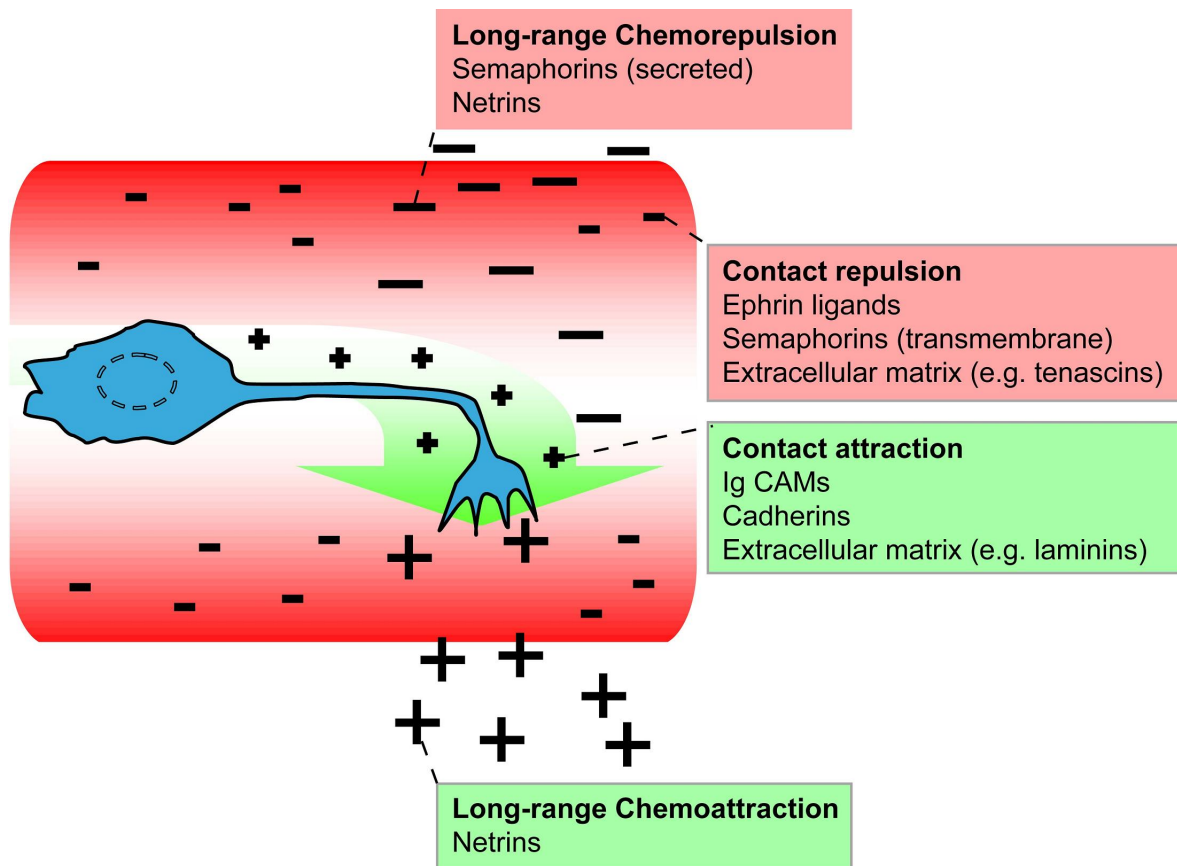


**Figure 1: Overview of guidance cues involved in neuronal migration.**

There are several developmental brain diseases that are caused by defects in migration of neuronal precursors from proliferation zones (birthplace) to their final target region. Among the neurological diseases characterized by the misplacement of neurons are Lissencephaly and the Miller-Dieker Syndrome. Here, a defect of neuronal migration results in a disturbed layer formation of the cerebral cortex and the absence of sulci and gyri. As a consequence children born with these conditions are among other defects severely neurologically impaired.

## **1.3 The Cerebellum**

For my studies I have focused on the cerebellum (latin: “little brain”) as this part of the brain provides the advantage of being comprised of only few cell types and it exhibits a high grade of conservation among vertebrates (Altman, 1997; Bae et al., 2009; Nieuwenhuys, 1967). The morphology, neurotransmitters and circuitry of the neurons in the mature vertebrate cerebellum have been well characterized but the development of the cerebellum is only partly understood leaving many interesting questions open.

### **1.3.1 Cerebellar functions**

The main functions of the mammalian cerebellum are balance control, motor coordination, motor learning and comparison between intention and action during movements. Via feedback modulation the cerebellum is able to compare an ongoing movement and the sensory input derived from it (Altman, 1997). The cerebellum is responsible for the modulation and smooth execution of movements. Thus diseases associated with a dysfunction of the cerebellum like cerebellar ataxia (Joubert syndrome, Dandy-Walker malformation, Pontocerebellar hypoplasia, Cerebellar vermis hypoplasia, Rhombencephalo synapsis) are characterized by a disturbed balance and gait as well as a lack of coordination in the movements of the eyes and extremities resulting in overshooting movements (Millen and Gleeson, 2008).

### **1.3.2 Cerebellar development**

The cerebellum is located dorsally to the pons. During embryonic development the cerebellar anlage (primordium) is formed from the dorsal part (the alar plate) of the rhombomere 1 (the anterior hindbrain region) adjacent to the midbrain-hindbrain boundary (MHB) or isthmic organizer. The cerebellar anlage undergoes a 90 degrees rotation during the opening of the hindbrain ventricle that turns the rostro-caudal axis of the cerebellar primordium into a medio-lateral orientation resulting in the formation of the bilateral symmetric cerebellar lobes (Altman, 1997; Distel et al., 2006; Sgaier et al., 2005). During further embryonic development the cerebellum grows in size and several subcompartments are formed (see this study). After birth the cerebellum of anamniotic vertebrates

undergoes foliation that leads to the formation of characteristic lobes, lobules and sublobules. In teleosts the cerebellum remains as a dorsally positioned unfoliated layered structure just underneath the epidermis making it easily accessible for time-lapse imaging approaches.

### **1.3.3 The cell types of the cerebellum - morphology and organization**

The mature cerebellar cortex exhibits a highly organized layered structure which is conserved throughout vertebrates. Directly under the cerebellar surface lies the molecular layer consisting of neuropil (axons and dendrites) and few interneurons (Figure 2). Underneath spreads the Purkinje cell layer and the innermost layer is the granule cell layer formed by the Purkinje cells and the cerebellar granule cells respectively (Figure 2). Granule cells have small cell bodies with 3-5 short dendrites with claw-shaped endings and extend a T-shaped axon into the molecular layer termed parallel fiber. Purkinje cells have large drop shaped cell bodies that form a monolayer between molecular and granule cell layer. Purkinje cells extend huge, tree-shaped dendrites into the molecular layer, where they are innervated by the parallel fibers (Figure 2). The parallel fibers and the planar dendritic trees of the Purkinje cells are orientated orthogonally to one another. The Purkinje cell axon is projecting to the deep cerebellar nuclei at the base of the cerebellum. The neurons of the deep cerebellar nuclei in turn have axons that are targeting areas outside the cerebellum.

Two types of interneurons are located in the molecular layer – the stellate and the basket cells. Basket cells have their soma in the lower half of the molecular layer close to the Purkinje cells (Figure 2). Their flattened irregular dendrites are directed towards the surface. The axons form extensive pericellular baskets around the somata of Purkinje cells and make contact to the soma and the initial portion of the Purkinje cell axon (Figure 2). The stellate cells have their somata in the upper two thirds of the molecular layer. Their axons terminate in the molecular layer contacting the smooth dendrites of Purkinje cells (Figure 2). The dendrites of basket cells as well as stellate cells are orientated in a translobular plane and are innervated by parallel fibers running orthogonally through them (Altman, 1997).

An interneuron type with the cell bodies sitting in the granule cell layer are the Golgi cells. These neurons have dendrites arborizing in the molecular layer being innervated by parallel fibers whereas their axons are synapsing with the somata of

the granule cells (Figure 2). Another type of interneurons that was identified and described recently is localized completely in the granule cell layer - the unipolar brush cells. They are characterized by a single thick dendrite ending in a typical brush of dendrioles (Harris et al., 1993; Mugnaini and Floris, 1994) and were recently also described for the cerebellum of the mormyrid fish *Gnathonemus petersii* (Meek et al., 2008).

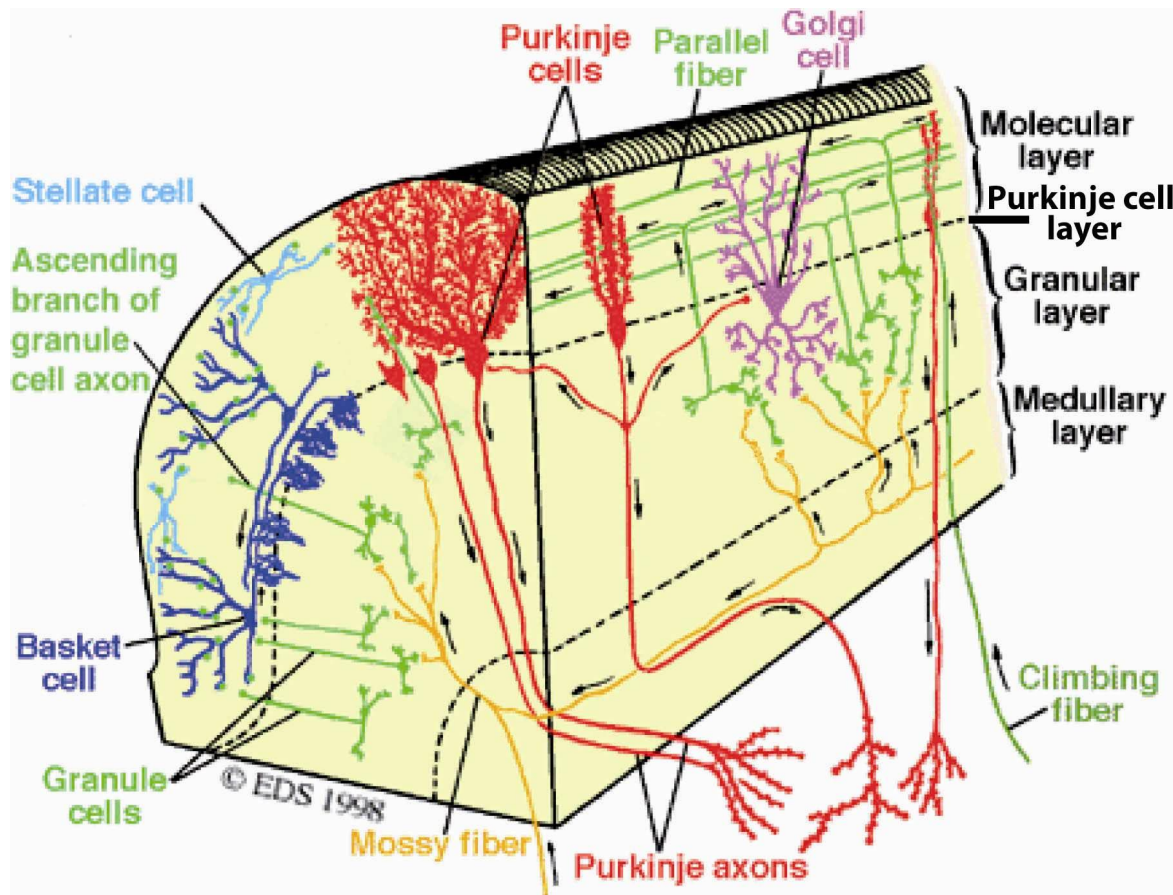


**Figure 2: Layers, cell types and circuitry of the mammalian cerebellar cortex.**

Schematic drawing showing the main neuronal cell types of the mammalian cerebellar cortex with their main connections. Arrows indicate the anterograde direction. Adapted from De Schutter, 1998. Web. <http://www.tnb.ua.ac.be/models/index.shtml>.

#### 1.3.4 Cerebellar circuitries and neurotransmitters

The cerebellum receives excitatory glutamatergic input from the precerebellar system: the pontine gray, the reticulotegmental, the lateral reticular and the external cuneate nucleus synapse via mossy fibers with the somata of granule cells in so called glomeruli (Altman, 1997; Nieuwenhuys, 1967). A single

glomerulus consists of a mossy fiber terminal, the granule cell dendrites, the Golgi cell terminal and is enclosed by glia cells (Jakab and Hamori, 1988). The parallel fibers of the granule cells in turn give excitatory glutamatergic input on the distal spiny dendrites of the Purkinje cells.

The second source of precerebellar input are the climbing fibers from the inferior olive that form excitatory synapses with the Purkinje cell dendrites in the molecular layer (Figure 2). Purkinje cells in turn project to the neurons of the deep cerebellar nuclei (dentate, interpositus and fastigial nucleus) at the base of the mammalian cerebellum. These neurons are the main output neurons of the cerebellum by projecting e.g. to the premotor areas of the ventrolateral (motor) thalamus. The input from the Purkinje cell axons on the neurons of the deep nuclei is inhibitory via GABAergic synapses. In addition, these nuclei receive both inhibitory and excitatory signals from other parts of the brain via collaterals of mossy and climbing fibers. This simple circuitry is further modulated by the inhibitory interneurons located in the granule cell layer and the molecular layer.

The axons of Golgi cells terminate in the glomeruli of the granule cell layer, where they alter the mossy fiber - granule cell synapse via GABAergic inhibition, whereas their dendritic tree reaches into the molecular layer, where it receives excitatory glutamatergic input from the parallel fibers. Interneurons found in the molecular layer are stellate cells and basket cells. Stellate cells get excitatory glutamatergic input from parallel fibers on their dendrites. Their axons innervate the dendritic trees of the Purkinje cells with inhibitory GABAergic synapses. The basket cells lie completely in the molecular layer, their axons synapse on the Purkinje cells providing inhibitory GABAergic input, whereas their own dendrites are innervated by the parallel fibers in the molecular layer with excitatory glutamatergic synapses. In contrast unipolar brush cells are excitatory glutamatergic interneurons of the granule cell layer which receive input from vestibular ganglia and vestibular nuclei and synapse on the dendrites of the granule cells (Nunzi et al., 2001).

### **1.3.5 Similarities and differences – brief comparison of the mammalian and teleostean cerebellum**

#### **1.3.5.1 *The mammalian cerebellum***

The cerebellum of mammals can be spatially subdivided by morphology, function and evolution. The evolutionary oldest part is called the vermis, this medial structure (Figure 3) receives input from the spinal cord, the posterior olivary complex and the lateral reticular nucleus. Lateral to the vermis lies the paravermis (Figure 3) that obtains input from the pontine and the reticulotegmental nucleus. Together with the vermis the paravermis forms the spinocerebellum (Paleocerebellum) that is responsible for the control of body and limb movements. The hemispheres lie lateral to the paravermis (Figure 3), they are the evolutionary youngest parts that form the cerebrocerebellum (Neocerebellum) receiving input from the pontine gray nucleus and the anterior olivary complex. The hemispheres have a role in the planning of movements, the control of limb movements and the evaluation of sensory information for actions, furthermore they are involved in motor learning. The caudal-most part of the cerebellum is called the flocculonodulus (flocculonodular lobe) (Figure 3), which receives input from vestibular nuclei and thus is also called the vestibulocerebellum (Archicerebellum), it is responsible for the regulation of balance and of eye movements (Altman, 1997).

The cerebellar compartments have specialized functions and different input and output. For example the deep nuclei at the base of the cerebellum receive projections from regions of the cerebellar cortex depending on their medio-lateral position. The laterally positioned dentate nucleus receives most of its input from the lateral hemispheres, the nucleus interpositus from the paravermis, and the fastigial nucleus at the medial base of the cerebellum from the vermis (Altman, 1997).



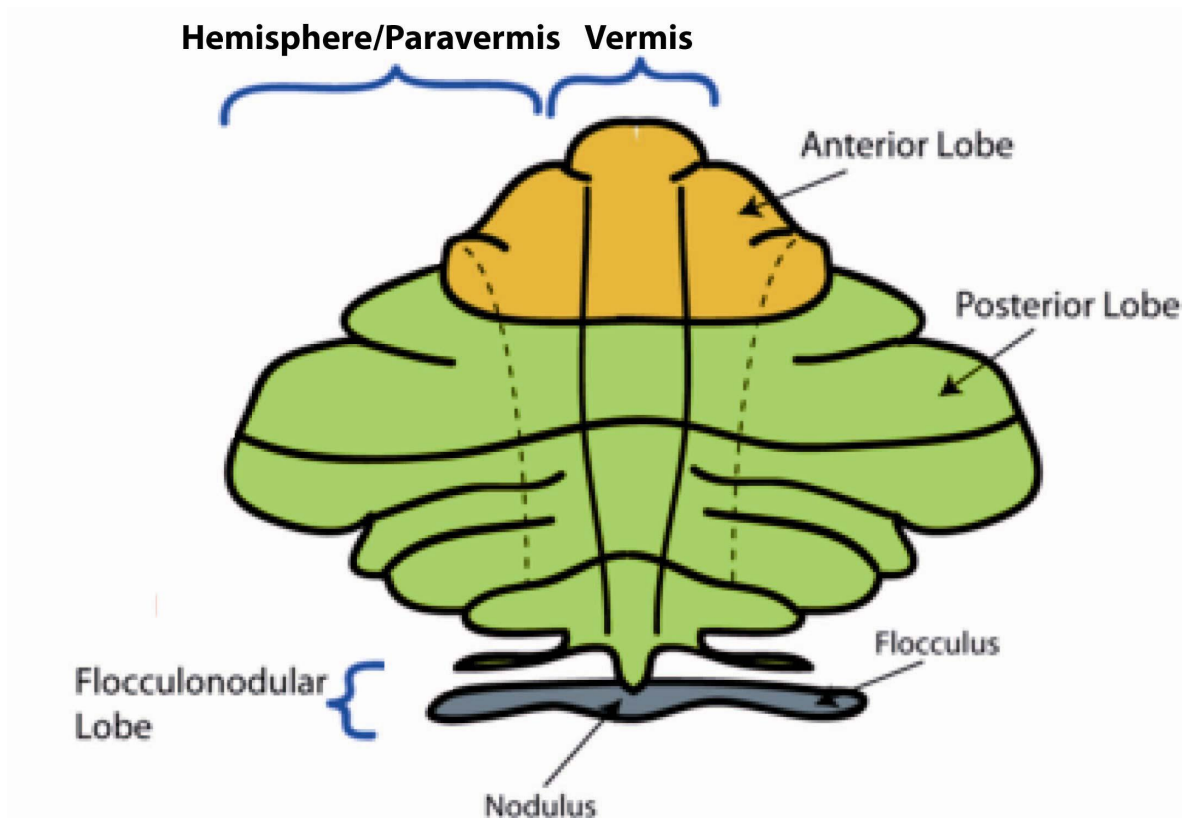


**Figure 3: The mammalian cerebellum.**

Schematic drawing of the adult mammalian cerebellum showing the main compartments: vermis, paravermis, hemispheres and flocculonodular lobe. The cerebellum is further subdivided by a prominent fissure into two main lobes: the anterior lobe and the posterior lobe. Adapted from Wikipedia. Wikimedia Foundation, Inc., 2005. Web. <http://en.wikipedia.org/wiki/File:CerebellumDiv.png>.

### **1.3.5.2 The zebrafish cerebellum**

In contrast to the mammalian and avian cerebellum the cerebellar cortex of teleost fish is not foliated and hence obtains a smooth surface (Nieuwenhuys, 1967). The zebrafish cerebellum has four major parts the corpus cerebelli, the eminentia granularis, the caudal lobe and the valvula cerebelli (Figure 4C) (Wullmann et al., 1996). The corpus cerebelli is a medial structure with the typical well organized layers: molecular layer, Purkinje cell layer and granule cell layer. It receives input from the spinal cord (tectocerebellar and spinocerebellar fibers) and is responsible for locomotion control. According location, input and function the corpus cerebelli is homologous to the vermis of the mammalian cerebellum. The paired lateral situated eminentia granularis together with the caudal lobe located

posterior to the corpus are called the auricles and comprise the vestibulocerebellum (Figure 4C). The caudal lobe receives input from the vestibulo nucleus and the lateral line nerves. The vestibulocerebellum is responsible for balance control and thus corresponds to the flocculo-nodulus of the mammals. The valvula cerebelli is a paired medial structure that extends anteriorly under the optic tectum. In mormyrid fish it receives input from transformed lateral line organs that function as electric sensors. Its specialized function in electroreception is associated with a massive increase in size (Nieuwenhuys and Nicholson, 1967). The valvula can only be found in ray-finned fishes with no homologous structure in mammals (Wullimann and Meyer, 1993). Another fish specific structure is the crista cerebellaris or cerebellar crest an extension of the molecular layer of the cerebellum that covers the anterior hindbrain (Nieuwenhuys, 1967; Wullimann et al., 1996) (Figure 4C). The crista cerebellaris contains the Purkinje cell-like cerebellar crest cells and parallel fibers but no granule cells (Nieuwenhuys, 1967). Only granule cells of the vestibulocerebellum - the eminentia granularis and the caudal lobe extend parallel fibers into the crista cerebellaris, where they receive input from the vestibulo nucleus and the lateral line system (Montgomery, 1981; Puzdrowski, 1989).

In contrast to the situation in mammals in teleost fish the output neurons of the cerebellar cortex do not sit as nuclei at the base of the cerebellum but are dispersed in the Purkinje cell layer. These homologues of the deep cerebellar nuclei are called eurydendroid cells (Ikenaga et al., 2005; Nieuwenhuys et al., 1974). The target regions of their axons are thalamic regions similar to the target regions of the deep cerebellar nuclei of mammals in the thalamus and brainstem. Eurydendroid cells have dendritic trees reaching into the molecular layer, where they are innervated by the Purkinje cell axons (Babaryka, 2009; McFarland et al., 2008). The precursors of the eurydendroid cells are born in the domain defined by the expression of the transcription factors *olig2* in zebrafish and arise and migrate as an early population starting from 36hpf (Babaryka, 2009; McFarland et al., 2008).

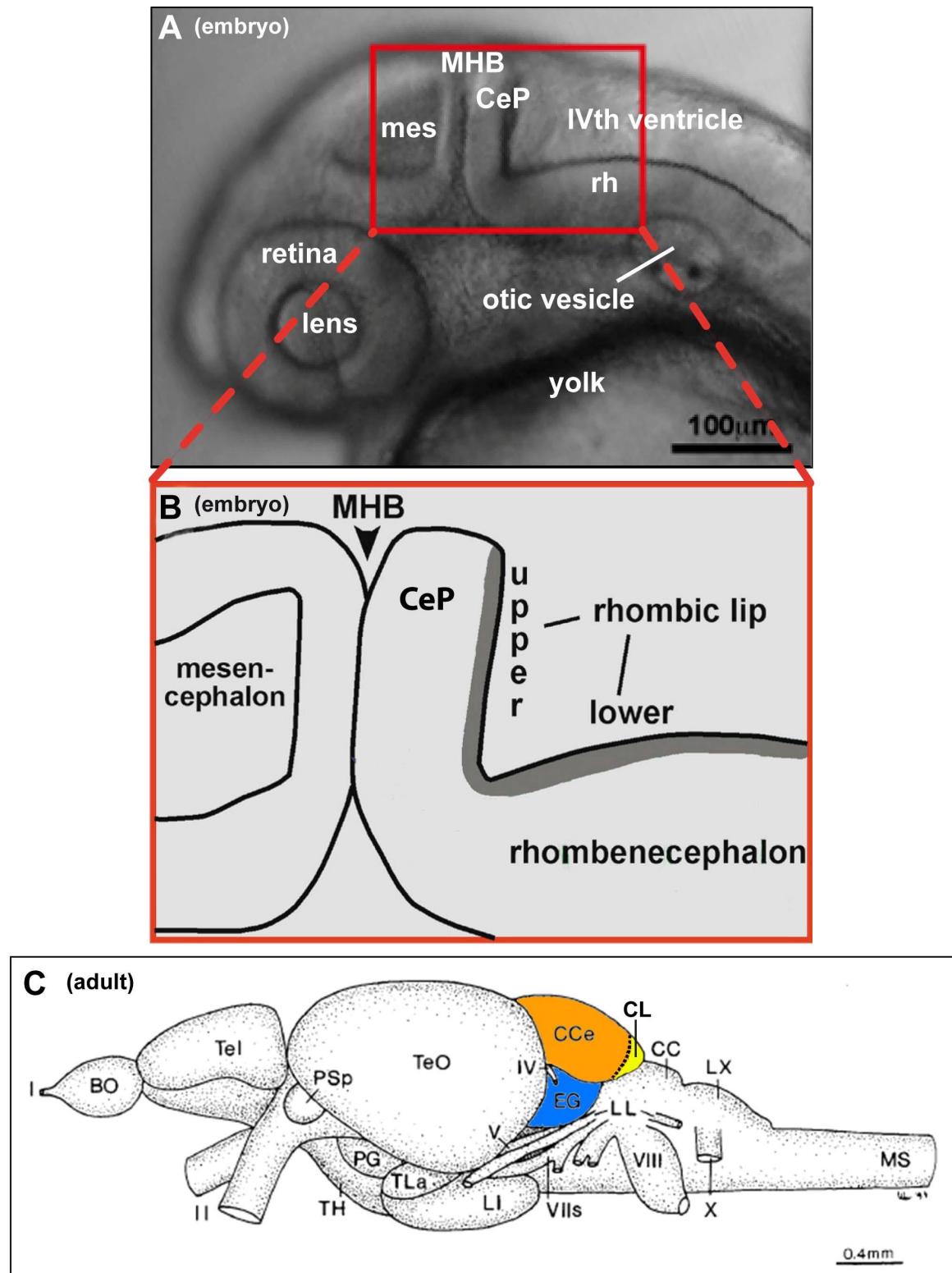


**Figure 4: The embryonic and adult zebrafish cerebellum.**

(A) Lateral view of the head of a zebrafish embryo at 28hpf showing the cerebellar anlage in the context of other structures. After (Köster and Fraser, 2001a).

(B) Schematic drawing of the boxed region in (A) depicting the upper and lower rhombic lip. After (Köster and Fraser, 2001a).

(C) Lateral view of an adult zebrafish brain. Rostral is to the left. The major cerebellar compartments are marked Corpus cerebelli (orange), eminentia granularis (blue), caudal lobe (yellow). After (Wullimann et al., 1996).

**Abbr.:** CC, cerebellar crest; CCe, corpus cerebelli; CeP, cerebellar plate; EG, eminentia granularis; IL, inferior lobe; I-X, cranial nerves; LL, lateral line nerve; LX, vagal lobe; mes, mesencephalon; MHB, midbrain–hindbrain boundary; MO, medulla oblongata; MS, medulla spinalis; BO, olfactory bulb; PG, preglomerular region; Pit, pituitary; PSp, parvocellular superficial pretectal nucleus; rh, rhombencephalon; Tel, telencephalon; TH, tuberal hypothalamus; TLa, torus longitudinalis; TeO, optic tectum.

There are two cerebellar proliferations zones where neuronal precursors are born: the upper rhombic lip (URL) and the ventricular zone (VZ), they are characterized by the expression of two transcription factors *math1* and *ptf1a* respectively (see chapter 1.4.1). Strikingly the situation with two distinct proliferation zones URL and VZ and the expression of the marker genes *atonal1a* (zebrafish homolog of *math1*) and zebrafish *ptf1a* is very similar in zebrafish and mouse embryos (Babaryka, 2009). Moreover the set of genes (*fgf8* (Reifers et al., 1998), *otx2* (Foucher et al., 2006), *gbx2* (Rhinn et al., 2003), *wnt1* (Lekven et al., 2003; McFarland et al., 2008), *atonal1a/math1* (Adolf et al., 2004), *zic1* (Elsen et al., 2008; Grinblat et al., 1998), *pax6* (Foucher et al., 2006)) expressed during cerebellar development are conserved between zebrafish and mammals. In contrast to the situation in mammals, the URL and EGL exist throughout life in zebrafish with continuous proliferation and migration in the adult zebrafish cerebellum (Adolf et al., 2006; Grandel et al., 2006; Kaslin et al., 2009; Zupanc, 2006; Zupanc et al., 2005).

#### **1.4 Migratory neuronal cell populations arising from the upper rhombic lip of the developing zebrafish cerebellum**

The cell types and histology of the cerebellum are described in detail for more than hundred years, but many questions about the cerebellar development remain elusive. In the past few years fate map studies as well as *in vivo* time-lapse analysis have shed some light on the origin and migration of cerebellar progenitor cells in mammals.

#### **1.4.1 The cerebellar rhombic lip or upper rhombic lip (URL) – a proliferation zone**

First described at 1891 by W. His (His, 1891) the rhombic lip is the dorsal-most portion of the hindbrain proliferative neuroepithelium lining the fourth ventricle. The rhombic lip of the hindbrain running longitudinally along the rim of the rhombic fossa is called the lower rhombic lip (also called caudal or hindbrain) rhombic lip. The rhombic lip of the cerebellar plate is termed the upper rhombic lip (URL) (for zebrafish compare (Wullimann and Knipp, 2000)). The URL of the cerebellum was thought to produce cerebellar granule cells only (Alder et al., 1996), but recent fate mapping studies in the mouse have revealed that the rhombic lip undergoes a temporal shift and produces different neuronal cell types in a subsequent manner. Starting with mesencephalic nuclei (parabigeminal, pedunculo-pontine, microcellular tegmental, laterodorsal tegmental, lateral parabrachial) (Machold and Fishell, 2005) from E9.5 to E10.5 followed by deep cerebellar nuclei (dentate, interpositus and fastigial) from E10.5 to E12.5 and finally by cerebellar granule cell progenitors starting from E13 on and ending after birth (Machold and Fishell, 2005; Wang et al., 2005). In addition the URL is the source of the precursors of unipolar brush cells (glutamatergic interneurons in the cerebellar cortex, see 1.3.3 and 1.3.4) (Englund et al., 2006). The URL thus produces the glutamatergic neurons of the cerebellum, whereas the VZ predominantly gives rise to GABAergic neuronal cell types: Purkinje cell precursors and precursors of stellate and basket cells (Millen and Gleeson, 2008). These studies also defined the URL molecularly by the expression of the transcription factor *Math1* and the VZ by the expression a different transcription factor *Ptf1a* (Hoshino et al., 2005; Wingate, 2005).

##### ***1.4.1.1 The expression of the transcription factor *Math1/Atonal1* defines the URL molecularly***

Recently the rhombic lip of the mouse and cerebellum was molecularly defined by the expression of the basic helix loop helix transcription factor *Math1*. Moreover the formation of several URL-derived nuclei was shown to be *Math1* dependent (Machold and Fishell, 2005; Wang et al., 2005), *Math1* is thus one key gene for cerebellar development. *Math1*-expression is induced by PC3

(Canzoniere et al., 2004) and repressed by the binding of the zinc finger transcription factor *Zic1* to the *math1* enhancer (Ebert et al., 2003).

The zebrafish homologue of the mouse *Math1* is *Atonal1*; as its avian and mammalian homologue zebrafish *atona1* is a marker gene for the hindbrain proliferation zones upper and lower rhombic lip. The genome duplication of teleosts resulted in the generation of two *atona1* homologues *atoh1.1* (*atona1a*) and *atoh1.2* (*atona1b*) in zebrafish, they show sequence homologies and exhibit a similar temporally and spatially overlapping expression pattern in the embryo (Adolf et al., 2004). *atona1a* is known to be expressed also by hair cell precursors of the ear in mouse (Bermingham et al., 1999; Chen et al., 2002) and the ear and lateral line in zebrafish (Itoh and Chitnis, 2001). In contrast to mammalian *math1* that is expressed throughout postnatal cerebellar development in the zebrafish embryo the expression of *atona1a* and *atona1b* in the rhombic lip is inactivated after 48hpf. Thus a third *atona1* homologue may exist that overtakes *atona1* function at later time points. Consistent with this assumption proliferation in the URL can be observed in the 5dpf larval zebrafish cerebellum (Wullmann and Knipp, 2000).

To evaluate the universality and thus the relevance of these interesting insights about URL derivatives drawn by the fate map studies in the mouse the grade of conservation among species has to be confirmed by studies in other vertebrate organisms. Furthermore the migration paths of the earliest URL-derived neuronal populations remain unclear. To identify potential guidance factors and regulators of neuronal migration of these neurons that arise in the URL settle in tegmental and brainstem regions, it is necessary to enlighten their migratory behavior in detail.

The teleost zebrafish offers the possibility of *in vivo* analysis of brain development with the help of time-lapse imaging combined with cell and tissue specific expression of transgenes (Köster and Fraser, 2001a; Mione et al., 2008; Rieger et al., 2009) offering means to find answers to these open questions.

#### 1.4.2 Mammalian tegmental hindbrain nuclei arise from the *wnt1*-expressing URL

Previous fate mapping studies in the mouse have identified various derivatives of the URL including the early parabrachial nucleus, parabigeminal nucleus and laterodorsal-pedunculo-pontine nucleus tegmental populations, but the migratory behavior of these early URL-derived neuronal populations that leave the cerebellum remained unclear (Machold and Fishell, 2005; Wang et al., 2005).

In an elegant study mice expressing a LacZ reporter under control of the *wnt1* enhancer were used to investigate the fate of *wnt1*-expressing cells in the murine hindbrain, (Nichols and Bruce, 2006). This fate map analysis confirmed that the *wnt1*-expressing rhombic lip of rhombomere 1 gives rise to several cell populations besides the granule cell precursors. The earliest cells migrate superficially and ventro-rostrally starting from E9/E11 to form cell aggregates in the isthmus, among them cells of the later parabrachial nuclear complex (Nichols and Bruce, 2006). In mouse the putative precursors of the neurons of the parabrachial nucleus migrate from the URL via the nuclear transitory zone (NTZ) (located below the pial surface at the rostral end of the cerebellar plate) into the dorsal tegmentum (Wang et al., 2005). Precursors of the deep cerebellar nuclei migrate from the *wnt1*-expressing cerebellar rhombic lip at E12/E13 whereas granule cell precursors only arise by E13 (Nichols and Bruce, 2006).

The murine parabrachial nuclear complex is a secondary relay area for ascending information from the primary viscerosensory (including gustatory) nucleus solitarius, to the thalamus, but also to the amygdala, hypothalamus and cerebral cortex (Saper and Loewy, 1980). The parabrachial complex in mammals has three main regions: the lateral parabrachial nucleus, the medial parabrachial nucleus and the Kölliker-Fuse nucleus. These regions are further subdivided into several subpopulations, among them the external medial, ventral lateral and external lateral subnuclei. This parabrachial nuclear complex includes partly cholinergic neurons (Jones and Beaudet, 1987; Tago et al., 1989).

Also located in this area is the parabigeminal nucleus, a visual structure of the mesencephalon, located in the isthmus region in the dorsolateral part of the caudal mesencephalic tegmentum, which has reciprocal connections with the superior colliculus and also projects to the parvocellular and/or magnocellular superficial

pretectal nucleus. The parabigeminal nucleus also contains excitatory cholinergic neurons (Mufson et al., 1986; Tago et al., 1989; Woolf, 1991).

Tegmental nuclei that arise early from the upper rhombic lip in the mouse further include the laterodorsal-pedunculopontine tegmental nuclei in the caudal portion of the mesencephalic tegmentum, which represent the brainstem cholinergic ascending system innervating mostly diencephalic and mesencephalic targets, but also the basal telencephalon.

The homologues of the mammalian parabrachial nuclear complex in teleost fish are the secondary gustatory nucleus (SGN) and the secondary viscerosensory nucleus (SVN) that is directly ventrally adjacent to the secondary gustatory nucleus ((Finger and Kanwal, 1992), see also Discussion). These nuclei are located in the hindbrain tegmentum of rhombomere 1 close to the valvula cerebelli, with the nucleus lateralis valvulae (NLV) rostrally adjacent to them (Figure 5). The secondary gustatory nuclei of both brain halves are connected by a broad commissure in cyprinids (Wullimann M.F., 1996) (Figure 5). Both extra-oral gustatory input (via facial sensory nerve) and intra-oral (via glossopharyngeal and vagal nerves) gustatory stimuli converge on the SGN in the rhombencephalon.

The secondary gustatory nucleus and likely also the viscerosensory nucleus neurons send axons into the tertiary gustatory tract that traverses the tegmentum from caudodorsally to rostroventrally and end in the preglomerular tertiary gustatory nucleus (TGN), and the inferior lobe of the hypothalamus in the diencephalon (Folgueira et al., 2003). Similar to the parabrachial nuclear complex in mammals, the secondary viscerosensory (and maybe partly the secondary gustatory) nucleus of the adult zebrafish brain contains cholinergic neurons (Ahrens and Wullimann, 2002; Castro et al., 2006; Mueller et al., 2004).

The teleostean nucleus isthmi (NI) is thought to be the homologue of the parabigeminal nucleus in mammals (Clark, 1933; Ito et al., 1982; Sakamoto et al., 1981). It is located in the tegmentum of rhombomere 1 close to the secondary gustatory/viscerosensory nucleus, but it projects to and receives excitatory visual input from the ipsilateral optic tectum and the parvocellular and/or magnocellular superficial pretectal nucleus (Northmore, 1991; Striedter and Northcutt, 1989; Vinogradova and Manteifel' lu, 1977; Xue et al., 2001). Many nucleus isthmi neurons are cholinergic in zebrafish (Clemente et al., 2004; Mueller et al., 2004)



and this was shown previously for the goldfish *Carassius* as well (Zottoli et al., 1988).

Teleosts furthermore possess in the isthmic region a cholinergic projection nucleus, the superior reticular nucleus (SRN), likely corresponding to the laterodorsal-pedunculo-pontine complex of mammals (Mueller et al., 2004).

Another very large nucleus that populates the teleost tegmental hindbrain region of rhombomere 1 is the nucleus lateralis valvulae (NLV) (Figure 5). This nucleus and the valvula cerebelli, which is a cerebellar structure extending under the optic tectum are specific to teleost fish and have no known homologues in mammals (Wullimann and Meyer, 1993). The nucleus lateralis valvulae is positioned adjacent to the valvula cerebelli and rostrally to the secondary gustatory nucleus (Figure 5) and it forms a very prominent projection into the corpus cerebelli and the valvula cerebelli (Wullimann and Northcutt 1988; 1989; Ito and Yoshimoto, 1990; Xue et al., 2004; Yang et al., 2004; Folgueira et al., 2006). Whether neurons of the mature nucleus lateralis valvulae in zebrafish are partly cholinergic like the secondary gustatory nucleus and nucleus isthmi neurons is a matter of debate (Castro et al., 2006; Clemente et al., 2004; Mueller et al., 2004; Yokogawa et al., 2007).

These four nuclei, that is the secondary gustatory/viscerosensory nucleus, nucleus isthmi, superior reticular nucleus and nucleus lateralis valvulae can be identified in the adult zebrafish brain based on their position (Figure 5), projections and neurotransmitter identity. However their origin, developmental time course and differentiation have remained unknown. These questions are of particular interest though, for the clarification of the evolutionary conservation of how the cerebellar rhombic lip produces a sequence of specific neuronal populations.

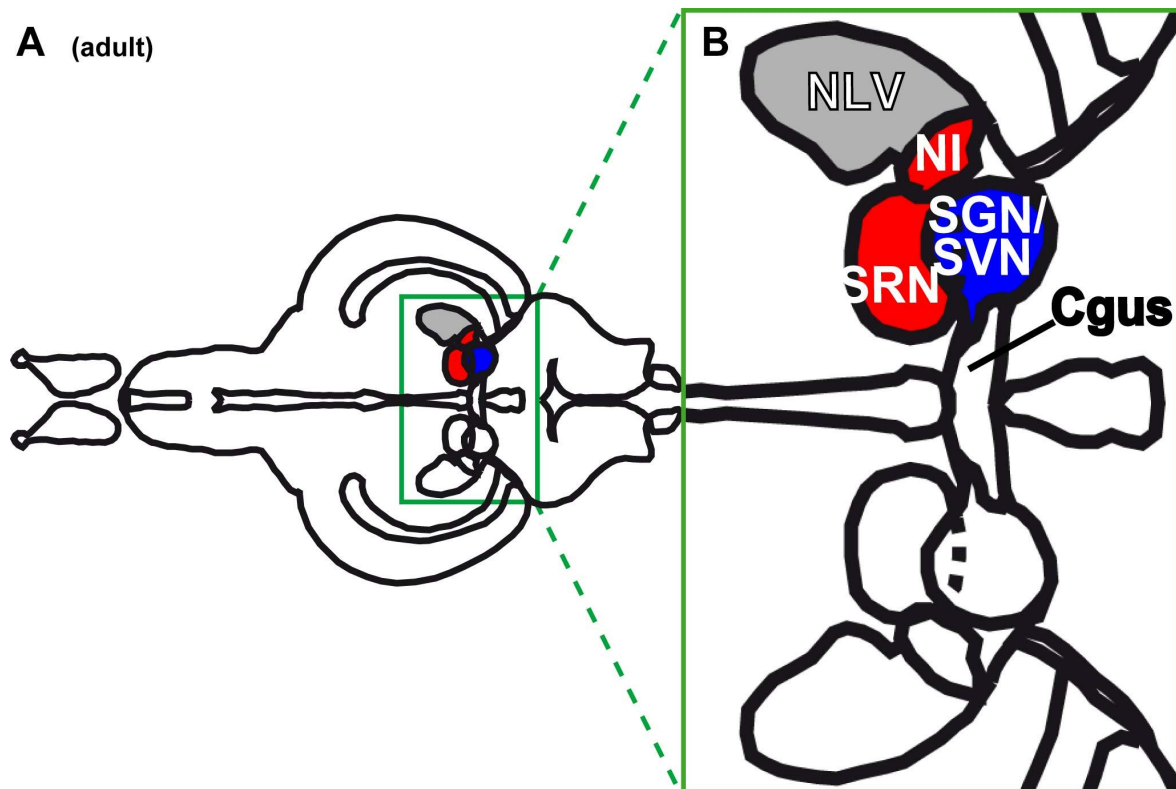


**Figure 5: Zebrafish tegmental hindbrain nuclei.**

(A) Schematic drawing depicting overview of adult brain section in dorsal view, the boxed area is magnified in (B) delineating the tegmental hindbrain nuclei of the isthmic region.

**Abbr.:** *Cgus*, commissure of the secondary gustatory nuclei; *NI*, nucleus isthmi; *NLV*, nucleus lateralis valvulae; *SGN/SVN*, secondary gustatory/viscerosensory nucleus; *SRN*, superior reticular nucleus.

The nearly transparent embryos of the teleost zebrafish (Figure 4A) offer the possibility for *in vivo* analysis of brain development with help of time-lapse imaging (Köster and Fraser, 2001a; Mione et al., 2008; Rieger et al., 2009). Intriguingly, by transient transgenic labeling experiments migration from the zebrafish URL was reported to start already around 24hpf (Köster and Fraser, 2001a) while zebrafish granule cells only begin to emerge at about 48hpf (this study) suggesting that similar to mammals the zebrafish URL produces different cell types over time.

I therefore aimed to characterize the migratory behavior of early URL-derived neuronal populations and to reveal their fates.

The analysis of certain cell lineages in zebrafish is complicated by the high number of neuronal cell populations as well as the current unavailability of a long term inducible labeling system. To overcome these restrictions the present study

takes advantage of a stable transgenic strain allowing the analysis of a defined cell population arising early from the *wnt1*-positive URL in the embryonic and larval brain. The *wnt1:Gal4-VP16-14xUAS-GFP* strain used in this study carries a construct containing the zebrafish *wnt1* promoter/enhancer element driving the expression of Gal4VP16 and via binding of Gal4 to UAS sites the expression of GFP. For simplicity the *wnt1:Gal4-VP16-14xUAS-GFP* strain will be referred to as *wnt1-GVP-UG* strain from hereon.

### **1.4.3 Cerebellar granule cells**

Cerebellar granule cells are the most numerous neuronal cell type in the brain (see chapter 1.3.3 and 1.3.4 for detailed description of morphology and connectivity). Granule cell precursors in the mouse have their origin in the URL (Altman, 1997) as confirmed by recent fate map studies (Machold and Fishell, 2005; Wang et al., 2005) (see chapter 1.4.1). In fact in the mouse embryonic cerebellum subsequent to E12.5 the URL starts to produce granule cell progenitors (Machold and Fishell, 2005; Wang et al., 2005). After leaving the URL granule cell precursors migrate tangentially towards anterior directions to populate the external granule cell layer (EGL), a secondary germinal zone where the progenitors further proliferate. After birth proliferation continues and recently studies observed tangential migration of postmitotic granule cell precursors within the EGL of mouse and chicken (Komuro et al., 2001; Ryder and Cepko, 1994). The postproliferative cells in the inner portion of the EGL start to extend a perpendicular axonal processes that will later become the parallel fiber, while a third process is extended in ventral directions (Figure 6). Then the cells start to migrate radially along radial Bergmann glia fibers through the Purkinje cell layer into the granule cell layer where they finally settle (Hatten and Mason, 1990; Rakic, 1990); (for review, see (Rakic, 1981)) (Figure 6).

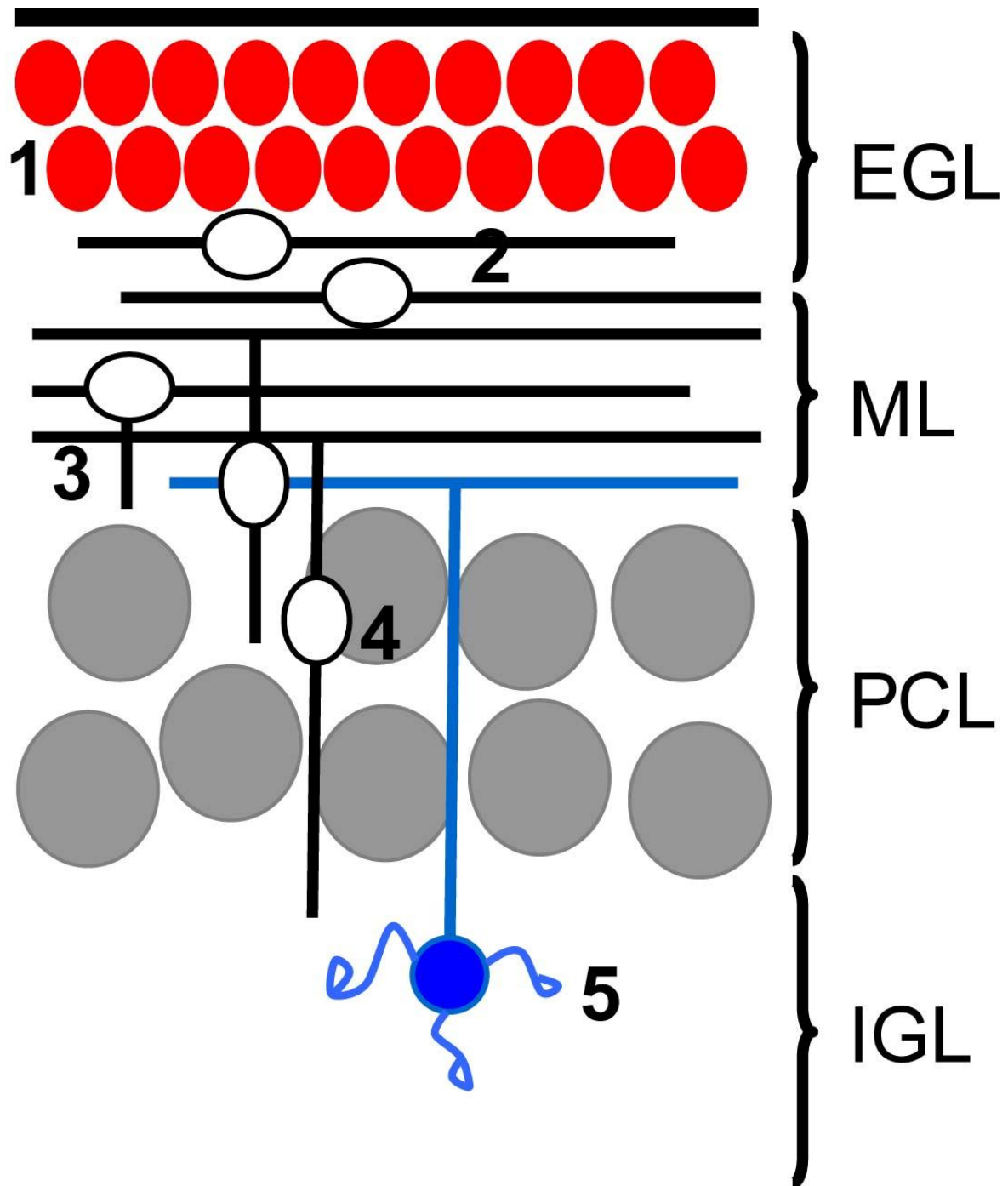


**Figure 6: Mammalian radial granule cell migration.**

Phases of granule cell development. (1) Granule cell precursors proliferate in the outer portion of the external granule cell layer (EGL). (2) Postmitotic granule cells in the deeper EGL extend two horizontal processes and migrate tangentially. They next send a third process perpendicular (3) and migrate radially through the molecular layer and Purkinje cells layer (grey circles) along radial glia (4) to settle in the internal granule cell layer (IGL) (5). After (Kerjan et al., 2005).

#### 1.4.4 Granule cells of the zebrafish cerebellum

Although it is the main cell type in the cerebellum little is known about granule cell development in zebrafish. The onset of zebrafish cerebellar granule cell development as well as the migration routes followed by the precursor cells are unclear. So are the gene expression profile and the differentiation time course. A further unanswered question was at which developmental stage the formation of the cerebellar layers is initiated. Similar to mammals an EGL is formed under the pial surface of the cerebellar plate between 3dpf and 4dpf (Mueller and Wullimann, 2002). However this layer of proliferating granule cell precursors is less prominent than the EGL of the mammalian developing cerebellum.

A prerequisite for the investigation of the development of cerebellar granule cells in zebrafish is the establishment of reliable cell type specific marker genes. The adhesion molecule Tag1 and the transcription factor NeuroD are expressed in differentiating migratory cerebellar granule cell precursors in the mouse embryo (Hatten et al., 1997; Miyata et al., 1999; Schüller et al., 2006), but whether they are expressed in zebrafish granule cells is unclear. There are marker genes known to be expressed by zebrafish granule cells like the zebrafish homologues of Reelin and Pax6a (Costagli et al., 2002; Foucher et al., 2006) but the mouse homologues of these genes are also expressed in other neuronal cell types arising from the URL like deep cerebellar nuclei neurons (D'Arcangelo et al., 1995; Fink et al., 2006; Schüller et al., 2006). Therefore it is necessary to identify definite marker genes for zebrafish cerebellar granule cells.

One granule cell specific marker gene involved in terminal differentiation throughout vertebrate species is the GABA<sub>A</sub>-receptor alpha 6 subunit (GABA<sub>A</sub>Rα6 subunit) which is expressed exclusively in the granule cell layer in the cerebellum of mouse, chicken and goldfish (Aller et al., 2003; Bahn et al., 1996; Fünfschilling and Reichardt, 2002; Jones et al., 1996). Therefore this gene represents a good candidate to identify granule cells in zebrafish.

#### 1.4.5 Is the URL spatially subdivided?

An interesting question in brain development is how the formation of different compartments from one single proliferation zone is organized. There are distinct compartments in the mouse cerebellum that contain granule cells but they are all supposed to arise from the URL. One possible explanation could be a determination of the precursor fate already inside the proliferation zone, this could occur by a spatial regionalization of the neuroepithelium, alternatively fate could be determined after the onset of migration.

Genetic fate mapping in mouse embryos showed that ventricular zone-derived cells maintain their embryonic medio-lateral identity until adulthood (Sgaier et al., 2005). In contrast URL-derived granule cell progenitors maintain their medio-lateral coordinates after emigration from the URL until the initiation of cerebellar foliation but then undergo transverse migration from lateral to medial-posterior during foliation. In particular granule cell progenitors from lateral positions of the URL migrate medially to preferentially populate the posterior-most folia of the mouse cerebellum (Sgaier et al., 2005). Recent genetic experiments suggest that different cerebellar functional subdomains are generated by a differential sensitivity to *engrailed* gene function (Sgaier et al., 2007) suggesting that *engrailed* causes a spatial subdivision of the URL in mice.

#### 1.4.6 The *gata1*:GFP transgenic strain shows GFP expression in a migratory population in the developing zebrafish cerebellum

For this study I took advantage of a stable transgenic zebrafish strain that expresses GFP under control of the *gata1* enhancer that normally drives GFP-expression only in blood cells. In the *gata1*:GFP 781-strain (Long et al., 1997) however GFP-expression can be observed ectopically in the midbrain, the hindbrain as well as in the eye of the embryo. This is probably due to a positional effect at the integration site in the genome. In addition the stable transgenic *gata1*:GFP strain shows GFP-expression in a migrating cell population of the cerebellum starting at 48hpf. It was recently shown that in embryos of the transgenic *gata1*:GFP 781-strain (for simplification *gata1*:GFP from hereon) GFP-expressing neuronal precursors migrate from the dorsoposterior region of the cerebellum, likely the upper rhombic lip anteriorly towards the MHB (Köster and Fraser, 2006). Some cells settle in a dorsal region close to the MHB, whereas

others migrate ventrally along the MHB to cease migration at the ventrolateral base of the cerebellum. During their migration the cells extend short leading processes into anterior-ventral directions. Time-lapse movies revealed that migration has nearly ceased after 80hpf and that most of the cells migrate during the second and third day of development.

Starting at ca. 75hpf the growth of long GFP-positive axons at least partly crossing the dorsal midline was observed. The formation of axonal projections, together with the observation that there are no glia cells present in the zebrafish cerebellum by this developmental time point as indicated by the lack of expression of glia marker genes in the cerebellum before 4dpf (Babaryka, 2009; Rieger et al., 2009) hints on a neuronal identity for the GFP-positive cells. However the cell type of this migratory cerebellar population of neurons as well as their definite origin remained unclear.

### **1.5 Input for the cerebellum - the precerebellar system and mossy fiber-like projections**

The precerebellar system that provides input to the cerebellum consists of five different nuclei. The inferior olive projects axons called climbing fibers to the Purkinje cells in the Purkinje cell layer of the cerebellum, while mossy fibers that terminate in the glomeruli of the granule cell layer at granule cell somata are formed by the pontine gray, reticulotegmental, lateral reticular and external cuneate nucleus. In mammals all neurons of the precerebellar system are born in the lower rhombic lip of the hindbrain. Precursors of the inferior olive arise from hindbrain rhombomere 7 while the other nuclei arise from rhombomere 6-8 (Farago et al., 2006). Interestingly the precursors of the pontine gray, reticulotegmental, lateral reticular, external cuneate nucleus neurons are migrating on an extramural path and arise from the *wnt1*-expressing lower rhombic lip whereas the intramurally migrating precursors of the inferior olive are born in the *wnt1*-negative part of the lower rhombic lip (Rodriguez and Dymecki, 2000).

Only little is known about the precerebellar system in the developing and adult zebrafish brain, including the migration paths of the precursors and the equivalent of the pontine nucleus in zebrafish. A very recent study though describes

precerebellar neurons with origin in the *hoxb4a* expression domain of rhombomere 7-8 (Ma et al., 2009). In addition to the precerebellar system the cerebellum receives input via mossy fiber-like projections from various sources outside the cerebellum, these axons terminate in the granule cell layer and provide excitatory glutamatergic on the granule cell somata and dendrites in glomeruli.

Among mossy fiber-like neurons known to project to the corpus cerebelli in zebrafish are sensory medullary nuclei (MON/DON/NDV), the premotor centers (reticular formation, lateral reticular nucleus) and the locus coeruleus (LC). Visual input is received from several nuclei of the pretectum (central pretectal nucleus (CPN), the dorsal part of the periventricular pretectal nucleus (PPd)) and the accessory optic system (dorsal accessory optic nucleus (DAO) and ventral accessory optic nucleus (VAO)). These inputs are similar to other vertebrates whereas the mossy fiber-like projections from the nucleus lateralis valvulae (NLV), the dorsal tegmental nucleus (DTN) the nucleus paracommissuralis (PCN) (providing telencephalic input) are teleost specific (Wullimann M.F., 1996).

## 1.6 Adhesion factors in cerebellar development

In the developing brain cell-cell adhesion factors have a role in axon fasciculation, neuronal motility and the directionality of migration which makes them interesting candidate molecules for the regulation of neuronal precursor migration and neuronal wiring in the developing cerebellum.

Neuroilin originally cloned from the goldfish (*Carassius auratus*) is the fish homologue of a cell surface glycoprotein is that is also known as ALCAM/CD166 (Bowen et al., 1997; Bowen et al., 1995). Neuroilin has a role in axon guidance and axon fasciculation that is mediated through homophilic adhesions or heterophilic interactions with the ligands CD6 and NgCAM (Bowen et al., 1995; Corbel et al., 1992; Fashena and Westerfield, 1999; Ott et al., 2001; Skonier et al., 1997; Swart et al., 2005). The ALCAM (activated leukocyte cell adhesion molecule) knockout mice show no morphological defects, only a subtle misdirection and poor fasciculation of axons is described.

The expression and function of Neuroilin in zebrafish was investigated with help of a monoclonal antibody named zn-5 or alternatively zn-8 that was isolated twice from the same hybridoma (Trevarrow et al., 1990). In zebrafish Neuroilin-



expression was reported in cranial motorneurons, cerebellar nuclei and hindbrain nuclei (data not shown in (Fashena and Westerfield, 1999)) after 24hpf. Thus Neurolin is an interesting potential adhesion factor for neuronal populations arising from the cerebellar rhombic lip (see **Appendix 1**).

The neuronal cell adhesion molecule (NCAM) has been shown to be involved in the regulation of neural migration (Wang et al., 1994; Hu et al., 1996) in the brain. Attachment of polysialic acid (PSA) to NCAM resulting in steric modification is required for the regulation of cell-cell adhesion and is thus an interesting candidate factor for the regulation of neuronal precursor migration from the URL (see chapter 3.2 and **Appendix 2**).

Furthermore the studies of my colleague in the lab Dr. Sandra Rieger have revealed a role of N-cadherin in the migration of cerebellar granule cell precursors (Rieger et al., 2009). This study was based on the identification and characterization of the granule cell population of the zebrafish cerebellum (see chapter 3.4 and **Appendix 4**).

### **1.7 The receptor/ligand pairs Dcc/Netrin-1 and Unc5c/Netrin-1 as candidate factors for the guidance of URL-derived migratory cell populations**

Netrins are a family of proteins that was named after the Sanskrit word for 'one who guides'. Netrin-1 is a multidomain protein that shares homology with Laminin. In particular Netrin-1 has a Laminin VI-like domain, a Laminin V-like domain, and a C-terminal domain with homology to the complement factors C3, C4, and C5. The Netrin-1 protein was shown to form a gradient in the embryonic chick, mouse and rat spinal cord with high concentration close to the ventral midline and low concentration in the dorsal part (Kennedy et al., 2006).

Both Netrin-1 receptors Dcc (Deleted in colorectal carcinoma/Deleted in colorectal cancer) and Unc5c (Unc-5 homolog c) are type I transmembrane proteins and belong to the Ig superfamily. The receptor Dcc has 10 extracellular domains - four Ig domains and six fibronectin type III domains. The cytoplasmic domain of Dcc is necessary for signaling whereas the extracellular domain is responsible for Netrin-

1 binding upon dimerization. In particular the receptor Dcc binds to Netrin-1 through the fourth fibronectin type III domain, whereas the ligand Netrin-1 binds through multiple domains to the receptors Dcc and Unc5c (Kruger et al., 2004).

In fact Netrin-1-mediated attraction requires multimerization of the Dcc cytoplasmic domain. Thus a truncated Dcc variant that is lacking the cytoplasmic domain acts as a dominant negative inhibiting the function of wild-type Dcc (Stein et al., 2001).

The ligand Netrin-1 is expressed in the floorplate of mice and chicken (Kennedy et al., 1994) during embryonic stages. At postnatal stages (P1 and P10) the expression of the ligand Netrin-1 in the rat cerebellum is localized to the external half of the EGL, an area that is associated with granule cell proliferation (Livesey and Hunt, 1997). In the mouse the Dcc protein and mRNA was found in postmitotic premigratory cerebellar granule cells sitting in the inner half of the EGL and the white matter of the developing cerebellum (Bloch-Gallego et al., 1999; Gad et al., 1997; Livesey and Hunt, 1997). The Netrin-1 receptor Unc5c is expressed postnatally in the mouse cerebellum in proliferating and premigratory granule cells of the EGL, in migratory granule cells in the molecular layer but also postmigratory cerebellar granule cells inside the IGL (Ackerman et al., 1997).

Netrin-1 signaling is known to promote the attraction of commissural axons towards the floor plate in the spinal chord (Kennedy et al., 1994). The *netrin-1* and the *dcc* knockout mice show similar phenotypes, and have severe reduction in commissural axon projections in the spinal chord and in several forebrain commissures. Moreover the absence of the pontine nucleus suggests a role in the migration of specific precerebellar neuronal precursors (Fazeli et al., 1997; Serafini et al., 1996; Yee et al., 1999). Netrin-1 signaling also has been implicated in the guidance of inferior olive precursor migration (Bloch-Gallego et al., 1999).

In addition to its role in the mediation of Netrin-1 signaling in axon guidance and neuronal migration (Cooper et al., 1999) the Netrin-1 receptor Dcc is a so-called dependence receptor that triggers apoptosis in the absence of Netrin-1 binding (Figure 7) (Bernet and Mehlen, 2007). Furthermore Dcc was thus suggested to have a tumor suppressor function (Mehlen and Mazelin, 2003).

Besides a severe size reduction of the cerebellum and abnormal foliation mice deficient for *Unc5c* display a defect in migration of granule cell precursors that fail to stop and migrate rostrally beyond the anterior cerebellar boundary to settle ectopically in the midbrain, whereas initial Purkinje cell development and migration occurs normal. Thus Netrin-1 signaling via the *Unc5c* receptor is important for the establishment of the rostral cerebella boundary (Ackerman et al., 1997; Eisenman and Brothers, 1998; Lane et al., 1992; Przyborski et al., 1998). Interestingly *Unc5c* can mediate both attraction and repulsion. Upon homodimerization Netrin-1 binding results in activation of a pathway causing repulsion whereas heterodimerization with *Dcc* can induce attraction (Hong et al., 1999) (Figure 7). Like *Dcc*, *Unc5c* is a dependence receptor that triggers programmed cell death in the absence of Netrin-1 binding (Bernet and Mehlen, 2007) (Figure 7).

In summary the ligand Netrin-1 is known to be involved in axon guidance, axonal outgrowth, neuronal precursor migration, cell proliferation and survival. The receptors *Dcc* and *Unc5c* can act as a tumor suppressor that mediates apoptosis in the absence of Netrin-1. Whether Netrin-1 signaling is involved in the guidance of ventral migration of early URL-derived precursor populations as it is for migrating populations from the caudal rhombic lip (Bloch-Gallego et al., 2005; Bloch-Gallego et al., 1999; Gad et al., 1997; Livesey and Hunt, 1997) is still unclear. A chicken cerebellar explants study only described an effect of Netrin-1 on the leading process of early URL derivatives (Gilthorpe et al., 2002). Also a possible role of Netrin-1 in the regulation of tangential migration of granule cell precursors from the URL as suggested by the phenotype of *Unc5c* knockout cerebella remains elusive and has to be investigated *in vivo*.

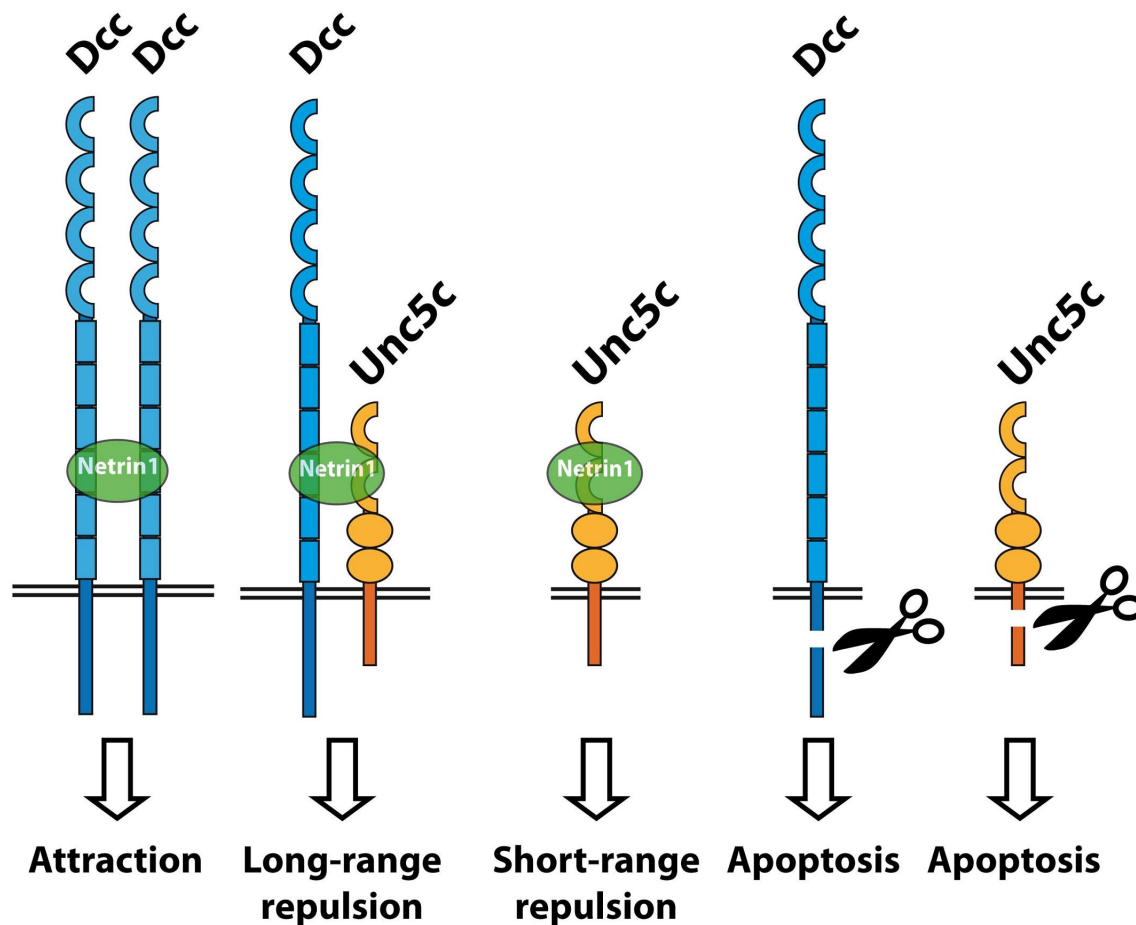


**Figure 7: Schematic drawing of Dcc and Unc5c receptor-mediated signaling.**

Upon Netrin-1 binding homodimerization of Dcc mediates attraction, whereas heterodimerization of Dcc and Unc5c mediates long-range repulsion. Netrin-1 binding to Unc5c alone leads to short-range repulsion and the absence of Netrin-1 binding induces apoptosis via both receptors.

### 1.7.1 Netrin-1 and Netrin-1 receptors in zebrafish

The two *netrin-1* homologues in zebrafish *netrin-1a* and *netrin-1b* are expressed in cells of the ventral midline in the hindbrain and spinal cord (Lauderdale et al., 1997; Strahle et al., 1997). The receptor Dcc is expressed in the forebrain, midbrain (tectum), hindbrain, spinal cord, pectoral fins, retina and heart (Fricke and Chien, 2005; Hjorth et al., 2001). A recent study could show via morpholino knockdown that Netrin-1 acts as a guidance cue for dendrites of zebrafish octavolateralis efferent neurons during midline crossing (Suli et al., 2006). Whether Netrin-1 signaling via the receptors Dcc or Unc5c also plays a role in the regulation of migration of precursor populations in rhombomere 1 remains

elusive. For the zebrafish homologue of *unc5c* no cDNA was isolated and the expression pattern was unknown.

Chi-Bin Chien and colleagues cloned and fully sequenced the zebrafish homologue for *dcc* as fragments but no full length cDNA was available. Thus to investigate Dcc/Netrin-1 signaling in the zebrafish cerebellum with help of over-expression and knockdown experiments I aimed to clone a full length cDNA for zebrafish *dcc*.

Keeping in mind that Netrin-1 signaling can be mediated by Dcc or Unc5c alone but also by heterodimers of both receptors with opposing effect on the migrating neuron/growing axon I had to find out if there is co-expression of Unc5c and Dcc in the cerebellum to interpret the data correctly. Thus I have aimed to isolate a partial cDNA for zebrafish *unc5c* to analyze *unc5c*-expression in the developing zebrafish cerebellum.

## 1.8 In vivo retrograde labeling of neurons in zebrafish larvae

Neuronal circuitries are established within a brain compartment but also by sending axonal projections over long distances connecting neurons localized in distinct structures but comprising a functional unit (see chapter 3.1.4, 3.4.3, **Appendix 1** and **Appendix 4**). One possible method to analyze such neuronal projections is the injection of fluorescent tracer dyes. Lipophilic dyes such as Dil spread passively by diffusion in the cell membrane of neurons anterogradely and retrogradely and thus can be used *in vivo* and on fixed tissue. Although occurring rarely, some degree of transmission to membranes of axons or somata in contact with the labeled cells is possible and provides risk of false positive results. In contrast rhodamine dextran is transported actively in the injured axon in retrograde direction only. Thus rhodamine dextran can only be used in living specimens or tissues but no transfer to neighboring cells is possible. **Appendix 5** describes a detailed method of how rhodamine dextran can be used in living zebrafish larvae (Volkman and Köster, 2007).

## 1.9 Retrograde labeling as potential means to analyze *parkin* function in the posterior tuberculum

The mammalian *parkin* gene is known to be involved in the development of Parkinson's Disease that is characterized by the degeneration of dopaminergic neurons in the substantia nigra (Cookson et al., 2008).

Interestingly the group of Oliver Bandmann found that a morpholino knockdown of the *parkin* mRNA causes a significant reduction of tyrosine hydroxylase (TH)-expressing cells in the posterior tuberculum of the ventral diencephalon in zebrafish embryos. This observation in a structure which is thought to be homologous to the substantia nigra in humans (Holzschuh et al., 2001; Rink and Wullmann, 2001; 2002) hints to a loss of dopaminergic neurons (see **Appendix 6**). An alternative interpretation of this observed reduction of TH-expression could be a delayed differentiation of the neurons resulting in low levels of this neurotransmitter synthesizing enzyme rather than a decrease in cell number. To discriminate between these two explanations one experimental approach could be the specific labeling of the dopaminergic neurons in the posterior tuberculum via their axonal projections into the subpallium of the telencephalon. For this purpose rhodamine dextran could be injected into the subpallium of *parkin* morphants followed by analysis for the presence of labeled cell bodies in the region of the posterior tuberculum. Also it was not addressed in the current study whether the missing dopaminergic neurons of the posterior tuberculum in *parkin* morphants undergo a sudden cell death or degenerate progressively over a longer time. Degeneration is possibly leading to a retraction of the axons preceding the death of the neuron. Here the proportion of labeled dopaminergic neurons in the posterior tuberculum after rhodamine dextran injections into the subpallium over time could give a hint on how dopaminergic neurodegeneration might progress. Thus my protocol for precise rhodamine dextran injections into zebrafish embryos and larvae (described in **Appendix 5** (Volkman and Köster, 2007)) could be applied to address these important questions regarding *parkin* function in the zebrafish model.

## 2 Aims and Achievements

The major aim of my PhD project was to identify and characterize migratory neuronal populations arising from the URL in the developing zebrafish cerebellum. At the beginning of my research none of the neuronal cell types in the developing zebrafish cerebellum had been characterized. Also nothing was known about the origins of these cell types and populations. Therefore my experiments concentrated on revealing the migratory behavior (migration path, migration speed) of these progenitor cells from their origin to their final destination as well as the characterization of their terminal differentiation.

(I) The comparison of cerebellar development in zebrafish with mammalian model organisms like the mouse helps to obtain insights into the grade of conservation among vertebrate species and thus the relevance of studies in model organisms for human development. The upper rhombic lip of mice was found to produce several different neuronal populations over time, among those the precursors of the tegmental hindbrain nuclei: the parabrachial nuclear complex, the parabigeminal and the laterodorsal-pedunculo pontine nuclei (Machold and Fishell, 2005; Wang et al., 2005). To find out if this holds true for other vertebrates I conducted a study investigating the origin and development of tegmental hindbrain nuclei of rhombomere 1 in the teleost fish zebrafish (*Danio rerio*). Taking advantage of a stable transgenic *wnt1:Gal4-VP16-14xUAS:GFP* zebrafish strain, which labels the embryonic *wnt1*-expressing neuronal precursor population and combining marker gene expression analysis with retrograde axonal labeling, I found the precursors of the zebrafish homologues of the parabrachial nuclear complex, the parabigeminal and the laterodorsal-pedunculo pontine nuclei, namely the secondary gustatory/viscerosensory nucleus and the nucleus isthmi and/or superior reticular nucleus to arise from the URL. Thus I could reveal that origin and developmental program of these populations is conserved between zebrafish and mouse and therefore likely holds true for the human cerebellum as well. With help of time-lapse imaging I focused on the characterization of the migratory behavior of these precursor populations. Furthermore, I analyzed the expression of the adhesion factors PSA and Neurolin in these neuronal populations. I could contribute in revealing a role of PSA-NCAM in the regulation of migration in this

population. Moreover, my co-expression studies provide insights into the neurotransmitter composition of the secondary gustatory/viscerosensory nucleus containing besides cholinergic also glutamatergic neurons. To achieve URL-specific expression of transgenes I created a stable transgenic *atoh1a:KaTA4* strain that drives Gal4 expression under control of the *atoh1a* enhancer. This strain was used in a study analyzing the migration of URL-cells on a subcellular level and investigating the role of the centrosome during migration and axogenesis of this population.

Thus my work lays the ground for further studies investigating the molecular base of these migration and neuronal wiring events (e.g. on guidance factors and the role of adhesion factors). This project is described in chapter 03.1, chapter 3.2, chapter 3.3 and in **Appendix 1**, **Appendix 2** and **Appendix 3**.

(II) Only little is known about how functional compartments of the adult cerebellum are laid down during embryogenesis. I have lead a study that revealed how the granule cell populations of the different cerebellar compartments are established. With help of marker gene expression analysis, and retrograde labeling in the stable transgenic *gata1:GFP* zebrafish strain I contributed to the identification of the granule cell population of the larval and juvenile zebrafish cerebellum. The granule cell precursors were found to be generated by the URL, consistent with what was described for the mouse and confirming the conserved role of this proliferation zone in producing granule neurons in vertebrates. Moreover, with help of time-lapse analysis in combination with single cell tracing I could reveal that this germinal zone not only undergoes a temporal shift generating different neuronal cell types in a subsequent manner but also features a regionalization into spatial domains producing different functional subtypes of granule neurons, namely the granule cells of the vestibulo- and non-vestibulocerebellum. Also it has not been shown so far, how the zebrafish cerebellum grows during larval stages. With help of proliferation studies, time-lapse analysis of larvae and histological examinations I could narrow this knowledge gap and provide information about the development of the most numerous cell population in the cerebellum the granule cells during later stages of cerebellar development after the first period of massive embryonic cell migration.

This work is presented in chapter 3.4 and **Appendix 4**.



To reveal the axonal connections of the developing cerebellar granule cell population, I established an *in vivo* retrograde labeling technique by microinjection of rhodamine dextran into the larval zebrafish brain (Volkman and Köster, 2007). This protocol is described in **Appendix 5**.

(III) In addition I aimed to elucidate the role of Netrin-1 signaling in the guidance of neuronal migration during zebrafish cerebellar development. Using expression analysis I could show that *netrin-1a/1b* is expressed in the floorplate of the hindbrain neural tube ventral to the cerebellar anlage potentially providing guidance information for neuronal migration in ventral directions. Remarkably, I found that the receptors Dcc and Unc5c are expressed by migrating cerebellar granule cells. However, I could not observe an effect on migration when knocking down *dcc* and *netrin-1a/1b* mRNA by antisense morpholino injection. Thus I provided more precise means of dissecting Dcc function in the cerebellum by cloning full length and dominant negative zebrafish Dcc variants that can be expressed via the Gal4-UAS system. These genetic tools are now available for a cell type specific analysis of Netrin-1/Dcc signaling in the developing cerebellum. This project is summarized in chapter 3.5.1.

Taken together my work reveals novel insights into the development and especially the migratory behavior of URL-derived neuronal populations. Furthermore I have provided tools to investigate the role of guidance factors during the migration of URL-derived neuronal precursors.

(IV) Finally in a collaborative effort with the group of Oliver Bandmann I have contributed to a morpholino based study developing zebrafish as a vertebrate model organism for early onset Parkinson's Disease. With help of transmission electron microscopy I have analyzed the effect of *parkin* deficiency on mitochondria. Surprisingly I could observe a novel phenotype affecting the t-tubules in the muscle tissue of the zebrafish trunk.

This collaboration is described in chapter 3.6 and **Appendix 6**.

## 3 Results

### 3.1 Characterization of GFP-expressing cell populations in the cerebellar anlage of the *wnt1*-GVP-UG stable transgenic zebrafish strain

**Published Article (Volkman et al. 2010) (see Appendix 1)**

To analyze the migration, developmental time course, differentiation and eventual fate of early arising neuronal populations from the URL I made use of a stable transgenic *wnt1:Gal4-VP16-14xUAS:GFP* zebrafish strain (*wnt1*-GVP-UG from hereon) (created by Yi-Yen Chen). In embryos from this strain GFP-expression under control of the *wnt1* promoter/enhancer drives GFP-fluorescence that persists over several days declining in rhombomere 1 at about 5dpf.

#### 3.1.1 Early cerebellar *wnt1*-expressing cells represent URL-derived cell types that migrate over long distances (Appendix 1: Figure 2 and 3)

For the mouse it was shown that the two proliferation zones of the cerebellum are characterized by the expression of two different transcription factors *math1* for the rhombic lip and *ptf1a* for the ventricular zone (Machold and Fishell, 2005; Wang et al., 2005). As this situation was recently shown to be conserved in the zebrafish cerebellum (Babaryka, 2009) I could use the zebrafish homologues of *math1 atonal1a* (Kim et al., 1997) and zebrafish *ptf1a* (Zecchin et al., 2004) as marker genes for the rhombic lip and ventricular zone respectively. *In situ* hybridization for the two marker genes combined with immunohistochemistry for GFP on *wnt1*-GVP-UG embryos revealed GFP-expressing cells to express *atonal1a* but not *ptf1a*. Thus the GFP-expressing cells in the cerebellar plate of *wnt1*-GVP-UG embryos represent a cell population derived from the cerebellar rhombic lip.

The pre-migratory GFP-expressing cells in the URL of *wnt1*-GVP-UG embryos were found to be in a proliferative state based on time-lapse imaging (**Movie 1**)

and immunohistochemical analysis and thus represent the complete cell lineage starting from the undifferentiated proliferating progenitor rather than from a postmitotic stage after onset of differentiation. *In vivo* observation can therefore be used to follow their fate from birth until terminal differentiation.

Time-lapse movies (**Movie 2 and Movie 3**) revealed that migration of GFP-expressing cells is initiated at about 24hpf shortly after the rotation of the zebrafish cerebellar primordium (Distel et al., 2006) and this migration peaks at about 36hpf and ceases until 48hpf. The *wnt1*-expressing neuronal progenitors leave the URL and move rostrally to the MHB. After reaching the MHB these cells turn ventrally and migrate along the MHB into the depth of the neural tube. Eventually these neurons settle in the tegmentum forming bilateral symmetric clusters in the ventral part of rhombomere 1 where they terminally differentiate. I have used transient DNA injection to obtain Gal4-VP16-mediated cell population specific but mosaic red-fluorescent labeling. Combining this technique with *in vivo* time-lapse confocal microscopy allowed us to trace individual cells along their migratory route and to quantify their characteristic behavior (**Movie 4**). I have determined the migration speed and persistence in migratory directionality of individual precursors that now can be compared to other migratory cell populations in the brain and used as reference for the analysis of migration phenotypes.

### **3.1.2 Ventrally migrating *wnt1*-GVP-UG cells do not contribute to zebrafish deep cerebellar neurons or eurydendroid cells: (Appendix 1, Figure 4)**

The homologous neurons of the deep cerebellar nuclei neurons are the eurydendroid cells of the teleost cerebellum. Like their mammalian counterpart they are receiving input from the Purkinje cells and they project outside of the cerebellum to innervate thalamic regions, thus they are the output neurons of the cerebellum. In contrast to the deep nuclei neurons that are sitting at the base of the mammalian cerebellum eurydendroid are not organized in nuclei but instead are dispersed in the Purkinje cell layer, with their dendrites spreading in the molecular layer. This cell type was recently characterized in the embryonic zebrafish cerebellum (Babaryka, 2009; McFarland et al., 2008). As fate map studies in the mouse have found the precursors of the deep cerebellar nuclei neurons to arise from the *wnt1*-expressing URL, I analyzed *wnt1*-GVP-UG cells for a possible identity as homologous of these deep nuclei neurons.

The results of my co-expression and axon projection analysis exclude that the ventral clusters formed by the *wnt1*-GVP-UG cells are related to the deep cerebellar nuclei of mammals. However whether the mouse homologues of deep cerebellar nuclei the eurydendroid cells are among the cell populations arising from the zebrafish URL at later stages in zebrafish is an interesting question that needs to be answered in further studies.

### **3.1.3 *wnt1*-GVP-UG cells are tegmental hindbrain nuclei of rhombomere 1 (Appendix 1: Figure 5 and 6)**

With help of ChAT immunohistochemistry I could demonstrate that *wnt1*-expressing progenitors that leave the cerebellar rhombic lip acquire a cholinergic fate in the tegmental area of rhombomere 1. Some *wnt1*-GVP-UG neurons, however, were glutamatergic based on *vglut2.1*-expression.

Further co-expression analysis revealed that postmigratory *wnt1*-GVP-UG cells express the marker genes *reelin* (Costagli et al., 2002) and Calretinin (Castro et al., 2006) known to be expressed by the nucleus isthmi or secondary gustatory/viscerosensory nucleus respectively.

Taken together the early origin of the *wnt1*-GVP-UG cells in the URL, their characteristic ventral migration, their final position in the tegmentum of rhombomere 1, their co-expression of tegmental nuclei marker genes and their neurotransmitter identity strongly suggest, that these GFP-expressing cells in the early URL are progenitors of the zebrafish tegmental hindbrain nuclei known to be positioned in the ventral rhombomere 1 in the adult brain, likely including the secondary gustatory/viscerosensory nucleus, nucleus isthmi (Arenzana et al., 2005), superior reticular nucleus or nucleus lateralis valvulae (Figure 5).

### **3.1.4 Axonal projections and adhesion factors (Appendix 1: Figure 3, 4 , 7 and 8)**

By retrograde labeling via microinjection of the red fluorescent lipophilic dye Dil I found that *wnt1*-GVP-UG URL-derived neurons settle in tegmental areas of rhombomere 1 from where they project towards the optic tectum, the hypothalamus and the preglomerular tertiary gustatory nucleus which allows to possibly identify them as neurons of the nucleus isthmi and/or superior reticular

nucleus (ventrorostral to the cerebellar tract) and the secondary gustatory/viscerosensory nucleus (caudal to the cerebellar tract), respectively. These different efferent projections define the region of the secondary gustatory/viscerosensory nucleus as the posterior part and the nucleus isthmi and/or superior reticular nucleus as the anteroventral part of the *wnt1*-GVP-UG cell cluster respectively. Furthermore, these connectional studies suggest that *wnt1*-expressing neuronal progenitors emanating from the URL do not contribute to the nucleus lateralis valvulae. Thus I could further discriminate between these tegmental hindbrain nuclei by means of their distinct axonal projections.

Furthermore my axonal projection analysis identified the origin of a prominent GFP-fluorescent mossy fiber-like projection into the IGL of the corpus cerebelli of *wnt1*-GVP-UG larvae and juvenile fish. Via retrograde and anterograde axonal labeling I found the respective cell bodies to be situated in the pretectal area most likely in the paracommissural nucleus (PC) or dorsal periventricular pretectal nucleus (PP) providing relayed telencephalic input to the non-vestibular granule cell population of the zebrafish cerebellum (**Appendix 1**: Figure 8).

With double-immunohistochemistry I found high levels of PSA (see chapter 3.2 and **Appendix 2**) localizing to the *wnt1*-expressing cells along their migration path close to the MHB, which is indicative for the presence of polysialylated NCAM. Moreover double-immunohistochemistry revealed the expression of the neuronal adhesion factor Neurolin on the somata of terminal differentiating secondary gustatory/viscerosensory nucleus and nucleus isthmi and/or superior reticular nucleus neurons in the tegmentum. Notably, at least the initial portion of their axons close to the cell bodies was also positive for the Neurolin protein.

## Conclusion

The progenitors of the tegmental hindbrain nuclei secondary gustatory/viscerosensory nucleus and nucleus isthmi and/or superior reticular nucleus arise from the *wnt1*-expressing URL and migrate on a migration path along the MHB into ventral directions to finally settle in the tegmentum of rhombomere 1. There they terminally differentiate and integrate into neuronal circuitries. Migrating NI/SRN and SGN/SVN precursors belong to the URL-derived

population that regulates motility by the enzymatic attachment of PSA to NCAM. Furthermore *wnt1*-expressing neurons of the pretectum provide input to the granule cells of the corpus cerebelli via mossy fiber-like projections. These connections are already established in the larvae at 4dpf.

### **3.2 Enzymatic removal of PSA results in impaired migration of NI/SRN and SGN/SVN precursors**

***Published Article (Rieger et al., 2008) (see Appendix 2)***

With help of *in situ* hybridization and antibody staining we have described the expression of the zebrafish homologues of the neural adhesion molecule NCAM, PSA as well as the polysialyltransferases STX and PST in the developing brain with focus on rhombomere 1. We found NCAM, STX and PSA to be linked to regions of neuronal migration. Strikingly we found in an *in vivo* time-lapse study that upon enzymatic removal of PSA ventral migration of URL-derived progenitors in rhombomere 1 is impaired.

My co-expression analysis in the *wnt1*-GVP-UG strain (chapter 3.1.4) revealed that the migrating NI/SRN and SGN/SVN precursors express PSA along their ventral migration path along the MHB (**Appendix 1**: Figure 3).

#### **Conclusion**

PSA-NCAM likely is involved in the regulation of migration of the tegmental hindbrain nuclei NI/SRN and SGN/SVN precursors during ventral migration.

### **3.3 Generation of a zebrafish *atonal1a* activator strain**

***Published Article (Distel et al. 2010) (see Appendix 3)***

To achieve a stable transgenic strain for driving expression of transgenes in the cells of the URL I aimed to isolate the regulatory element of the rhombic lip marker gene *atonal1a*.

To identify the *atonal1a* enhancer the flanking genomic regions of the zebrafish *atonal1a* locus were compared with the loci of other vertebrate species. The interspecies alignment revealed a region with high homology to the zebrafish genomic sequence. This sequence conservation hinted on the presence of regulatory elements in this region. To isolate the genomic region likely to contain regulatory elements primers were designed to amplify a 3kb fragment upstream and a 6kb fragment downstream of the zebrafish *atonal1a* gene. Using a BAC containing the *atonal1a* genomic DNA together with 5' and 3' flanking regions (RZPD) as template these fragments were amplified by PCR.

The KalTA4 pA sequence coding for an optimized Gal4 (Distel et al., 2009) was cloned in frame between these genomic fragments. For better insertion into the genome the whole expression cassette was flanked by I-SceI restriction sites (Babaryka et al., 2009) (Figure 8A).

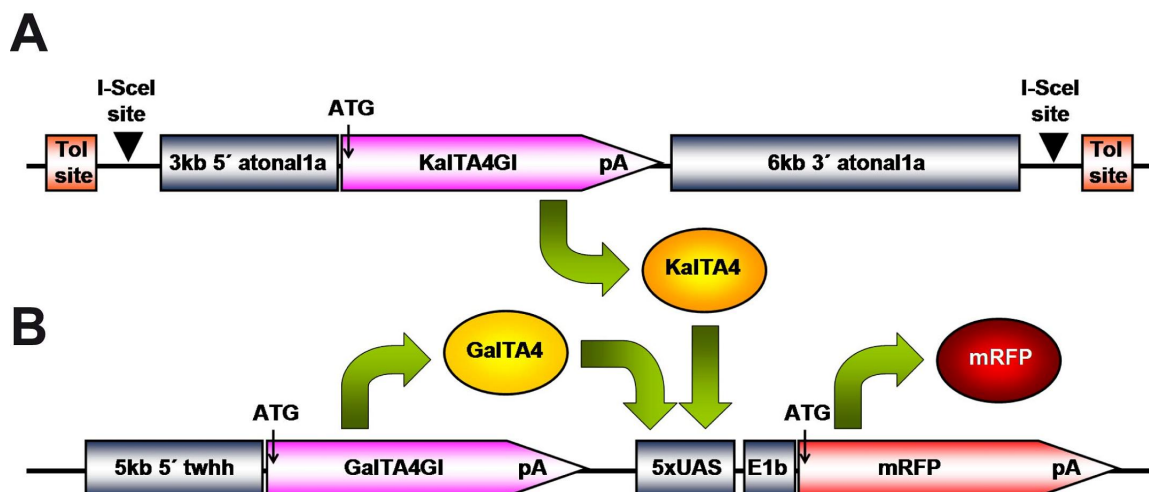


**Figure 8: *atoh1a*:KalTA4 activator cassette and activator/reporter cassette of TG5xR RFP reporter strain.**

Schematic drawing of activator (A) and activator/reporter (B) cassettes depicting the basal promoter (E1b), the upstream activating sequence (UAS), the polyadenylation site (pA), the transcription factors GalTA4 (GalTA4) and optimized GalTA4 (KalTA4), the *atonal1a* and *twhh* enhancer elements, translation start (ATG), red fluorescent protein (mRFP) and the flanking restriction enzyme I-SceI sites (I-SceI) as well as the Tol transposase recognition sites (Tol site).

The construct was tested by transient injections, via co-injection with I-SceI coding RNA into a *twhh:GalTApA-5xUAS:mRFPpA* (TG5xR from hereon) stable transgenic background (Figure 8B) resulting in mosaic RFP-expression in the rhombic lip cell population but also ectopically elsewhere in the embryos (data not shown). From this observation I concluded that the construct is not suitable for transient transgenic experiments but needs stable integration into the genome for full transcriptional control. Thus to create a stable strain the construct was co-injected with I-SceI coding RNA into the one-cell stage in a heterozygous TG5xR stable transgenic background (Figure 8B) and the injected embryos were raised to adulthood. Identification of transgenic carriers was achieved by outcrossing with the TG5xR stable transgenic strain (Figure 8B) and the observation of red fluorescent cells in these embryos was used as indication for stable insertion of the expression cassette into the germ line. 8 founder fish could be isolated that gave rise to offspring with different red fluorescent expression patterns (Table 1): embryos of one carrier displayed expression in yolk cells probably due to a positional effect at the integration site. In embryos derived from five founders the hair cells of the lateral line and the otic vesicle were labeled. These cell populations are known to express *atonal1a* endogenously (Itoh and Chitnis, 2001). There were three founders that gave rise to embryos with expression in the heart suggesting that the isolated genomic sequence used in the activator cassette contains a regulatory element driving expression in the heart. Two founders though had offspring with red-fluorescent transgene expression in the cerebellum and hindbrain reminiscent of endogenous *atonal1a*-expression.



Founder #	Expression
1	<b>hair cells of lateral line, ear</b> and head; skin; eye
2	cells on yolk - probably keratinocytes
3	<b>cerebellum</b> and <b>hindbrain</b> ; ( <b>hair cells of ear</b> and <b>lateral line</b> ); pectoral fin
4	<b>hair cells of ear</b> and <b>lateral line</b> ; few <b>cells in cerebellum</b> and <b>hindbrain</b>
5	heart
6	heart
7	heart; <b>hair cells of ear</b> and <b>lateral line</b>
8	<b>hair cells of ear</b> and <b>lateral line</b>

**Table 1: RFP-expression in *atonal1a:KalTA4GI/TG5xR* double transgenic founder strains.**

Cell types in bold represent cells with endogenous *atonal1a*-expression.

Because of this specific expression in the cerebellum founder III was chosen for further experiments. This stable transgenic strain drives mosaic red-fluorescent RFP-expression in the upper and lower rhombic lip, a medial cell population in the midbrain tegmentum and ectopically in cells of the pectoral fin. F1 offspring of founder III were raised to adulthood for further breeding and will be referred to as *atoh1a:KalTA4* from hereon. Embryos of the F3 and F4 generation still showed the same expression pattern that was transmitted at Mendelian ratio confirming a stable insertion of the transgene into the genome. *In vivo* time-lapse movies revealed that *atoh1a:KalTA4* cells showed the typical migratory behavior of early URL-derived precursors (**Movie 5**).

When crossed into a stable transgenic 4xUAS:GFP reporter strain GFP was expressed in all rhombic lip cells, as shown by *in situ* hybridization against *atonal1a* and immunohistochemistry for GFP (done by Martin Distel, **Appendix 3: Figure 2**). Thus the mosaicism is dependent on the reporter strain used: TG5xR or 4xUAS:GFP, allowing the analysis of single cells or whole populations respectively.

The strain was able to transactivate various UAS reporter constructs that were injected transiently into *atoh1a:KalTA4* carriers at the 1 cell stage (done by Martin Distel) allowing one to address molecular and cellular mechanisms of neuronal migration in a cell population specific manner. Thus it was used in a study that investigated the migration and axonogenesis of early URL-derived cells on a subcellular level. Moreover the behavior of the centrosome during migration and axon outgrowth could be visualized in detail. Here we could show that the centrosome does not permanently stay ahead of the nucleus but is overtaken by the nucleus. Furthermore our *in vivo* time-lapse analysis revealed that the position of the centrosome does not determine the site of axon outgrowth (Distel et al., 2010, see **Appendix 3**).

## **Conclusion**

I have generated and initially characterized a stable transgenic zebrafish strain that drives KalTA4-mediated transgene expression under control of the *atoh1a* enhancer in the cells of the rhombic lip. This strain has already proven a powerful tool to obtain novel insights into the role of the centrosome in early URL-derived precursors during migration and axonogenesis. My *atoh1a:KalTA4* strain now can be used to elucidate the role of guidance molecules during the migration and differentiation of early URL-derived populations *in vivo*.

## **3.4 Characterization of the GFP-expressing cell population in the cerebellum of the *gata1:GFP* stable transgenic zebrafish strain**

*Published Article (Volkman et al., 2008) (see Appendix 4)*

### **3.4.1 *gata1:GFP* cells represent the granule cell population of the embryonic, larval and juvenile zebrafish cerebellum (Appendix 4: Figure 1, 2, 3)**

It was recently shown that in embryos of the transgenic *gata1:GFP* 781-strain (Long et al., 1997) (for simplification *gata1:GFP* from hereon) GFP-expressing neuronal precursors migrate from the dorsoposterior region of the cerebellum,

likely the upper rhombic lip, toward and along the midbrain–hindbrain boundary (Köster and Fraser, 2006). The identity of this cerebellar neuronal cell type, however, remained unclear.

To molecularly confirm that GFP-expressing cells in the cerebellum of the *gata1:GFP* zebrafish strain are derived from the rhombic lip, I used zebrafish *atonal1a* (Kim et al., 1997) and *ptf1a* (Zecchin et al., 2004) as marker genes for the rhombic lip and the ventricular zone respectively. With help of *in situ* hybridization for *atonal1a* and *ptf1a* combined with immunohistochemistry for GFP I could clearly show that the granule cells arise from the URL as they express *atonal1a* consistent with what is known from the mouse cerebellum.

The URL is known to produce mainly glutamatergic cell types in mouse whereas the VZ gives rise to GABAergic neurons (Hoshino et al., 2005). The granule cells did not co-express the GABAergic marker gene *GAD65* (data not shown), but they expressed the *vesicular glutamate transporter 1* (*vglut1*) and thus are glutamatergic neurons. This is consistent with an origin from the URL that produces mainly glutamatergic cell types and also with a cerebellar granule cell fate. Interestingly the expression of *vglut1* in contrast to the broader expression of the other homologues *vglut2.1* and *vglut2.2* (data not shown) appeared to be restricted to *gata1:GFP* cells in the cerebellum (Bae et al., 2009).

The mouse cerebellar rhombic lip sequentially generates different migratory neuronal cell types. Granule neurons are the last of the cell types to be produced (Machold and Fishell, 2005; Wang et al., 2005; Wingate, 2005; Wilson and Wingate, 2006). Neuronal migration from the zebrafish rhombic lip is initiated at around 28hpf (Köster and Fraser, 2001). In contrast, GFP-expression and onset of rhombic lip-derived migration in *gata1:GFP* embryos is not observed prior to 48hpf (Köster and Fraser, 2006). This suggests that the *gata1:GFP* population represents a cell type arising late from the zebrafish rhombic lip.

To find out if *gata1:GFP* cells are granule cells we analyzed *gata1:GFP* cells for expression of genes expressed in cerebellar granule cell progenitors in the mouse, namely the transcription factor *neuroD* (3dpf), the adhesion factor *tag1* (3dpf), the transcription factor *pax6* (6dpf) and the extracellular matrix protein *reelin* (6dpf). *In*

*situ* hybridization combined with immunohistochemistry for GFP revealed that these early and late granule cell marker genes are expressed by cerebellar *gata1*:GFP cells. This developmental expression profile suggests an identity for cerebellar *gata1*:GFP cells as granule cell progenitors of the zebrafish cerebellum.

In contrast to the genes mentioned above that are in addition expressed in other cerebellar cell types like deep cerebellar nuclei the GABA<sub>A</sub>Rα6 subunit was found to be expressed exclusively in the granule cells of the mouse and goldfish cerebellum (Aller et al., 2003; Bahn et al., 1996; Fünfschilling and Reichardt, 2002; Jones et al., 1996). In order to find a definite granule cell marker gene in zebrafish we cloned a partial cDNA of the zebrafish homologue of the *gaba<sub>A</sub>Rα6* subunit (which has the conserved arginin residue associated with the special pharmacological features of this subunit). My mRNA expression analysis revealed that *gaba<sub>A</sub>Rα6* subunit-expression in the adult zebrafish cerebellum is confined to the granule cell layer of corpus cerebelli, caudal lobe, eminentia granularis and valvula cerebelli. Thus the exclusive expression in the granule cell layers of all cerebellar compartments identifies *gaba<sub>A</sub>Rα6* as a specific marker gene for cerebellar granule cells. mRNA expression analysis of zebrafish *gaba<sub>A</sub>Rα6* followed by immunohistochemistry against GFP on 1-, 2-, and 4-week old larval and juvenile *gata1*:GFP transgenic brains revealed that expression of *gaba<sub>A</sub>Rα6* was confined to the internal granule cell layer of the zebrafish corpus cerebelli, the granule cell-containing caudal lobe and the eminentia granularis co-localizing with *gata1*:GFP cells (Appendix 4: Supplementary Figure 1).

Taken together, these data identify the GFP-expressing cells in the cerebellum of *gata1*:GFP embryos and larvae as cerebellar granule neurons.

### **3.4.2 *gata1*:GFP cells in the cerebellum represent all cerebellar granule cell populations in teleost fish**

First, we aimed to reveal when layer formation in the cerebellum occurs as layer formation likely represents a developmental period when granule progenitor cells settle in their final location and can be attributed to distinct granule cell populations. We could show with *in vivo* Bodipy Ceramide stainings to label the neuropil of the developing molecular layer that cerebellar layer formation is

initiated between 60hpf and 72hpf. Thus, cerebellar lamination must be well under way after 1 week of zebrafish embryonic development.

To address the final localization of the GFP-expressing embryonic granule cell clusters, *gata1:GFP* larvae at 8dpf and juvenile fish were sectioned, processed for immunohistochemistry against GFP and subsequently counterstained with Bodipy 630/650-X to outline the cellular organization of the cerebellum. In these sagittal and transverse sections *gata1:GFP* cells were found in all granule cell containing cerebellar compartments corpus cerebelli, eminentia granularis, caudal lobe.

Thus *gata1:GFP* cells represent all granule cell subpopulations of the zebrafish cerebellum.

### **3.4.3 The URL of the embryonic zebrafish cerebellum is spatially subdivided and simultaneously gives rise to granule cells of different fate and function (Appendix 4: Figure 4, 5, 6, 7; Movie 6)**

With help of time-lapse movies combined with individual cell tracking we have analyzed the migratory routes of the granule cell subpopulations existing in the zebrafish cerebellum. This analysis revealed that progenitors from the medial rhombic lip form the granule cell population of the corpus cerebelli whereas progenitors from the lateral rhombic lip contribute to the eminentia granularis. Furthermore *in vivo* time-lapse imaging allowed us to visualize the growth of first parallel fibers in the cerebellar anlage. With help of retrograde labeling of parallel fibers in the crista cerebellaris I could further distinguish between the vestibulo- and non-vestibulocerebellum as only parallel fibers of the vestibulocerebellar system (composed of eminentia granularis and caudal lobe), but not of the corpus cerebelli, project into the crista cerebellaris (see **Figure 18** for summary).

These retrograde labeling experiments were performed by microinjection of the lipophilic dye Dil as well as rhodamine dextran into the putative target area of the axons. The use of rhodamine dextran for retrograde labeling in living zebrafish larvae is described in detail in **Appendix 5** (Volkman and Köster, 2007).

Based on our tracing of individual granule cell progenitors, the embryonic zebrafish rhombic lip is spatially patterned, with the lateral upper rhombic lip generating granule cells of the vestibulocerebellum, while granule cells of the

zebrafish non-vestibulocerebellar system originate from the medial upper rhombic lip.

#### **3.4.4 Migration of cerebellar granule cell precursors continues at larval and juvenile stages and the regionalization of the URL is maintained (Appendix 4: Figure1, Movie 7 and Movie 8)**

In my time course histological analysis a massive growth of the cerebellar granule cell layer could be observed. This observation poses the question how the granule cell population of the maturing cerebellum grows – by divisions of proliferative precursors inside the IGL or by supply of granule cells from outside the IGL? With help of staining for the mitosis marker PH3 the *gata1:GFP* cells were found to proliferate at a low rate close to the URL, but never in their target region inside the granule cell layer of the eminentia granularis or the corpus cerebelli. Moreover most of the *gata1:GFP* cells that left the URL region expressed the postmitotic neuronal marker gene *HuC/D*.

Time-lapse movies at larval stages between 4 to 5hpf (**Movie 7**) and 6 to 7hpf (**Movie 8**) revealed the continued migration of granule cell precursors from the URL into the growing eminentia granularis and corpus cerebelli. Furthermore single cell tracking showed that the subdomains of the URL are maintained in the larva. Continued migration could also be observed in sections of juvenile cerebellum granule cells descending from the posterior molecular layer into the granule cell layer. This observation is consistent with proliferation found in the adult cerebellum in other studies (Grandel et al., 2006; Kaslin et al., 2009; Zupanc et al., 2005).

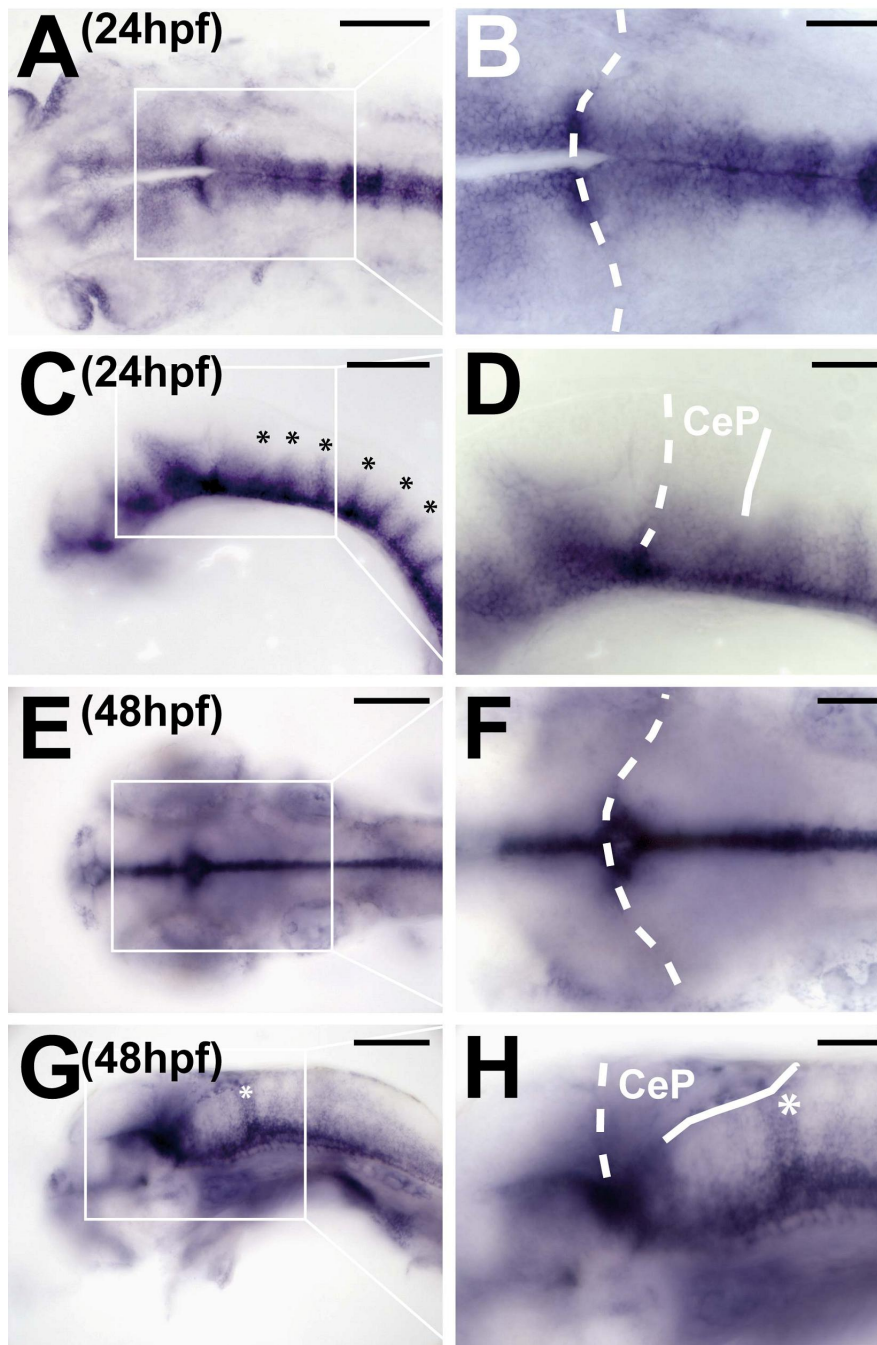
#### **Conclusion**

After the generation of tegmental hindbrain nuclei the zebrafish URL gives rise to cerebellar granule cells. Granule cells of the eminentia granularis arise from the lateral URL whereas granule cells of the corpus cerebelli have their origin in the medial URL. Thus the URL is spatially subdivided in producing the granule cell subpopulations of the vestibulo- and non-vestibulocerebellum. Migration of granule cell precursors from the URL and the spatial subdomains are maintained at larval stages.

### 3.5 Zebrafish Netrin-1 and its receptors in URL-derived precursor populations

#### 3.5.1 The guidance molecules zebrafish *netrin-1a* and *netrin-1b* are expressed at embryonic stages when migration from the URL occurs

Netrin-1 is known to have a role in axon guidance and neuronal migration (see chapter 1.7). To evaluate Netrin-1 as a potential guidance molecule for migrating neuronal precursors or outgrowing cerebellar axons I analyzed the mRNA expression in the zebrafish embryo. *In situ* hybridization revealed that at 24hpf and 48hpf both zebrafish homologues of *netrin-1* – *netrin-1a* (Figure 9A-H) and *netrin-1b* (Figure 9I-P) are expressed by cells of the floorplate reaching from the mesencephalon to the posterior hindbrain. Note the dorsally extending stripes of *netrin-1a*-expression in each hindbrain rhombomere at 24hpf (Figure 9C, asterisks). All these stripes except one (Figure 9G, H, asterisk) have diminished at 48hpf. Both *netrin-1* homologues show a similar expression pattern. Interestingly *netrin-1a* and *netrin-1b*-expression could still be detected in the floorplate of the adult zebrafish brain (data not shown). Thus the ligand Netrin-1 is present during the phase of neuronal migration directly ventral to the embryonic zebrafish cerebellar anlage.





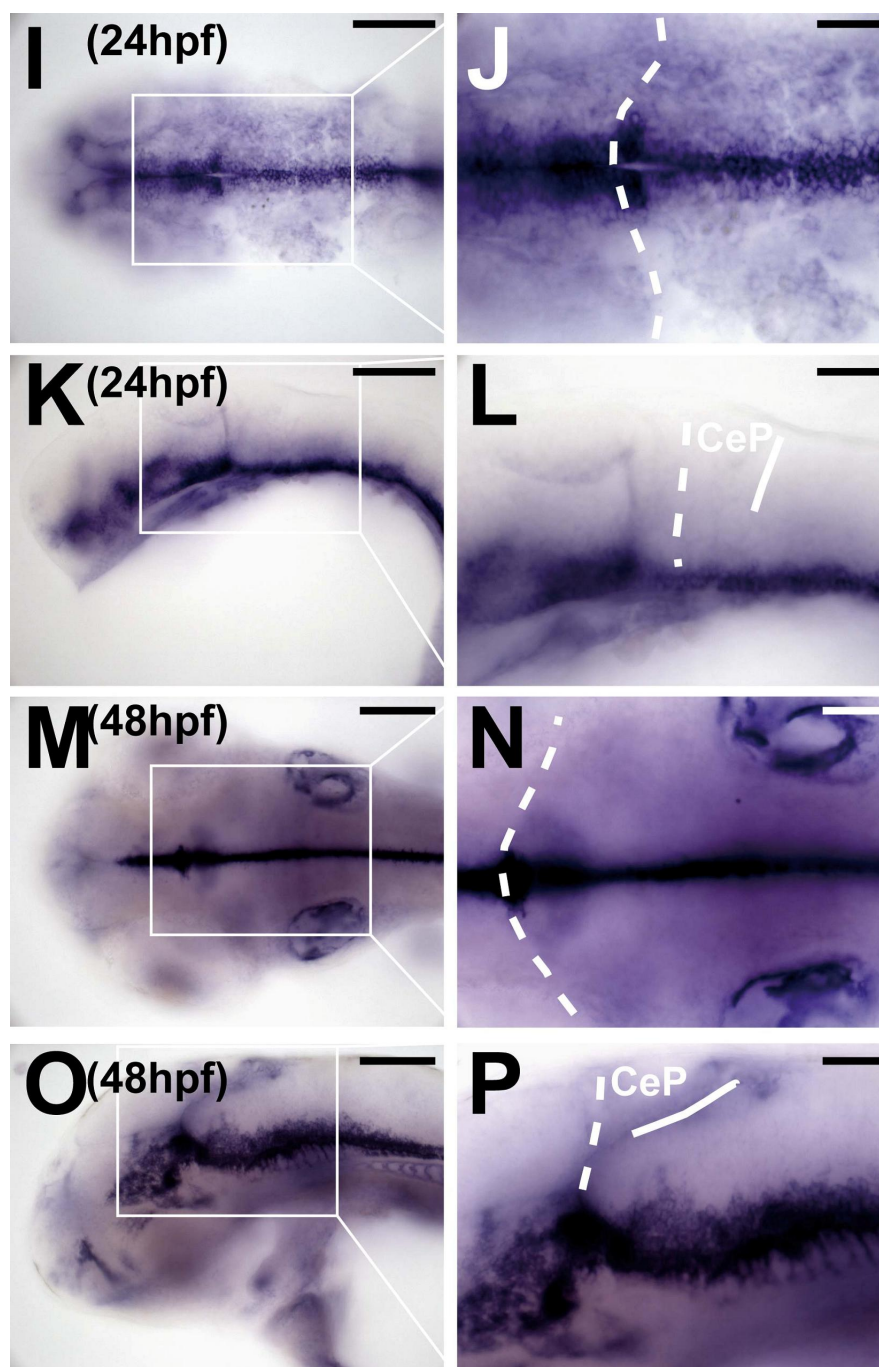


**Figure 9: Expression of *netrin-1a* and *netrin-1b* in the zebrafish embryonic brain.**

*In situ* hybridization for zebrafish *netrin-1a* (A-H) and *netrin-1b* (I-P) at 24hpf (A-D, I-L) and 48hpf (E-H, M-P). Dorsal (A, B, E, F, I, J, M, N) and lateral (C, D, G, H, K, L, O, P) views of whole mount embryos are shown. Asterisks in C, G and H mark dorsally extending stripes of *netrin-1a*-expression associated with hindbrain rhombomeres. The URL is indicated by a dashed line and the MHB by a solid line. *netrin-1a* and *netrin-1b* are expressed along the ventral neural tube in the floorplate. This expression domain extends from the mesencephalic tegmentum to the posterior hindbrain. *netrin-1a* and *netrin-1b* are similarly expressed. Scale bars = 50 $\mu$ m in A, C, E, G, I, K, M, O; 20 $\mu$ m in B, D, F, H, J, L, N, P.

**Abbr.:** CeP, cerebellar plate.

### 3.5.2 *dcc*-expression in the embryonic zebrafish cerebellum is confined to regions of neuronal migration

To evaluate Dcc as a candidate guidance receptor for neuronal migration in the developing zebrafish cerebellum it needed to be clarified if *dcc* is expressed in regions where migration of cerebellar neuronal precursors occurs (Köster and Fraser, 2001a). For expression analysis a partial cDNA of zebrafish *dcc* was used to synthesize Dig labeled RNA probes (Hjorth et al., 2001). The *in situ* hybridization staining revealed *dcc*-expression in the anterior part of the rhombomere 1 adjacent to the MHB starting from 24hpf (Figure 10A-G). As development progresses the expression domain appears to extend dorsally (Figure 10C, E). A transversal section (Figure 10H) shows that the expression domain at 24hpf in both halves of rhombomere 1 spread continuously from dorsal to ventral but is excluded from the proliferative zones along the ventricle and the dorsal cerebellar plate including the pial surface. Furthermore the transverse section of triple *in situ* hybridization for *dcc* receptor and *netrin-1a/1b* ligand at 24hpf (Figure 11A) reveals the *dcc*-expression domain along the migration path of early URL-derived precursors with the ligand expressed ventral in the target regions where the precursors finally settle.

The medial expression of *dcc* in rhombomere 1 diminishes after 40hpf and at 48hpf the expression domain is restricted to the surface of the cerebellar plate along the migration path of granule cell precursor cells (data not shown). At 4 and 7dpf *dcc*-expression can be found in the posterior cerebellum in the region of the URL (data not shown). Thus the expression of zebrafish *dcc* in the zebrafish cerebellum at embryonic and larval stages is highly dynamic and spatially and temporarily tightly regulated. Strikingly *dcc*-expression is observed in regions of neuronal migration in the embryonic cerebellum during the main events of migration from the URL between 1dpf to 3dpf.

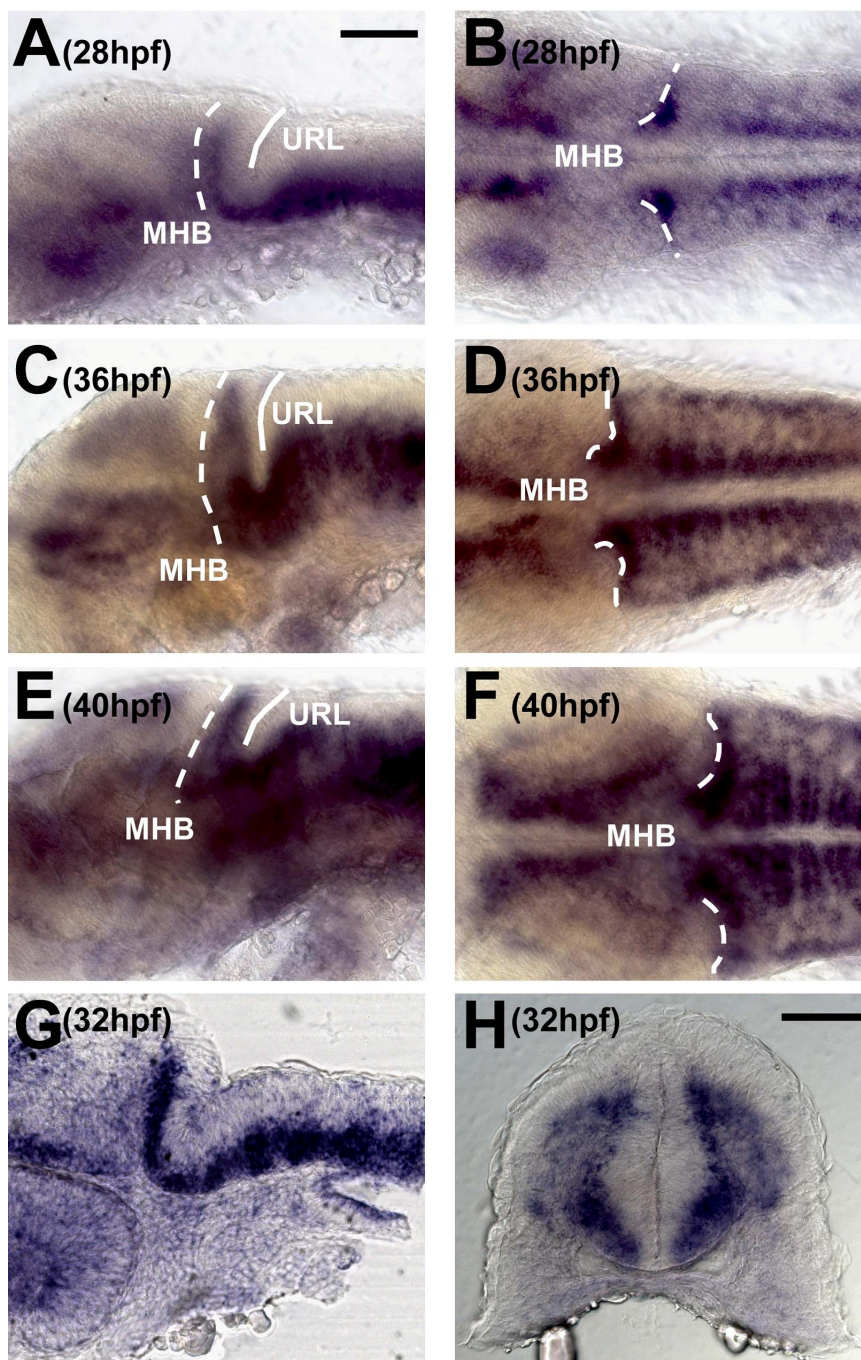


**Figure 10: Expression of the Netrin-1 receptor *dcc* in the developing zebrafish cerebellum.**

*In situ* hybridization for zebrafish *dcc* at 28hpf (A, B), 36hpf (C, D), 40hpf (E, F) and 32hpf (G, H). Lateral (A, C, E) and dorsal (B, D, F) views of whole mount embryos or sagittal (G) and transverse (H) sections of embryonic brains are shown. Panel (G) shows a sagittal section of a 32hpf embryo, at this stage *dcc* is expressed in the anterior part of the cerebellum along the MHB, the URL zone shows no *dcc*-expression. (H) shows a transverse section through the cerebellum of an embryo of the same age. The expression domain of *dcc* is extending from dorsal to ventral in each lobe of rhombomere 1. Scale bars = 50 $\mu$ m in A (applies to A-G), H.

**Abbr.:** MHB, midbrain-hindbrain boundary; URL, upper rhombic lip.

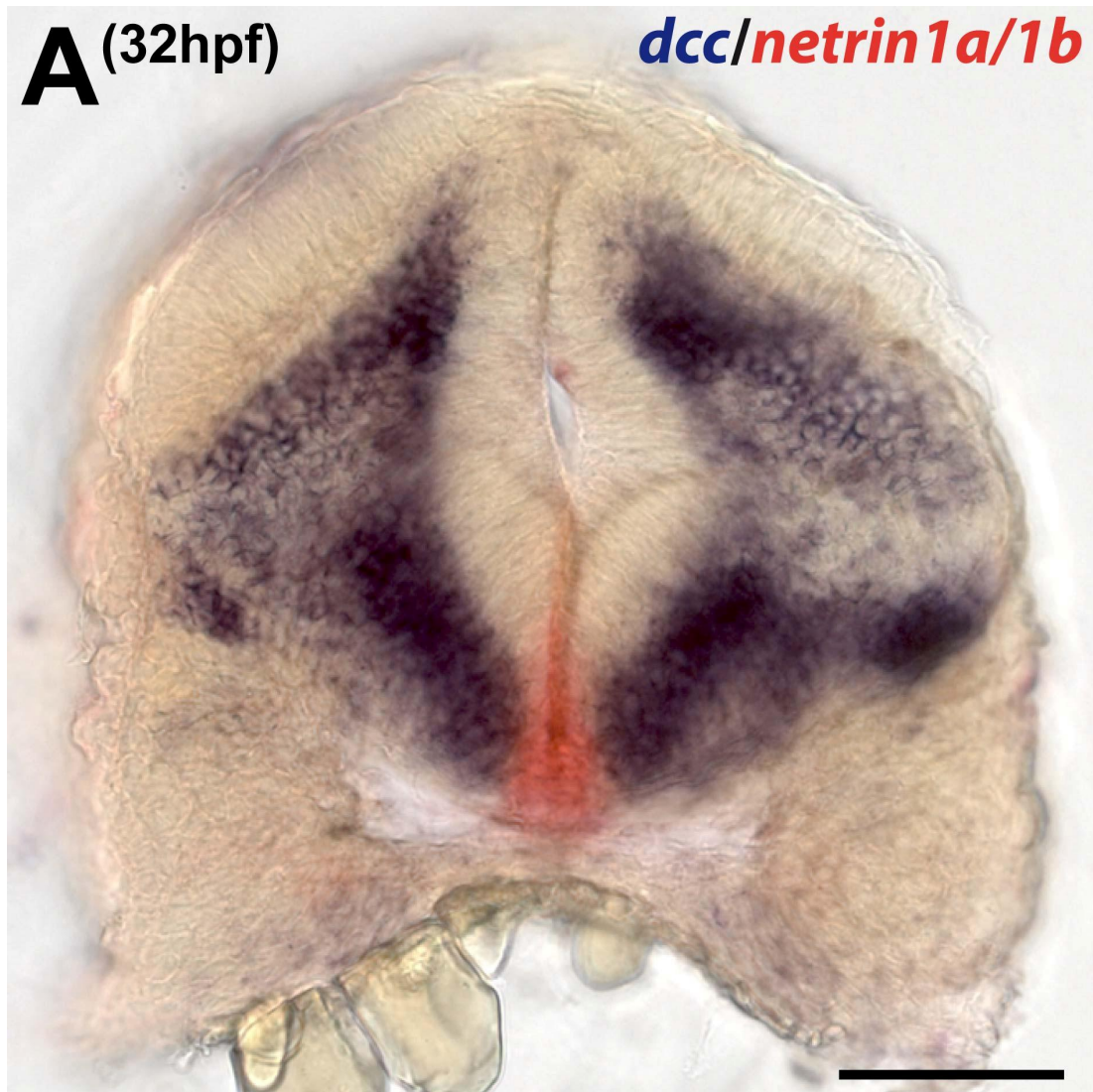


**Figure 11: Expression of *dcc* and *netrin-1a/1b* in rhombomere 1.**

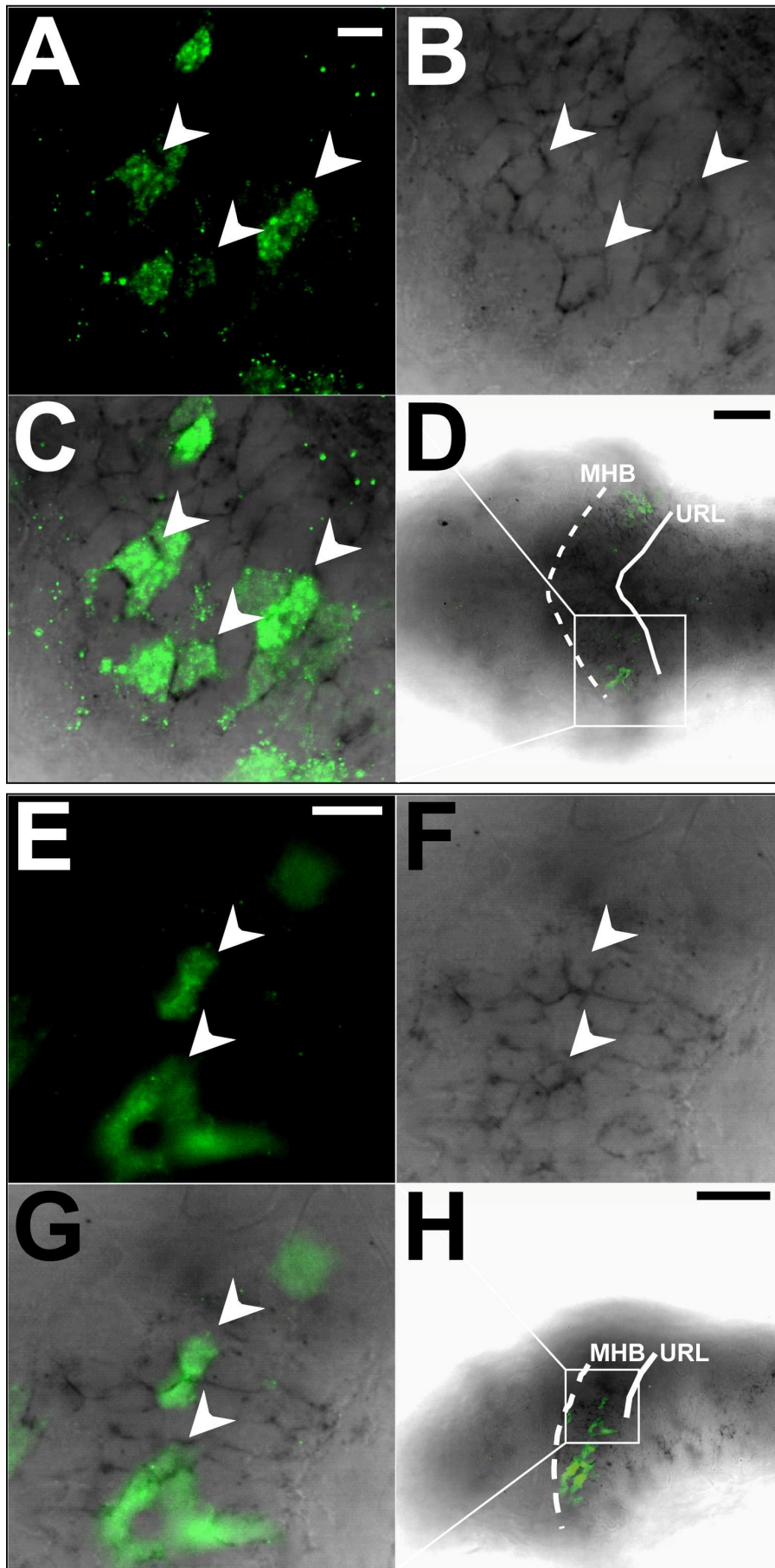
Transverse section through the cerebellar plate of a 32hpf embryo after triple *in situ* hybridization with probes against *netrin-1a* and *netrin-1b* (red) and *dcc* (blue). The expression domain of *dcc* is extending from dorsal to ventral, whereas *netrin-1a/1b* is expressed in the floor plate. Scale bar = 50 $\mu$ m in A.

### 3.5.3 The Netrin-1 receptor *dcc* is expressed in URL-derived precursors in zebrafish

To find out whether URL-derived cells express the Netrin-1 receptor *dcc* double *in situ* hybridization against *dcc* and the URL marker gene *atona1a* was performed. Interestingly the expression domains were overlapping indicating that *dcc* is expressed in neuronal precursors born in the URL (data not shown).

### 3.5.4 The Netrin-1 receptor *dcc* is expressed in migrating cerebellar granule cell precursors

Previously I could show that the GFP-expressing cells in the cerebellum of *gata1:GFP* transgenic strain represent the granule cell population of the zebrafish cerebellum (chapter 3.4; **Appendix 4**). To find out if Netrin-1/Dcc could be involved in the migration of the granule cell precursors *in situ* hybridization for *dcc* was performed on *gata1:GFP* embryos followed by immunohistochemistry against GFP. Interestingly this double staining revealed *dcc*-expression in all migratory granule cell subpopulations (Figure 12A-H). The dorsal view reveals expression in granule cell precursors migrating towards the MHB (Figure 12A-D) whereas lateral views show the *dcc*-expression in granule cell precursors migrating ventrally to form the granule cell layer of the eminentia granularis (Figure 12E-H). In a transverse view it becomes obvious that *dcc*-expression is confined to the cerebellar surface along the migration route of the granule cell precursors during tangential migration, at time points when this migration step takes place (Figure 12I-L). This specific expression pattern localized to cerebellar granule cells suggests a role of Dcc-mediated signaling in granule cell migration.



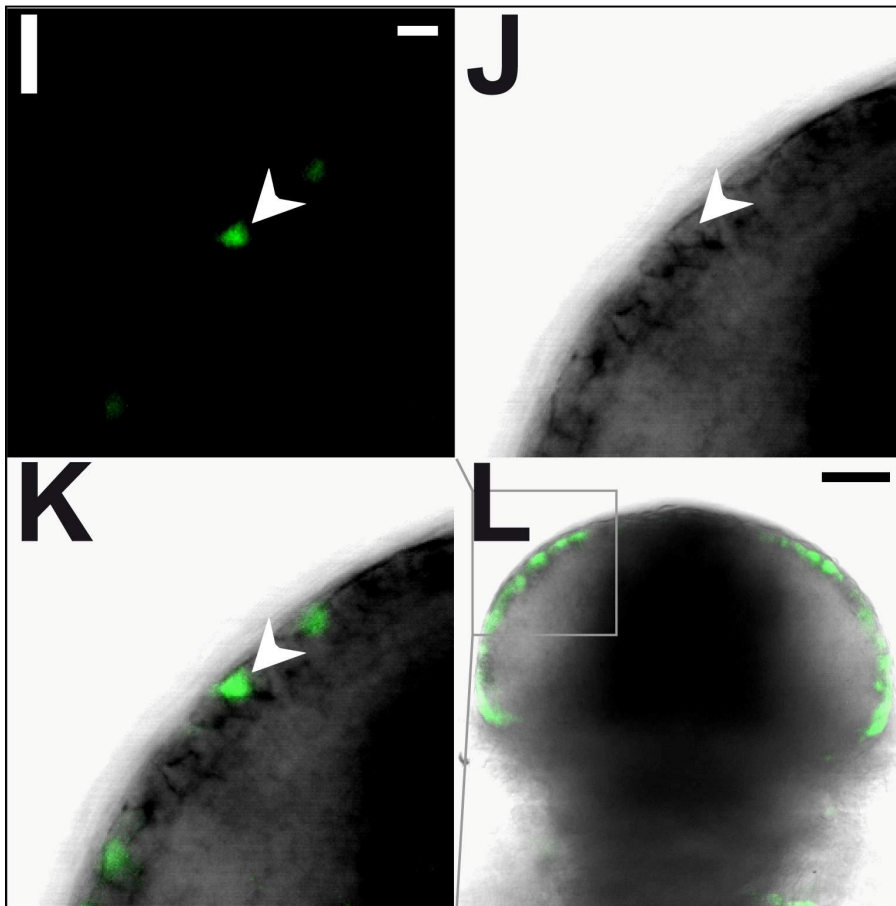


**Figure 12: *dcc*-expression in cerebellar granule cells.**

Dorsal (D), lateral (H) and transverse view (L) of cerebellar plate at 54hpf or magnification of boxed area showing a single optical section recorded by confocal microscopy (A–C, E–G, I–K). Embryos were analyzed by immunohistochemistry for GFP protein and by *in situ* hybridization for zebrafish *dcc* mRNA expression. Most GFP-expressing cells in the dorsal and lateral view (white arrowheads) are co-expressing *dcc* (B, C, F, G). (I–L) The transverse view reveals *dcc*-expression directly under the surface of the cerebellar plate the position of the GFP-expressing cells with many cells showing co-expression of *dcc* and GFP (white arrowhead). Scale bars = 10 $\mu$ m in A (applies to A–C), E (applies to E–G), I (applies to I–K); 50 $\mu$ m in D, H, L.

**Abbr.:** MHB, midbrain-hindbrain boundary; URL, upper rhombic lip.

### 3.5.5 Cloning of a partial cDNA of zebrafish *unc5c*

Besides Dcc the guidance molecule Netrin-1 is known to bind to two additional receptors in zebrafish and mouse: Neogenin and Unc5c (see chapter 1.7). Neogenin-expression in the zebrafish embryonic rhombencephalon is broad and not linked to neuronal migration (Shen et al., 2002). Unc5c though has been shown to be involved in mouse cerebellar development (Ackerman et al., 1997;

Eisenman and Brothers, 1998; Lane et al., 1992; Przyborski et al., 1998). To find out if *unc5c* is expressed in the embryonic zebrafish cerebellum a partial zebrafish *unc5c* cDNA was amplified by RT-PCR from cDNA at 35hpf. The fragment was sequenced completely and the sequence comparison revealed a high similarity to *unc5c* of other vertebrate species. Thus I have successfully isolated a 491bp fragment of zebrafish *unc5c*. After subcloning this partial *unc5c* cDNA was used for expression analysis.

### **3.5.6 The Netrin-1 receptor zebrafish *unc5c* is expressed in the embryonic cerebellum and hindbrain**

To find out whether *unc5c* is expressed in the developing zebrafish cerebellar plate during phases of neuronal migration the partial *unc5c* cDNA was used for probe synthesis and *in situ* hybridization.

The mRNA of zebrafish *unc5c* can be first detected in the brain at 36hpf. At 48hpf *unc5c*-expression can be observed in the hindbrain and the cerebellum (Figure 13A, C). The cerebellar expression appears patchy and spreads on the surface between URL and MHB (Figure 13B, D). At larval stages of 4dpf and 7dpf weak *unc5c*-expression can be observed at the posterior rim and the dorsal midline of the cerebellum (data not shown).

Thus the expression analysis revealed that zebrafish *unc5c* is indeed expressed in the cerebellar plate during the migration of URL-derived precursors.



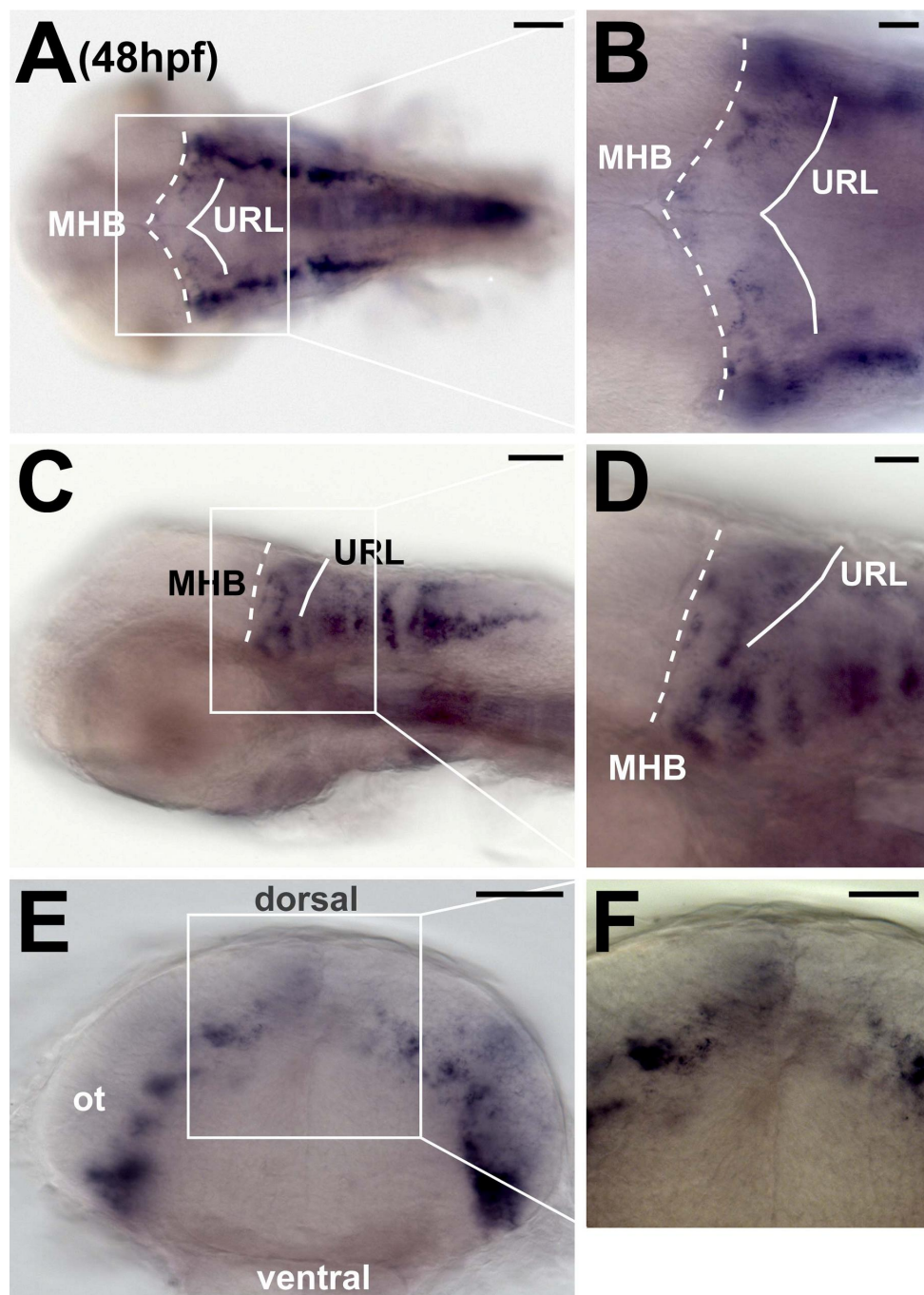


**Figure 13: Expression of the Netrin-1 receptor *unc5c* in the developing zebrafish cerebellum.**

*In situ* hybridization for zebrafish *unc5c* on 48hpf embryos. Dorsal (A, B), lateral (C, D) and transverse (E, F) views are shown. At this stage *unc5c* is expressed in the hindbrain and the dorsal cerebellum between the MHB and the URL zone. A higher magnification of the cerebellum is shown in (B) and (D) revealing the patchy expression of *unc5c*. (E, F) shows a transverse section through the cerebellum with *unc5c* expressed in groups of cells close to the surface of the cerebellar plate (note that the optic tectum is partially included in this section). Scale bars = 50 $\mu$ m in A, C, E; 20 $\mu$ m in B, D, F.

**Abbr.:** MHB, midbrain-hindbrain boundary; ot, optic tectum; URL, upper rhombic lip.

### 3.5.7 The Netrin-1 receptor *unc5c* is expressed in migrating cerebellar granule cell precursors

The Netrin-1 transmembrane receptors Dcc and Unc5c can form homodimers as well as heterodimers upon Netrin-1 binding resulting in attraction or repulsion (Hong et al., 1999). Thus it was of interest to know for Dcc knockdown and over-expression experiments whether *dcc* and *unc5c* are co-expressed in cerebellar neuronal precursors. To find out if the latter Netrin-1 receptor is expressed in migrating granule cell precursors in the zebrafish cerebellum, *in situ* hybridization for *unc5c* was performed on *gata1:GFP* embryos followed by immunohistochemistry against GFP.

Nearly all GFP-positive cells in the cerebellar plate showed *unc5c*-expression (Figure 14). The dorsal view shows *unc5c*-expression in granule cell precursors migrating towards the MHB (Figure 14A-D). In a lateral view *unc5c*-expression in granule cell precursors migrating ventrally to form the granule cell layer of the eminentia granularis is visible (Figure 14E-H). Thus *unc5c* seems to be expressed at the cerebellar surface along the tangential migration route of the granule cell precursors. This suggests a role of Unc5c-mediated Netrin-1 signaling in the development of all migratory granule cell subpopulations. Moreover both Netrin-1 receptors Dcc and Unc5c are expressed in the granule cell precursor population at the same stage.

### Conclusion

My expression analysis revealed that the guidance factor Netrin-1 is expressed in the target region of migratory URL-derived precursors ventral to the cerebellar anlage. Whereas the Netrin-1 receptor Dcc is expressed in early URL-derived precursors and the migratory subpopulations of cerebellar granule cells. Furthermore I have for the first time isolated a partial cDNA for the Netrin-1 receptor *unc5c*. Interestingly I found *unc5c* to be expressed by the migrating granule cell precursor subpopulations. The expression of the ligand in the target region and the receptors in neuronal precursors migrating towards this region suggests a role of Dcc/Unc5c-mediated Netrin-1 signaling in the guidance of URL-derived populations during ventral migration.

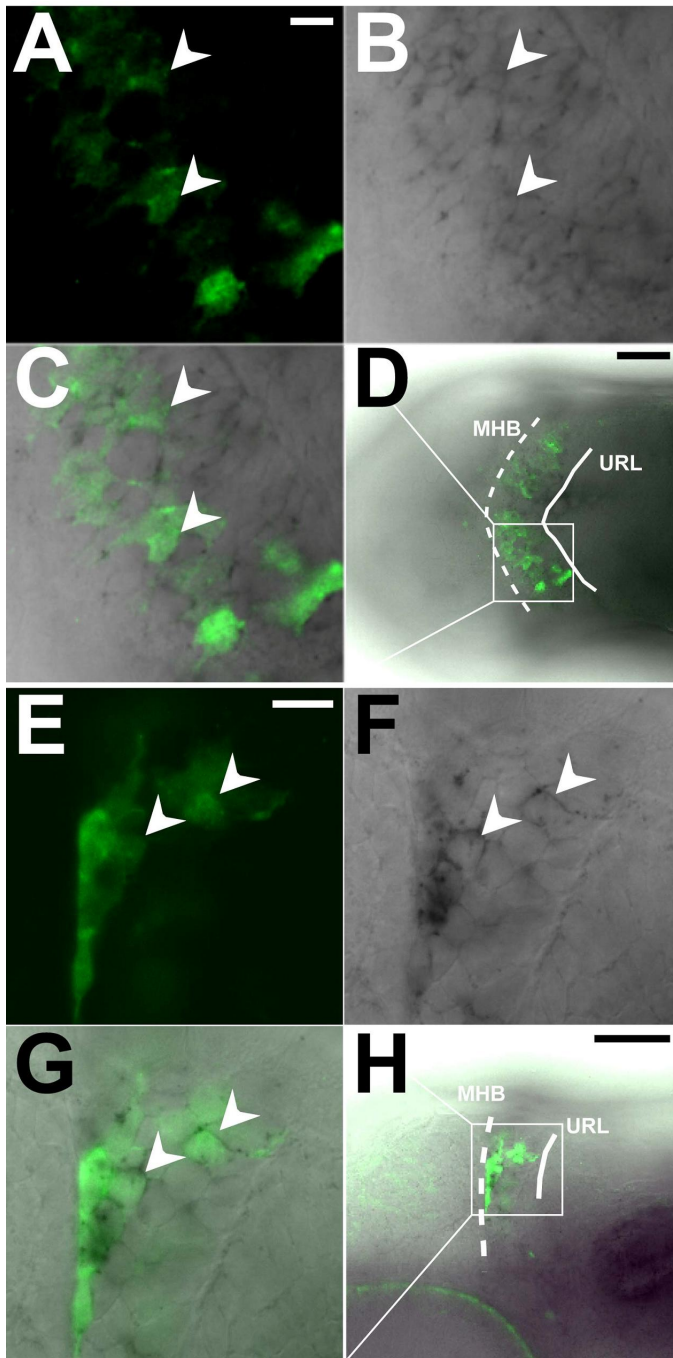


**Figure 14: *unc5c*-expression in cerebellar granule cells.**

Dorsal (D) and lateral (H) of cerebellar plate at 54hpf or magnification of boxed area showing a single optical section recorded by confocal microscopy (A–C, E–G). Embryos were analyzed by immunohistochemistry for GFP protein and by *in situ* hybridization for zebrafish *unc5c* mRNA expression. Many GFP-expressing cells in the dorsal and lateral (white arrowheads) are co-expressing *unc5c* (B–C, F–G). Scale bars = 10 $\mu$ m in A (applies to A–C), E (applies to E–G); 50 $\mu$ m in D, H.

**Abbr.:** MHB, midbrain-hindbrain boundary; ot, optic tectum; URL, upper rhombic lip.

### 3.5.8 Cloning of full length zebrafish *dcc*

Chi-Bin Chien and colleagues recently published the full length sequence of the *dcc* homologue in zebrafish (Fricke and Chien, 2005). However there was no full length cDNA available. Thus I aimed to clone full length *dcc* from 35hpf whole embryo cDNA with primers designed against the known sequence and flanked by additional restriction sites. I successfully amplified three fragments flanked by restriction sites that were subsequently subcloned to assemble the fragments to a full length cDNA. The complete cDNA was sequenced and the obtained result was compared with the sequence published previously. Surprisingly the sequence analysis revealed an additional insert of 66bps. Comparison with Dcc homologues of other vertebrate species (human, mouse, rat, *Xenopus*) revealed that length and position of this fragment was highly conserved among these species whereas the base pair and amino acid sequence showed low conservation (Figure 15A). Interestingly the *Xenopus* Dcc homologue also lacks these base pairs. Thus the previously published sequence might represent an alternative splicing variant of *dcc* in zebrafish. Alternatively a polymorphism of the *dcc* gene locus in the zebrafish population might have resulted in the isolation of different cDNAs. To generate a dominant negative variant of the zebrafish Dcc receptor another primer was used to amplify a truncated variant of *dcc* lacking the intracellular domain, known to mediate Netrin-1 signaling (Stein et al., 2001) (Figure 15B). This cDNA was also completely sequenced to confirm correctness of the sequence. Thus I have successfully cloned a full length and a dominant negative variant of zebrafish Dcc.

**A**

	(800)	800	810	820	830	840	850	860
zf DCC chien (795)		FNNAGEGVPLYESAVTRSM	TD	-----	-----	-----	SSSAPMI	PPVGVQAVALTSDSVRV
zf DCC new (226)		FNNAGEGVPLYESAVTRSM	TD	DFSDPSDDDLFHLFDNVATAAP	SSSAPMI	PPVGVQAVALTSDSVRV		
human DCC (799)		FNNAGEGVPLYESATTRSI	TD	PTDPVD	--	YYPLLDDFPTSVPDI	-	STPMLPPVGVQAVALTHDAVRV
mouse DCC (799)		FNNAGEGVPLYESATTRSI	TD	PTDPVD	--	YYPLLDDFPTS	GPDV	-
rat DCC (799)		FNNAGEGVPLYESATTRSI	TD	PTDPVD	--	YYPLLDDFPTS	GPDV	-
xenopus DCC (799)		FNNAGEGVPLYESATTRSI	QIVP	-----	-----	DM	-	STPMLPPVGVQAVALTHDAVRV
Consensus (800)		FNNAGEGVPLYESATTRSI	TD	PTDPVD		YYPLLDDFPTS	GPDV	STPMLPPVGVQAVALTHDAVRV

**B**

	(1089)	1089	1100	1110	1120	1130	1140	1150
ratDcc fl(1085)		PPHGSVTPQKNSNLLVITVVT	VGVLTVLVVIVAVICTRRS	SAQQRKKRATHSASKRKG	SQKDI			
ratDcc dn(1085)		PPHGSVTPQKNSNLLVITVVT	VGVLTVLVVIVAVICTRRS	-----	-----	-----	-----	-----
zfDcc fl(1084)		PPHGSVTPQKNSNLLVITVVT	VGAVTVVVVLI	VALICTRRS	SAQQRKKRATHSAGK	KRKG	SQKDI	
zfDcc dn(1084)		PPHGSVTPQKNSNLLVITVVT	VGAVTVVVVLI	VALICTRRS	-----	-----	-----	-----
Consensus(1089)		PPHGSVTPQKNSNLLVITVVT	VGVLTVLVVLI	VALICTRRSSA	QQRKKRATHSA	KRKG	SQKDI	

**Figure 15: Dcc amino acid sequence alignments.**

(A) Partial amino acid sequence comparison of published zebrafish Dcc (Fricke and Chien, 2005) (zf Dcc chien), human Dcc, mouse Dcc, rat Dcc and *Xenopus* Dcc showing additional 22 AAs in the isolated sequence aligned with the corresponding region of the other vertebrate species. At the same position in the protein the mammalian proteins have additional 19 AAs while there is a gap in the Dcc sequence of (Fricke and Chien, 2005) and *Xenopus* Dcc.

(B) Partial amino acid sequence alignment of zebrafish and rat Dcc showing the published full length (fl) and dominant negative (dn) truncated rat Dcc protein lacking the cytoplasmic domain (Hong et al., 1999) and the full length amino acid sequence of zebrafish Dcc with the truncated variant designed accordingly.

### 3.5.9 Bicistronic expression constructs for driving simultaneous expression of Dcc and the red-fluorescent Cherry protein

To achieve expression in a specific cell population the full length as well as the dominant negative Dcc variant were subcloned into a bicistronic expression vector (Figure 16A) that was supposed to allow expression of two transgenes simultaneously in the same cell. In these constructs expression of Dcc and the red-fluorescent reporter protein Cherry is under control of UAS sites and a basal E1b promoter. To increase the export out of the nucleus by targeting the mRNA to the splicing machinery of the cell the sequence of the globin intron (GI) was added (Distel et al., 2009). For high integration efficiency in transient transgene experiments the expression construct was flanked with Tol2 transposase recognition sites (Kawakami et al., 2004) (Figure 16A, B).

I used the stable transgenic *wnt1*-GVP-UG zebrafish strain to test the constructs (see chapter 3.1 for description). Microinjection of plasmids containing the expression constructs together with Tol2 transposase coding mRNA into the one cell stage of *wnt1*-GVP-UG zygotes resulted in a broad mosaic expression of Cherry protein in rhombomere 1 (and other brain regions with *wnt1*-GVP-UG-expression e.g. the optic tectum). However, *in situ* hybridization against the *dcc* mRNA revealed only sparse ectopic expression of *dcc*. As it was shown that both transgenic proteins in similar designed bicistronic expression cassettes are expressed equally ((Köster and Fraser, 2001a) see also **Appendix 3**) this could be explained by the fact that the *wnt1* enhancer/promotor is only active in the rhombic lip proliferation zone of the cerebellum. Thus most neuronal precursors switch of

*wnt1/gal4-VP16/gfp/dcc* mRNA expression when they leave the rhombic lip. The transgenic *dcc* mRNA expression is thus supposed to be restricted to the endogenous *wnt1* expression domain and not maintained in migrating precursors. In contrast due to high protein stability the GFP and Cherry protein is maintained during migration and subsequent terminal differentiation. Thus to find out whether Cherry and Dcc protein expression correlates the presence of the recombinant Dcc protein itself has to be addressed, by immunohistochemistry for Dcc or epitope tagging of the recombinant Dcc protein.

To achieve high expression levels of transgenic Dcc or any other candidate guidance receptor during migration and terminal differentiation expression needs to be controlled by an enhancer that is active throughout migration in neuronal precursors of the cerebellum.

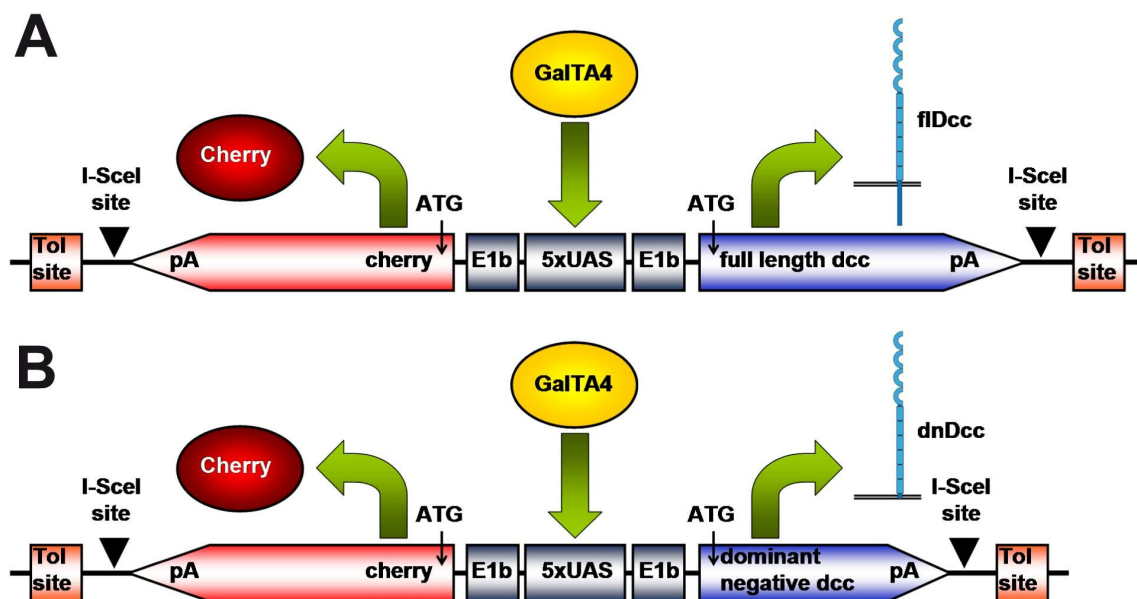


**Figure 16: Bicistronic Dcc expression constructs.**

Schematic drawing of full length (A) and dominant negative (B) Dcc expression cassettes depicting the basal promoter (E1b), the upstream activating sequence (UAS), the polyadenylation site (pA), the transcription factors GalTA4 (GalTA4), translation start (ATG), red fluorescent protein (Cherry) and the flanking restriction enzyme I-SceI sites (I-SceI) as well as the Tol transposase recognition sites (Tol site).

### 3.5.10 Injection of antisense MOs against *netrin-1a*, *netrin-1b* and *dcc*

To knockdown Dcc-expression in the embryo I have used translation blocking antisense morpholinos against *dcc*, *netrin-1a* and *netrin-1b* with the sequences published previously (Suli et al., 2006). The morpholinos were injected at a concentration of 4ng/nl into the one cell stage of the *wnt1-GVP-UG*, *atoh1a:KalTA4* and *gata1:GFP* transgenic strains. To analyze the overall migratory behavior of the neuronal precursors stacks of the morphant cerebelli were recorded to compare the position at the endpoint of migration with control embryos. Furthermore to reveal changes in migration dynamics or altered migration paths time-lapse movies were recorded. Both approaches revealed that the migration of the different neuronal precursor populations in these transgenic strains was not affected. The migration appeared normal in cerebellar granule cell precursors, the precursors of the neurons forming the tegmental hindbrain nuclei, and *atoh1a*-expressing precursors arising from the URL in general. Interestingly at 4dpf in *netrin-1a/1b* but not *dcc* morpholino injected larvae a reduction in granule cell number in the corpus cerebelli could be observed but normal positioning and number of eminentia granularis cells.

### Conclusion

Netrin-1 signaling appears not to be involved in the regulation of neuronal migration from the URL in zebrafish embryos. However the reduction of the eminentia granularis population in *netrin-1a/1b* but not *dcc* morpholino injections hints on a possible role in survival of cerebellar granule cell precursors. I have cloned a complete cDNA for zebrafish *dcc* as well as a dominant negative variant that now can be used for future gain and loss of function studies. After further validation my bicistronic expression Dcc/Cherry constructs can be used together with appropriate transgenic activator strains to dissect Dcc function in URL-derived populations.

### 3.6 TEM study of *parkin* knockdown zebrafish embryos

#### ***Published Article (Flinn et al., 2009) (see Appendix 6)***

The lab of Oliver Bandmann found that in zebrafish embryos the knockdown of *parkin* function with antisense morpholinos resulted in loss of dopaminergic neurons in the posterior tuberculum a structure that is homologous to the substantia nigra of humans. Moreover the *parkin* knockdown embryos show a specific reduction in the activity of the mitochondrial respiratory chain complex I. My TEM analysis of fast muscle cells in the somites of the trunk of control and *parkin* morpholino injected larvae revealed that mitochondria morphology and number was not affected. The mitochondrial cristae had a normal and shape and structure. Furthermore the tissue showed no sign of muscle necrosis as myofibrils and sarcoplasmic reticulum appeared normal. Surprisingly I found an increase in electron-dense material in the transverse (t)-tubules within the muscle tissue of *parkin* knockdown zebrafish larvae compared to control larvae.

#### **Conclusion**

The knockdown of *parkin* mRNA resulted in an impaired mitochondrial function but normal mitochondrial morphology and number in the fast muscle cells of the trunk. Surprisingly the *parkin* knockdown embryos displayed a novel phenotype affecting the t-tubules in the muscle tissue of the trunk.



## 4 Discussion

To validate the teleost fish zebrafish as a model system for the development of the vertebrate CNS it is of great interest to investigate the grade of conservation compared to the development of mammalian model organisms like the mouse. This aim includes facing the challenge to identify cell types and brain structures, known and often well described in the brain of adult zebrafish and other teleost fish species in the developing embryonic and larval brain. This identification is complicated by the occurrence of the massive morphological changes and growth processes shaping the brain during maturation. In this study I have focused on the development of URL-derived neuronal populations in zebrafish.

### 4.1 Identification and characterization of tegmental hindbrain nuclei precursor populations

#### 4.1.1 Tegmental hindbrain nuclei of the isthmic region originate in the URL

The expression of *wnt1* in the embryonic zebrafish cerebellum is of transient nature ceasing at 48hpf and being restricted to the pre-migratory cells localized in the URL (Lekven et al., 2003; McFarland et al., 2008). Compared to the high expression levels in the mesencephalic isthmus *wnt1*-expression is low in the cerebellar anlage. Using a *wnt1* promotor/enhancer in combination with Gal4-VP16-mediated GFP-expression, which has an exceptional stability, the migration and differentiation of *wnt1*-expressing progeny can be followed over several days in *wnt1*-GVP-UG transgenic embryos. The expression of GFP in early embryos of this strain represents the endogenous expression of *wnt1* (Matthew Harris personal communication).

In this study, I have analyzed a GFP-expressing migratory cell population in the embryonic cerebellum of the stable transgenic *wnt1*-GVP-UG zebrafish strain. With the help of *in vivo* time-lapse imaging, expression and retrograde axon projection analysis I could identify these cells as the likely precursors of the secondary gustatory/viscerosensory nucleus and the nucleus isthmi and/or the superior reticular nucleus, the zebrafish homologues of the parabrachial and parabigeminal and/or the laterodorsal-pedunculopontine nuclei in mammals.

Recent fate map studies in the mouse reported these hindbrain nuclei to arise in the URL of the cerebellum (Machold and Fishell, 2005; Wang et al., 2005) with the parabrachial nucleus originating from the *wnt1*-expressing URL (Nichols and Bruce, 2006), but the relevance of this studies for anamniotic vertebrates including teleosts remained elusive. Based on my data I found the neurons of the secondary gustatory/viscerosensory nucleus and nucleus isthmi and/or superior reticular nucleus to have their origin in the *wnt1*-expressing URL in zebrafish. Whether the parabigeminal nucleus and/or the laterodorsal-pedunculo-pontine nucleus in mammals also arise from the *wnt1*-expressing cells of the URL as does the nucleus isthmi and/or superior reticular nucleus in zebrafish has to be clarified in future fate map studies in mice.

#### 4.1.2 Migratory behavior of tegmental hindbrain nuclei precursors

Combining transient DNA injection into embryos of the *wnt1*-GVP-UG zebrafish strain with time-lapse imaging and software supported individual cell tracing I have described their migratory behavior in detail, revealing their migration path, migration speed and the persistence of directionality. Consistently the migration speed was similar to the velocity reported for early migrating neuronal cerebellar precursors in our recent study as were the migration routes and the origin of these zebrafish cells in the URL (see **Appendix 2**) (Rieger et al., 2008).

The tegmental hindbrain nuclei precursors migrate between 24hpf and 48hpf from the URL before the onset of granule cell migration at 48hpf. The migration paths of NI/SRN and SGN/SVN and granule cell precursors show similarities - both progenitors migrate towards the MHB and migrate along the MHB into ventral directions. After reaching the MHB immature hindbrain tegmental nuclei neurons turn ventrally and migrate along the MHB into the depth of the neural tube, thereby leaving the cerebellar plate. Eventually these neurons settle in the tegmentum forming bilateral symmetric clusters in the ventral part of rhombomere 1 where they terminally differentiate. In contrast migrating granule neurons take a superficial path directly underneath the surface of the neural tube and either settle mediodorsally in the corpus cerebelli or migrate lateroventrally to form the eminentia granularis (Volkman et al., 2008) (**Appendix 4**). Thus the neuronal populations generated early by the zebrafish URL namely the precursors of the

secondary gustatory/viscerosensory nucleus and nucleus isthmi and/or superior reticular nucleus follow clearly different migration routes than the late arising cerebellar granule cell population.

#### **4.1.3 Tegmental nuclei of rhombomere 1 contain besides cholinergic also glutamatergic subpopulations of neurons**

The mammalian parabrachial nucleus contains several neuronal subpopulations, among them the external medial, ventral lateral and external lateral subnuclei. Cholinergic cells have been observed in the external medial and external lateral subnuclei (Jones and Beaudet, 1987; Ruggiero et al., 1990; Tago et al., 1989). Thus if the neurons in at least the external lateral parabrachial subnucleus of mice are at the same time cholinergic and project to the hypothalamus, they may correspond to the secondary general viscerosensory system in teleosts. The external medial and ventral lateral subnuclei have ascending projections, contributing to tertiary gustatory projections to (the ventroposterior parvicellular nucleus of) the dorsal thalamus (Saper, 2002; Yasui et al., 1989), the relay nucleus to the gustatory opercular/insular cortex speaking for a secondary gustatory, not a general viscerosensory nature. Thus, the teleostean secondary gustatory nucleus represents the homologue of the external medial and ventral lateral subnuclei of the mammalian parabrachial nuclear complex.

With help of ChAT immunohistochemistry I could demonstrate that *wnt1*-expressing progenitors of the secondary gustatory/viscerosensory nucleus and nucleus isthmi and/or superior reticular nucleus that leave the cerebellar rhombic lip acquire a cholinergic fate in the tegmental area of rhombomere 1. In summary, the secondary/viscerosensory (and maybe also the secondary gustatory) nucleus, nucleus isthmi and superior reticular nucleus of the zebrafish brain contain cholinergic neurons as do their mammalian homologues the parabrachial, parabigeminal and laterodorsal-pedunculopontine tegmental nucleus (Jones and Beaudet, 1987; Tago et al., 1989).

*vglut2.1*-expression revealed that some neurons of the tegmental hindbrain nuclei were glutamatergic. This is in good agreement with the idea that the URL

predominantly produces glutamatergic neurons. As well as with the recent finding in rat showing that the mammalian secondary gustatory nucleus area homologue the parabrachial nuclear complex is of a dual composition formed by cholinergic and glutamatergic (*vglut2*-expressing) neurons that are projecting to the ventral tegmental area (Geisler et al., 2007).

Interestingly the cholinergic neurons of the secondary gustatory nucleus in zebrafish and the trout project exclusively to the hypothalamus (Perez et al., 2000). Thus it was suggested for the secondary gustatory nucleus in zebrafish that only a subset of the neurons in the secondary gustatory nucleus are cholinergic whereas another subpopulation within this nucleus might exist that uses a different neurotransmitter and that projects to the preglomerular tertiary gustatory nucleus. The existence of this subpopulation as well as the nature of this neurotransmitter remained unclear however (Clemente et al., 2004). My study suggests that this unidentified neurotransmitter might be glutamate. Whether the glutamatergic neurons project to the preglomerular tertiary gustatory nucleus whereas the cholinergic neurons project to the hypothalamus has to be tested e.g. by a combination of retrograde axonal labeling and immunohistochemistry. A potential correlation between the use of different neurotransmitters in different subpopulations with different projections and even with a different function has to be investigated for the secondary gustatory nucleus.

#### **4.1.4 Expression of adhesion factors in the cells of the NI/SRN and SGN/SVN during distinct differentiation steps**

Software-supported individual cell tracing allowed us to calculate the speed of cell migration of tegmental hindbrain nuclei precursors being similar to the velocity reported for early migrating neuronal precursors in our recent zebrafish study (**Appendix 2**) (Rieger et al., 2008). The neuronal progenitors analyzed in this study also originated in the URL and followed similar migration routes as do the tegmental hindbrain nuclei progenitors. Interestingly we could demonstrate that polysialylation of NCAM is required for their migration along the anteroventral pathway into ventral rhombomere 1, but the identity of these cells remained unclear.

As I could show here that *wnt1*-expressing URL-derived cells express PSA during migration, neuronal progenitors of the secondary gustatory/viscerosensory nucleus

and nucleus isthmi and/or superior reticular tegmental nuclei are among these PSA-dependent migrating neuronal precursors with URL origin. These tegmental hindbrain nuclei are thus likely to regulate their motility via modulating NCAM mediated cell-cell adhesion through polysialylation. To answer the question whether progenitors forming the parabrachial nuclear complex, the parabigeminal nucleus or laterodorsal-pedunculo pontine complex in mammals might use PSA for regulation of motility requires *in vivo* studies in the future.

At 3dpf *wnt1-GVP-UG* cells are postmigratory and have started to differentiate indicated by the expression of the acetylcholine neurotransmitter synthesizing enzyme ChAT and the glutamate transporter Vglut2.1.

Double immunohistochemistry for the adhesion factor Neurolin and GFP revealed that the expression of Neurolin in the tegmentum of rhombomere 1 is restricted to *wnt1-GVP-UG* cells and they are thus molecularly distinct from surrounding cell populations. Based on the expression data one could speculate that the cell adhesion molecule Neurolin/DM-GRASP might have a function during the final steps of migration of the *wnt1-GVP-UG* precursor cells. The progenitors loose contact during migration from the URL but form aggregates in their target region (**Movie 2**, **Movie 3** and **Movie 4**). Via the promotion of homotypic somata interactions the surface protein Neurolin could mediate the clustering of the *wnt1-GVP-UG* cells. Another possible function for Neurolin could be in regulating terminal differentiation like the outgrowth, guidance or fasciculation (Ott et al., 1998; Ott et al., 2001) of the axonal processes to ventral regions as the neurons of the different nuclei initially send their axons into the same axon tract.

As I have characterized the migratory behavior of these precursor populations and identified the projections of secondary gustatory/viscerosensory nucleus and nucleus isthmi and/or superior reticular nucleus via retrograde labeling in the developing zebrafish brain, thus the ground for functional studies investigating the role of Neurolin has been laid.

#### **4.1.5 Tegmental hindbrain nuclei can be discriminated by their different axonal projections in the larval brain**

After settling in the tegmentum of rhombomere 1 the precursors of the teleostean nucleus isthmi, superior reticular nucleus and secondary gustatory/viscerosensory nucleus integrate into distinct neuronal circuitries fulfilling functions different than those of the cerebellum. These nuclei are responsible for processing sensory information as are their mammalian counterparts that have the same developmental origin. In retrograde Dil labeling studies (see Figure 17 for summary) I observed the neurons of the ventrostral portion of the GFP fluorescent cluster to project to the optic tectum. I thus identified these tegmental neurons anteroventral to the cerebellar output tract as the nucleus isthmi and/or superior reticular nucleus of the zebrafish larval brain. Tegmental neurons located posterior to this tract were found to innervate the hypothalamus and the preglomerular tertiary gustatory nucleus (TGN) in the ventrostral diencephalon. These neurons thus belong to the secondary gustatory/viscerosensory nucleus and are likely to mediate gustatory/viscerosensory information to diencephalic areas. The cerebellar output tract can therefore serve to distinguish nucleus isthmi and/or superior reticular nucleus and secondary gustatory/viscerosensory nucleus neurons by their relative position.

The superior reticular nucleus was shown to project to the subpallium (Rink and Wullmann, 2004), interestingly in our transgenic strain no GFP-fluorescent axons could be observed in the telencephalon throughout the larval stages. Thus one might rule out that *wnt1*-GVP-UG cells contribute to the superior reticular nucleus. However this telencephalic projection is known to be quite weak and also might thus be not yet established at 4dpf. Nevertheless the mammalian homologue of the superior reticular nucleus the laterodorsal tegmental nucleus was not among the populations found to be derived from the *wnt1*-positive rhombic lip in the mouse (Nichols and Bruce, 2006). Together this supports an identity of the tectal projecting neurons as nucleus isthmi rather than superior reticular nucleus.

My Dil retrograde labeling experiments revealed that the efferent connections of secondary gustatory/viscerosensory nucleus and nucleus isthmi and/or superior reticular nucleus as described for the adult brain are already established at 4dpf in the zebrafish larval brain. Thus the formation of these evolutionary conserved

neuronal circuitries occurs in zebrafish in a very condensed time frame allowing their dynamics to be studied *in vivo* by time-lapse microscopy.

In addition, my anterograde and retrograde labeling experiments identified afferents of the larval zebrafish cerebellum that are not derived from the *wnt1*-positive rhombic lip. Such input was found to arise from the nucleus lateralis valvulae which apparently does not contain *wnt1*-expressing cells. The teleost lateralis valvulae of teleost fish has been compared to the pontine nuclei of mammals (Yang et al., 2004). If these structures are related our findings would contrast to the situation in the mouse, where the pontine nuclei were found to arise from the *wnt1*-expressing caudal rhombic lip (Nichols and Bruce, 2006; Rodriguez and Dymecki, 2000). We think though that a homology of this large nuclear mass with the mammalian pontine nuclei is unlikely for the following reasons. Firstly, the nucleus lateralis valvulae does not receive a telencephalic input in teleosts (Wullimann and Meyer, 1993) like the mammalian pontine nucleus. More importantly, a phylogenetic comparison involving amphibians and reptiles indicates that pontine nuclei do not exist in basal tetrapods (Wullimann and Meyer, 1993) and thus, nucleus lateralis valvulae and pontine nuclei are at best a case of parallel evolution.

#### **4.1.6 Pretectal input to the corpus cerebelli**

I have identified the origin of the mossy fiber-like projection in the IGL of the corpus cerebelli that is formed by a population of *wnt1*-expressing neuronal progenitors that is not derived from the URL. These neurons are situated in the pretectal area of the diencephalon, and likely contribute to the paracommissural nuclei (PC) and/or the dorsal periventricular pretectal nucleus (PP) (Folgueira et al., 2006; 2008; Imura et al., 2003; Wullimann and Northcutt, 1988). By antero- and retrograde axonal tracing (see Figure 17 for summary) I identified these neurons rather than the nucleus lateralis valvulae as the source of the observed GFP-fluorescent axonal input into the corpus cerebelli in *wnt1*-GVP-UG transgenic embryos. Interestingly, the afferents provide differentially weighted visual (if from PP) or telencephalic (if from PC) input via both ipsilateral and contralateral projections to the corpus cerebelli where they end in characteristic mossy fiber-like terminals. This suggests that their efferents are cerebellar granule neurons. In this

study the origin of these *wnt1*-expressing cells was not a matter of investigation. However in time-lapse movies of mosaicly labeled embryos no migration of fluorescent *wnt1*-expressing cells across the MHB neither in rostral nor caudal directions could be observed between 24 and 72hpf (data not shown). Thus the precursors of these pretectal projection neurons appear to have their origin in the midbrain most likely in the proliferation centers of the pretectum (Mueller and Wullimann, 2003).

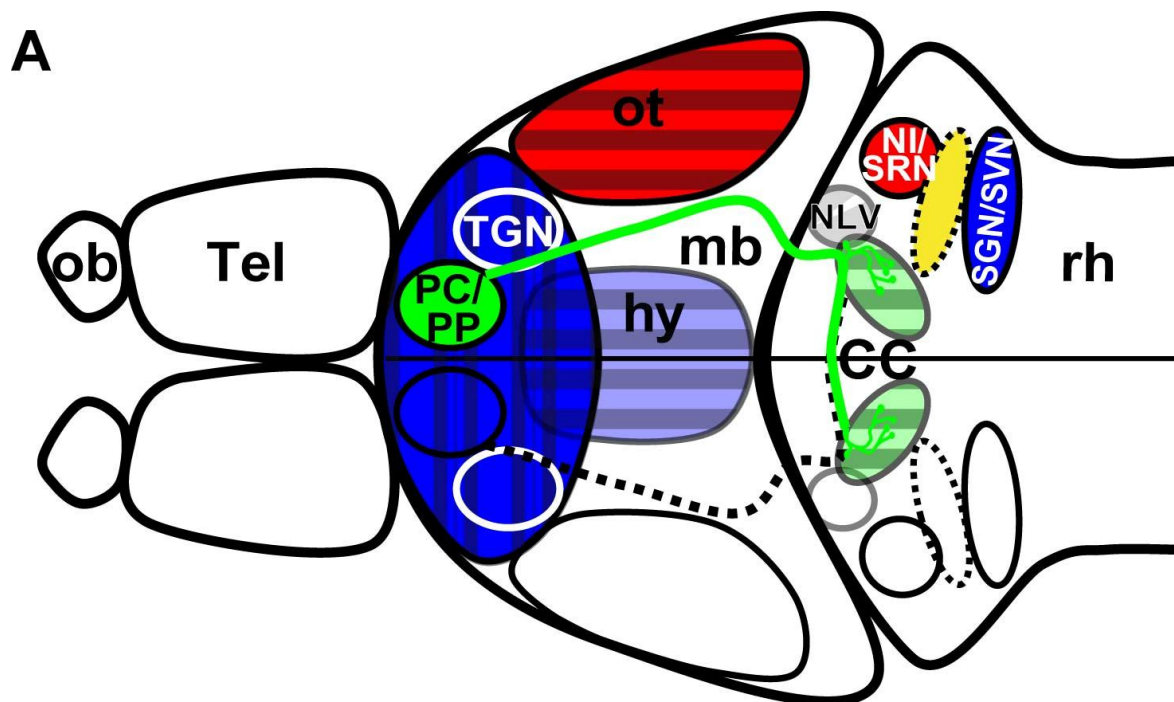


**Figure 17: Summary of retrograde labeling experiments as schematic drawing from a dorsal view of a larval zebrafish brain.**

Dil injection sites (shaded) and the correspondingly labeled nuclei are depicted in the same color, the position of the cerebellar tract is marked in yellow. The nucleus isthmi and/or superior reticular nucleus (red circle) and the secondary gustatory/viscerosensory nucleus (blue oval) in the tegmentum of rhombomere 1 have axonal projections targeting areas in the midbrain and diencephalon, respectively. The nucleus isthmi and the superior reticular nucleus are projecting to the optic tectum, whereas the secondary gustatory/viscerosensory nucleus projects to hypothalamus and preglomerular tertiary gustatory nucleus in the ventral rostral diencephalon. The nucleus lateralis valvulae (grey circle) in close neighborhood to the nucleus isthmi and secondary gustatory/viscerosensory nucleus has prominent projection into the corpus cerebelli but it does not appear to be derived from *wnt1*-expressing URL progenitors. Mossy fiber-like projections from the paracommissural nucleus and/or periventricular pretectal nucleus (green circle) are terminating in the granule cell layer of the ipsi- and contralateral corpus cerebelli (shaded in green) formed by the granule neurons of the non-vestibular cerebellar system in zebrafish.



**Abbr.:** CC, corpus cerebelli; hy, hypothalamus; mb, midbrain; NI, nucleus isthmi; NLV, nucleus lateralis valvulae; ob, olfactory bulb; ot, optic tectum; PC, paracommissural nucleus; PP, dorsal periventricular preectal nucleus, rh, rhombencephalon; SGN/SVN, secondary gustatory/viscerosensory nucleus; SRN, superior reticular nucleus; Tel, telencephalon; TGN, preglomerular tertiary gustatory nucleus.

#### 4.1.7 Constraints of the study

It has to be noted that GFP-expression under control of the *wnt1*-promoter/enhancer in the *wnt1*-GVP-UG strain is not covering all *wnt1*-expressing URL-derived neuronal populations observed in the mouse (e.g. precerebellar neurons sending mossy fibers into the cerebellum) (Nichols and Bruce, 2006). This observation might be partly explained by the functional redundancy and overlapping but not completely identical expression patterns of the two Wnt family members Wnt1 and Wnt10b in zebrafish (Lekven et al., 2003). Thus in this study, we can only report about the origin and migratory behavior of neuronal populations labeled in our transgenic *wnt1*-GVP-UG strain, but we cannot exclude that additional neuronal populations are generated by *wnt10b*-expressing progenitors in the URL or lower rhombic lip that resemble the residual neurons derived from the *wnt1*-expressing rhombic lip in the mouse. Furthermore, we do not know whether the *wnt1*-GVP-UG strain represents the entire endogenous expression of *wnt1* in spatial and temporal means although it does in early embryonic stages (Matthew Harris personal communication).

#### 4.2 PSA-NCAM regulates motility of URL-derived tegmental hindbrain precursors

I have contributed to work of Dr. Sandra Rieger in investigating the function of PSA-NCAM in an early arising migratory neuronal population of the zebrafish embryonic cerebellum (see **Appendix 2**). For this *in vivo* study the effect of enzymatic removal of PSA on migration was analyzed with help of time-lapse movies. However, the identity of these early precursor populations arising between 24hpf and 48hpf had remained unclear so far. As part of my own PhD project I have clarified the identity of precursors belonging to this PSA-dependent migrating population with help of the transgenic *wnt1*-GVP-UG strain (see **Appendix 1**) and

could show that the precursors of the NI/SRN and SGN/SVN likely migrate ventrally in a PSA dependent manner.

### **4.3 New Gal4 activator strain allows transgene expression in *atona1a*-expressing rhombic lip derived populations**

I succeeded in isolating a promoter fragment sufficient to drive transgene expression in all *atona1a*-expressing cell populations of the zebrafish embryo including the early cell populations arising from the URL. Combined with a Gal4 expression cassette this allows for driving expression specifically in these populations enabling expression of gain or loss of function protein variants, labeling of subcellular components or fate mapping constructs. Moreover this transgenic strain can be crossed in other transgenic backgrounds to compare development of the *atona1a* cells with that of other cell populations in the same embryo. Moreover by simple crossing this Gal4 activator strain into reporter or effector strains one can achieve cell population specific expression in URL progenitors cells but leave e.g. VZ-derived cells unaffected. The Gal4 expression cassette inserted into the genome is a pure activator, which means that there is no endogenous fluorescence and thus the full range of fluorescence molecules can be used. As the construct was inserted into the genome with help of the I-SceI restriction enzyme, the transient integration of expression constructs can be efficiently increased by use of the Tol transposon system without the risk of remobilizing the *atoh1a:KalTA4* expression cassette (Kawakami et al., 2004). This transgenic strain has already proven as a powerful tool to address the subcellular orchestration of NI/SRN and SGN/SVN neuron migration in an *in vivo* study.

## **4.4 Characterization of the granule cell population of the developing zebrafish cerebellum**

### **4.4.1 *gata1*:GFP cells represent the granule cell population of the embryonic, larval and juvenile zebrafish cerebellum**

With help of extensive marker gene expression studies I could identify the granule cell population of the embryonic, larval and juvenile zebrafish cerebellum and described their differentiation in detail.

In sections of larval and juvenile brains the *gata1*:GFP cells revealed the typical morphology of cerebellar granule cells with small cell bodies in the granule cell layer, ascending axons passing through the Purkinje cell layer and most likely bifasciculating in the molecular layer (see chapter 1.3.3). To visualize individual granule cells and analyze processes like axon outgrowth, axon bifurcation and dendrite formation together with other changes of morphology during maturation *in vivo* transplantation experiments of *gata1*:GFP cells into wild-type fish could be performed.

I could establish a gene expression profile for the zebrafish cerebellar granule cells and their progenitors that is useful for further studies involving differentiation, fate specification etc. of cell types of the cerebellum in teleosts.

### **4.4.2 The URL of the embryonic zebrafish cerebellum is spatially subdivided and simultaneously gives rise to granule cells of different fate and function**

With help of time-lapse movies combined with individual cell tracking we have analyzed the migratory routes of the granule cell subpopulations existing in the zebrafish cerebellum. Furthermore *in vivo* time-lapse imaging allowed us to visualize the growth of first parallel fibers in the cerebellar anlage. With help of retrograde labeling of parallel fibers in the crista cerebellaris I could further distinguish between the vestibulo- and non-vestibulocerebellum (see Figure 18 for summary).

These retrograde labeling experiments were performed by microinjection of the lipophilic dye Dil as well as rhodamine dextran into the putative target area of the

axons. The use of rhodamine dextran for retrograde labeling in living zebrafish larvae is described in detail in **Appendix 5** (Volkmann and Köster, 2007).

Consistent with proliferation in the adult cerebellum found in other studies (Grandel et al., 2006; Kaslin et al., 2009; Zupanc et al., 2005) I observed continuous migration of granule cell precursors from the URL into the corpus cerebelli and the eminentia granularis at larval stages. Strikingly the regionalization of the URL found in the embryo is maintained.

This study revealed that granule cell populations not only have different origins, migratory routes and final positions but they also have different projections and thus serve different functions. Taken together our results show that the cerebellar rhombic lip is spatially subdivided along its medio-lateral axis in simultaneously producing granule cells of different connectivity and function. The temporal shift of the URL in producing different cell types combined with the regionalization could specify the cerebellar rhombic lip precursor population to give rise to spatial subpopulations of neurons that will form specific neuronal circuits - supporting a model how mature functional compartments are laid down in the embryonic brain.

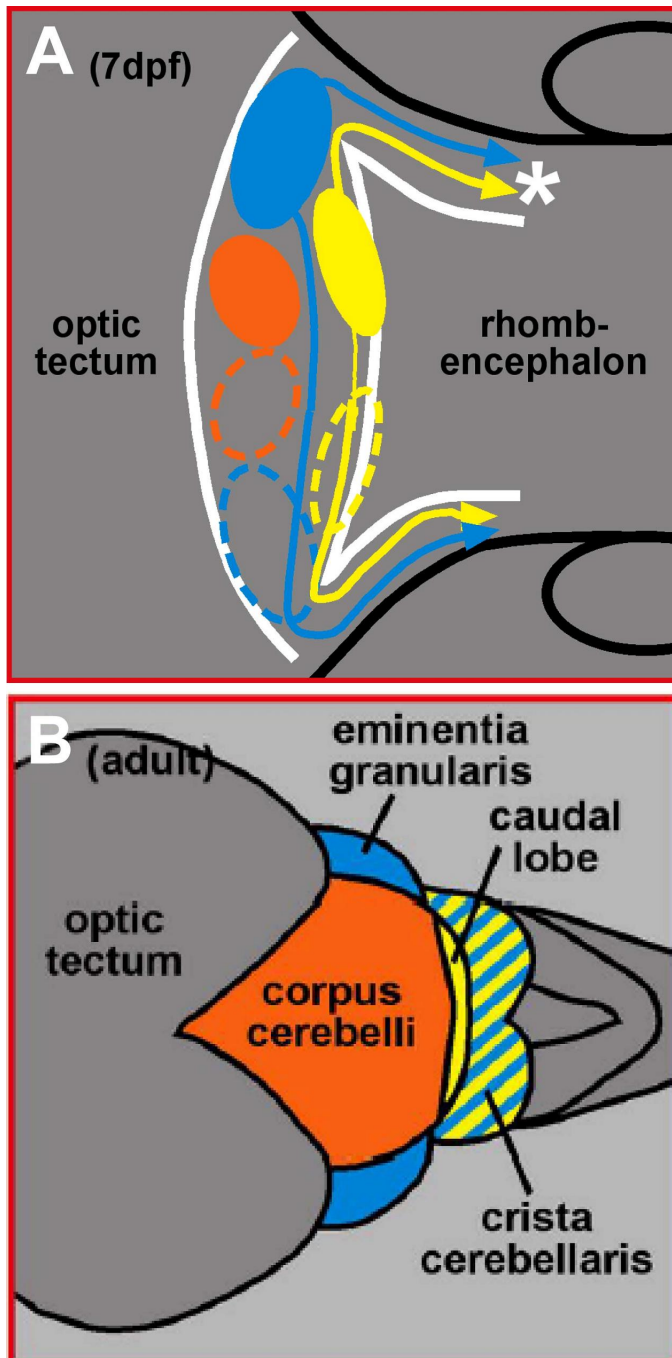


**Figure 18: Schematic drawing of granule cell projections deduced from rhodamine dextran retrograde labeling.**

The schematic drawing of a dorsal view of (A) larval and (B) adult granule cell populations and projections reveals the embryonic ventrolateral (A, blue dashed circle) and dorsoposterior (A, yellow dashed circle) *gata1*:GFP granule cell clusters as the granule cells of the adult vestibulocerebellar system in zebrafish (B) formed by the eminentia granularis (blue) and the caudal lobe (yellow) respectively. The embryonic dorsomedial cluster (orange circle) does not project into the crista cerebellaris supporting together with their medial position an identity as the granule cell population of the corpus cerebelli forming the non-vestibulocerebellum (marked orange).

#### **4.4.3 Comparison of granule cell migration in the mammalian (avian) and the zebrafish cerebellum**

In the developing mammalian cerebellum granule cell precursors initially migrate tangentially over the pial surface of the cerebellar anlage to form the secondary germinal zone of the external granule cell layer (EGL). In postnatal stages the progenitor cells start to migrate radially along radial glia fibers through the Purkinje cell layer to populate the internal granule cell layer (IGL) resulting in the formation of the prominent layers of the cerebellar cortex (IGL, ML, PCL see Introduction chapter 1.3). In contrast to the situation in mammals and what was reported previously for the embryonic zebrafish brain (Mueller and Wullmann, 2002) we could not find a prominent secondary proliferation zone or an accumulation of granule cell precursors similar to the EGL in the zebrafish embryos or larvae up to 4dpf. In our time-lapse study the migration of zebrafish granule cell precursors was tangential between 2dpf and 4dpf. This early lack of a radial migration step is consistent with the lack of glia marker gene expression in the cerebellum up to day 4 post fertilization together with the observation that granule cell precursors use a homotypic neurophilic migration mode (Rieger et al., 2009). By neuropil stainings with the lipophilic dye Bodipy a prominent molecular layer could be first observed after 4 days of development indicating that the formation of layers in the cerebellum has started at 3 days of development. As the cerebellar layers are growing in size (which can be observed with help of the BODIPY staining in my time course), it may become necessary for granule cells to include a radial migration step to pass through the molecular and Purkinje cell layer. Thus I assume that radial migration is prominent at later stages of development as radial glia cells can be found in the adult zebrafish cerebellum (Grandel et al., 2006; Kaslin et al., 2009).

#### **4.4.4 Possible molecular bases of the regionalization of the URL**

Whether a single progenitor cell in the URL gives rise to several neuronal cell types of the cerebellum over time or if different progenitor cells producing a single but different cell type co-exist in the URL is still an open question. The analysis of double transgenic zebrafish embryos with fluorescence protein expression in early and late URL-derived cell populations could give a first hint on whether distinct progenitor populations are present in the URL simultaneously. Furthermore it is

unknown at which point the cellular fate is determined – already in the proliferative epithelium - before or after the final division of the progenitor cell, or after the progenitors have left the URL. Also only little is known about the factors involved in fate determination of cerebellar cell types - they might be provided by URL cells or via long distance signaling from a source elsewhere in the neural tube or during migration from neighboring cells e.g. via contact to the MHB. Also how the different granule cell subpopulations are specified remains unclear. The granule cells might already be determined inside the URL or specification might take place after onset of migration. This open question could be answered by transplantation of medial URL cells to lateral positions and vice versa. If fate is an intrinsic feature of the progenitor cells the migratory behavior and the projections of the granule cells should be maintained whereas the new fate should be acquired if the information is provided by the environment. However the observation in our time-lapse analysis that the migrating cells have very directional routes that do not cross even close to the URL suggests that the progenitors are already specified when they leave the URL.

Neuronal fate specification can be mediated by the exposition to different concentrations of extracellular cues providing a positional information (Dessaud et al., 2008; Sansom and Livesey, 2009), in the cerebellar plate e.g. a gradient of BMP protein secreted by the roofplate could determine the fate of the granule cell precursors in the URL. Interestingly the roofplate was already implicated in the regulation of cerebellar proliferation and cell type specification (Chizhikov et al., 2006).

#### **4.5 Comparison of mouse and zebrafish URL-derived cell types**

To allow a comparison of cerebellar development of the model organisms mouse and zebrafish first the homologous phases in development have to be identified both on a tissue and cellular level. Different steps may be regulated by completely different sets of molecular factors. This is also important for the comparison of *in vivo* and *in vitro* systems (e.g. explants).

In the mouse the URL produces mesencephalic nuclei (parabigeminal, pedunculo pontine, microcellular tegmental, laterodorsal tegmental, lateral parabrachial) from E9.5 – E10.5 followed by the precursors of the deep cerebellar

nuclei (dentate, interpositus and fastigial) from E10.5 to E12.5 and finally cerebellar granule cell progenitors starting from E13 on and ending after birth (Machold and Fishell, 2005; Wang et al., 2005).

This correlates well with the situation observed in zebrafish with *wnt1*-expressing precursors contributing to several tegmental nuclei of the hindbrain (the secondary gustatory/viscerosensory nucleus and nucleus isthmi and/or superior reticular nucleus) migrating between 24-48hpf and the cerebellar granule cell precursors leaving the URL from 48hpf onwards. Thus the generation of different neuronal cell populations from the URL over time that was reported for the embryonic mouse cerebellum is conserved among vertebrate species. The neurons of the deep cerebellar nuclei arise from the URL in mouse, while preliminary data suggests that the zebrafish homologues of the deep cerebellar nuclei neurons, the eurydendroid cells, arise from the VZ (Babaryka, 2009), however their origin needs to be further investigated.

In zebrafish though this temporal change of the URL in producing different neuronal cell populations is more condensed occurring within 24 hours compared to about 3 days in mouse. This makes zebrafish embryos well suited for analyzing the underlying *in vivo* dynamics of cerebellar development. Furthermore, my data revealed that the zebrafish cerebellar rhombic lip is spatially patterned along its mediolateral axis with subdomains giving rise to different subpopulations of cerebellar granule cells with different positions, connectivities and functions in the mature brain. Subdomains were also observed recently in the mouse cerebellum (Sgaier et al., 2007; Sgaier et al., 2005). Thus, rather than being a simple proliferative zone, the zebrafish cerebellar rhombic lip is a complex germinal structure with distinct characteristics in time and space.

Before this study the only population of the zebrafish cerebellum that was identified and characterized in the embryonic brain was the eurydendroid cell population (McFarland et al., 2008). I could identify and characterize additional migratory neuronal cell populations in the zebrafish embryonic and larval cerebellum – the neurons of the nucleus isthmi and/or superior reticular nucleus and secondary gustatory/viscerosensory nucleus and the cerebellar granule cells that are derived from the URL. Fate mapping studies in the mouse and in the chicken (Machold and Fishell, 2005; Nichols and Bruce, 2006; Wang et al., 2005;



Wilson and Wingate, 2006) have delineated the migration paths existing for URL-derived neuronal cell populations - this study now adds detailed *in vivo* data for individual cells and cell populations. Furthermore we provide new insights into the dynamics of migratory processes in rhombomere 1.

My data reveal that neuronal identity not only depends on the time point in development when cells migrate but it is also fine-tuned by the spatial position of the progenitors inside the rhombic lip. This spatio-temporal fate determination might also hold true for other proliferation zones of the brain.

#### **4.6 The function of Netrin-1/Dcc in URL-derived populations remains elusive**

URL-derived neuronal precursors follow distinct migration routes inside rhombomere 1. Only little is known about the guidance factors involved in these migratory processes. Based on our time-lapse analysis, that revealed the migration of neuronal precursors from the URL into ventral directions, I have focused on the guidance factor Netrin-1 as it is expressed in the floorplate (Lauderdale et al., 1997; Strahle et al., 1997) and thus could potentially be the cue providing ventral direction information during migration.

My expression analysis indeed revealed that *netrin-1a/1b*-expression ventrally to rhombomere 1 during ventral migration of URL-derived populations. Moreover I found expression of the Netrin-1 receptor *dcc* in the zone of early precursor migration along the MHB in rhombomere 1 during NI/SRN and SGN/SVN migration. Furthermore migrating granule cell precursors in the cerebellar plate express *dcc* at 48hpf.

To analyze the expression of both Netrin-1 receptors in the embryonic zebrafish cerebellum I have isolated a partial cDNA for the zebrafish homologue of the Netrin-1 receptor *Unc5c*. Using this fragment as template for synthesis of a situ hybridization probe I could characterize *unc5c*-expression in the zebrafish embryonic brain. Interestingly I found *unc5c*-expression in the migrating granule neurons of the zebrafish cerebellum. This finding is consistent with the expression of *unc5c* in granule cells of the mouse cerebellum (Przyborski et al., 1998). Thus *unc5c* and *dcc* are probably co-expressed by migrating granule cell precursors but not by the early migrating precursors of tegmental hindbrain nuclei.

The expression of *dcc* and *unc5c* in migrating URL precursors with the ligand expressed in the ventral target regions of the precursors is suggesting a role of Dcc/Unc5c/Netrin-1 signaling in the guidance of URL-derived neuronal precursors during their migration into ventral directions.

In morpholino knockdown experiments for *dcc* and *netrin-1a* together with *netrin-1b*, however, I could not observe an effect on neuronal migration or axon guidance in the following populations arising from the URL: cerebellar granule cells, tegmental hindbrain nuclei or early *atona1a*-expressing precursors in general.

Strikingly, in tissue explant experiments in mouse embryos, cells of the URL did not respond to a Netrin-1 source although they expressed the Dcc receptor. In contrast at postnatal stages a strong chemorepulsive effect of Netrin-1 on growing granule cell axons from the EGL and a chemorepulsive effect on migrating granule cells was observed (Alcantara et al., 2000). Moreover Netrin-1 knockout mice have a nearly intact EGL (Bloch-Gallego et al., 1999) and do form an IGL (Eisenman and Brothers, 1998) suggesting that Netrin 1 is not required for early granule cell development. Furthermore in chicken cerebellar explants of the late rhombic lip migrating cells (likely granule cell precursors) showed no responsiveness to Netrin-1 (Gilthorpe et al., 2002). These published together with my current data suggest that Dcc in the zebrafish cerebellum could have a function other than axon guidance or guidance of neuronal migration in response to Netrin-1 binding (see chapter 1.7).

Interestingly though after knockdown of *netrin-1a/1b* but not after *dcc* knockdown a reduction of granule cell numbers in the corpus cerebelli could be observed, while the eminentia granularis cell number and migrating appeared normally. Dcc is a dependence receptor triggering apoptosis in absence of the Netrin-1 protein. The *netrin-1a/1b* morpholino injections are likely to cause an incomplete knockdown of protein expression levels, resulting in residual Netrin-1 secretion from the floorplate cells in the morphants. The cerebellar corpus represents a dorsal population whereas the eminentia is a ventral population, thus as the Netrin-1 ligand is expressed ventrally in the floorplate, the cells of the corpus cerebelli have a wider distance to the Netrin-1 source and are thus exposed to a lower protein

concentration in the Netrin-1 gradient possibly leading to increased Dcc-mediated programmed cell death.

Due to this complex network of interactions Dcc function has to be manipulated and analyzed in a single cell population. Thus I have cloned a full length cDNA for zebrafish *dcc* and a dominant negative variant that can be used in future functional studies in combination with the Gal4-UAS system.

The formation of the brain involves the migration of thousands of neuronal precursors from the proliferation zones to their final target place. How does the growing brain deal with precursors that took the wrong turn? There are phases of frequent apoptosis events in the embryonic zebrafish brain, anyhow apoptosis is occurring on a lower level throughout embryonic brain development (Cole and Ross, 2001). Could Dcc and Unc5c-mediated apoptosis be involved in the elimination of migrating neuronal precursors that got stuck on the way or followed the wrong path and that did not reach the Netrin-1 source? In this model movement up the Netrin-1 protein gradient could be the direction on the route to survival. Strikingly in a recent study Netrin-1 signaling was implicated as survival factor for the precursors of the inferior olivary nucleus in the mouse hindbrain (Marcos et al., 2009).

#### **4.7 Zebrafish as novel vertebrate model system for early onset Parkinson's Disease**

The *parkin* antisense morpholino study in the lab of Oliver Bandmann revealed that *parkin*-knockdown zebrafish embryos and human *parkin*-mutant Parkinson patients share both the pathogenic mechanisms (i.e. complex I deficiency) and the pathological hallmark (i.e. dopaminergic cell loss). Thus the zebrafish embryo is ideally suited for future studies (e.g. drug screens see chapter 1.1) investigating which functional mechanism are underlying the death of dopaminergic neurons in early onset Parkinson's Disease.

Moreover in collaboration with Oliver Bandmann and his lab my TEM study of *parkin* knockdown embryos revealed an unexpected phenotype, namely an increase of electron-dense material of unknown nature in the t-tubules in the muscle tissue of the trunk. This observation suggests protein aggregation in these invaginations of the surface membrane, which are important for the calcium ( $\text{Ca}^{2+}$ )

homeostasis of the muscle tissue (Brette and Orchard, 2007). Interestingly, a recent review implicates mitochondrial calcium homeostasis with Parkinson's Disease (Celsi et al., 2009). Thus the aggregations in the t-tubules might be linked to the impaired mitochondrial function observed in *parkin* knockdown embryos.

In TEM images of the analyzed early larval stages no signs of muscle degeneration could be observed and the larvae displayed no obvious locomotive defects. The MO knockdown of *parkin* is of transient nature. Thus whether the aggregates in the t-tubules might lead to muscle necrosis over time in mutants with permanent Parkin depletion has to be investigated in future studies.

T-tubules are studded with voltage dependent L-type calcium channels. Upon stimulation with an action potential these channels open and cause calcium influx from the sarcoplasmic reticulum into the cytoplasm of muscle cells leading to increase in intracellular calcium levels. Our work might also provide a tentative link between genetically determined early onset Parkinson's Disease and recent studies implicating these L-type calcium channels in late onset sporadic Parkinson's Disease (Chan et al., 2007).

## 5 Table of Figures

Figure 1: Overview of guidance cues involved in neuronal migration. ....	5
Figure 2: Layers, cell types and circuitry of the mammalian cerebellar cortex. ....	8
Figure 3: The mammalian cerebellum.....	11
Figure 4: The embryonic and adult zebrafish cerebellum.....	13
Figure 5: Zebrafish tegmental hindbrain nuclei. ....	20
Figure 6: Mammalian radial granule cell migration.....	22
Figure 7: Schematic drawing of Dcc and Unc5c receptor-mediated signaling. ....	30
Figure 8: <i>atoh1a</i> :KalTA4 activator cassette and activator/reporter cassette of TG5xR RFP reporter strain.....	41
Figure 9: Expression of <i>netrin-1a</i> and <i>netrin-1b</i> in the zebrafish embryonic brain.	51
Figure 10: Expression of the Netrin-1 receptor <i>dcc</i> in the developing zebrafish cerebellum.....	53
Figure 11: Expression of <i>dcc</i> and <i>netrin-1a/1b</i> in rhombomere 1.....	54
Figure 12: <i>dcc</i> -expression in cerebellar granule cells. ....	57
Figure 13: Expression of the Netrin-1 receptor <i>unc5c</i> in the developing zebrafish cerebellum.....	59
Figure 14: <i>unc5c</i> -expression in cerebellar granule cells. ....	61
Figure 15: Dcc amino acid sequence alignments.....	63
Figure 16: Bicistronic Dcc expression constructs.....	64
Figure 17: Summary of retrograde labeling experiments as schematic drawing from a dorsal view of a larval zebrafish brain. ....	74
Figure 18: Schematic drawing of granule cell projections deduced from rhodamine dextran retrograde labeling. ....	79



## 6 Movie Legends

### **Movie 1: Proliferation of NI/SRN and SGN/SVN precursors**

Time-lapse movie recorded by *in vivo* three dimensional confocal microscopy showing in a dorsal view GFP-expressing precursors in the dorsal cerebellar plate of a transgenic *wnt1-GVP-UG* embryo between 24 and 34hpf. Stacks of 35 pictures (at 2.5 $\mu$ m distance) were recorded every 12min; pictures of individual time-points were projected into a single maximum intensity projection that were subsequently animated as a QuickTime movie at a frame-rate of 6 frames per second. A dividing GFP-positive cell at the URL is marked by a yellow arrowhead. After division the daughter cells are marked by a yellow and a red arrowhead respectively.

**Abbr.:** *IV*, fourth ventricle; *mb*, midbrain; *MHB*, midbrain-hindbrain boundary; *URL*, upper rhombic lip.

### **Movie 2 and 3: Migration paths of NI/SRN and SGN/SVN precursors**

Time-lapse movie recorded by *in vivo* three dimensional confocal microscopy showing in a dorsal view (movie 2) and a lateral view (movie 3) GFP-expressing precursors in the cerebellar plate of a transgenic *wnt1-GVP-UG* embryo between 24 and 64hpf. Stacks of 30-35 pictures (at 2-2.5 $\mu$ m distance) were recorded every 12min; pictures of individual time-points were projected into a single maximum intensity projection and subsequently animated as a QuickTime movie at a frame-rate of 6 frames per second. GFP-expressing progenitors, after cell divisions leave the URL and move anterior towards the MHB, where they turn ventrally and migrate along the MHB to tegmental regions ventral to the cerebellar plate where they form a cluster (marked by a green circle).

**Abbr.:** *IV*, fourth ventricle; *mb*, midbrain; *MHB*, midbrain-hindbrain boundary; *URL*, upper rhombic lip.

### **Movie 4: Mosaic labeling and individual cell tracking**

Lateral view time-lapse movie recorded by *in vivo* three dimensional confocal microscopy showing mosaic Gal4-VP16-dependent expression of the red fluorescent mCherry protein in *wnt1-GVP-UG* cells in the cerebellar plate of a

transgenic embryo between 24 and 72hpf. Stacks of 21 pictures (at 3 $\mu$ m distance) were recorded every 12min; pictures of individual time-points were projected into a single maximum intensity projection that were subsequently animated as a QuickTime movie at a frame-rate of 10 frames per second. The same time-lapse movie is played again showing in the second sequence individual migratory precursor cells showing both GFP- and mCherry-expression that were traced manually and marked with colored dots. In addition in the third sequence, the migratory routes were visualized by ImageJ supported cell tracing, which reveals that these progenitor cells migrate along the MHB into ventral directions and settle in a tegmental cluster ventral to the cerebellum and close to the MHB. This movie is summarized in Fig. 2A-J.

**Abbr.:** *IV*, fourth ventricle; *cb*, cerebellar anlage; *mb*, midbrain; *MHB*, midbrain-hindbrain boundary; *ot*, optic tectum; *rh*, rhombencephalon; *URL*, upper rhombic lip.

#### **Movie 5: NI/SRN and SGN/SVN precursor migration in *atoh1a:KaITa4/TG5xR* double transgenic embryo**

Time-lapse movie starting at approximately 24hpf and ending at approximately 54hpf showing in a lateral view the cerebellar anlage of an *atoh1a:KaITa4/TG5xR* double transgenic zebrafish embryo. Images are maximum projections of z-stacks (stack of 38 images, 2.5 $\mu$ m apart) recorded every 12min using a 40x water objective and a Zeiss LSM 510 confocal microscope. The images were animated as a QuickTime movie at a frame-rate of 6 frames per second.

**Abbr.:** *cb*, cerebellar anlage; *mb*, midbrain; *MHB*, midbrain-hindbrain boundary; *URL*, upper rhombic lip.

#### **Movie 6: Parallel fiber outgrowth**

Time-lapse movie recorded by 3-D *in vivo* confocal microscopy showing, in a dorsal view, neuronal migration and axon projections of GFP-expressing granule cell precursors in one half of the cerebellum of a transgenic *gata1:GFP* embryo. Starting at around 48hpf neuronal migration is initiated from the cerebellar rhombic lip towards the midbrain–hindbrain boundary. The formation of several neuronal clusters along the mediolateral axis of the cerebellum can be observed. Axons (blue arrows) arise from GFP-expressing granule cells in the cerebellum and



project dorsally towards the dorsal midline with some of these axons beginning to fasciculate (e.g., 1, 3 see slow motion sequence). At the dorsal midline axons originating from both cerebellar halves (blue and red arrows respectively) meet while crossing the midline. Contacts of their growth cones last shortly, followed by retraction and avoidance (see yellow circle in slow motion sequence). Subsequently, the projection continues ventrolaterally along the posterior border of the contralateral cerebellar half and posteriorly into the hindbrain (green arrow). Stacks of 21 pictures (at 3 $\mu$ m distance) were recorded every 12min; pictures of individual time-points were projected in a maximum intensity projection into a single image per time-point with these images subsequently being animated as a movie at a frame-rate of 6 frames per second, the slow-motion sequence was animated at 1 frame per second or 0.6 frames per second, respectively.

**Abbr.:** *cb*, cerebellar anlage; *MHB*, midbrain–hindbrain boundary; *ot*, optic tectum; *rh*, rhombencephalon; *URL*, upper rhombic lip.

### **Movie 7 and 8: Granule cell precursor migration at larval stages**

Time-lapse movie recorded by 3-D *in vivo* confocal microscopy showing in a dorsal view granule cell precursors in one half of the cerebellum of a transgenic *gata1:GFP* larvae between 4 and 5dpf (Movie 7) and 6 and 7 dpf (Movie 8), respectively. These movies show that differentiating granule cells do not leave their respective clusters and thus cease migration within the clusters and become stationary. At these later developmental stages, migration from the upper rhombic lip, although significantly reduced, still feeds into the clusters contributing to their expansion. Consistent with the tracing results during embryonic stages granule cell precursors from the medial part of the cerebellar rhombic lip migrate to the dorsomedial cluster (orange dot), whereas granule cell precursors from the lateral cerebellar rhombic lip contribute to the ventrolateral cluster (blue dots). This indicates that the spatial subdivision of the cerebellar rhombic lip is still maintained until 7dpf. Stacks of 35 images (at 4 $\mu$ m distance) were recorded every 12min; pictures of individual time-points were projected in a maximum intensity projection into a single image per time-point with these images subsequently being animated as a movie at a frame rate of 6 frames per second.

**Abbr.:** *cb*, cerebellum; *MHB*, midbrain–hindbrain boundary; *ot*, optic tectum; *rh*, rhombencephalon; *URL*, upper rhombic lip.

## 7 Abbreviations

Abbr.	Abbreviations
atoh1a	zebrafish atonal homolog 1a
BAC	bacterial artificial chromosome
BCIP	5-bromo-4-chloro-3'-indolyphosphate p-toluidine salt
bHLH	basic Helix-Loop-Helix
BO	olfactory bulb
bp	base pair
BSA	bovine serum albumin
cb	cerebellum
CC	cerebellar crest/crista cerebellaris
CCe	corpus cerebelli
cDNA	complementary DNA
<i>CeP</i>	<i>cerebellar plate</i>
<i>Cgus</i>	<i>commissure of the secondary gustatory nuclei</i>
Chat	choline acetyl-transferase
ChAT	choline acetyltransferase
CL	caudal lobe
DAB	diaminobenzidine
DAPI	di-aminobenzidine
Dcc	Deleted in colorectal carcinoma/Deleted in colorectal cancer
DMSO	di-methyl sulfoxide
dn	dominant negative
DNA	Deoxyribonucleic acid
dpf	days post fertilization
E	embryonic day
EG	eminentia granularis
EGL	external granule cell layer

Fig.	figure
fl	full length
GABA <sub>A</sub> Rα6	GABA <sub>A</sub> receptor α6 subunit
GFP	green fluorescent protein
hpf	hours post fertilization
IGL	internal granule cell layer
IL	inferior lobe
kb	kilo bases
LL	lateral line nerve
math1	mouse atonal homolog 1
MHB	midbrain-hindbrain boundary
ML	molecular layer
MO	medulla oblongata
mRNA	messenger ribonucleic acid
MS	medulla spinalis
NBT	nitro-blue tetrazolium chloride
NCAM	neuronal cell adhesion molecule
NGS	normal goat serum
NI	nucleus isthmi
NLV	nucleus lateralis valvulae
OB	olfactory bulb
PBS	phosphate buffered saline
PCR	polymerase chain reaction
pFA	paraformaldehyde
PG	preglomerular region
PH3	phospho-histone 3
Pit	pituitary
PSA	polysialic acid
PSp	parvocellular superficial pretectal nucleus
r1	rhombomere 1
RFP	red fluorescent protein
rh	rhombencephalon

RNA	ribonucleic acid
SGN	secondary gustatory nucleus
SGN/SVN	secondary gustatory/viscerosensory nucleus
SRN	<i>superior reticular nucleus</i>
Tel	telencephalon
TEM	transmission electron microscopy
TeO	optic tectum
TH	tuberal hypothalamus
THN	tegmental hindbrain nuclei
TLa	torus longitudinalis
twhh	<i>tiggy winkle hedgehog</i>
UAS	upstream activator sequence
Unc5c	Unc-5 homolog c
URL	upper rhombic lip
VZ	ventricular zone
wpf	weeks post fertilization
zic1	zic family member 1

## 8 References

- Ackerman SL, Kozak LP, Przyborski SA, Rund LA, Boyer BB, Knowles BB. 1997. The mouse rostral cerebellar malformation gene encodes an UNC-5-like protein. *Nature* 386(6627):838-842.
- Adolf B, Bellipanni G, Huber V, Bally-Cuif L. 2004. *atoh1.2* and *beta3.1* are two new bHLH-encoding genes expressed in selective precursor cells of the zebrafish anterior hindbrain. *Gene Expr Patterns* 5(1):35-41.
- Adolf B, Chapouton P, Lam CS, Topp S, Tannhauser B, Strahle U, Gotz M, Bally-Cuif L. 2006. Conserved and acquired features of adult neurogenesis in the zebrafish telencephalon. *Dev Biol* 295(1):278-293.
- Ahrens K, Wullmann MF. 2002. Hypothalamic inferior lobe and lateral torus connections in a percomorph teleost, the red cichlid (*Hemichromis lifalili*). *J Comp Neurol* 449(1):43-64.
- Alcantara S, Ruiz M, De Castro F, Soriano E, Sotelo C. 2000. Netrin 1 acts as an attractive or as a repulsive cue for distinct migrating neurons during the development of the cerebellar system. *Development* 127(7):1359-1372.
- Alder J, Cho NK, Hatten ME. 1996. Embryonic precursor cells from the rhombic lip are specified to a cerebellar granule neuron identity. *Neuron* 17(3):389-399.
- Aller MI, Jones A, Merlo D, Paterlini M, Meyer AH, Amtmann U, Brickley S, Jolin HE, McKenzie AN, Monyer H, Farrant M, Wisden W. 2003. Cerebellar granule cell Cre recombinase expression. *Genesis* 36(2):97-103.
- Altman J, Bayer, S.A. 1997. Development of the Cerebellar System in Relation to its Evolution, Structure, and Functions. Petralia P, editor. Boca Raton, FL.: CRC Press, Inc.
- Alvarez-Buylla A. 1997. Mechanism of migration of olfactory bulb interneurons. *Semin Cell Dev Biol* 8(2):207-213.
- Andrews WD, Barber M, Parnavelas JG. 2007. Slit-Robo interactions during cortical development. *J Anat* 211(2):188-198.
- Arenzana FJ, Clemente D, Sanchez-Gonzalez R, Porteros A, Aijon J, Arevalo R. 2005. Development of the cholinergic system in the brain and retina of the zebrafish. *Brain Res Bull* 66(4-6):421-425.
- Babaryka A. 2009. Characterization of the zebrafish cerebellar efferent system. München: Technische Universität München. 132 p.
- Babaryka A, Kühn E, Köster RW. 2009. In vivo synthesis of meganuclease for generating transgenic zebrafish *Danio rerio*. *Journal of Fish Biology* 74:452-457.
- Bae YK, Kani S, Shimizu T, Tanabe K, Nojima H, Kimura Y, Higashijima S, Hibi M. 2009. Anatomy of zebrafish cerebellum and screen for mutations affecting its development. *Dev Biol* 330(2):406-426.
- Bahn S, Harvey RJ, Darlison MG, Wisden W. 1996. Conservation of gamma-aminobutyric acid type A receptor alpha 6 subunit gene expression in cerebellar granule cells. *J Neurochem* 66(5):1810-1818.
- Bak M, Fraser SE. 2003. Axon fasciculation and differences in midline kinetics between pioneer and follower axons within commissural fascicles. *Development* 130(20):4999-5008.
- Balciunas D, Davidson AE, Sivasubbu S, Hermanson SB, Welle Z, Ekker SC. 2004. Enhancer trapping in zebrafish using the Sleeping Beauty transposon. *BMC Genomics* 5(1):62.
- Bermingham NA, Hassan BA, Price SD, Vollrath MA, Ben-Arie N, Eatock RA, Bellen HJ, Lysakowski A, Zoghbi HY. 1999. *Math1*: an essential gene for the generation of inner ear hair cells. *Science* 284(5421):1837-1841.
- Bernet A, Mehlen P. 2007. Dependence receptors: when apoptosis controls tumor progression. *Bull Cancer* 94(4):E12-17.
- Bianco IH, Carl M, Russell C, Clarke JD, Wilson SW. 2008. Brain asymmetry is encoded at the level of axon terminal morphology. *Neural Dev* 3:9.
- Blin M, Norton W, Bally-Cuif L, Vernier P. 2008. NR4A2 controls the differentiation of selective dopaminergic nuclei in the zebrafish brain. *Mol Cell Neurosci* 39(4):592-604.
- Bloch-Gallego E, Causeret F, Ezan F, Backer S, Hidalgo-Sanchez M. 2005. Development of precerebellar nuclei: instructive factors and intracellular mediators in neuronal migration, survival and axon pathfinding. *Brain Res Brain Res Rev* 49(2):253-266.
- Bloch-Gallego E, Ezan F, Tessier-Lavigne M, Sotelo C. 1999. Floor plate and netrin-1 are involved in the migration and survival of inferior olivary neurons. *J Neurosci* 19(11):4407-4420.
- Bowen MA, Bajorath J, D'Egidio M, Whitney GS, Palmer D, Kobarg J, Starling GC, Siadak AW, Aruffo A. 1997. Characterization of mouse ALCAM (CD166): the CD6-binding domain is conserved in different homologs and mediates cross-species binding. *Eur J Immunol* 27(6):1469-1478.

- Bowen MA, Patel DD, Li X, Modrell B, Malacko AR, Wang WC, Marquardt H, Neubauer M, Pesando JM, Francke U, et al. 1995. Cloning, mapping, and characterization of activated leukocyte-cell adhesion molecule (ALCAM), a CD6 ligand. *J Exp Med* 181(6):2213-2220.
- Brette F, Orchard C. 2007. Resurgence of cardiac t-tubule research. *Physiology (Bethesda)* 22:167-173.
- Canzoniere D, Farioli-Vecchioli S, Conti F, Ciotti MT, Tata AM, Augusti-Tocco G, Mattei E, Lakshmana MK, Krizhanovsky V, Reeves SA, Giovannoni R, Castano F, Servadio A, Ben-Arie N, Tirone F. 2004. Dual control of neurogenesis by PC3 through cell cycle inhibition and induction of Math1. *J Neurosci* 24(13):3355-3369.
- Castro A, Becerra M, Manso MJ, Anadon R. 2006. Calretinin immunoreactivity in the brain of the zebrafish, *Danio rerio*: distribution and comparison with some neuropeptides and neurotransmitter-synthesizing enzymes. II. Midbrain, hindbrain, and rostral spinal cord. *J Comp Neurol* 494(5):792-814.
- Celsi F, Pizzo P, Brini M, Leo S, Fotino C, Pinton P, Rizzuto R. 2009. Mitochondria, calcium and cell death: a deadly triad in neurodegeneration. *Biochim Biophys Acta* 1787(5):335-344.
- Chan CS, Guzman JN, Ilijic E, Mercer JN, Rick C, Tkatch T, Meredith GE, Surmeier DJ. 2007. 'Rejuvenation' protects neurons in mouse models of Parkinson's disease. *Nature* 447(7148):1081-1086.
- Chen P, Johnson JE, Zoghbi HY, Segil N. 2002. The role of Math1 in inner ear development: Uncoupling the establishment of the sensory primordium from hair cell fate determination. *Development* 129(10):2495-2505.
- Chizhikov VV, Lindgren AG, Currie DS, Rose MF, Monuki ES, Millen KJ. 2006. The roof plate regulates cerebellar cell-type specification and proliferation. *Development* 133(15):2793-2804.
- Chuang JC, Mathers PH, Raymond PA. 1999. Expression of three Rx homeobox genes in embryonic and adult zebrafish. *Mech Dev* 84(1-2):195-198.
- Clark WE. 1933. The Medial Geniculate Body and the Nucleus Isthmi. *J Anat* 67(Pt 4):536-548 531.
- Clemente D, Porteros A, Weruaga E, Alonso JR, Arenzana FJ, Aijon J, Arevalo R. 2004. Cholinergic elements in the zebrafish central nervous system: Histochemical and immunohistochemical analysis. *J Comp Neurol* 474(1):75-107.
- Cole LK, Ross LS. 2001. Apoptosis in the developing zebrafish embryo. *Dev Biol* 240(1):123-142.
- Cookson MR, Hardy J, Lewis PA. 2008. Genetic neuropathology of Parkinson's disease. *Int J Clin Exp Pathol* 1(3):217-231.
- Cooper HM, Gad JM, Keeling SL. 1999. The Deleted in Colorectal Cancer netrin guidance system: a molecular strategy for neuronal navigation. *Clin Exp Pharmacol Physiol* 26(9):749-751.
- Corbel C, Bluestein HG, Pourquie O, Vaigot P, Le Douarin NM. 1992. An antigen expressed by avian neuronal cells is also expressed by activated T lymphocytes. *Cell Immunol* 141(1):99-110.
- Costagli A, Kapsimali M, Wilson SW, Mione M. 2002. Conserved and divergent patterns of Reelin expression in the zebrafish central nervous system. *J Comp Neurol* 450(1):73-93.
- D'Arcangelo G, Miao GG, Chen SC, Soares HD, Morgan JI, Curran T. 1995. A protein related to extracellular matrix proteins deleted in the mouse mutant reeler. *Nature* 374(6524):719-723.
- Dessaud E, McMahon AP, Briscoe J. 2008. Pattern formation in the vertebrate neural tube: a sonic hedgehog morphogen-regulated transcriptional network. *Development* 135(15):2489-2503.
- Distel M, Babaryka A, Köster RW. 2006. Multicolor in vivo time-lapse imaging at cellular resolution by stereomicroscopy. *Dev Dyn* 235(4):1100-1106.
- Distel M, Hocking JC, Volkman K, Köster RW. 2010. The centrosome neither persistently leads migration nor determines the site of axonogenesis in migrating neurons in vivo. *J Cell Biol* 191(4):875-890.
- Distel M, Wullmann MF, Köster RW. 2009. Optimized Gal4 genetics for permanent gene expression mapping in zebrafish. *Proc Natl Acad Sci U S A*.
- Dynes JL, Ngai J. 1998. Pathfinding of olfactory neuron axons to stereotyped glomerular targets revealed by dynamic imaging in living zebrafish embryos. *Neuron* 20(6):1081-1091.
- Ebert PJ, Timmer JR, Nakada Y, Helms AW, Parab PB, Liu Y, Hunsaker TL, Johnson JE. 2003. Zic1 represses Math1 expression via interactions with the Math1 enhancer and modulation of Math1 autoregulation. *Development* 130(9):1949-1959.
- Edmondson JC, Hatten ME. 1987. Glial-guided granule neuron migration in vitro: a high-resolution time-lapse video microscopic study. *J Neurosci* 7(6):1928-1934.
- Eisenman LM, Brothers R. 1998. Rostral cerebellar malformation (rcm/rcm): a murine mutant to study regionalization of the cerebellum. *J Comp Neurol* 394(1):106-117.
- Ekker SC. 2008. Zinc finger-based knockout punches for zebrafish genes. *Zebrafish* 5(2):121-123.
- Elsen GE, Choi LY, Millen KJ, Grinblat Y, Prince VE. 2008. Zic1 and Zic4 regulate zebrafish roof plate specification and hindbrain ventricle morphogenesis. *Dev Biol* 314(2):376-392.

- Englund C, Kowalczyk T, Daza RA, Dagan A, Lau C, Rose MF, Hevner RF. 2006. Unipolar brush cells of the cerebellum are produced in the rhombic lip and migrate through developing white matter. *J Neurosci* 26(36):9184-9195.
- Farago AF, Awatramani RB, Dymecki SM. 2006. Assembly of the brainstem cochlear nuclear complex is revealed by intersectional and subtractive genetic fate maps. *Neuron* 50(2):205-218.
- Fashena D, Westerfield M. 1999. Secondary motoneuron axons localize DM-GRASP on their fasciculated segments. *J Comp Neurol* 406(3):415-424.
- Fazeli A, Dickinson SL, Hermiston ML, Tighe RV, Steen RG, Small CG, Stoeckli ET, Keino-Masu K, Masu M, Rayburn H, Simons J, Bronson RT, Gordon JL, Tessier-Lavigne M, Weinberg RA. 1997. Phenotype of mice lacking functional Deleted in colorectal cancer (Dcc) gene. *Nature* 386(6627):796-804.
- Finger TE, Kanwal JS. 1992. Ascending general visceral pathways within the brainstems of two teleost fishes: *Ictalurus punctatus* and *Carassius auratus*. *J Comp Neurol* 320(4):509-520.
- Fink AJ, Englund C, Daza RA, Pham D, Lau C, Nivison M, Kowalczyk T, Hevner RF. 2006. Development of the deep cerebellar nuclei: transcription factors and cell migration from the rhombic lip. *J Neurosci* 26(11):3066-3076.
- Flinn L, Bretaud S, Lo C, Ingham PW, Bandmann O. 2008. Zebrafish as a new animal model for movement disorders. *J Neurochem* 106(5):1991-1997.
- Flinn L, Mortiboys H, Volkmann K, Köster RW, Ingham PW, Bandmann O. 2009. Complex I deficiency and dopaminergic neuronal cell loss in parkin-deficient zebrafish (*Danio rerio*). *Brain* 132(Pt 6):1613-1623.
- Folgueira M, Anadon R, Yanez J. 2003. Experimental study of the connections of the gustatory system in the rainbow trout, *Oncorhynchus mykiss*. *J Comp Neurol* 465(4):604-619.
- Folgueira M, Anadon R, Yanez J. 2006. Afferent and efferent connections of the cerebellum of a salmonid, the rainbow trout (*Oncorhynchus mykiss*): a tract-tracing study. *J Comp Neurol* 497(4):542-565.
- Folgueira M, Anadon R, Yanez J. 2008. The organization of the pretectal nuclei in the trout: a revision based on experimental hodological studies. *Brain Res Bull* 75(2-4):251-255.
- Foucher I, Mione M, Simeone A, Acampora D, Bally-Cuif L, Houart C. 2006. Differentiation of cerebellar cell identities in absence of Fgf signalling in zebrafish Otx morphants. *Development* 133(10):1891-1900.
- Fricke C, Chien CB. 2005. Cloning of full-length zebrafish dcc and expression analysis during embryonic and early larval development. *Dev Dyn* 234(3):732-739.
- Fünfschilling U, Reichardt LF. 2002. Cre-mediated recombination in rhombic lip derivatives. *Genesis* 33(4):160-169.
- Gad JM, Keeling SL, Wilks AF, Tan SS, Cooper HM. 1997. The expression patterns of guidance receptors, DCC and Neogenin, are spatially and temporally distinct throughout mouse embryogenesis. *Dev Biol* 192(2):258-273.
- Geisler S, Derst C, Veh RW, Zahm DS. 2007. Glutamatergic afferents of the ventral tegmental area in the rat. *J Neurosci* 27(21):5730-5743.
- Gilmour D, Knaut H, Maischein HM, Nusslein-Volhard C. 2004. Towing of sensory axons by their migrating target cells in vivo. *Nat Neurosci* 7(5):491-492.
- Gilthorpe JD, Papantoniou EK, Chedotal A, Lumsden A, Wingate RJ. 2002. The migration of cerebellar rhombic lip derivatives. *Development* 129(20):4719-4728.
- Grandel H, Kaslin J, Ganz J, Wenzel I, Brand M. 2006. Neural stem cells and neurogenesis in the adult zebrafish brain: origin, proliferation dynamics, migration and cell fate. *Dev Biol* 295(1):263-277.
- Grinblat Y, Gamse J, Patel M, Sive H. 1998. Determination of the zebrafish forebrain: induction and patterning. *Development* 125(22):4403-4416.
- Gutzman JH, Graeden EG, Lowery LA, Holley HS, Sive H. 2008. Formation of the zebrafish midbrain-hindbrain boundary constriction requires laminin-dependent basal constriction. *Mech Dev* 125(11-12):974-983.
- Gutzman JH, Sive H. 2010. Epithelial relaxation mediated by the myosin phosphatase regulator Mypt1 is required for brain ventricle lumen expansion and hindbrain morphogenesis. *Development* 137(5):795-804.
- Harrington MJ, Chalasani K, Brewster R. 2010. Cellular mechanisms of posterior neural tube morphogenesis in the zebrafish. *Dev Dyn* 239(3):747-762.
- Harris J, Moreno S, Shaw G, Mugnaini E. 1993. Unusual neurofilament composition in cerebellar unipolar brush neurons. *J Neurocytol* 22(12):1039-1059.
- Hatten ME. 1999. Central nervous system neuronal migration. *Annu Rev Neurosci* 22:511-539.
- Hatten ME, Alder J, Zimmerman K, Heintz N. 1997. Genes involved in cerebellar cell specification and differentiation. *Curr Opin Neurobiol* 7(1):40-47.

- Hatten ME, Mason CA. 1990. Mechanisms of glial-guided neuronal migration in vitro and in vivo. *Experientia* 46(9):907-916.
- He Z, Wang KC, Koprivica V, Ming G, Song HJ. 2002. Knowing how to navigate: mechanisms of semaphorin signaling in the nervous system. *Sci STKE* 2002(119):RE1.
- Higginbotham HR, Gleeson JG. 2007. The centrosome in neuronal development. *Trends Neurosci* 30(6):276-283.
- His W. 1891. Die Entwicklung des menschlichen Rautenhirns vom Ende des ersten bis zum Beginn des dritten Monats. I. Verlängertes Mark. *Abhandlungen der königlicher sachsische Gesellschaft der Wissenschaften, Mathematische-physikalische Klasse* 29:1-74.
- Hjorth JT, Gad J, Cooper H, Key B. 2001. A zebrafish homologue of deleted in colorectal cancer (zdcc) is expressed in the first neuronal clusters of the developing brain. *Mech Dev* 109(1):105-109.
- Holzschuh J, Ryu S, Aberger F, Driever W. 2001. Dopamine transporter expression distinguishes dopaminergic neurons from other catecholaminergic neurons in the developing zebrafish embryo. *Mech Dev* 101(1-2):237-243.
- Hong CC. 2009. Large-scale small-molecule screen using zebrafish embryos. *Methods Mol Biol* 486:43-55.
- Hong K, Hinck L, Nishiyama M, Poo MM, Tessier-Lavigne M, Stein E. 1999. A ligand-gated association between cytoplasmic domains of UNC5 and DCC family receptors converts netrin-induced growth cone attraction to repulsion. *Cell* 97(7):927-941.
- Hoshino M, Nakamura S, Mori K, Kawauchi T, Terao M, Nishimura YV, Fukuda A, Fuse T, Matsuo N, Sone M, Watanabe M, Bito H, Terashima T, Wright CV, Kawaguchi Y, Nakao K, Nabeshima Y. 2005. Ptf1a, a bHLH transcriptional gene, defines GABAergic neuronal fates in cerebellum. *Neuron* 47(2):201-213.
- Hutson LD, Chien CB. 2002. Pathfinding and error correction by retinal axons: the role of astray/robo2. *Neuron* 33(2):205-217.
- Ikenaga T, Yoshida M, Uematsu K. 2005. Morphology and immunohistochemistry of efferent neurons of the goldfish corpus cerebelli. *J Comp Neurol* 487(3):300-311.
- Imura K, Yamamoto N, Sawai N, Yoshimoto M, Yang CY, Xue HG, Ito H. 2003. Topographical organization of an indirect telencephalo-cerebellar pathway through the nucleus paracommissuralis in a teleost, *Oreochromis niloticus*. *Brain Behav Evol* 61(2):70-90.
- Ito H, Sakamoto N, Takatsuji K. 1982. Cytoarchitecture, fiber connections, and ultrastructure of nucleus isthmi in a teleost (*Navodon modestus*) with a special reference to degenerating isthmic afferents from optic tectum and nucleus pretectalis. *J Comp Neurol* 205(3):299-311.
- Itoh M, Chitnis AB. 2001. Expression of proneural and neurogenic genes in the zebrafish lateral line primordium correlates with selection of hair cell fate in neuromasts. *Mech Dev* 102(1-2):263-266.
- Jakab RL, Hamori J. 1988. Quantitative morphology and synaptology of cerebellar glomeruli in the rat. *Anat Embryol (Berl)* 179(1):81-88.
- Jones A, Bahn S, Grant AL, Kohler M, Wisden W. 1996. Characterization of a cerebellar granule cell-specific gene encoding the gamma-aminobutyric acid type A receptor alpha 6 subunit. *J Neurochem* 67(3):907-916.
- Jones BE, Beaudet A. 1987. Distribution of acetylcholine and catecholamine neurons in the cat brainstem: a choline acetyltransferase and tyrosine hydroxylase immunohistochemical study. *J Comp Neurol* 261(1):15-32.
- Kaslin J, Ganz J, Geffarth M, Grandel H, Hans S, Brand M. 2009. Stem cells in the adult zebrafish cerebellum: initiation and maintenance of a novel stem cell niche. *J Neurosci* 29(19):6142-6153.
- Kawakami K, Takeda H, Kawakami N, Kobayashi M, Matsuda N, Mishina M. 2004. A transposon-mediated gene trap approach identifies developmentally regulated genes in zebrafish. *Dev Cell* 7(1):133-144.
- Kawauchi T, Hoshino M. 2008. Molecular pathways regulating cytoskeletal organization and morphological changes in migrating neurons. *Dev Neurosci* 30(1-3):36-46.
- Kennedy TE, Serafini T, de la Torre JR, Tessier-Lavigne M. 1994. Netrins are diffusible chemotropic factors for commissural axons in the embryonic spinal cord. *Cell* 78(3):425-435.
- Kennedy TE, Wang H, Marshall W, Tessier-Lavigne M. 2006. Axon guidance by diffusible chemoattractants: a gradient of netrin protein in the developing spinal cord. *J Neurosci* 26(34):8866-8874.
- Kerjan G, Dolan J, Haumaitre C, Schneider-Maunoury S, Fujisawa H, Mitchell KJ, Chedotal A. 2005. The transmembrane semaphorin Sema6A controls cerebellar granule cell migration. *Nat Neurosci* 8(11):1516-1524.
- Kim CH, Bae YK, Yamanaka Y, Yamashita S, Shimizu T, Fujii R, Park HC, Yeo SY, Huh TL, Hibi M, Hirano T. 1997. Overexpression of neurogenin induces ectopic expression of HuC in zebrafish. *Neurosci Lett* 239(2-3):113-116.



- Kirby BB, Takada N, Latimer AJ, Shin J, Carney TJ, Kelsh RN, Appel B. 2006. In vivo time-lapse imaging shows dynamic oligodendrocyte progenitor behavior during zebrafish development. *Nat Neurosci* 9(12):1506-1511.
- Klein R. 2004. Eph/ephrin signaling in morphogenesis, neural development and plasticity. *Curr Opin Cell Biol* 16(5):580-589.
- Komuro H, Yacubova E, Yacubova E, Rakic P. 2001. Mode and tempo of tangential cell migration in the cerebellar external granular layer. *J Neurosci* 21(2):527-540.
- Kosodo Y, Toida K, Dubreuil V, Alexandre P, Schenk J, Kiyokage E, Attardo A, Mora-Bermudez F, Arai T, Clarke JD, Huttner WB. 2008. Cytokinesis of neuroepithelial cells can divide their basal process before anaphase. *EMBO J* 27(23):3151-3163.
- Köster RW, Fraser SE. 2001a. Direct imaging of in vivo neuronal migration in the developing cerebellum. *Curr Biol* 11(23):1858-1863.
- Köster RW, Fraser SE. 2001b. Tracing transgene expression in living zebrafish embryos. *Dev Biol* 233(2):329-346.
- Köster RW, Fraser SE. 2004. Time-lapse microscopy of brain development. *Methods Cell Biol* 76:207-235.
- Köster RW, Fraser SE. 2006. FGF signaling mediates regeneration of the differentiating cerebellum through repatterning of the anterior hindbrain and reinitiation of neuronal migration. *J Neurosci* 26(27):7293-7304.
- Kruger RP, Lee J, Li W, Guan KL. 2004. Mapping netrin receptor binding reveals domains of Unc5 regulating its tyrosine phosphorylation. *J Neurosci* 24(48):10826-10834.
- Lane PW, Bronson RT, Spencer CA. 1992. Rostral cerebellar malformation, (rcm): a new recessive mutation on chromosome 3 of the mouse. *J Hered* 83(4):315-318.
- Lauderdale JD, Davis NM, Kuwada JY. 1997. Axon tracts correlate with netrin-1a expression in the zebrafish embryo. *Mol Cell Neurosci* 9(4):293-313.
- Lekven AC, Buckles GR, Kostakis N, Moon RT. 2003. Wnt1 and wnt10b function redundantly at the zebrafish midbrain-hindbrain boundary. *Dev Biol* 254(2):172-187.
- Livesey FJ, Hunt SP. 1997. Netrin and netrin receptor expression in the embryonic mammalian nervous system suggests roles in retinal, striatal, nigral, and cerebellar development. *Mol Cell Neurosci* 8(6):417-429.
- Long Q, Meng A, Wang H, Jessen JR, Farrell MJ, Lin S. 1997. GATA-1 expression pattern can be recapitulated in living transgenic zebrafish using GFP reporter gene. *Development* 124(20):4105-4111.
- Luo J. 2005. The role of matrix metalloproteinases in the morphogenesis of the cerebellar cortex. *Cerebellum* 4(4):239-245.
- Ma LH, Punnamoottil B, Rinkwitz S, Baker R. 2009. Mosaic *hoxb4a* neuronal pleiotropism in zebrafish caudal hindbrain. *PLoS One* 4(6):e5944.
- Machold R, Fishell G. 2005. Math1 is expressed in temporally discrete pools of cerebellar rhombic-lip neural progenitors. *Neuron* 48(1):17-24.
- Marcos S, Backer S, Causeret F, Tessier-Lavigne M, Bloch-Gallego E. 2009. Differential roles of Netrin-1 and its receptor DCC in inferior olivary neuron migration. *Mol Cell Neurosci* 41(4):429-439.
- McClintock JM, Jozefowicz C, Assimacopoulos S, Grove EA, Louvi A, Prince VE. 2003. Conserved expression of *Hoxa1* in neurons at the ventral forebrain/midbrain boundary of vertebrates. *Dev Genes Evol* 213(8):399-406.
- McFarland KA, Topczewska JM, Weidinger G, Dorsky RI, Appel B. 2008. Hh and Wnt signaling regulate formation of olig2+ neurons in the zebrafish cerebellum. *Dev Biol* 318(1):162-171.
- McGraw HF, Nechiporuk A, Raible DW. 2008. Zebrafish dorsal root ganglia neural precursor cells adopt a glial fate in the absence of neurogenin1. *J Neurosci* 28(47):12558-12569.
- McLean DL, Fetcho JR. 2008. Using imaging and genetics in zebrafish to study developing spinal circuits in vivo. *Dev Neurobiol* 68(6):817-834.
- McLean DL, Fetcho JR. 2009. Spinal interneurons differentiate sequentially from those driving the fastest swimming movements in larval zebrafish to those driving the slowest ones. *J Neurosci* 29(43):13566-13577.
- Meek J, Yang JY, Han VZ, Bell CC. 2008. Morphological analysis of the mormyrid cerebellum using immunohistochemistry, with emphasis on the unusual neuronal organization of the valvula. *J Comp Neurol* 510(4):396-421.
- Mehlen P, Mazelin L. 2003. The dependence receptors DCC and UNC5H as a link between neuronal guidance and survival. *Biol Cell* 95(7):425-436.

- Metin C, Vallee RB, Rakic P, Bhide PG. 2008. Modes and mishaps of neuronal migration in the mammalian brain. *Journal of Neuroscience* 28:11746-11752.
- Millen KJ, Gleason JG. 2008. Cerebellar development and disease. *Curr Opin Neurobiol* 18(1):12-19.
- Mione M, Baldessari D, Deflorian G, Nappo G, Santoriello C. 2008. How neuronal migration contributes to the morphogenesis of the CNS: insights from the zebrafish. *Dev Neurosci* 30(1-3):65-81.
- Miyata T, Maeda T, Lee JE. 1999. NeuroD is required for differentiation of the granule cells in the cerebellum and hippocampus. *Genes Dev* 13(13):1647-1652.
- Moens CB, Donn TM, Wolf-Saxon ER, Ma TP. 2008. Reverse genetics in zebrafish by TILLING. *Brief Funct Genomic Proteomic* 7(6):454-459.
- Montgomery JC. 1981. Origin of the parallel fibers in the cerebellar crest overlying the intermediate nucleus of the elasmobranch hindbrain. *J Comp Neurol* 202(2):185-191.
- Mueller T, Vernier P, Wullmann MF. 2004. The adult central nervous cholinergic system of a neurogenetic model animal, the zebrafish *Danio rerio*. *Brain Res* 1011(2):156-169.
- Mueller T, Wullmann MF. 2002. BrdU-, neuroD (nrd)- and Hu-studies reveal unusual non-ventricular neurogenesis in the postembryonic zebrafish forebrain. *Mech Dev* 117(1-2):123-135.
- Mueller T, Wullmann MF. 2003. Anatomy of neurogenesis in the early zebrafish brain. *Brain Res Dev Brain Res* 140(1):137-155.
- Mufson EJ, Martin TL, Mash DC, Wainer BH, Mesulam MM. 1986. Cholinergic projections from the parabrachial nucleus (Ch8) to the superior colliculus in the mouse: a combined analysis of horseradish peroxidase transport and choline acetyltransferase immunohistochemistry. *Brain Res* 370(1):144-148.
- Mugnaini E, Floris A. 1994. The unipolar brush cell: a neglected neuron of the mammalian cerebellar cortex. *J Comp Neurol* 339(2):174-180.
- Neuhauss SC. 2003. Behavioral genetic approaches to visual system development and function in zebrafish. *J Neurobiol* 54(1):148-160.
- Nichols DH, Bruce LL. 2006. Migratory routes and fates of cells transcribing the Wnt-1 gene in the murine hindbrain. *Dev Dyn* 235(2):285-300.
- Nieuwenhuys R. 1967. Comparative anatomy of the cerebellum. *Prog Brain Res* 25:1-93.
- Nieuwenhuys R, Nicholson C. 1967. Cerebellum of mormyrids. *Nature* 215(5102):764-765.
- Nieuwenhuys R, Pouwels E, Smulders-Kersten E. 1974. The neuronal organization of cerebellar lobe C1 in the mormyrid fish *Gnathonemus petersii* (teleostei). *Z Anat Entwicklungsgesch* 144(3):315-336.
- Nomura T, Holmberg J, Frisen J, Osumi N. 2006. Pax6-dependent boundary defines alignment of migrating olfactory cortex neurons via the repulsive activity of ephrin A5. *Development* 133(7):1335-1345.
- Northmore DP. 1991. Visual responses of nucleus isthmi in a teleost fish (*Lepomis macrochirus*). *Vision Res* 31(3):525-535.
- Nunzi MG, Birnstiel S, Bhattacharyya BJ, Slater NT, Mugnaini E. 2001. Unipolar brush cells form a glutamatergic projection system within the mouse cerebellar cortex. *J Comp Neurol* 434(3):329-341.
- O'Rourke NA. 1996. Neuronal chain ganglia: homotypic contacts support migration into the olfactory bulb. *Neuron* 16(6):1061-1064.
- Ott H, Bastmeyer M, Stuermer CA. 1998. Neurodin, the goldfish homolog of DM-GRASP, is involved in retinal axon pathfinding to the optic disk. *J Neurosci* 18(9):3363-3372.
- Ott H, Diekmann H, Stuermer CA, Bastmeyer M. 2001. Function of Neurodin (DM-GRASP/SC-1) in guidance of motor axons during zebrafish development. *Dev Biol* 235(1):86-97.
- Perez SE, Yanez J, Marin O, Anadon R, Gonzalez A, Rodriguez-Moldes I. 2000. Distribution of choline acetyltransferase (ChAT) immunoreactivity in the brain of the adult trout and tract-tracing observations on the connections of the nuclei of the isthmus. *J Comp Neurol* 428(3):450-474.
- Piper M, Little M. 2003. Movement through Slits: cellular migration via the Slit family. *Bioessays* 25(1):32-38.
- Przyborski SA, Knowles BB, Ackerman SL. 1998. Embryonic phenotype of *Unc5h3* mutant mice suggests chemorepulsion during the formation of the rostral cerebellar boundary. *Development* 125(1):41-50.
- Puzdrowski RL. 1989. Peripheral distribution and central projections of the lateral-line nerves in goldfish, *Carassius auratus*. *Brain Behav Evol* 34(2):110-131.
- Rakic P. 1981. Neuron-glia interaction during brain development. *Trends Neurosci* 4:184-187.
- Rakic P. 1990. Principles of neural cell migration. *Experientia* 46(9):882-891.
- Reifers F, Bohli H, Walsh EC, Crossley PH, Stainier DY, Brand M. 1998. *Fgf8* is mutated in zebrafish acerebellar (*ace*) mutants and is required for maintenance of midbrain-hindbrain boundary development and somitogenesis. *Development* 125(13):2381-2395.

- Rhinn M, Lun K, Amores A, Yan YL, Postlethwait JH, Brand M. 2003. Cloning, expression and relationship of zebrafish *gbx1* and *gbx2* genes to Fgf signaling. *Mech Dev* 120(8):919-936.
- Rieger S, Senghaas N, Walch A, Köster RW. 2009. Cadherin-2 controls directional chain migration of cerebellar granule neurons. *PLoS Biol* 7(11):e1000240.
- Rieger S, Volkmann K, Köster RW. 2008. Polysialyltransferase expression is linked to neuronal migration in the developing and adult zebrafish. *Dev Dyn* 237(1):276-285.
- Rink E, Wullmann MF. 2001. The teleostean (zebrafish) dopaminergic system ascending to the subpallium (striatum) is located in the basal diencephalon (posterior tuberculum). *Brain Res* 889(1-2):316-330.
- Rink E, Wullmann MF. 2002. Development of the catecholaminergic system in the early zebrafish brain: an immunohistochemical study. *Brain Res Dev Brain Res* 137(1):89-100.
- Rink E, Wullmann MF. 2004. Connections of the ventral telencephalon (subpallium) in the zebrafish (*Danio rerio*). *Brain Res* 1011(2):206-220.
- Rodriguez CI, Dymecki SM. 2000. Origin of the precerebellar system. *Neuron* 27(3):475-486.
- Ruggiero DA, Giuliano R, Anwar M, Stornetta R, Reis DJ. 1990. Anatomical substrates of cholinergic-autonomic regulation in the rat. *J Comp Neurol* 292(1):1-53.
- Rutishauser U. 2008. Polysialic acid in the plasticity of the developing and adult vertebrate nervous system. *Nat Rev Neurosci* 9(1):26-35.
- Ryder EF, Cepko CL. 1994. Migration patterns of clonally related granule cells and their progenitors in the developing chick cerebellum. *Neuron* 12(5):1011-1028.
- Sakamoto N, Ito H, Ueda S. 1981. Topographic projections between the nucleus isthmi and the optic tectum in a teleost. *Navodon modestus*. *Brain Res* 224(2):225-234.
- Sansom SN, Livesey FJ. 2009. Gradients in the brain: the control of the development of form and function in the cerebral cortex. *Cold Spring Harbor Perspect Biol* 1(2):a002519.
- Saper CB. 2002. The central autonomic nervous system: conscious visceral perception and autonomic pattern generation. *Annu Rev Neurosci* 25:433-469.
- Saper CB, Loewy AD. 1980. Efferent connections of the parabrachial nucleus in the rat. *Brain Res* 197(2):291-317.
- Schier AF, Talbot WS. 2005. Molecular genetics of axis formation in zebrafish. *Annu Rev Genet* 39:561-613.
- Schüller U, Kho AT, Zhao Q, Ma Q, Rowitch DH. 2006. Cerebellar 'transcriptome' reveals cell-type and stage-specific expression during postnatal development and tumorigenesis. *Mol Cell Neurosci* 33(3):247-259.
- Scott EK, Mason L, Arrenberg AB, Ziv L, Gosse NJ, Xiao T, Chi NC, Asakawa K, Kawakami K, Baier H. 2007. Targeting neural circuitry in zebrafish using GAL4 enhancer trapping. *Nat Methods* 4(4):323-326.
- Serafini T, Colamarino SA, Leonardo ED, Wang H, Beddington R, Skarnes WC, Tessier-Lavigne M. 1996. Netrin-1 is required for commissural axon guidance in the developing vertebrate nervous system. *Cell* 87(6):1001-1014.
- Sgaier SK, Lao Z, Villanueva MP, Berenshteyn F, Stephen D, Turnbull RK, Joyner AL. 2007. Genetic subdivision of the tectum and cerebellum into functionally related regions based on differential sensitivity to engrailed proteins. *Development* 134(12):2325-2335.
- Sgaier SK, Millet S, Villanueva MP, Berenshteyn F, Song C, Joyner AL. 2005. Morphogenetic and cellular movements that shape the mouse cerebellum; insights from genetic fate mapping. *Neuron* 45(1):27-40.
- Shen H, Illges H, Reuter A, Stuermer CA. 2002. Cloning, expression, and alternative splicing of *neogenin1* in zebrafish. *Mech Dev* 118(1-2):219-223.
- Skonier JE, Bowen MA, Aruffo A, Bajorath J. 1997. CD6 recognizes the neural adhesion molecule BEN. *Protein Sci* 6(8):1768-1770.
- Stein E, Zou Y, Poo M, Tessier-Lavigne M. 2001. Binding of DCC by netrin-1 to mediate axon guidance independent of adenosine A2B receptor activation. *Science* 291(5510):1976-1982.
- Strahle U, Fischer N, Blader P. 1997. Expression and regulation of a netrin homologue in the zebrafish embryo. *Mech Dev* 62(2):147-160.
- Striedter GF, Northcutt RG. 1989. Two distinct visual pathways through the superficial pretectum in a percomorph teleost. *J Comp Neurol* 283(3):342-354.
- Suli A, Mortimer N, Shepherd I, Chien CB. 2006. Netrin/DCC signaling controls contralateral dendrites of octavolateralis efferent neurons. *J Neurosci* 26(51):13328-13337.
- Suzuki SC, Takeichi M. 2008. Cadherins in neuronal morphogenesis and function. *Dev Growth Differ* 50 Suppl 1:S119-130.

- Swart GW, Lunter PC, Kilsdonk JW, Kempen LC. 2005. Activated leukocyte cell adhesion molecule (ALCAM/CD166): signaling at the divide of melanoma cell clustering and cell migration? *Cancer Metastasis Rev* 24(2):223-236.
- Tago H, McGeer PL, McGeer EG, Akiyama H, Hersh LB. 1989. Distribution of choline acetyltransferase immunopositive structures in the rat brainstem. *Brain Res* 495(2):271-297.
- Tiveron MC, Cremer H. 2008. CXCL12/CXCR4 signalling in neuronal cell migration. *Curr Opin Neurobiol* 18(3):237-244.
- Trevarrow B, Marks DL, Kimmel CB. 1990. Organization of hindbrain segments in the zebrafish embryo. *Neuron* 4(5):669-679.
- Vinogradova VM, Manteifel' lu B. 1977. [Responses of neurons in the nucleus isthmi region of the frog to optic nerve stimulation]. *Neirofiziologija* 9(1):33-40.
- Volkman K, Chen YY, Harris MP, Wullmann MF, Koster RW. 2010. The zebrafish cerebellar upper rhombic lip generates tegmental hindbrain nuclei by long-distance migration in an evolutionary conserved manner. *J Comp Neurol* 518(14):2794-2817.
- Volkman K, Köster RW. 2007. In Vivo Retrograde Labeling of Neurons in the Zebrafish Embryo or Larva with Rhodamine Dextran. *CSH Protocols* doi:10.1101/pdb.prot4832.
- Volkman K, Rieger S, Babaryka A, Köster RW. 2008. The zebrafish cerebellar rhombic lip is spatially patterned in producing granule cell populations of different functional compartments. *Dev Biol* 313(1):167-180.
- Wang VY, Rose MF, Zoghbi HY. 2005. Math1 expression redefines the rhombic lip derivatives and reveals novel lineages within the brainstem and cerebellum. *Neuron* 48(1):31-43.
- Wilson LJ, Wingate RJ. 2006. Temporal identity transition in the avian cerebellar rhombic lip. *Dev Biol* 297(2):508-521.
- Wingate R. 2005. Math-Map(ic)s. *Neuron* 48(1):1-4.
- Woods IG, Schier AF. 2008. Targeted mutagenesis in zebrafish. *Nat Biotechnol* 26(6):650-651.
- Wolf NJ. 1991. Cholinergic systems in mammalian brain and spinal cord. *Prog Neurobiol* 37(6):475-524.
- Wullmann MF, Knipp S. 2000. Proliferation pattern changes in the zebrafish brain from embryonic through early postembryonic stages. *Anat Embryol (Berl)* 202(5):385-400.
- Wullmann MF, Meyer DL. 1993. Possible multiple evolution of indirect telencephalo-cerebellar pathways in teleosts: studies in *Carassius auratus* and *Pantodon buchholzi*. *Cell Tiss Res* 274:447-455.
- Wullmann MF, Northcutt RG. 1988. Connections of the corpus cerebelli in the green sunfish and the common goldfish: a comparison of perciform and cypriniform teleosts. *Brain Behav Evol* 32(5):293-316.
- Wullmann MF, Rupp B, Reichert H. 1996. *Neuroanatomy of the zebrafish brain*. CH-4010 Basel: Switzerland: Birkhaeuser Verlag.
- Xue HG, Yamamoto N, Yoshimoto M, Yang CY, Ito H. 2001. Fiber connections of the nucleus isthmi in the carp (*Cyprinus carpio*) and tilapia (*Oreochromis niloticus*). *Brain Behav Evol* 58(4):185-204.
- Yang CY, Yoshimoto M, Xue HG, Yamamoto N, Imura K, Sawai N, Ishikawa Y, Ito H. 2004. Fiber connections of the lateral valvular nucleus in a percomorph teleost, tilapia (*Oreochromis niloticus*). *J Comp Neurol* 474(2):209-226.
- Yasui Y, Saper CB, Cechetto DF. 1989. Calcitonin gene-related peptide immunoreactivity in the visceral sensory cortex, thalamus, and related pathways in the rat. *J Comp Neurol* 290(4):487-501.
- Yee KT, Simon HH, Tessier-Lavigne M, O'Leary DM. 1999. Extension of long leading processes and neuronal migration in the mammalian brain directed by the chemoattractant netrin-1. *Neuron* 24(3):607-622.
- Yokogawa T, Marin W, Faraco J, Pezeron G, Appelbaum L, Zhang J, Rosa F, Mourrain P, Mignot E. 2007. Characterization of sleep in zebrafish and insomnia in hypocretin receptor mutants. *PLoS Biol* 5(10):2379-2397.
- Zecchin E, Mavropoulos A, Devos N, Filippi A, Tiso N, Meyer D, Peers B, Bortolussi M, Argenton F. 2004. Evolutionary conserved role of ptf1a in the specification of exocrine pancreatic fates. *Dev Biol* 268(1):174-184.
- Zottoli SJ, Rhodes KJ, Corrodi JG, Mufson EJ. 1988. Putative cholinergic projections from the nucleus isthmi and the nucleus reticularis mesencephali to the optic tectum in the goldfish (*Carassius auratus*). *J Comp Neurol* 273(3):385-398.
- Zupanc GK. 2006. Neurogenesis and neuronal regeneration in the adult fish brain. *J Comp Physiol A Neuroethol Sens Neural Behav Physiol* 192(6):649-670.
- Zupanc GK, Hinsch K, Gage FH. 2005. Proliferation, migration, neuronal differentiation, and long-term survival of new cells in the adult zebrafish brain. *J Comp Neurol* 488(3):290-319.

## **9 Appendices**



## Appendix 1

Article in **The Journal of Comparative Neurology**

### **The Zebrafish Cerebellar Upper Rhombic Lip Generates Tegmental Hindbrain Nuclei by Long-Distance Migration in an Evolutionary Conserved Manner**

Katrin Volkmann, Yi-Yen Chen, Matthew P. Harris, Mario F.  
Wullimann, and Reinhard W. Köster

The Journal of Comparative Neurology 518: 2794-2817 (2010)

#### **Contribution**

The stable transgenic *wnt1-GVP-UG* zebrafish strain was generated by Yi-Yen Chen under supervision of Matthew P. Harris. I conducted all other experiments (control experiments for of the anti-Calretinin and anti-ChAT antibody and sense *in situ* probes were performed by Enrico Kühn) and the analysis of the data shown in this manuscript. I also designed all Figures except for Figure 1 and wrote the first version of the manuscript independently and subsequently revised the changes suggested by the co-authors. Mario F. Wullimann contributed especially to some paragraphs of Introduction and Discussion, designed Figure 1 and reviewed the manuscript.

# The Zebrafish Cerebellar Upper Rhombic Lip Generates Tegmental Hindbrain Nuclei by Long-Distance Migration in an Evolutionary Conserved Manner

Katrin Volkmann,<sup>1</sup> Yi-Yen Chen,<sup>2</sup> Matthew P. Harris,<sup>2</sup> Mario F. Wullmann,<sup>3</sup> and Reinhard W. Köster<sup>1\*</sup>

<sup>1</sup>Helmholtz Zentrum München, German Research Center for Environmental Health, Institute of Developmental Genetics, 85764 Neuherberg-Munich, Germany

<sup>2</sup>Department of Genetics, Max-Planck-Institute for Developmental Biology, 72076 Tübingen, Germany

<sup>3</sup>Department of Biology II, Graduate School of Systemic Neurosciences, Ludwig-Maximilians-University Munich, 82152 Planegg-Martinsried, Germany

## ABSTRACT

The upper rhombic lip (URL) of the developing mammalian cerebellum produces different neuronal cell types in a temporal sequence. The first neuronal populations arising from this proliferation zone include the progenitors of the parabrachial, parabigeminal, and laterodorsal-pedunculopontine tegmental hindbrain nuclei. By means of expression analysis, histology, and retrograde neuronal tracing, we have identified the zebrafish homologues of these nuclei, namely, the secondary gustatory/viscerosensory nucleus, the nucleus isthmi, and the superior reticular nucleus, respectively, in the embryonic and larval brain of a stable transgenic *wnt1:Gal4-VP16-14 × UAS:GFP* zebrafish strain. Combining time-lapse confocal imaging with individual cell tracing, we characterize the migratory behavior of these neuronal precursor populations in detail by revealing their migration path, velocity, and directionality. In addition, we identify neuronal progenitors of the secondary

gustatory/viscerosensory nucleus and nucleus isthmi/superior reticular nucleus as belonging to the polysialic acid (PSA)-expressing cell population in the cerebellar plate that migrates in a PSA-dependent manner. Finally, we reveal that circuitries involved in the processing of sensory information (visual, gustatory, general viscerosensory) are already established in the zebrafish larva at day 4 of development. Also the *wnt1*-expressing pre-tectal neuronal precursors (not originating from the URL) sending mossy fiber-like projections into the cerebellar corpus are established at that time. In sum, our results show that the origin of neurons of some tegmental hindbrain nuclei, namely, nucleus isthmi/superior reticular nucleus and secondary gustatory/viscerosensory nucleus is in the URL, and that the temporal order of cell types produced by the URL and their developmental program are conserved among vertebrate species. *J. Comp. Neurol.* 518:2794–2817, 2010.

© 2010 Wiley-Liss, Inc.

**INDEXING TERMS:** zebrafish; neuronal migration; cell tracing; cerebellum; upper rhombic lip (URL); bioimaging; secondary gustatory nucleus (SGN); secondary viscerosensory nucleus (SVN); nucleus isthmi (NI); superior reticular nucleus (SRN); parabrachial nuclear complex; parabigeminal nucleus (PBG); laterodorsal-pedunculopontine complex; paracommissural nucleus (PC); dorsal periventricular pre-tectal nucleus (PP)

Additional Supporting Information may be found in the online version of this article.

Grant sponsor: German Ministry for Education and Research (BMBF); Grant number: BioFuture Award 0311889; Grant sponsor: European Commission Coordination Action ENINET; Grant number: LSHM-CT-2005-19063; Grant sponsor: Graduate School for Systemic Neurosciences of the Ludwig-Maximilians-University Munich (to M.W.F.).

\*CORRESPONDENCE TO: Reinhard W. Köster, Helmholtz Zentrum München, German Research Center for Environmental Health, Institute of

Developmental Genetics, Ingolstädter Landstraße 1, 85764 Neuherberg-Munich, Germany. E-mail: reinhard.koester@helmholtz-muenchen.de

Received December 22, 2009; Revised January 31, 2010; Accepted February 12, 2010

DOI 10.1002/cne.22364

Published online March 23, 2010 in Wiley InterScience (www.interscience.wiley.com)



The dorsalmost portion of the proliferative neuroepithelium lining the fourth ventricle of the hindbrain is termed the *rhombic lip*. It includes an anteriormost cerebellar part, the upper rhombic lip (URL; also termed *cerebellar or rostral rhombic lip*; Machold and Fishell, 2005; Wang et al., 2005), which is represented by transversely oriented paired ventricular proliferation zones in the dorsal cerebellar plate (CeP; for zebrafish, compare Wullimann and Knipp, 2000; Fig. 1A). The second part of the rhombic lip runs longitudinally along the rim of the rhombic fossa and is termed *caudal* (also called *lower or hindbrain*) *rhombic lip* (Fig. 1A). Recent fate mapping studies in the mouse have revealed that the URL produces different neuronal cell types in a specific temporal sequence: starting with tegmental nuclei (parabigeminal, laterodorsal tegmental, pedunculopontine tegmental, microcellular tegmental, lateral parabrachial), followed by deep cerebellar nuclei and, finally, cerebellar granule cells (Machold and Fishell, 2005; Wang et al., 2005). Furthermore, the early migratory progenitor populations of the tegmental nuclei were found to express *wnt1* inside the cerebellar rhombic lip, among them cells of the later parabrachial nuclear complex (Nichols and Bruce, 2006).

The tegmental nuclei that arise early from the upper rhombic lip in the mouse include in the caudal portion of the mesencephalic tegmentum the laterodorsal-pedunculopontine tegmental nuclei, which represent the brainstem cholinergic ascending system innervating mostly diencephalic and mesencephalic targets, but also the basal telencephalon. Also located in this area is the parabigeminal nucleus, which has reciprocal connections with the superior colliculus and also contains excitatory cholinergic neurons (Mufson et al., 1986; Tago et al., 1989; Woolf, 1991). The parabrachial nuclear complex is a secondary relay area for ascending information from the primary viscerosensory (including gustatory) nucleus solitarius, to the thalamus, but also to the amygdala, hypothalamus, and cerebral cortex (Saper and Loewy, 1980). This parabrachial nuclear complex also includes partially cholinergic neurons (Jones and Beaudet, 1987; Tago et al., 1989).

The homologues of the mammalian parabrachial nuclear complex in teleost fish are the secondary gustatory nucleus (SGN) and the secondary viscerosensory nucleus (SVN; Herrick, 1905; Finger and Kanwal, 1992; see also Discussion). These nuclei are located in the hindbrain tegmentum of rhombomere 1 close to the valvula cerebelli, with the nucleus lateralis valvulae (NLV) rostrally adjacent to them. The secondary gustatory nuclei of both brain halves are connected in all teleosts by a commissure, which is especially broad in cyprinids (Morita et al., 1980, 1983), including zebrafish (Wullimann and Reichert, 1996). The cyprinid secondary general viscerosensory nu-

cleus (SVN) is a cholinergic cell group directly ventrally adjacent to the secondary gustatory nucleus (Finger and Kanwal, 1992; see also Discussion). The secondary gustatory nucleus and likely also the viscerosensory nucleus neurons send axons into the preglomerular tertiary gustatory nucleus (TGN) and the inferior lobe of the hypothalamus in the diencephalon (Rink and Wullimann, 1998; Figueira et al., 2003). Similar to the parabrachial nuclear complex in mammals, the secondary viscerosensory (and maybe partially the secondary gustatory) nucleus of the adult zebrafish brain contains cholinergic neurons (Ahrens and Wullimann, 2002; Mueller et al., 2004; Castro et al., 2006; Fig. 1B).

The teleostean nucleus isthmi is thought to be the homologue of the parabigeminal nucleus in mammals (Clark, 1933; Sakamoto et al., 1981; Ito et al., 1982). It is located in the tegmentum of rhombomere 1 close to the secondary gustatory/viscerosensory nucleus (Fig. 1B,C), but it projects to and receives excitatory visual input from the ipsilateral optic tectum and the parvocellular and/or magnocellular superficial pretectal nucleus (Vinogradova and Manteifel'lu, 1977; Striedter and Northcutt, 1989; Northmore, 1991; Xue et al., 2001). Many nucleus isthmi neurons are cholinergic (Clemente et al., 2004; Mueller et al., 2004; Fig. 1B). Teleosts furthermore possess in the isthmic region a cholinergic projection nucleus, the superior reticular nucleus, likely corresponding to the laterodorsal-pedunculopontine complex of mammals (Mueller et al., 2004; Fig. 1B).

Another very large nucleus that populates the teleost tegmental hindbrain region of rhombomere 1 is the nucleus lateralis valvulae (NLV). This nucleus and the valvula cerebelli have no known homologues in mammals (Wullimann and Meyer, 1993). The nucleus lateralis valvulae is positioned adjacent to the valvula cerebelli and rostrally to the secondary gustatory nucleus, and it forms a very prominent projection into the corpus cerebelli and the valvula cerebelli (Wullimann and Northcutt, 1988, 1989; Ito and Yoshimoto, 1990; Xue et al., 2004; Yang et al., 2004; Figueira et al., 2006). Whether neurons of the mature nucleus lateralis valvulae in zebrafish are partially cholinergic like the secondary gustatory nucleus and nucleus isthmi neurons is a matter of debate (Clemente et al., 2004; Mueller et al., 2004; Castro et al., 2006; Yokogawa et al., 2007). These four nuclei, that is, the secondary gustatory/viscerosensory nucleus, nucleus isthmi, superior reticular nucleus, and nucleus lateralis valvulae, can be identified in the adult zebrafish brain based on their position, projections, and neurotransmitter identity. However, their origin, developmental time course, and differentiation have remained unknown. These questions are of particular interest, though, for the clarification of the evolutionary conservation of the

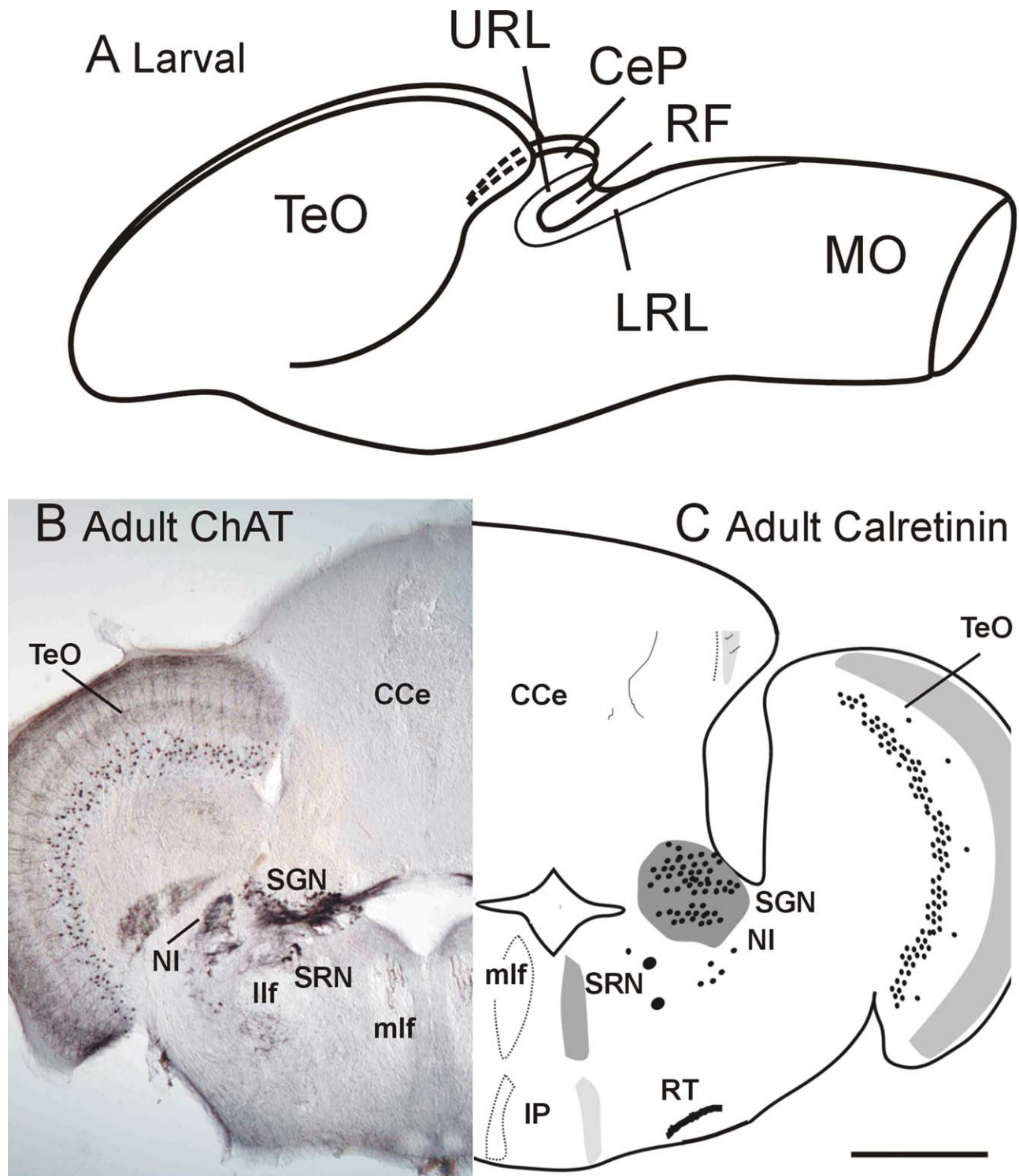


**Figure 1.** Overview of rhombic lip in the zebrafish larva and cholinergic and calretinin-positive systems at the isthmus of the adult zebrafish brain. **A:** Sketch of larval zebrafish midbrain and hindbrain showing the position of the upper and lower rhombic lip. **B:** Distribution of cholinergic systems at isthmus level (Reprinted from *Brain Research*, Vol. 1011: Thomas Mueller, Philippe Vernier and Mario F. Wullmann, the adult central nervous cholinergic system of a neurogenetic model animal, the zebrafish *Danio rerio*, pages 156–169, 2004, by permission of Elsevier). **C:** Distribution of calretinin-positive systems at isthmus levels (slightly adapted from *Journal of Comparative Neurology*, Vol. 494: Antonio Castro, Manuela Becerra, María Jesús Manso, and Ramón Anadón, calretinin immunoreactivity in the brain of the zebrafish, *Danio rerio*: distribution and comparison with some neuropeptides and neurotransmitter-synthesizing enzymes. II. Midbrain, hindbrain, and rostral spinal cord, pages 792–814, 2006, by permission of John Wiley & Sons). CCe, corpus cerebelli; CeP, cerebellar plate; IP, interpeduncular nucleus; llf, lateral longitudinal fascicle; LRL, lower rhombic lip; mlf, medial longitudinal fascicle; MO, medulla oblongata; NI, nucleus isthmi; RF, reticular formation; RT, raphe tract; SGN, secondary gustatory nucleus; SRN, superior reticular nucleus; TeO, optic tectum; URL, upper rhombic lip. Scale bar = 250  $\mu\text{m}$ . [Color figure can be viewed in the online issue, which is available at [www.interscience.wiley.com](http://www.interscience.wiley.com).]

cerebellar rhombic lip in producing a sequence of specific neuronal populations.

Previous fate-mapping studies in the mouse have identified various derivatives of the URL, including the early parabrachial nucleus, parabigeminal nucleus, and latero-dorsal-pedunculo-pontine tegmental populations, but the migratory behavior of these early URL-derived neuronal populations that leave the cerebellum has remained unclear (Machold and Fishell, 2005; Wang et al., 2005). The nearly transparent embryos of the teleost zebrafish offer the possibility for in vivo analysis of brain development with help of time-lapse imaging (Köster and Fraser, 2001a; Mione et al., 2008; Rieger et al., 2008; Volkman et al., 2008). We therefore sought to characterize the migratory behavior of early URL-derived neuronal populations and to reveal their fate. In zebrafish, cerebellar granule cell migration from the URL does not start before 48 hours postfertilization (hpf; Volkman et al., 2008). Intriguingly, in transient transgenic labeling experiments, migration from the zebrafish URL was reported to start already at about 24 hpf (Köster and Fraser, 2001a), suggesting that, similarly to the case in mammals, the zebrafish URL produces different cell types over time. Recent in vivo studies showed that, in this early-arising neuronal population, migratory motility is regulated by the expression of polysialic acid (PSA), a steric modifier of the neuronal cell adhesion molecule (NCAM; Rieger et al., 2008). However, the identity of these early precursor populations arising between 24 hpf and 48 hpf has remained unclear. Based on their early origin, though, they represent good candidates for progenitors of the URL-derived tegmental hindbrain nuclei, such as the secondary gustatory/viscerosensory nucleus, the nucleus isthmi, and the superior reticular nucleus.

## MATERIALS AND METHODS

### Maintenance of fish

Raising, spawning, and maintaining of zebrafish lines were performed as described previously (Kimmel et al., 1995; Westerfield, 1995). For simplification purposes, stable transgenic *wnt1:Gal4-VP16-14* × *UAS-GFP* embryos and juvenile fish will be called *wnt1-GVP-UG* throughout this paper. For mosaic labeling of migrating neuronal precursors in zebrafish embryos, plasmid DNA injection was carried out as described previously (Köster and Fraser, 2001b) using a 5 × *UASE1b:mCherry* expression construct.

### Generation of the *wnt1-GVP-UG* strain

A 6.6-kb upstream promoter and a 6.7 kb-downstream enhancer of the *wnt1* coding region were obtained by using the primers 5'-ACCTCACGCAATAGCACACTG-3',

5'-GGTAAGCACTGGCTCTCCTG-3', and 5'-GTTCTCAGCTC TTGCCCTGGAGGAGT-3', 5'-ATTAAGTCTCGCTTTGTCCCG CATCC-3', respectively, with zebrafish BAC zk166N8 as a template for genomic DNA surrounding the *wnt1* locus. The promoter and enhancer fragments were cloned 5' and 3' of the Gal4-VP16 ORF, respectively, within a Gal4-VP16pA-14 × *UASE1b-EGFPpA* reporter construct (Köster and Fraser, 2001b). The construct was linearized by the restriction enzyme I-SceI and injected into one-cell-stage embryos as described previously (Köster and Fraser, 2001b).

### In situ hybridization and immunohistochemistry

For mRNA in situ hybridization, embryos and larvae were fixed in 4% paraformaldehyde in phosphate-buffered saline (PBS; pH 7.4) containing 0.1% Tween 20 (Sigma, St. Louis, MO) overnight at 4°C. The in situ hybridization procedure was carried out as described previously (Westerfield, 1995; Köster and Fraser, 2006; Volkman et al., 2008). Complementary RNA probes were labeled with digoxigenin (Roche, Penzberg, Germany), which was detected by antidigoxigenin antibody conjugated with alkaline phosphatase (AP; 1:2,000; Roche). NBT/BCIP (Roche) was used as substrate for the AP.

The following probes for in situ hybridization were used in this study: *atona1a* (accession No. AF024536; bp 1–938; Kim et al., 1997), *calretinin* (accession No. BC059467; bp 76–882), *eomes* (accession No. AF 287 007; bp 1–2450; Mione et al., 2001), *ptf1a* (accession No. NM\_207641; bp 1–1211; Zecchin et al., 2004), *reelin* (accession No. AF427524; bp 1–3238; Costagli et al., 2002), *tbr1* (accession No. AF287006; bp 1–2218; Mione et al., 2001), and *vglut2.1* (accession No. AB183386; bp 939–1889; Higashijima et al., 2004). As control, the in situ hybridization procedure was performed with sense probes showing no signal.

Three different anti-GFP antibodies were employed to detect GFP expression. After in situ hybridization, a rabbit anti-GFP antibody was used [1:500; Torrey Pines Biolabs, Houston, TX; detected with Cy2-conjugated anti-rabbit IgG antibody (1:200; Jackson ImmunoResearch, West Grove, PA)]; for double antibody stainings, a monoclonal mouse anti-GFP [1:500; Molecular Probes, Eugene, OR; detected with anti-mouse Alexa Fluor 488 antibody (1:200; Molecular Probes)] or a polyclonal chicken anti-GFP antibody [1:500; Aves Labs, Inc., Tigard, OR; detected with a donkey anti-chicken FITC conjugated antibody (1:100; Jackson ImmunoResearch)] was used.

Further antibodies used were monoclonal mouse anti-zn-8 antibody [1:50; Developmental Studies Hybridoma Bank; detected with goat anti-mouse Alexa 546 (1:200;

Molecular Probes)], antiphosphohistone H3 (PH3) antibody [06-570; 1:200; Upstate Biotechnology, Lake Placid, NY; detected with anti-rabbit Cy5-conjugated antibody (1:200; Jackson ImmunoResearch)], monoclonal mouse anti-PSA antibody [1:750; (Marx et al., 2001); detected with anti-mouse IgG-Alexa 546 antibody (1:200; Molecular Probes)], polyclonal rabbit anti-calretinin [1:250; Chemicon International, Temecula, CA; detected with a anti-rabbit Cy5-conjugated antibody (1:200; Jackson ImmunoResearch)], and polyclonal goat anti-choline acetyltransferase (ChAT) antibody [1:100; Chemicon International; detected with a donkey anti-goat Alexa 546 (1:100; Invitrogen, San Diego, CA)].

For immunohistochemistry, larvae were fixed in 4% paraformaldehyde in PBS containing 0.1% Tween 20 overnight at 4°C. The specimens were washed out of the fixative with the following washing solutions: PBS containing 0.1% Tween 20 (PH3; PSA), PBS containing 0.1% Tween 20, 1% DMSO (Sigma; zn8), or PBS 0.2% Triton X-100 (Sigma; ChAT) five times for 5 minutes each. For zn8, PH3, and PSA antibody stainings, the tissue was permeabilized by dehydration with 100% methanol for 5 minutes, and, after exchange with fresh 100% methanol, it was stored overnight (o/n) or long term at -20°C. For better penetration, the larvae were transferred directly from 100% methanol into -20°C cold 100% acetone for 7 minutes, followed by deionized water for 5 minutes, 5 minutes PBS, and two 5-minute washes with in PBS containing 0.1% Tween 20. In the case of ChAT and calretinin immunohistochemistry, the larvae were soaked in 20% sucrose solution in PBS for at least 1 hour to up to 1 day, mounted in TissueTek OCT medium (Sakura, Torrance, CA), and cryosectioned with a cryostat (Microm, HM 560, Walldorf, Germany) to slices of 20 µm thickness prior to blocking and antibody incubation. Before blocking, the sections used for calretinin immunohistochemistry additionally were treated for 2 × 5 minutes with PBS, 10 minutes with dH<sub>2</sub>O, and 10 minutes with 10 mM NaCitrate, pH 6, at 95°C for epitope unmasking; after cooling to room temperature (RT), the sections were washed twice with PBS. For blocking, specimens were incubated for 1 hour in 10% normal goat serum (NGS) in PBS containing 0.1% Tween 20 at room temperature; for zn8 detection, 1% dimethyl sulfoxide (DMSO) was added to the blocking solution. The cryosections for ChAT immunohistochemistry were blocked with 5% BSA in PBS containing 0.2% Triton X-100. The specimens were incubated with the primary antibodies diluted in their blocking solutions o/n at 4°C. The whole-mount embryos and larvae were washed for 5 × 15 minutes and the cryosections for 3 × 30 minutes at room temperature (ChAT, calretinin) in their washing solutions. The secondary antibodies were diluted in blocking solution, and the specimens were incu-

bated with the antibody solution o/n at 4°C and washed as described above.

For preparation of vibratome sections after in situ hybridization, immunohistochemistry or GFP expression analysis samples were mounted in 4% agarose (Sigma), 1× PBS and sectioned on a vibratome (Microm HM 650 V) into slices of 30–50 µm thickness.

### Antibody characterization

In the present study, we used three independent antibodies for GFP, two polyclonal antibodies raised in rabbit and chicken and one monoclonal antibody. All three antibodies showed an identical staining pattern when used on the transgenic zebrafish embryos or larvae. In addition, the staining pattern for all three anti-GFP antibodies was identical to the intrinsic fluorescence by the GFP protein. As a control, siblings not carrying the construct, indicated by the lack of green fluorescence before and after fixation, did not show any staining.

The antibody against neurolin was tested on Western blots of zebrafish embryo extracts and recognized a single band of 75 kD (Fashena and Westerfield, 1999). As a control, there was no band on the lane with no primary antibody. In addition, a polyclonal antibody raised against recombinant neurolin protein tested on Western blots recognized a band of the same size, confirming that that the zn-5 antibody detects the neurolin protein (Fashena and Westerfield, 1999).

The anti-phosphohistone H3 (PH3) antibody stains a single band of 17 kD molecular weight on Western blot with HeLa cell protein extracts (manufacturer's technical information). In our hands, the antiserum gave positive chromosome staining in mitotic zebrafish cells identified by DNA counterstaining with DAPI.

The anti-PSA antibody recognized a broad band between 120 and 240 kD on Western blots with zebrafish brain membranes. This band disappeared completely when the membranes were treated with the PSA-degrading enzyme Endo N before electrophoresis (Marx et al., 2001). In addition, PSA immunoreactivity in the hindbrain was abolished in embryos injected with Endo N into the hindbrain ventricle compared with control embryos injected with PBS (Rieger et al., 2008).

The staining pattern detected by the anti-calretinin antibody at 4 dpf was similar to the *calretinin* mRNA expression detected by in situ hybridization at 3 dpf (data not shown). In addition, expression vectors containing the cDNAs for GFP as control or zebrafish calretinin were transfected in 293 cells and lysates were analyzed by Western blot analysis with the anti-calretinin antibody used in this study. A single band for zebrafish calretinin of 31 kD was detected in the lysate of zebrafish calretinin-transfected cells only.

The anti-choline acetyltransferase (ChAT) antibody used in this study has been used before in several studies with zebrafish, and the staining pattern observed was similar to the expression reported previously for the larval (Arenzana et al., 2005) and adult zebrafish brain (Clemente et al., 2004, 2005; Mueller et al., 2004). In addition, expression vectors containing the cDNAs for GFP as control or zebrafish ChAT were transfected in 293 cells, and lysates were analyzed by Western blot analysis with the anti-ChAT antibody used in this study. A single band for zebrafish ChAT of 70 kD was detected in the lysate of zebrafish *chat*-transfected cells only. This value found for zebrafish ChAT conforms closely to bands between 68 and 72 kD found in Western blots for a cartilaginous fish (dogfish), a basal ray-finned fish (sturgeon), and even the relatively closely related teleost fish trout (Anadon et al., 2000) and goldfish (Giraldez-Perez et al., 2009).

### Retrograde neuronal labeling

Transgenic *wnt1*-GVP-UG zebrafish larvae were fixed at 3, 4, or 5 dpf with 4% paraformaldehyde in PBS at 4°C o/n. Brains were dissected, followed, if necessary, by embedding in a drop of 1.2% ultralow-gelling agarose (Sigma) with the injection side facing upward. Cell Tracker CM-Dil (Invitrogen) dissolved to 5 nmol/μl in DMSO (Invitrogen) was pressure injected with a Femtojet express microinjector (Eppendorf, Hamburg, Germany) into the pretectum, ventrorostral diencephalon (preglomerular area), hypothalamus, optic tectum, or corpus cerebelli. The injection was performed with a fluorescent stereomicroscope (MZ 16FA equipped with filters for GFP and Texas red; Leica, Wetzlar, Germany). After dye application, the agarose was removed, and larvae were incubated in 4% PFA in PBS at RT for 2 days in the dark. The fixative was removed by rinsing twice with PBS, and the larvae were processed for confocal image acquisition. As control, Dil was injected into the tegmentum in a region adjacent to hypothalamus and optic tectum, not resulting in Dil labeling of any GFP-expressing cells of the URL-derived population (Supp. Info. Fig. 11–O).

### Imaging of stained sections, whole mounts, or living embryos

In embryos destined for expression or time-lapse microscopy analysis, pigment formation was inhibited by adding 0.15 mM phenylthiourea (PTU; Sigma) to the rearing medium starting from 10 hpf. Vibratome and cryosections were mounted in 90% glycerol; stained whole mounts or living zebrafish embryos for time-lapse microscopy were embedded in a drop of 1.2% ultralow-gelling agarose (Sigma) as described previously (Köster and Fraser, 2004). To stain the nuclei on fixed tissue, diamino-

benzidine (DAPI; 10 236 276 001, 1 μg/μl; Roche) was used. All images were recorded using a LSM510 or LSM510 Meta laser scanning confocal microscope (both from Zeiss, Oberkochen, Germany). The thickness of the single optical sections shown is 2–3 μm.

### Image rendering

Images were adjusted for brightness, contrast, sharpness (Smart Sharpen filter: amount 44%, radius 0.4 pixels; Gaussian blur filter: radius 0.5 pixels), and size in Adobe Photoshop CS2 software, and figures were produced with Adobe Illustrator CS2 (both from Adobe, San Jose, CA). For analysis of time-lapse movies, z-stacks were converted into maximum intensity projections using the LSM510 software version 4.0 (Zeiss) and subsequently animated with QuickTime Player 7.4.5 (Apple Computer, Inc.). Migrating GFP- and mCherry-expressing cells were tracked, and migration distance and persistence of directionality were calculated using the NIH open-source software ImageJ (1.34 S; <http://rsb.info.nih.gov/ij/>) together with the Manual Tracking plugin. Statistical calculations [standard deviation (SD) and mean], and drawing of diagrams was performed in Microsoft Excel.

## RESULTS

To analyze the migration, developmental time course, differentiation, and eventual fate of early-arising neuronal populations from the URL, we made use of a stable transgenic *wnt1:Gal4-VP16-14* × *UAS:GFP* zebrafish strain (*wnt1*-GVP-UG from hereon). In embryos from this line, the early GFP expression under control of the *wnt1* promoter/enhancer combination represents the early endogenous expression of *wnt1* as shown by in situ hybridization (data not shown). GFP expression is visible in the cerebellum as early as 16hpf, when the primordium of the cerebellum becomes morphologically distinguishable, and GFP fluorescence persists in URL-derived cells over several days, declining in the hindbrain tegmentum at about 5 dpf.

### Expression of *atonal1a* but not *ptf1a* in cerebellar *wnt1*-GVP-UG cells

The upper and the lower rhombic lip areas are characterized by the expression of the marker gene *atonal1* (mouse *Math1* homologue) and give rise to many neuronal populations that migrate over long distances during brain development (see the introductory paragraphs). Ventrally to the rhombic lip, expression of *ptf1a* localizes to the cerebellar ventricular zone, a germinal zone giving rise to cerebellar neuronal populations different from those of the rhombic lip. These ventricular zone-derived neuronal cells migrate only over shorter distances in the

mouse (Hoshino et al., 2005), so we used *in situ* hybridization for the zebrafish homologues *atonal1a* (Fig. 2A–D) and *ptf1a* (Fig. 2E–H) as markers for the rhombic lip and the ventricular zone, respectively. This analysis was combined with immunohistochemistry for GFP to clarify the origin of the GFP-expressing cells in the cerebellar plate of *wnt1*-GVP-UG embryos. Single optical sections recorded by laser scanning confocal microscopy revealed an overlap of GFP-expressing cells with *atonal1a* expression at 24 hpf (Fig. 2C). Strikingly, *ptf1a* expression is not initiated prior to 36 hpf in the zebrafish cerebellar plate and thus occurs significantly later than the first *wnt1* promoter/enhancer driven GFP expression. Coexpression studies at these later stages (40 hpf) indeed revealed no coexpression for GFP and the *ptf1a* mRNA expression domain, which is located ventrally to *atonal1a* and the GFP-expressing cells (insets in Fig. 2F–H, focus on ventral *ptf1a*-expressing regions of the cerebellar plate). Thus, the GFP-expressing cells in the cerebellar plate of *wnt1*-GVP-UG embryos represent a cell population that is derived from the cerebellar rhombic lip at early cerebellar differentiation stages.

### Proliferation of cerebellar *wnt1*-GVP-UG cells

To answer whether GFP is already expressed in dividing progenitors of the URL or is turned on later in postmitotic cells that have started to differentiate, we recorded time-lapse movies of GFP-expressing cells in *wnt1*-GVP-UG embryos starting at about 24 hpf. These movies frequently revealed divisions of *wnt1*-GVP-UG cells at the URL, showing that GFP-expressing cells are still mitotic (see Supp. Info. Movie 1). Immunohistochemistry for the M-phase marker phosphohistone H3 (PH3) confirmed this finding. Double-positive cells could be observed to be strictly localized to the URL even at later stages of 48 hpf (Fig. 2I–L), indicating that *wnt1*-GVP-UG are still mitotic inside the URL at a low rate [mean number of  $4.4 \pm 3.21$  (SD) cells per embryo, with five embryos analyzed]. In contrast, outside the URL, no PH3-positive GFP-expressing cells could be found, suggesting that, similarly to granule neuron progenitors, these GFP-expressing cells start to differentiate upon leaving the URL (Volkman et al., 2008). Consistently with this finding, PH3 expression did not colocalize to any GFP-fluorescent cell in more ventral regions, where these GFP-fluorescent cells accumulated ( $n = 5$  analyzed embryos; Fig. 2M–P). Laser scanning confocal microscopy revealed that *wnt1*-GVP-UG cells formed stable clusters at 3 dpf ventral to the cerebellum in the tegmentum of rhombomere 1 and remained positioned in this area (Fig. 2Q–S, ovals). Thus, in the *wnt1*-GVP-UG strain, URL-derived progenitors can be followed already from their birthplace onward, likely to

their final position of terminal differentiation in the hind-brain tegmentum.

### Migration analysis of cerebellar *wnt1*-GVP-UG cells

URL-derived cells commonly migrate over long distances. To confirm directly that *wnt1*-GVP-UG cells from the URL populate the ventrally positioned tegmental clusters, time-lapse imaging of *wnt1*-GVP-UG transgenic embryos from 24 hpf up to 72 hpf ( $n = 5$ ) was performed. Combined analysis of time-lapse recordings from either a dorsal view (see Supp. Info. Movie 2;  $n = 2$ ) or a lateral view (see Supp. Info. Movie 3;  $n = 3$ ) indeed revealed long-distance migration emanating from the URL. In detail, rostral migration of *wnt1*-GVP-UG-expressing cells started at about 24 hpf toward the midbrain–hind-brain boundary (MHB), followed by a ventrolateral migration to tegmental areas beneath the cerebellum. This symmetric migration in both cerebellar halves resulted in the formation of bilateral ventral clusters close to but not in contact with the MHB (Fig. 2Q–S). Migration occurred mainly between 24 hpf and 48 hpf and, thus, prior to the generation of cerebellar granule neurons. Lateral (24–72 hpf)- and dorsal (24–64 hpf)-view time-lapse recordings from older embryos confirmed that the GFP-expressing cells remained stably in these tegmental clusters (not shown), representing their final position of terminal differentiation.

To characterize the migratory behavior of *wnt1*-GVP-UG cells in detail, we aimed to follow individual cells. For this, a  $5 \times$  UAS:mCherry construct was injected into *wnt1*-GVP-UG embryos at the one-cell stage (25 ng/ $\mu$ l), leading to a Gal4-dependent mosaic expression of the red fluorescent mCherry protein in the *wnt1*-expressing URL-derived cells. After time-lapse recording ( $n = 3$ ), ImageJ software was used to trace individual GFP and mCherry double-positive cells ( $n = 9$ ) for up to 18 hours. Cells were followed during their migration after they had left the neuroepithelium of the URL to their target area ventral to the cerebellar plate (Fig. 3A–D,F–I; Supp. Info. Movie 4; and data not shown). In lateral (Fig. 3A–D) and transverse (Fig. 3F–I) maximum-intensity projections of a lateral image stack of rhombomere 1, these tracings confirmed the initially observed migration path on an individual cellular basis. Moreover, the individual tracks revealed that the migration route close to the MHB was directional, following a tangential path in deeper layers of the neural tube (see lateral and transversal view of migratory routes in Fig. 3E,J). In addition, all cells migrated along the same route, and a different behavior of cells such as a splitting up in different migratory populations could not be observed. The migratory routes of the *wnt1*-

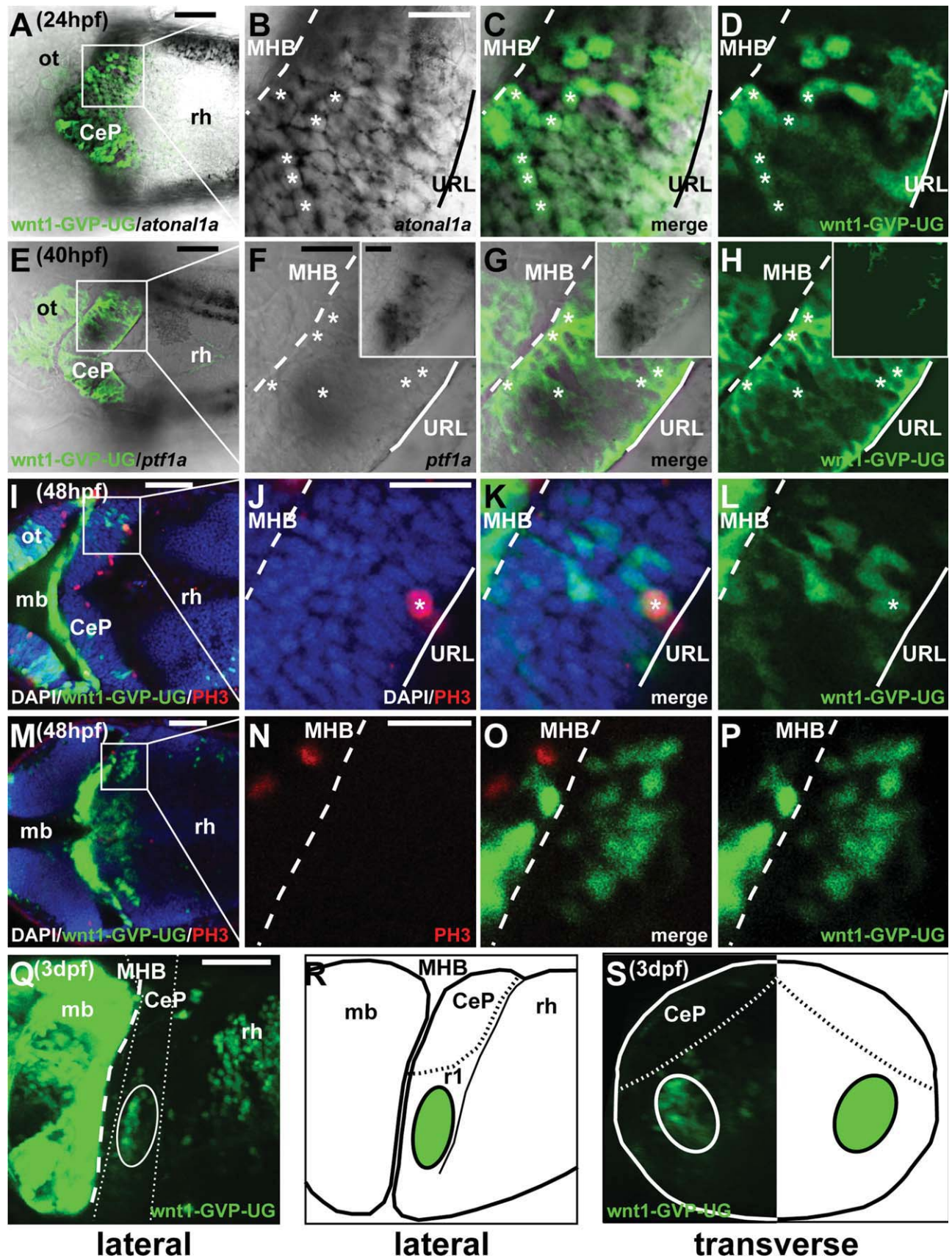


Figure 2

GVP-UG cells migrating from the URL between 24 hpf and 48 hpf and the cerebellar granule neurons, another URL-derived migratory neuronal population, emanating from the URL after 48 hpf (Volkman et al., 2008), are schematically compared in Figure 3M. Both neuronal populations leave the URL and move rostrally toward the MHB (not shown), but subsequently they follow different ventral migratory routes with respect to the mediolateral organization of the zebrafish cerebellum. After reaching the MHB, the *wnt1*-GVP-UG cells turn ventrally and migrate along the MHB deep inside the neural tube finally to settle in the tegmentum of rhombomere 1. In contrast, migratory granule cell neurons take a superficial path directly beneath the surface of the cerebellar plate and either settle dorsomedially to contribute to the granule cell population of the corpus cerebelli or migrate lateroventrally along the MHB to settle in the eminentia granularis, both representing compartments of the zebrafish cerebellum in rhombomere 1.

The tracks that are shown in Figure 3D,E,I,J represent originally recorded data and thereby include the movements caused by the overall movement of the tissue and are thus longer than the real migration distance. Therefore, all the following measurements of migration distance were corrected for movements caused by drifting and growth of the embryo. The persistence of migratory directionality was calculated as the ratio of the direct distance from start to end point (D) divided by the total track distance (T). For the tracked cells that are shown in Figure 3A–J, this quantification revealed an average persistence of migratory directionality of  $0.59 \pm 0.16$  [SD; Fig. 3K; in total nine cells in three different *wnt1*-GVP-UG embryos were analyzed, with an average persistence of migratory directionality of  $0.55 \pm 0.16$  (SD)]. Compared

with other neuronal populations in the zebrafish embryonic hindbrain, such as migrating facial branchiomotor neurons, this value demonstrated a high degree of persistence of migratory directionality (Sittaramane et al., 2008). Individual cell tracing also allowed for quantifying the migration speed of the traced cells, which were also corrected for movements caused by drifting and growth of the embryo. GFP-expressing cells pass the distance between the URL and their final position close to the ventral isthmus in a mean of 14.2 hours ( $n = 9$ ). The average speed of cell migration of the tracked cells shown in Figure 3A–J was  $4.64 \pm 1.58 \mu\text{m}/\text{hour}$  [SD; Fig. 3L; the average speed of cell migration for all nine cells analyzed was  $4.19 \mu\text{m}/\text{h} \pm 1.52$  (SD)], which is in good agreement with recent measurements of the migratory speed of URL-derived cells in the cerebellum (Rieger et al., 2008). These cells have been shown to require polysialylation of NCAM for proper forward migration.

Immunohistochemistry for PSA on *wnt1*-GVP-UG embryos at 36 hpf revealed that *wnt1*-GVP-UG cells at the URL and along their migration path in the anterior part of the cerebellum close to the MHB express PSA (Fig. 3M–O; see also insets). This identifies *wnt1*-GVP-UG cells as one of the PSA-dependent migrating neuronal precursor populations of the URL, but the final fate of these cells remained unclear.

### Expression of the neuronal surface protein neurolin by *wnt1*-GVP-UG cells

Expression of PSA suggested that the *wnt1*-GVP-UG cells in the zebrafish cerebellum are immature neurons. To confirm their neuronal identity further; *wnt1*-GVP-UG larvae were analyzed for the expression of neurolin (zn8),

**Figure 2.** GFP-expressing cells in the early embryonic cerebellum of the *wnt1*-GVP-UG line represent an URL-derived cell lineage. Dorsal views of cerebellar plate at 24 hpf (A) and 40 hpf (E) or magnification of boxed area showing a single optical section recorded by confocal microscopy (B–D,F–H). Embryos were analyzed by immunohistochemistry for GFP protein and by in situ hybridization for zebrafish *atonal1a* (A–D) and *ptf1a* mRNA (E–H) expression, respectively. Whereas GFP-expressing cells (C,D, white asterisks) are coexpressing *atonal1a* (B,C), they lack *ptf1a* expression and are located dorsal to the *ptf1a*-positive cell population in the cerebellum (F–H, white asterisks). Insets in F–H show more ventral optical sections of the same region; note the *ptf1a* expression emanating from the ventricular zone (insets in F,G) and the absence of GFP-positive cells (insets in G,H). I–P: Single optical sections recorded by confocal microscopy at 48 hpf of *wnt1*-GVP-UG embryo at 48 hpf stained by immunohistochemistry for the M-phase marker PH3 (I–K,M,O in red) and GFP (I,K–M,O,P in green). DAPI was used for counterstaining of nuclei (I–K,M, blue). I and M show a dorsal overview of the isthmus region. A magnified view of the boxed area in I shows a dividing GFP-expressing cell at the URL (K,L) that is positive for PH3 (J,K), whereas the magnified view of the boxed area in M shows the absence of PH3-expressing cells in the ventral cluster formed by *wnt1*-GVP-UG cells in the tegmentum of rhombomere 1 (N–P). Q,S: Maximum-intensity projection of confocal image stack (stack of 36 images each 2  $\mu\text{m}$  apart) of a *wnt1*-GVP-UG larva at 3 dpf in a lateral view (Q) and a transverse reconstruction (S). The ovals indicate the cluster formed by the aggregating GFP-expressing cells ventral to the cerebellar plate close to but not in contact to the MHB. The position of these bilateral clusters in the neural tube is depicted in schematic drawings in a lateral (R) and a transverse view (S). A magenta-green version of this figure is available online as Supporting Information Figure 1. CeP, cerebellar plate; mb, midbrain; MHB, midbrain–hindbrain boundary; ot, optic tectum; r1, rhombomere 1; rh, rhombencephalon; URL, upper rhombic lip. Scale bars = 50  $\mu\text{m}$  in A,E,I,M,Q; 20  $\mu\text{m}$  in B (applies to B–D); 20  $\mu\text{m}$  in F (applies to F–H); 20  $\mu\text{m}$  in J (applies to J–L); 20  $\mu\text{m}$  in N (applies to N–P); 10  $\mu\text{m}$  in insets. [Color figure can be viewed in the online issue, which is available at [www.interscience.wiley.com](http://www.interscience.wiley.com).]



a neuron-specific adhesion factor in the developing brain (Kanki et al., 1994; Laessing et al., 1994; Mann et al., 2006). This antibody staining indicated the coexpression of neuroilin in many GFP-expressing cells remote from the URL in a cluster in the tegmentum of rhombomere 1 (Fig. 4B–D,E–G, white arrowheads). Moreover, ventrally projecting axonal-like processes derived from *wnt1*-GVP-UG cells were immunoreactive for the neuroilin protein (not shown). In addition, neuroilin-positive commissural axons in tegmental areas were observed (Fig. 4E,F, yellow arrowhead); however, *wnt1*-GVP-UG cells could not be found to contribute to this commissural connection (Fig. 4F,G) that might represent the forming commissure of the secondary gustatory nuclei. Nevertheless, the coexpression of PSA and neuroilin on the cell somata and in forming axons indicated that the *wnt1*-GVP-UG progenitors acquire a neuronal fate along their migratory pathway.

### Expression of deep cerebellar nuclei markers

Among the neuronal cell types known to be produced early by the *wnt1*-expressing URL in mouse are the neurons of the deep cerebellar nuclei (Machold and Fishell, 2005; Wang et al., 2005; Nichols and Bruce, 2006) that are located at the base of the mammalian cerebellum. Insofar as the generation of granule neurons in the zebrafish cerebellum is initiated only after 48 hpf (Volkman et al., 2008), the *wnt1*-GVP-UG population emigrating from the URL to ventral regions starting already at 24 hpf could represent cell types contributing to hindbrain nuclei as well as homologues of deep cerebellar nuclei. The latter (eurydendroid cells), though, are dispersed throughout the teleostean Purkinje cell layer of the teleost fish cerebellum and are thus located in more dorsal regions of the cerebellum (Ikenaga et al., 2005, 2006), making a deep cerebellar nuclei identity of *wnt1*-GVP-UG cells unlikely.

Nevertheless, we performed zebrinIII antibody stainings at 4 dpf to visualize differentiated Purkinje cells, which are afferent to the deep cerebellar nuclei (Fig. 4H–L). Although Purkinje cells (Fig. 4H, white arrows) have developed prominent axonal projections to eurydendroid cells within the cerebellum and to the only extracerebellar target in the caudal medullary hindbrain (likely the primary vestibular area; see Brochu et al., 1990; Fig. 4H, white arrowhead) and dendrites at this developmental stage, zebrinIII-positive processes projecting to the position of the GFP-positive ventral cluster could not be observed (Fig. 4I–L, zebrinIII-positive processes marked with white arrowhead). Furthermore, the expression of the zebrafish homologues of *tbr1* and *tbr2* [*tbr1* (Fig. 4M–P) and *eomes*

(Supp. Info. Fig. 8A–D; Mione et al., 2001)], two markers for deep cerebellar nuclei neurons in mammals (Fink et al., 2006), did not colocalize with *wnt1*-GVP-UG cells at 3 dpf. Together, the lack of coexpression of deep cerebellar nuclei marker genes and the absence of Purkinje cell axons innervating the ventral *wnt1*-GVP-UG cell clusters are inconsistent with an homology or functional equivalence of *wnt1*-GVP-UG cells to the mammalian deep cerebellar nuclei neurons. These findings rather support an identity of *wnt1*-GVP-UG cells as neuronal progenitors of tegmental nuclei, in particular, the secondary gustatory/viscerosensory nucleus, nucleus isthmi, superior reticular nucleus, or nucleus lateralis valvulae (Fig. 5I,J), as is shown below.

### Expression of secondary gustatory/viscerosensory nucleus and nucleus isthmi markers

In the larval zebrafish brain at 5 dpf, expression of the extracellular matrix protein reelin was reported for neurons of the nucleus isthmi (Costagli et al., 2002). Thus we analyzed *wnt1*-GVP-UG larvae for *reelin* expression. Strikingly, GFP cells in the anteroventral part of the *wnt1*-GVP-UG cell cluster were found to coexpress *reelin* mRNA (Fig. 5A–D), suggesting that *wnt1*-GVP-UG cells might also contribute to the nucleus isthmi in the tegmentum of rhombomere 1 of the larval brain.

In adult zebrafish, secondary gustatory/viscerosensory nucleus neurons have been shown to express the calcium-binding protein calretinin, whereas the cells of the nucleus isthmi are calretinin negative (Castro et al., 2006; Fig. 1C). Therefore, we analyzed *wnt1*-GVP-UG larvae at 4 dpf (data not shown) and 7 dpf (Fig. 5E–H) for expression of calretinin and GFP by immunohistochemistry. Many of the GFP-positive cells coexpressed calretinin (Fig. 5G) in the dorsoposterior portion of the *wnt1*-GVP-UG cell cluster at 7 dpf, suggesting that these cells belong to the secondary gustatory/viscerosensory nucleus.

### Neurotransmitter expression analysis

The URL is known to produce mostly excitatory glutamatergic neurons, and this is consistent with the finding that the URL-derived parabrachial nucleus of the rat expresses the *vesicular glutamate transporter 2.1* (*vglut2.1*; Geisler et al., 2007). In addition several hindbrain nuclei derived from the URL in the mouse, such as the parabrachial, parabigeminal, pedunculo-pontine tegmental, and laterodorsal tegmental nuclei contain cholinergic neurons (see the introductory paragraphs; Machold and Fishell, 2005). Therefore, we analyzed the expression of *vglut2.1* and choline acetyltransferase (ChAT), the

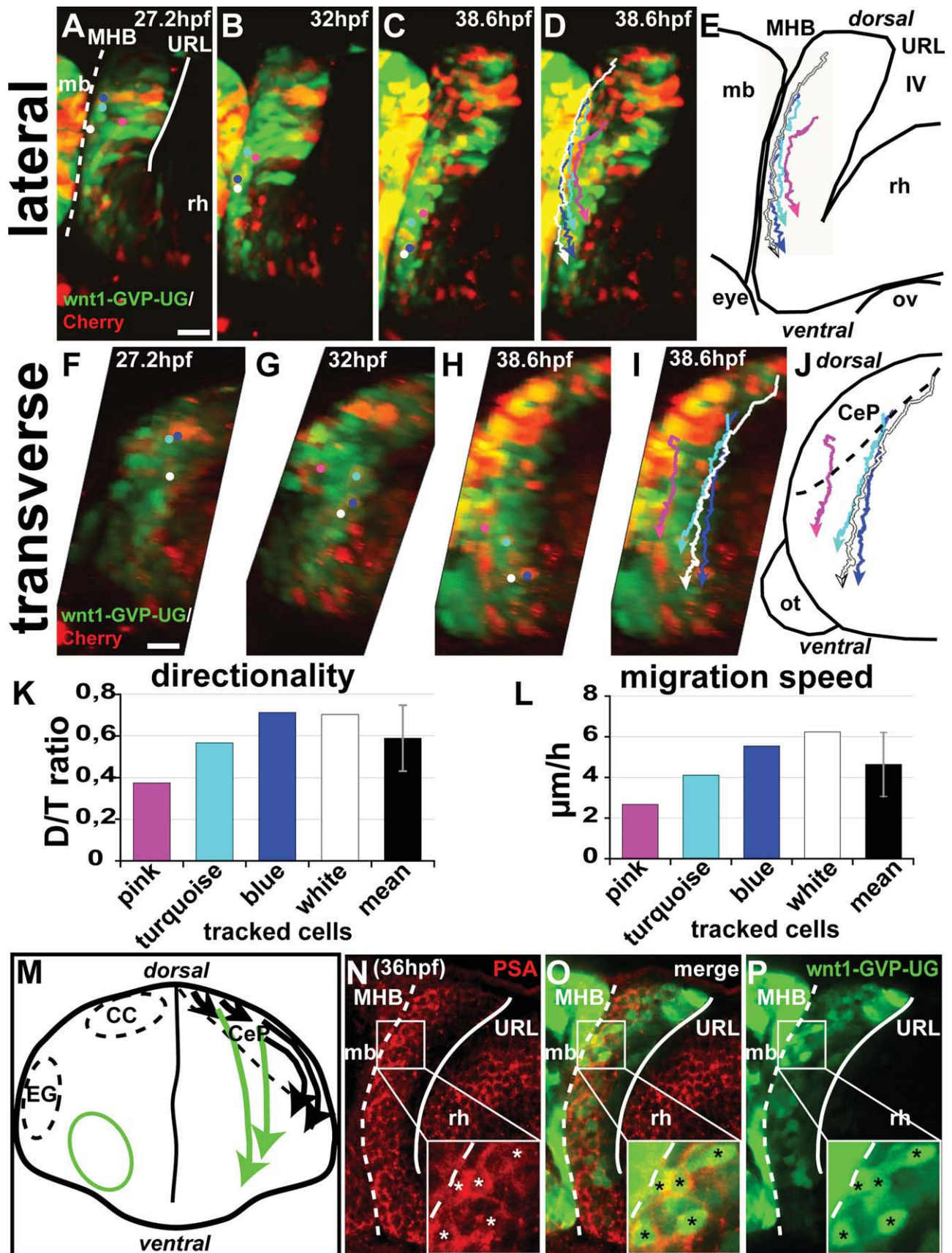


Figure 3

acetylcholine-synthesizing enzyme, in the tegmentum of *wnt1-GVP-UG* transgenic larvae. In situ hybridization against *vglut2.1* at 4 dpf indeed revealed coexpression in a subpopulation of the GFP-expressing URL-derived cell cluster (Fig. 6A–D). Similarly, ChAT immunohistochemistry identified GFP-expressing cells in this cluster as cholinergic neurons (Fig. 6E–H), which is consistent with the position of the cholinergic neurons of the tegmental nuclei in the mature brain (Fig. 1B). Taken together, the early origin of the *wnt1-GVP-UG* cells in the cerebellar rhombic lip, their characteristic ventral migration, their final position in the tegmentum of rhombomere 1, their coexpression of tegmental nuclei marker genes, and their neurotransmitter identity strongly suggest that these GFP-expressing cells in the early URL are progenitors of the zebrafish tegmental nuclei known to be positioned in the ventral rhombomere 1 in the adult brain, likely including the secondary gustatory/viscerosensory nucleus, nucleus isthmi (Arenzana et al., 2005), superior reticular nucleus, or nucleus lateralis valvulae (Fig. 5I,J).

### Axonal projection analysis

To discriminate further between these different tegmental nuclei, we sought to identify them by means of their distinct axonal projections. For example, the secondary gustatory/viscerosensory nucleus projects to the preglomerular tertiary gustatory nucleus (TGN) and the hypothalamus (Wullimann, 1988; Perez et al., 2000). The

nucleus isthmi and superior reticular nucleus instead project to the optic tectum (Sakamoto et al., 1981; Ito et al., 1982; Xue et al., 2001), whereas the nucleus lateralis valvulae projects into the granule cell layer of the corpus cerebelli (Finger, 1978; Wullimann and Northcutt, 1988, 1989; Ito and Yoshimoto, 1990; Xue et al., 2004). For retrograde labeling, the red fluorescent lipophilic dye Dil was injected into the ventrorostral diencephalon (including the preglomerular tertiary gustatory nucleus), the hypothalamus, the optic tectum, or the corpus cerebelli of 4-dpf *wnt1-GVP-UG* larvae, respectively. After 2 days of incubation, confocal microscopy analysis of the injected brains by maximum-intensity projection of recorded image stacks revealed Dil-positive cells in different clusters in the tegmental region of rhombomere 1 depending on the injection site (three brains were analyzed for each injection site; Fig. 7E,I,M,Q).

In brains injected into the corpus cerebelli (Fig. 7A, asterisk), a Dil-labeled cell cluster was observed close to the developing valvula cerebelli, which likely represents the nucleus lateralis valvulae (Fig. 7E,F). In single optical sections, cells of this nucleus were found to be located rostromedially and ventrally to the *wnt1-GVP-UG* cell population (Fig. 7D,H) and showed no overlap with the GFP-positive cells in this cluster (Fig. 7C,G). In contrast, Dil injection into the optic tectum (Fig. 7I–L), the hypothalamus (Fig. 7M–P), and the area of the preglomerular tertiary gustatory nucleus in the ventrorostral diencephalon (Fig. 7Q–T) all resulted in retrograde labeling of *wnt1-*

**Figure 3.** Migratory characteristics of *wnt1-GVP-UG* cells. Lateral (A–D) and transverse (F–I) view of rhombomere 1; maximum brightness projections (stack of 21 images each 3  $\mu\text{m}$  apart) from individual time points of a time-lapse microscopy study of a transgenic *wnt1-GVP-UG* embryo after injection with  $5\times$  UAS:mCherry construct are shown. In addition to GFP expression (green), the embryo shows mosaic Gal4-VP16-dependent expression of the red fluorescent protein mCherry in URL-derived cells (red). Double-positive cells were traced manually in lateral (A–C) and transverse (F–H) views and are marked with colored dots (note that each color corresponds to the same cell in both views). In addition, migratory routes were visualized by ImageJ-supported cell tracing. Routes have been overlaid onto pictures of individual time points (D,I, 38.6 hpf) at which tracing has been finished (arrowheads indicate direction of movements). Schematic drawings depict the individual migratory routes in lateral (E) and transversal (J) views in the context of other brain structures. For the cells tracked in A–C,F–H, the persistence of migratory directionality, the ratio of the direct distance from start to end point (D) divided by the total track distance (T), is displayed in K, and migration velocities are shown in L. Note that, for the calculation of persistence (K) and migration speed (L), the migration distances were corrected for tissue movements caused by the continued growth of the brain and thus are shorter than the tracks shown in D,E,I,J. M: Schematic drawing depicting hindbrain rhombomere 1 between 24 and 74 hpf in a transverse view, with the migratory routes of immature cerebellar granule cell neurons (black arrows) and URL-derived *wnt1-GVP-UG* cells (green arrows) shown in the right half of the scheme. The final target regions of the two migratory subpopulations of cerebellar granule cells, the corpus cerebelli and the eminentia granularis, are marked by dashed ovals, whereas the target region of *wnt1-GVP-UG* cells is marked by a solid green oval (on the left half of the scheme). Note that the different populations migrate consecutively; migration of URL-derived *wnt1-GVP-UG* cells peaks at 24–48 hpf, whereas the emanation of granule cells from the URL initiates at 48 hpf. N–P: Single optical sections recorded by confocal microscopy of a *wnt1-GVP-UG* embryo at 36 hpf after immunohistochemistry for GFP (green) and polysialic acid (PSA) expression (red), showing the cerebellar plate in a lateral view. The migrating GFP-positive precursor cells (O,P) express PSA (N,O) along their migration path close to the MHB. The insets show single migrating *wnt1-GVP-UG* cells in the boxed area at high magnification that are positive for PSA (insets N–P, asterisks). Note that PSA expression is low in the URL proliferation zone. A magenta-green version of this figure is available online as Supporting Information Figure 2. IV, fourth ventricle; CC, corpus cerebelli; CeP, cerebellar plate; EG, eminentia granularis; mb, midbrain; MHB, midbrain–hindbrain boundary; ot, optic tectum; ov, otic vesicle; rh, rhombencephalon; URL, upper rhombic lip. Scale bars = 20  $\mu\text{m}$  in A (applies to A–D); 20  $\mu\text{m}$  in F (applies to F–I); 20  $\mu\text{m}$  in N (applies to N–P); 10  $\mu\text{m}$  in insets. [Color figure can be viewed in the online issue, which is available at [www.interscience.wiley.com](http://www.interscience.wiley.com).]

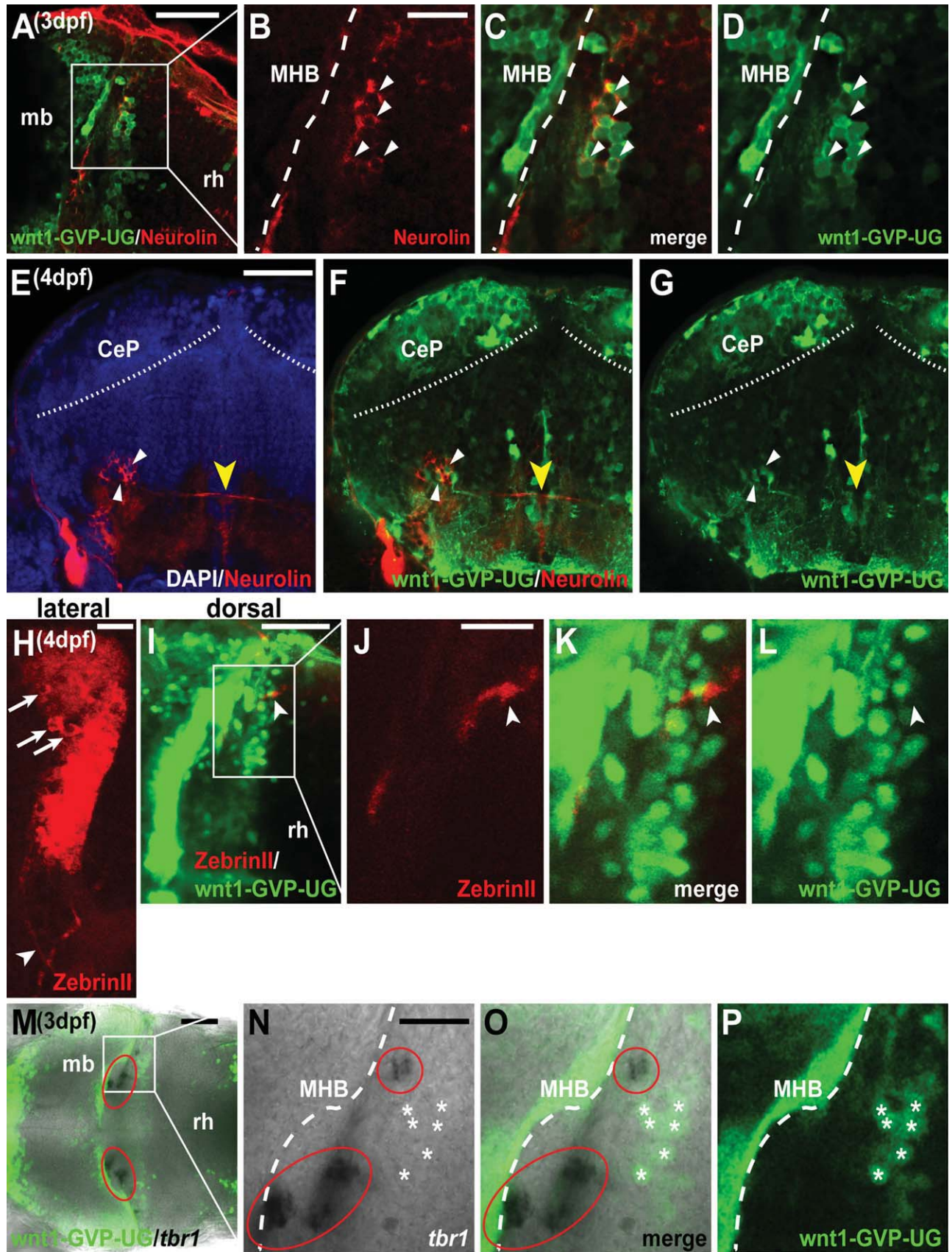


Figure 4

GVP-UG cells. These observations indicate that the URL-derived *wnt1*-GVP-UG-expressing neurons project to the optic tectum, the hypothalamus, and the area of the preglomerular tertiary gustatory nucleus. However, Dil injections into the optic tectum marked *wnt1*-GVP-UG neurons only ventrorostrally to the cerebellar tract close to the MHB (Fig. 7I–L, yellow dashed oval), whereas Dil application to the hypothalamic and preglomerular tertiary gustatory nucleus regions resulted in marked *wnt1*-GVP-UG neurons in positions caudal to this tract (Fig. 7M–T, yellow dashed oval). As control, Dil was injected into the tegmentum in a region adjacent to the hypothalamus and optic tectum; these injections did not result in Dil labeling of any GFP-expressing cells of the URL-derived population in the tegmentum of rhombomere 1 (Supp. Info. Fig. 8I–O).

Taken together, these retrograde labeling experiments indicate that *wnt1*-GVP-UG URL-derived neurons settle in tegmental areas of rhombomere 1 from which they project toward the optic tectum, the hypothalamus, and the preglomerular tertiary gustatory nucleus, which allows us possibly to identify them as neurons of the nucleus isthmi or superior reticular nucleus (ventrorostral to the cerebellar tract) and the secondary gustatory/viscerosensory nucleus (caudal to the cerebellar tract), respectively. These different efferent projections define the region of the secondary gustatory/viscerosensory nucleus as the posterior part and the nucleus isthmi/superior reticular nucleus as the anteroventral part of the *wnt1*-GVP-UG cell cluster respectively (Fig. 8M). Furthermore, these connectional studies suggest that *wnt1*-expressing neuronal progenitors emanating from the URL do not contribute to the nucleus lateralis valvulae.

### *wnt1*-Expressing pretectal neurons project to the corpus cerebelli

At this point, a prominent GFP-fluorescent, mossy fiber-like projection that can be observed in the granule cell layer of the corpus cerebelli in the *wnt1*-GVP-UG line up to 4 weeks has to be mentioned (Fig. 8A–D; note typical mossy fiber endings in insets of Fig. 8B–D). To identify the origin of these axonal projections, Dil was injected into the mossy fiber endings in the corpus cerebelli, resulting in bilateral labeling of cell bodies in the pretectal area most likely in the paracommissural nucleus or dorsal periventricular pretectal nucleus (Fig. 8E–H; Wullmann and Northcutt, 1988; Imura et al., 2003; Folgueira et al., 2006, 2008). In turn, Dil injections into the pretectum resulted in labeling of the GFP-positive mossy fibers in the corpus cerebelli (three brains were analyzed for each injection site; Fig. 8I–L). Furthermore, the retrograde as well as anterograde labeling visualized the axon tract transversing the ventral midbrain (Fig. 8E, yellow arrowhead) and forming a commissure in rhombomere 1 close to the MHB, thereby innervating the contralateral side of the corpus cerebelli. The corpus innervation by the mossy fibers was dual, predominantly of an ipsilateral but to a lesser extent also of a contralateral nature (Fig. 8J–L, yellow arrowhead). Thus, the GFP fluorescent mossy fiber-like axons that innervate the corpus cerebelli in *wnt1*-GVP-UG larvae originate not in the ventral URL-derived tegmental nuclei but rather in the pretectum, providing relayed telencephalic input to the nonvestibular granule cell population of the zebrafish cerebellum (Wullmann and Northcutt, 1988; Wullmann and Meyer, 1993;

**Figure 4.** *wnt1*-GVP-UG cells are a neuronal population not homologous to the neurons of the deep cerebellar nuclei. **A–G:** Single optical sections recorded by confocal microscopy of a *wnt1*-GVP-UG larvae at 3 dpf (A–D) or 4 dpf (E–G) after immunohistochemistry for GFP (green) and neurolin expression (red), showing rhombomere 1 in a dorsal (A–D) or transverse (E–G) view. GFP-positive *wnt1*-GVP-UG cells express neurolin in the ventral cell cluster (white arrowheads in B–G); note the gap between the MHB and the GFP/neurolin-coexpressing cells in the dorsal view (A–D). Neurolin-positive, GFP-negative cells form a commissure in the tegmentum of rhombomere 1 (yellow arrowhead in E–G). DAPI (blue) was used for counterstaining of nuclei in E. **H:** Maximum-brightness projection of confocal image stack (stack of 30 images each 3  $\mu$ m apart) shows lateral view of zebrinII expression in the cerebellum at 4 dpf. ZebrinII-immunoreactive Purkinje cell bodies (arrows) and dendrites are visible. Note the few Purkinje cell axons leaving the cerebellum ventrally and turning posteriorly to innervate the vestibular nucleus (arrowhead). **I–L:** ZebrinII immunoreactivity (red) in a *wnt1*-GVP-UG larvae of same age; maximum-brightness projections (stack of 17 images each 4  $\mu$ m apart) show tegmentum of rhombomere 1 in a dorsal view. Magnification of boxed area in I reveals no contacts of zebrinII-immunoreactive axons (J,K) with GFP-positive cells (K,L); instead, the zebrinII-immunoreactive Purkinje cell axons (arrowhead) leave the region of the *wnt1*-GVP-UG cell cluster in posterior directions. **M–P:** Dorsal views of isthmic region of a *wnt1*-GVP-UG larvae at 3 dpf showing a single optical section recorded by confocal microscopy at the level of the *wnt1*-GVP-UG cell cluster. Larvae were analyzed by immunohistochemistry for GFP and by in situ hybridization for zebrafish *tbr1* expression. Magnified views of boxed areas in M show GFP-expressing cells (white asterisks) and *tbr1* expression. **O,P:** GFP-expressing cells in a caudomedial position distinct from *tbr1*-expressing cells of rhombomere 1 located rostromedially (M–O, red ovals). A magenta-green version of this figure is available online as Supporting Information Figure 3. CeP, cerebellar plate; mb, midbrain; MHB, midbrain–hindbrain boundary; rh, rhombencephalon. Scale bars = 50  $\mu$ m in A; 20  $\mu$ m in B (applies to B–D); 50  $\mu$ m in E (applies to E–G); 20  $\mu$ m in H; 50  $\mu$ m in I,M; 20  $\mu$ m in J (applies to J–L); 20  $\mu$ m in N (applies to N–P). [Color figure can be viewed in the online issue, which is available at [www.interscience.wiley.com](http://www.interscience.wiley.com).]

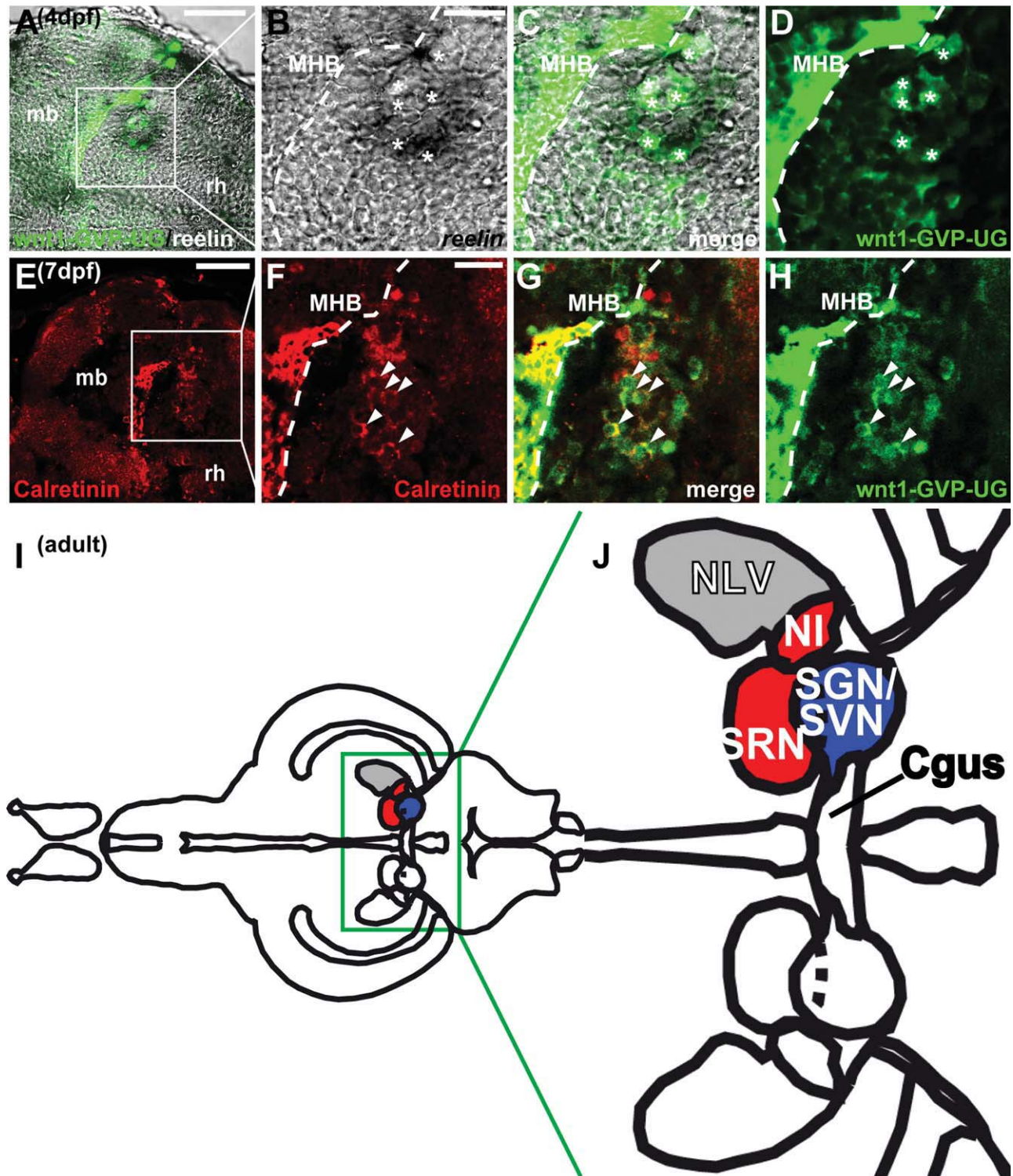


**Figure 5.** *wnt1-GVP-UG* cells express hindbrain tegmental nuclei markers. Single optical section recorded by confocal microscopy of 4 dpf (A–D) and 7 dpf (E–H) brain or a schematic drawings of adult brain section (I, J) all in dorsal views. *wnt1-GVP-UG* larvae were analyzed by immunohistochemistry for GFP (A–H) and by in situ hybridization for zebrafish *reelin* (A–D) expression or by immunohistochemistry for calretinin (E–H, K) protein expression. A–D: *reelin* Shows coexpression with GFP-expressing cells in the anteroventral portion of the *wnt1-GVP-UG* cell cluster (B–D, white asterisks). F–H: Magnified views of boxed area in E show GFP-expressing cells in the dorsoposterior portion coexpressing calretinin (white arrowheads). I: Schematic drawing depicting overview of adult brain section in dorsal view, the boxed area is magnified in J, delineating the tegmental hindbrain nuclei of the isthmus region. A magenta-green version of this figure is available online as Supporting Information Figure 4. Cgus, commissure of the secondary gustatory nuclei; mb, midbrain; MHB, midbrain-hindbrain boundary; NI, nucleus isthmi; NLV, nucleus lateralis valvulae; rh, rhombencephalon; SGN/SVN, secondary gustatory/viscerosensory nucleus; SRN, superior reticular nucleus. Scale bars = 50  $\mu$ m in A, E; 20  $\mu$ m in B (applies to B–D); 20  $\mu$ m in F (applies to F–H). [Color figure can be viewed in the online issue, which is available at [www.interscience.wiley.com](http://www.interscience.wiley.com).]

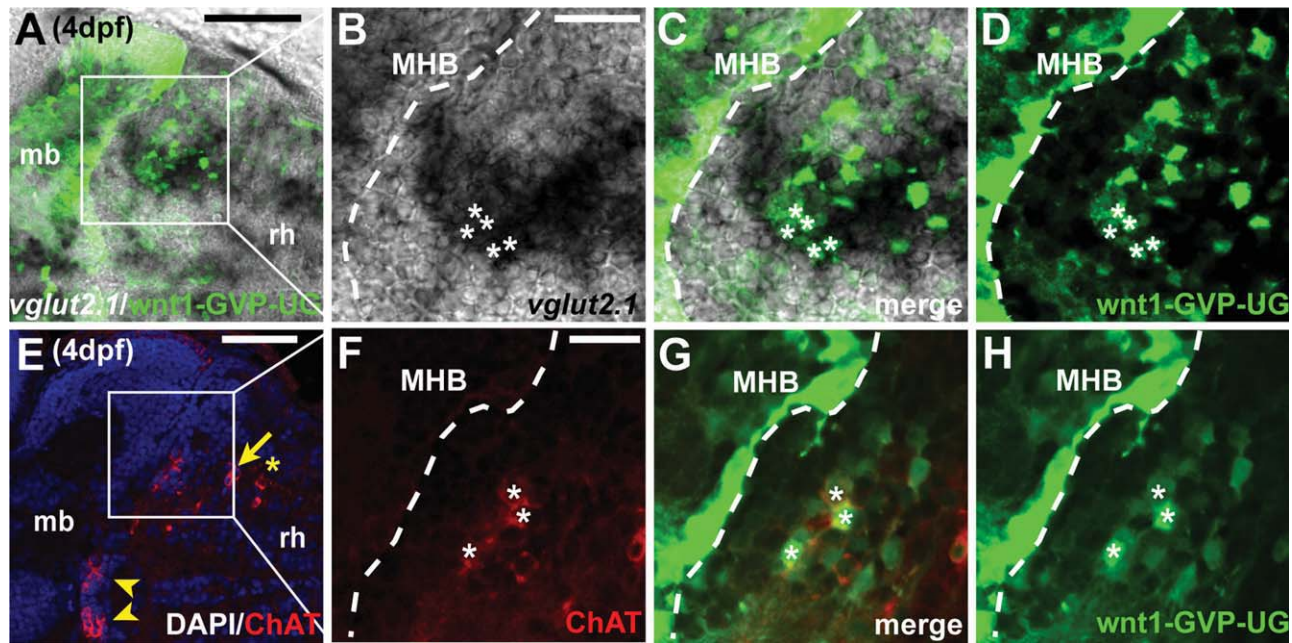


**Figure 6.** *wnt1*-GVP-UG cells of the ventral cluster are cholinergic and glutamatergic. Dorsal views of isthmus region at 4 dpf (A–H) showing single optical sections recorded by confocal microscopy at the level of the *wnt1*-GVP-UG cell cluster ventral to the cerebellum or schematic drawings of adult brain section (I, J). Larvae or adult brain were analyzed by immunohistochemistry for GFP protein and by in situ hybridization for zebrafish *vglut2.1* (A–D) and by immunohistochemistry for ChAT (E–H, K). A–D: A subpopulation of the GFP-expressing cells in the tegmental cluster is coexpressing *vglut2.1* (B–D, white asterisks). E: Overview of isthmus region with DAPI counterstaining of the nuclei (blue). ChAT-expressing cells (red) are observed in the oculomotor (yellow arrowheads), the trigeminal (yellow arrow and yellow asterisk) nuclei and the *wnt1*-GVP-UG cell cluster (boxed area). F–H: Magnified view of the boxed area in E showing a subset of GFP-expressing cells (green) coexpressing ChAT (red; white asterisks). A magenta-green version of this figure is available online as Supporting Information Figure 5. Cgus, commissure of the secondary gustatory nuclei; mb, midbrain; MHB, midbrain–hindbrain boundary; NI, nucleus isthmi; NLV, nucleus lateralis valvulae; rh, rhombencephalon; SGN/SVN, secondary gustatory/viscerosensory nucleus; SRN, superior reticular nucleus. Scale bars = 50  $\mu$ m in A, E; 20  $\mu$ m in B (applies to B–D); 20  $\mu$ m in F (applies to F–H). [Color figure can be viewed in the online issue, which is available at [www.interscience.wiley.com](http://www.interscience.wiley.com).]

Wullimann, 1998; Imura et al., 2003; Figueira et al., 2006, 2008; Volkmann et al., 2008).

## DISCUSSION

The expression of *wnt1* in the embryonic zebrafish cerebellum is of a transient nature, ceasing at 48 hpf and being restricted to the premigratory cells in the URL (Lekven et al., 2003; McFarland et al., 2008). By using the *wnt1* promoter/enhancer in combination with Gal4-VP16-mediated GFP expression, which has an exceptional stability, the migration and differentiation of *wnt1*-expressing progeny can be followed over several days in *wnt1*-GVP-UG transgenic embryos.

With the help of in vivo time-lapse expression and retrograde axon projection analysis, we could identify these cells as the likely precursors of the secondary gustatory/viscerosensory nucleus and the nucleus isthmi and/or the superior reticular nucleus, the zebrafish homologues of the parabrachial and parabigeminal and/or the laterodorsal-pedunclopontine nuclei in mammals. Recent fate

map studies in the mouse reported these hindbrain nuclei to arise in the URL of the cerebellum, but the relevance of this study for anamniotic vertebrates including teleosts remained elusive. Based on their expression of the transcription factor *atonal1a*, neurons of the secondary gustatory/viscerosensory nucleus and nucleus isthmi/superior reticular nucleus were found to have their origin in the *wnt1*-expressing URL in zebrafish. Moreover, our time-lapse study confirmed the sequence of cell populations produced by the cerebellar rhombic lip that was observed in the mouse, starting with *wnt1*-expressing precursors contributing to several tegmental nuclei of the hindbrain and finally granule neuron precursors (Nichols and Bruce, 2006; Volkmann et al., 2008). Thus, the generation of different neuronal cell populations from the URL over time that was reported for the embryonic mouse cerebellum is conserved among vertebrate species. In zebrafish, though, this temporal change of the URL in producing different neuronal cell populations is more condensed, occurring within 24 hours compared with about 3 days in mouse. This makes zebrafish embryos well suited for analyzing the underlying in vivo dynamics.

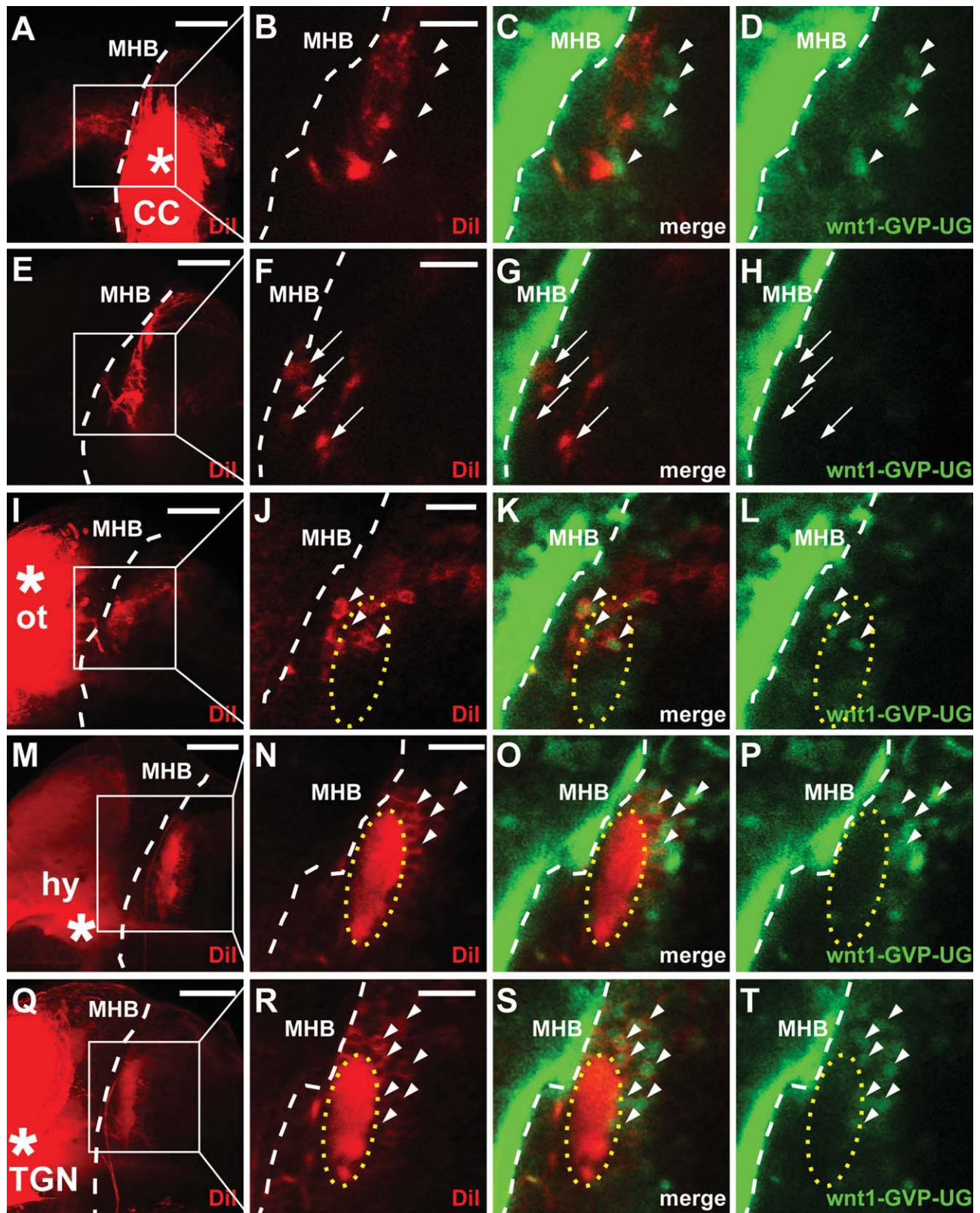


Figure 7



## Rhombic lip *wnt1*-expressing cells represent URL-derived cell types that migrate over long distances

The premigratory GFP-expressing cells in the URL of *wnt1*-GVP-UG embryos were found to be in a proliferative state based on time-lapse and immunohistochemical analysis. In vivo observation can therefore be used to follow their fate from birth until terminal differentiation. Combining transient DNA injection to obtain Gal4-VP16-mediated cell-population-specific but mosaic labeling with in vivo time-lapse confocal microscopy allowed us to trace individual cells along their migratory route and to quantify their characteristic behavior. Migration is initiated at about 24 hpf, shortly after the rotation of the zebrafish cerebellar primordium (Distel et al., 2006), and this migration peaks at about 36 hpf and ceases until 48 hpf, the time when granule progenitor cells begin to be generated in the URL. The neuronal progenitors leave the URL and move rostrally to the MHB, similarly to immature cerebellar granule neurons. After reaching the MHB, these immature hindbrain tegmental nuclei neurons turn ventrally and migrate along the MHB into the depth of the neural tube. Eventually, these neurons settle in the tegmentum, forming bilateral symmetric clusters in the ventral part of rhombomere 1, where they terminally differentiate. In contrast migrating granule neurons take a superficial path directly beneath the surface of the neural tube and either settle mediodorsally in the corpus cerebelli or migrate lateroventrally to form the eminentia granularis (Volkman et al., 2008). Thus, the neuronal populations generated early by the zebrafish URL, namely, the precursors of the secondary gustatory/viscerosensory nucleus and nucleus isthmi/superior reticular nucleus, follow migration routes clearly different from those of the late-arising cerebellar granule cell population.

Software-supported individual cell tracing allowed us to calculate the speed of cell migration, which was similar

to the velocity reported for early-migrating neuronal precursors in a recent zebrafish study (Rieger et al., 2008). In this study, the characterized neuronal progenitors also originated in the URL and followed similar migration routes. Interestingly, it was demonstrated that polysialylation of NCAM was required for their migration along the anteroventral pathway into ventral rhombomere 1, but the identity of these cells remained unclear. We show here that *wnt1*-expressing URL-derived cells express PSA during migration, that neuronal progenitors of the secondary gustatory/viscerosensory nucleus and nucleus isthmi/superior reticular tegmental nuclei are among these PSA-dependent migrating neuronal precursors with URL origin, and that they likely regulate their motility via modulating NCAM-mediated cell-cell adhesion through polysialylation.

In addition, we observed the expression of the neuron-specific adhesion factor neurolin in postmigratory neurons and axons, suggesting that it has a later function in regulating terminal differentiation, such as the proper formation of axonal projections. We have identified these projections of secondary gustatory/viscerosensory nucleus and nucleus isthmi/superior reticular nucleus via retrograde labeling in the developing zebrafish brain, so the groundwork for such functional studies has been laid.

## Tegmental nuclei of rhombomere 1 contain besides cholinergic also glutamatergic neurons

The neuronal population of the general viscerosensory nucleus, initially described as part of the goldfish secondary gustatory nucleus (Zottoli et al., 1988), was later shown to lie directly ventrally adjacent to the secondary gustatory nucleus, differing from it by its calcitonin gene-related peptide (CGRP) content and by its different input from primary sensory areas, clearly representing the

**Figure 7.** A–T: *wnt1*-GVP-UG neurons project to the hypothalamus, the ventrorostral diencephalon, and the optic tectum but not to the corpus cerebelli. Maximum-intensity projection of confocal image stack (stack of 30–40 images each 3  $\mu$ m apart) of 4-dpf brains microinjected with Dil into the corpus cerebelli (A,E), optic tectum (I), hypothalamus (M), and ventrorostral diencephalon (tertiary gustatory nucleus; Q; injection site is marked with white asterisk) in dorsal views. Right panels show boxed areas in the left panels in magnified views as single optical sections: Dil-labeled cells in red, overlay and GFP-expressing cells in green. Individual Dil-labeled GFP-positive cells of the ventral cluster are marked by white arrowheads. Injection of Dil into the molecular layer and the granule cell layer of the corpus cerebelli results in Dil-positive cells located ventrally and rostromedially to the GFP cell cluster, likely in the nucleus lateralis valvulae (F–H, white arrows); no Dil labeling was found in the GFP-expressing *wnt1*-GVP-UG neurons (B–D, white arrowheads; Dil in B,C are stained axonal fascicles). Note that F–H show an optical section 33  $\mu$ m ventral to the section in B–D. Dil-labeled GFP-expressing neurons can be found after injection into the optic tectum in a subpopulation of tegmental nuclei neurons anteroventral to the cerebellar tract (dashed ovals) close to the MHB (J–L, white arrowheads). After injection into the hypothalamus (N–P) and the ventrorostral diencephalon (R–T), Dil labeling is confined to GFP-positive cells (white arrowheads) posterior to the cerebellar tract (dashed ovals). A magenta-green version of this figure is available online as Supporting Information Figure 6. CC, corpus cerebelli; hy, hypothalamus; MHB, midbrain-hindbrain boundary; ot, optic tectum; TGN, preglomerular tertiary gustatory nucleus. Scale bars = 50  $\mu$ m in A,E,I,M,Q; 20  $\mu$ m in B (applies to B–D); 20  $\mu$ m in F (applies to F–H); 20  $\mu$ m in J (applies to J–L); 20  $\mu$ m in N (applies to N–P); 20  $\mu$ m in R (applies to R–T). [Color figure can be viewed in the online issue, which is available at [www.interscience.wiley.com](http://www.interscience.wiley.com).]

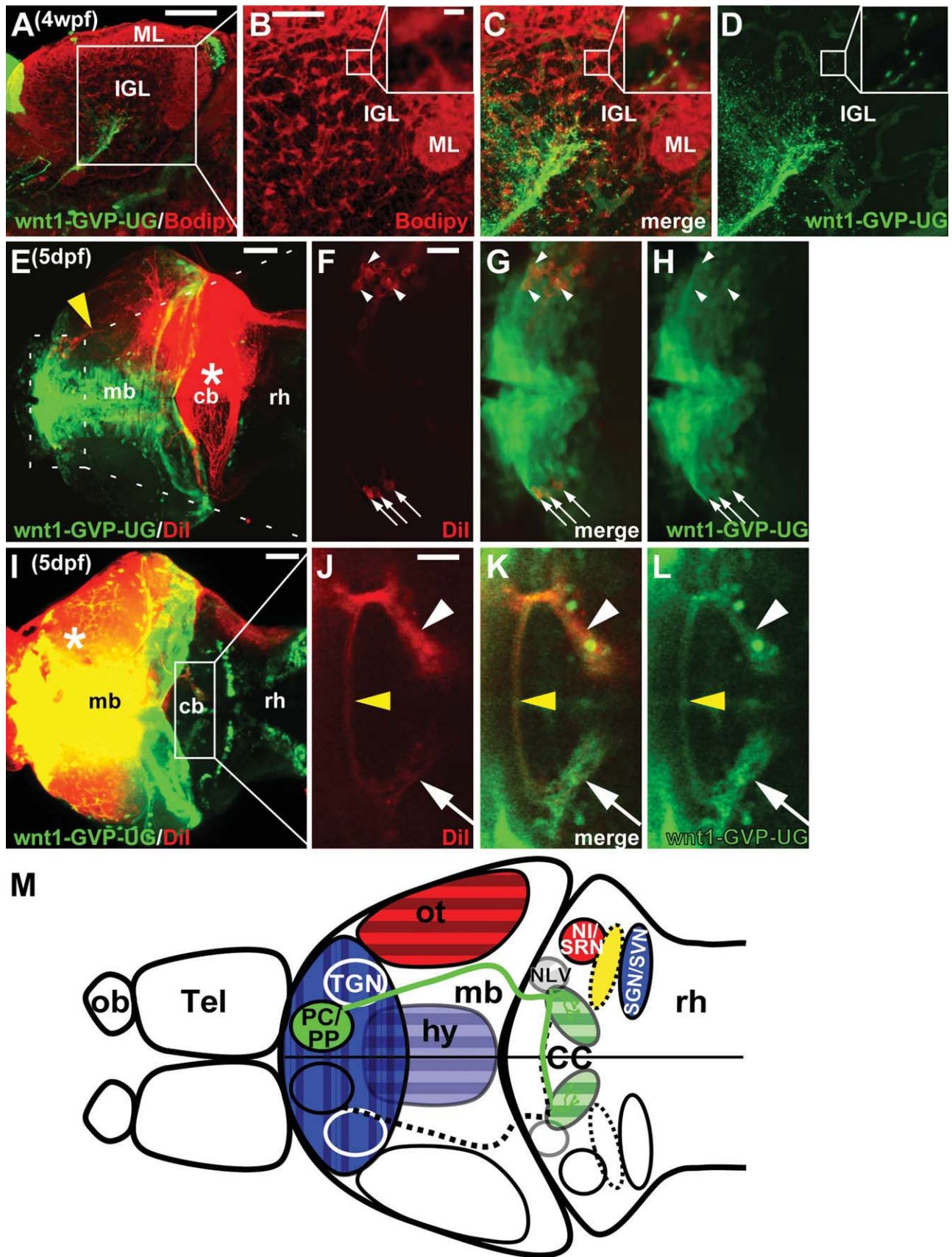


Figure 8

secondary general viscerosensory nucleus (Finger and Kanwal, 1992; also in the catfish). Later, a similar cholinergic population was shown in the African red cichlid (Ahrens et al., 2002), whereas, in the zebrafish (Mueller et al., 2004) and particularly in the trout (Perez et al., 2000), the cholinergic neurons seemed to extend into the secondary gustatory nucleus as well. The mammalian parabrachial nucleus also contains CGRP-containing neuronal subpopulations, namely, the external medial and ventral lateral subnuclei (Saper, 2002). However, their ascending projections speak for a secondary gustatory, not a general viscerosensory, nature, because these cells contribute to tertiary gustatory projections to (the ventroposterior parvicellular nucleus of) the dorsal thalamus (Yasui et al., 1989; Saper, 2002), the relay nucleus to the gustatory opercular/insular cortex. Thus, the teleostean secondary gustatory nucleus represents the homologue of the mammalian parabrachial nucleus.

What of the teleostean secondary general viscerosensory nucleus? There are additional CGRP-containing neurons in the central, dorsal, and external lateral subnuclei of the mammalian parabrachial nucleus (Yasui et al., 1989), and these nuclei project to the hypothalamus (Bester et al., 1997). Furthermore, ChAT-immunoreactive cells have been observed in the mammalian parabrachial nucleus (Jones and Beaudet, 1987; Tago et al., 1989) in the external medial and lateral subnuclei (Ruggiero et al.,

1990). Thus, if the CGRP cells in at least the external lateral parabrachial subnucleus are at the same time cholinergic and project to the hypothalamus, they may correspond to the secondary general viscerosensory system described above for teleosts.

With the help of ChAT immunohistochemistry, we could demonstrate that *wnt1*-expressing progenitors of the secondary gustatory/viscerosensory nucleus and nucleus isthmi/superior reticular nucleus that leave the cerebellar rhombic lip acquire at least partially a cholinergic fate in the tegmental area of rhombomere 1. In summary, the secondary viscerosensory (and maybe also the secondary gustatory) nucleus, nucleus isthmi, and superior reticular nucleus of the zebrafish brain contain cholinergic neurons, as do their mammalian homologues the parabrachial, parabigeminal, and laterodorsal-pedunculopontine tegmental nuclei (Jones and Beaudet, 1987; Tago et al., 1989).

Some *wnt1*-GVP-UG neurons positioned in the region of the tegmental nuclei of rhombomere 1 were glutamatergic based on *vglut2.1* expression. This is in good agreement with the idea that the URL produces predominantly glutamatergic neurons and the recent finding in rat showing that the mammalian secondary gustatory nucleus area homologue, namely, the parabrachial nuclear complex, is of a dual composition formed by cholinergic and glutamatergic (*vglut2*-expressing) neurons (Geisler et al., 2007).

**Figure 8.** GFP fluorescent mossy fiber-like projections in the granule cell layer of the corpus cerebelli originate in the pretectal area of the diencephalon. Maximum-intensity projection of confocal stacks (stack of 38 images each 2  $\mu\text{m}$  apart; A) and (stack of 83 images each 1  $\mu\text{m}$  apart; B–D) in a lateral view of the corpus cerebelli of a 4-wpf juvenile *wnt1*-GVP-UG fish. GFP-positive mossy fiber-like projections ending in glomeruli in the granule cell layer of the corpus cerebelli are visible. **Insets** show the synaptic thickenings typical for mossy fibers. **E–L:** Maximum-intensity projection of confocal image stack (stack of 40 images each 4  $\mu\text{m}$  apart) recorded in a dorsal view from 5-dpf *wnt1*-GVP-UG larvae after injection of Dil into the granule cell layer of the corpus cerebelli (E–H) or the pretectal area of the diencephalon (I–L; injection site marked with asterisk in E,I). The Dil-labeled axonal projection transversing the midbrain is marked by a yellow arrowhead in E. F–H show magnified view of single optical section of boxed area in E. GFP-positive cells labeled retrogradely by Dil in the ipsilateral pretectum are visible marked by white arrowheads. Dil-labeled cells on the contralateral side (arrows) are labeled via commissural axons within the pretectum (not shown). J–L show magnified view of single optical section of boxed area in I. The GFP-positive mossy fiber endings in the corpus cerebelli were found to be anterogradely labeled with Dil, predominantly on the ipsilateral side (white arrowheads) but also to a lesser extent on the contralateral side (arrows). The commissure formed in the cerebellum is marked by a yellow arrowhead. **M:** Summary of retrograde labeling experiments as a schematic drawing of larval zebrafish brain. Dil injection sites (shaded) and the correspondingly labeled nuclei are depicted in the same color; the position of the cerebellar tract is marked in yellow. The nucleus isthmi/superior reticular nucleus (red circle) and the secondary gustatory/viscerosensory nucleus (blue oval) in the tegmentum of rhombomere 1 have axonal projections targeting areas in the midbrain and diencephalon, respectively. The nucleus isthmi and the superior reticular nucleus are projecting to the optic tectum, whereas the secondary gustatory/viscerosensory nucleus projects to hypothalamus and preglomerular tertiary gustatory nucleus in the ventral rostral diencephalon. The nucleus lateralis valvulae (gray circle) in close proximity to the nucleus isthmi, and the secondary gustatory/viscerosensory nucleus has prominent projection into the corpus cerebelli but does not appear to be derived from *wnt1*-expressing URL progenitors. Mossy fiber-like projections from the paracommissural nucleus and/or periventricular pretectal nucleus (green circle) are terminating in the granule cell layer of the ipsi- and contralateral corpus cerebelli (shaded in green) formed by the granule neurons of the nonvestibular cerebellar system in zebrafish. A magenta-green version of this figure is available online as Supporting Information Figure 7. cb, Cerebellum; CC, corpus cerebelli; hy, hypothalamus; IGL, internal granule cell layer; mb, midbrain; ML, molecular layer; NI, nucleus isthmi; NLV, nucleus lateralis valvulae; ob, olfactory bulb; ot, optic tectum; PC, paracommissural nucleus; PP: dorsal periventricular pretectal nucleus, rh, rhombencephalon; SGN/SVN, secondary gustatory/viscerosensory nucleus; SRN, superior reticular nucleus; Tel, telencephalon; TGN, preglomerular tertiary gustatory nucleus. Scale bars = 100  $\mu\text{m}$  in A; 50  $\mu\text{m}$  in B (applies to B–D); 50  $\mu\text{m}$  in E,I; 20  $\mu\text{m}$  in insets; 20  $\mu\text{m}$  in F (applies to F–H); 20  $\mu\text{m}$  in J (applies to J–L). [Color figure can be viewed in the online issue, which is available at [www.interscience.wiley.com](http://www.interscience.wiley.com).]

## Tegmental hindbrain nuclei can be discriminated by their different axonal projections

We have shown by time-lapse analysis that the teleostean nucleus isthmi, superior reticular nucleus, and secondary gustatory/viscerosensory nucleus are formed by neuronal precursors that leave the primordium of the cerebellum to populate the tectum in rhombomere 1. Subsequently, they integrate into distinct neuronal circuitries, fulfilling functions different from those of the cerebellum. These nuclei are responsible for processing sensory information, as are their mammalian counterparts that have the same developmental origin. In our retrograde Dil labeling studies, we observed the neurons of the ventrorostral portion of the GFP-fluorescent cluster to project to the optic tectum. We thus identified these tegmental neurons anteroventral to the cerebellar tract as the nucleus isthmi or superior reticular nucleus of the zebrafish larval brain. Tegmental neurons located posterior to this tract were found to innervate the hypothalamus and the preglomerular tertiary gustatory nucleus (TGN) in the ventrorostral diencephalon. These neurons thus belong to the secondary gustatory/viscerosensory nucleus and are likely to mediate gustatory/viscerosensory information to diencephalic areas. The cerebellar tract can therefore serve to distinguish nucleus isthmi/superior reticular nucleus and secondary gustatory/viscerosensory nucleus neurons by their relative position (Fig. 7M). Moreover, these Dil retrograde labeling experiments revealed that the efferent connections of secondary gustatory/viscerosensory nucleus and nucleus isthmi/superior reticular nucleus as described for the adult brain are already established at 4 dpf in the zebrafish larval brain. Thus, the formation of these evolutionarily conserved neuronal circuitries occurs in zebrafish in a very condensed time frame, allowing their dynamics to be studied *in vivo* by time-lapse microscopy.

In addition, our anterograde and retrograde labeling experiments identified afferents of the zebrafish cerebellum that are not derived from the *wnt1*-positive URL. A first such input was shown to arise from the nucleus lateralis valvulae, which apparently does not contain *wnt1*-expressing cells. Thus it is possible that this large nuclear mass arises from the caudal rhombic lip, as do the mammalian pontine nuclei. However, for this to be true, these cell masses would have to cross the midbrain–hindbrain boundary, because they lie clearly anterior to it in the adult brain. A homology with the mammalian pontine nuclei is unlikely for additional reasons. First, the nucleus lateralis valvulae does not receive a telencephalic input in teleosts (Wullimann and Meyer, 1993), although the closely related and also cerebellar-projecting dorsal teg-

mental nucleus does and has been included in other studies in the nucleus lateralis valvulae (see Yang et al., 2004). More importantly, a phylogenetic comparison involving amphibians and reptiles indicates that there are no pontine nuclei in basal tetrapods (Wullimann and Meyer, 1993), so nucleus lateralis valvulae and pontine nuclei are at most a case of parallel evolution.

It has to be noted that GFP expression under control of the *wnt1* promoter/enhancer in the *wnt1*-GVP-UG line is not covering all *wnt1*-expressing URL-derived neuronal populations observed in the mouse (precerebellar neurons sending mossy fibers into the cerebellum; Nichols and Bruce, 2006). This observation might be partially explained by the functional redundancy and overlapping but not completely identical expression patterns of the two Wnt family members, Wnt1 and Wnt10b, in zebrafish (Lekven et al., 2003). Thus, from this study, we can report only on the origin and migratory behavior of neuronal populations labeled in our transgenic *wnt1*-GVP-UG line but cannot exclude that additional neuronal populations are generated by *wnt10b*-expressing progenitors in the URL or lower rhombic lip that resemble the residual neurons derived from the *wnt1*-expressing rhombic lip in the mouse. Furthermore, although the majority of the neurons of the larval secondary gustatory/viscerosensory nucleus and nucleus isthmi/superior reticular nucleus was found to be formed by *wnt1*-expressing progenitor cells originating from the URL, we cannot exclude that progenitors with other origin also contribute to these nuclei.

A second population of *wnt1*-expressing neuronal progenitors (not derived from the URL) is situated in the pretectal area of the diencephalon (Fig. 8I) and likely contributes to the paracommissural nuclei (PC) and/or the dorsal periventricular pretectal nucleus (PP; Wullimann and Northcutt, 1988; Imura et al., 2003; Folgueira et al., 2006, 2008). By antero- and retrograde axonal tracing, we identified these neurons rather than the nucleus lateralis valvulae as the source of the observed axonal input to the corpus cerebelli in *wnt1*-GVP-UG transgenic embryos. The afferents provide differentially weighted visual (if from PP) or telencephalic (if from PC) input via both ipsilateral and contralateral projections to the corpus cerebelli, where their terminals end in characteristic mossy fiber-like terminals.

The function of the cerebellum is conserved in vertebrates in regulating body posture and the smooth coordination of locomotion. In all vertebrates examined (including teleosts and mammals), the neuronal cell types of the cerebellar cortex and their morphology are highly conserved (Altman and Bayer, 1997). Less well studied so far is the evolutionary conservation of the developmental origin of these cell types, the underlying genetics, and their dynamic behavior during differentiation. Here we have

attempted to contribute toward filling this knowledge gap. So far, the differentiation of only two neuronal populations that originate in the zebrafish cerebellum has been characterized, the granule neurons (Volkman et al., 2008) and eurydendroid neurons, the homologue of the mammalian deep cerebellar nuclei (McFarland et al., 2008). Here we have provided evidence that, prior to the generation of granule neurons, the zebrafish URL gives rise to neurons of tegmental hindbrain nuclei. Thus, the temporal order of the cerebellar rhombic lip in producing different neuronal populations during neurogenesis as well as the fate and the migratory properties of these neurons is conserved between teleosts and mammals.

## ACKNOWLEDGMENTS

We thank Enrico Kühn and Petra Hammerl for excellent technical assistance and animal care. We are grateful to Laure Bally-Cuif, Corinne Houart, Francesco Argenton, John Kuwada, Shin-ichi Higashijima, and Marina Mione for kindly providing zebrafish cDNA constructs. We thank all members of the Köster laboratory for helpful discussions, particularly Jen Hocking and Kazuhiko Namikawa for helpful suggestions and critical reading of the manuscript.

## LITERATURE CITED

- Ahrens K, Wullimann MF. 2002. Hypothalamic inferior lobe and lateral torus connections in a percomorph teleost, the red chichlid (*Hemichromis lifalili*). *J Comp Neurol* 449: 43–64.
- Altman J, Bayer SA. 1997. Development of the cerebellar system in relation to its evolution, structure, and functions. Boca Raton, FL: CRC Press.
- Anadon R, Molist P, Rodriguez-Moldes I, Lopez JM, Quintela I, Cervino MC, Barja P, Gonzalez A. 2000. Distribution of choline acetyltransferase immunoreactivity in the brain of an elasmobranch, the lesser spotted dogfish (*Scyliorhinus canicula*). *J Comp Neurol* 420:139–170.
- Arenzana FJ, Clemente D, Sanchez-Gonzalez R, Porteros A, Aijon J, Arevalo R. 2005. Development of the cholinergic system in the brain and retina of the zebrafish. *Brain Res Bull* 66:421–425.
- Bester H, Besson JM, Bernard JF. 1997. Organization of efferent projections from the parabrachial area to the hypothalamus: a *Phaseolus vulgaris*-leucoagglutinin study in the rat. *J Comp Neurol* 383:245–281.
- Brochu G, Maler L, Hawkes R. 1990. Zebrin II: a polypeptide antigen expressed selectively by Purkinje cells reveals compartments in rat and fish cerebellum. *J Comp Neurol* 291:538–552.
- Castro A, Becerra M, Manso MJ, Anadon R. 2006. Calretinin immunoreactivity in the brain of the zebrafish, *Danio rerio*: distribution and comparison with some neuropeptides and neurotransmitter-synthesizing enzymes. II. Midbrain, hindbrain, and rostral spinal cord. *J Comp Neurol* 494: 792–814.
- Clark WE. 1933. The medial geniculate body and the nucleus isthmi. *J Anat* 67:536–548.
- Clemente D, Porteros A, Weruaga E, Alonso JR, Arenzana FJ, Aijon J, Arevalo R. 2004. Cholinergic elements in the zebrafish central nervous system: histochemical and immunohistochemical analysis. *J Comp Neurol* 474:75–107.
- Clemente D, Arenzana FJ, Sanchez-Gonzalez R, Porteros A, Aijon J, Arevalo R. 2005. Comparative analysis of the distribution of choline acetyltransferase in the central nervous system of cyprinids. *Brain Res Bull* 66:546–549.
- Costagli A, Kapsimali M, Wilson SW, Mione M. 2002. Conserved and divergent patterns of reelin expression in the zebrafish central nervous system. *J Comp Neurol* 450: 73–93.
- Distel M, Babaryka A, Koster RW. 2006. Multicolor in vivo time-lapse imaging at cellular resolution by stereomicroscopy. *Dev Dyn* 235:1100–1106.
- Fashena D, Westerfield M. 1999. Secondary motoneuron axons localize DM-GRASP on their fasciculated segments. *J Comp Neurol* 406:415–424.
- Finger TE. 1978. Cerebellar afferents in teleost catfish (Ictaluridae). *J Comp Neurol* 181:173–181.
- Finger TE, Kanwal JS. 1992. Ascending general visceral pathways within the brainstems of two teleost fishes: *Ictalurus punctatus* and *Carassius auratus*. *J Comp Neurol* 320: 509–520.
- Fink AJ, Englund C, Daza RA, Pham D, Lau C, Nivison M, Kowalczyk T, Hevner RF. 2006. Development of the deep cerebellar nuclei: transcription factors and cell migration from the rhombic lip. *J Neurosci* 26:3066–3076.
- Folgueira M, Anadon R, Yanez J. 2003. Experimental study of the connections of the gustatory system in the rainbow trout, *Oncorhynchus mykiss*. *J Comp Neurol* 465:604–619.
- Folgueira M, Anadon R, Yanez J. 2006. Afferent and efferent connections of the cerebellum of a salmonid, the rainbow trout (*Oncorhynchus mykiss*): a tract-tracing study. *J Comp Neurol* 497:542–565.
- Folgueira M, Anadon R, Yanez J. 2008. The organization of the pretectal nuclei in the trout: a revision based on experimental histological studies. *Brain Res Bull* 75:251–255.
- Geisler S, Derst C, Veh RW, Zahm DS. 2007. Glutamatergic afferents of the ventral tegmental area in the rat. *J Neurosci* 27:5730–5743.
- Giraldez-Perez RM, Gaytan SP, Torres B, Pasaro R. 2009. Colocalization of nitric oxide synthase and choline acetyltransferase in the brain of the goldfish (*Carassius auratus*). *J Chem Neuroanat* 37:1–17.
- Herrick CJ. 1905. The central gustatory paths in the brains of bony fishes. *J Comp Neurol* 15:374–457.
- Higashijima S, Mandel G, Fetcho JR. 2004. Distribution of prospective glutamatergic, glycinergic, and GABAergic neurons in embryonic and larval zebrafish. *J Comp Neurol* 480: 1–18.
- Hoshino M, Nakamura S, Mori K, Kawauchi T, Terao M, Nishimura YV, Fukuda A, Fuse T, Matsuo N, Sone M, Watanabe M, Bito H, Terashima T, Wright CV, Kawaguchi Y, Nakao K, Nabeshima Y. 2005. Ptf1a, a bHLH transcriptional gene, defines GABAergic neuronal fates in cerebellum. *Neuron* 47:201–213.
- Ikenaga T, Yoshida M, Uematsu K. 2005. Morphology and immunohistochemistry of efferent neurons of the goldfish corpus cerebelli. *J Comp Neurol* 487:300–311.
- Ikenaga T, Yoshida M, Uematsu K. 2006. Cerebellar efferent neurons in teleost fish. *Cerebellum* 5:268–274.
- Imura K, Yamamoto N, Sawai N, Yoshimoto M, Yang CY, Xue HG, Ito H. 2003. Topographical organization of an indirect telencephalo-cerebellar pathway through the nucleus paracommissuralis in a teleost, *Oreochromis niloticus*. *Brain Behav Evol* 61:70–90.
- Ito H, Yoshimoto M. 1990. Cytoarchitecture and fiber connections of the nucleus lateralis valvulae in the carp (*Cyprinus carpio*). *J Comp Neurol* 298:385–399.

- Ito H, Sakamoto N, Takatsuji K. 1982. Cytoarchitecture, fiber connections, and ultrastructure of nucleus isthmi in a teleost (*Navodon modestus*) with a special reference to degenerating isthmic afferents from optic tectum and nucleus pretectalis. *J Comp Neurol* 205:299–311.
- Jones BE, Beaudet A. 1987. Distribution of acetylcholine and catecholamine neurons in the cat brainstem: a choline acetyltransferase and tyrosine hydroxylase immunohistochemical study. *J Comp Neurol* 261:15–32.
- Kanki JP, Chang S, Kuwada JY. 1994. The molecular cloning and characterization of potential chick DM-GRASP homologs in zebrafish and mouse. *J Neurobiol* 25:831–845.
- Kim CH, Bae YK, Yamanaka Y, Yamashita S, Shimizu T, Fujii R, Park HC, Yeo SY, Huh TL, Hibi M, Hirano T. 1997. Overexpression of neurogenin induces ectopic expression of HuC in zebrafish. *Neurosci Lett* 239:113–116.
- Kimmel CB, Ballard WW, Kimmel SR, Ullmann B, Schilling TF. 1995. Stages of embryonic development of the zebrafish. *Dev Dyn* 203:253–310.
- Köster RW, Fraser SE. 2001a. Direct imaging of in vivo neuronal migration in the developing cerebellum. *Curr Biol* 11:1858–1863.
- Köster RW, Fraser SE. 2001b. Tracing transgene expression in living zebrafish embryos. *Dev Biol* 233:329–346.
- Köster RW, Fraser SE. 2004. Time-lapse microscopy of brain development. *Methods Cell Biol* 76:207–235.
- Köster RW, Fraser SE. 2006. FGF signaling mediates regeneration of the differentiating cerebellum through repatterning of the anterior hindbrain and reinitiation of neuronal migration. *J Neurosci* 26:7293–7304.
- Laessing U, Giordano S, Stecher B, Lottspeich F, Stuermer CA. 1994. Molecular characterization of fish neurolin: a growth-associated cell surface protein and member of the immunoglobulin superfamily in the fish retinotectal system with similarities to chick protein DM-GRASP/SC-1/BEN. *Differentiation* 56:21–29.
- Lekven AC, Buckles GR, Kostakis N, Moon RT. 2003. Wnt1 and wnt10b function redundantly at the zebrafish midbrain–hindbrain boundary. *Dev Biol* 254:172–187.
- Machold R, Fishell G. 2005. Math1 is expressed in temporally discrete pools of cerebellar rhombic-lip neural progenitors. *Neuron* 48:17–24.
- Mann CJ, Hinits Y, Hughes SM. 2006. Comparison of neurolin (ALCAM) and neurolin-like cell adhesion molecule (NLCAM) expression in zebrafish. *Gene Expr Patterns* 6:952–963.
- Marx M, Rutishauser U, Bastmeyer M. 2001. Dual function of polysialic acid during zebrafish central nervous system development. *Development* 128:4949–4958.
- McFarland KA, Topczewska JM, Weidinger G, Dorsky RI, Appel B. 2008. Hh and Wnt signaling regulate formation of olig2<sup>+</sup> neurons in the zebrafish cerebellum. *Dev Biol* 318:162–171.
- Mione M, Shanmugalingam S, Kimelman D, Griffin K. 2001. Overlapping expression of zebrafish T-brain-1 and eomesodermin during forebrain development. *Mech Dev* 100:93–97.
- Mione M, Baldessari D, Deflorian G, Nappo G, Santoriello C. 2008. How neuronal migration contributes to the morphogenesis of the CNS: insights from the zebrafish. *Dev Neurosci* 30:65–81.
- Morita Y, Ito H, Masai H. 1980. Central gustatory paths in the crucian carp, *Carassius carassius*. *J Comp Neurol* 191:119–132.
- Morita Y, Murakami T, Ito H. 1983. Cytoarchitecture and topographic projections of the gustatory centers in a teleost, *Carassius carassius*. *J Comp Neurol* 218:378–394.
- Mueller T, Vernier P, Wullimann MF. 2004. The adult central nervous cholinergic system of a neurogenetic model animal, the zebrafish *Danio rerio*. *Brain Res* 1011:156–169.
- Mufson EJ, Martin TL, Mash DC, Wainer BH, Mesulam MM. 1986. Cholinergic projections from the parabrachial nucleus (Ch8) to the superior colliculus in the mouse: a combined analysis of horseradish peroxidase transport and choline acetyltransferase immunohistochemistry. *Brain Res* 370:144–148.
- Nichols DH, Bruce LL. 2006. Migratory routes and fates of cells transcribing the Wnt-1 gene in the murine hindbrain. *Dev Dyn* 235:285–300.
- Northmore DP. 1991. Visual responses of nucleus isthmi in a teleost fish (*Lepomis macrochirus*). *Vis Res* 31:525–535.
- Perez SE, Yanez J, Marin O, Anadon R, Gonzalez A, Rodriguez-Moldes I. 2000. Distribution of choline acetyltransferase (ChAT) immunoreactivity in the brain of the adult trout and tract-tracing observations on the connections of the nuclei of the isthmus. *J Comp Neurol* 428:450–474.
- Rieger S, Volkman K, Köster RW. 2008. Polysialyltransferase expression is linked to neuronal migration in the developing and adult zebrafish. *Dev Dyn* 237:276–285.
- Rink E, Wullimann MF. 1998. Some forebrain connections of the gustatory system in the goldfish *Carassius auratus* visualized by separate Dil application to the hypothalamic inferior lobe and the torus lateralis. *J Comp Neurol* 394:152–170.
- Ruggiero DA, Giuliano R, Anwar M, Stornetta R, Reis DJ. 1990. Anatomical substrates of cholinergic-autonomic regulation in the rat. *J Comp Neurol* 292:1–53.
- Sakamoto N, Ito H, Ueda S. 1981. Topographic projections between the nucleus isthmi and the optic tectum in a teleost, *Navodon modestus*. *Brain Res* 224:225–234.
- Saper CB. 2002. The central autonomic nervous system: conscious visceral perception and autonomic pattern generation. *Annu Rev Neurosci* 25:433–469.
- Saper CB, Loewy AD. 1980. Efferent connections of the parabrachial nucleus in the rat. *Brain Res* 197:291–317.
- Sittaramane V, Sawant A, Wolman MA, Maves L, Halloran MC, Chandrasekhar A. 2008. The cell adhesion molecule Tag1, transmembrane protein Stbm/Vangl2, and Laminin alpha1 exhibit genetic interactions during migration of facial branchiomotor neurons in zebrafish. *Dev Biol* (in press).
- Striedter GF, Northcutt RG. 1989. Two distinct visual pathways through the superficial pretectum in a percomorph teleost. *J Comp Neurol* 283:342–354.
- Tago H, McGeer PL, McGeer EG, Akiyama H, Hersh LB. 1989. Distribution of choline acetyltransferase immunopositive structures in the rat brainstem. *Brain Res* 495:271–297.
- Vinogradova VM, Manteifel’lu B. 1977. [Responses of neurons in the nucleus isthmi region of the frog to optic nerve stimulation]. *Neirofiziologija* 9:33–40.
- Volkman K, Rieger S, Babaryka A, Köster RW. 2008. The zebrafish cerebellar rhombic lip is spatially patterned in producing granule cell populations of different functional compartments. *Dev Biol* 313:167–180.
- Wang VY, Rose MF, Zoghbi HY. 2005. Math1 expression redefines the rhombic lip derivatives and reveals novel lineages within the brainstem and cerebellum. *Neuron* 48:31–43.
- Westerfield M. 1995. The zebrafish book. Eugene, OR: University of Oregon Press.
- Wolf NJ. 1991. Cholinergic systems in mammalian brain and spinal cord. *Prog Neurobiol* 37:475–524.
- Wullimann MF. 1998. The central nervous system. In: Evans DH, editor. *The physiology of fishes*. Boca Raton, FL: CRC Press, Inc..
- Wullimann MF. 1988. The tertiary gustatory center in sunfishes is not nucleus glomerulosus. *Neurosci Lett* 86:9–10.
- Wullimann MF, Knipp S. 2000. Proliferation pattern changes in the zebrafish brain from embryonic through early post-embryonic stages. *Anat Embryol* 202:385–400.

- Wullimann MF, Meyer DL. 1993. Possible multiple evolution of indirect telencephalo-cerebellar pathways in teleosts: studies in *Carassius auratus* and *Pantodon buchholzi*. *Cell Tissue Res* 274:447–455.
- Wullimann MF, Northcutt RG. 1988. Connections of the corpus cerebelli in the green sunfish and the common goldfish: a comparison of perciform and cypriniform teleosts. *Brain Behav Evol* 32:293–316.
- Wullimann MF, Northcutt RG. 1989. Afferent connections of the valvula cerebelli in two teleosts, the common goldfish and the green sunfish. *J Comp Neurol* 289:554–567.
- Wullimann MF, Rupp B, Reichert H. 1996. *Neuroanatomy of the zebrafish brain*. Basel: Birkhaeuser Verlag.
- Xue HG, Yamamoto N, Yoshimoto M, Yang CY, Ito H. 2001. Fiber connections of the nucleus isthmi in the carp (*Cyprinus carpio*) and tilapia (*Oreochromis niloticus*). *Brain Behav Evol* 58:185–204.
- Xue HG, Yamamoto N, Yang CY, Imura K, Ito H. 2004. Afferent connections of the corpus cerebelli in holocentrid teleosts. *Brain Behav Evol* 64:242–258.
- Yang CY, Yoshimoto M, Xue HG, Yamamoto N, Imura K, Sawai N, Ishikawa Y, Ito H. 2004. Fiber connections of the lateral valvular nucleus in a percomorph teleost, tilapia (*Oreochromis niloticus*). *J Comp Neurol* 474:209–226.
- Yasui Y, Saper CB, Cechetto DF. 1989. Calcitonin gene-related peptide immunoreactivity in the visceral sensory cortex, thalamus, and related pathways in the rat. *J Comp Neurol* 290:487–501.
- Yokogawa T, Marin W, Faraco J, Pezeron G, Appelbaum L, Zhang J, Rosa F, Mourrain P, Mignot E. 2007. Characterization of sleep in zebrafish and insomnia in hypocretin receptor mutants. *PLoS Biol* 5:2379–2397.
- Zecchin E, Mavropoulos A, Devos N, Filippi A, Tiso N, Meyer D, Peers B, Bortolussi M, Argenton F. 2004. Evolutionary conserved role of ptf1a in the specification of exocrine pancreatic fates. *Dev Biol* 268:174–184.
- Zottoli SJ, Rhodes KJ, Corrodi JG, Mufson EJ. 1988. Putative cholinergic projections from the nucleus isthmi and the nucleus reticularis mesencephali to the optic tectum in the goldfish (*Carassius auratus*). *J Comp Neurol* 273:385–398.

## **Appendix 2**

Article in **Developmental Dynamics**

### **Polysialyltransferase Expression Is Linked to Neuronal Migration in the Developing and Adult Zebrafish**

Sandra Rieger, Katrin Volkmann and Reinhard W. Köster

Developmental Dynamics 237: 276–285 (2008)

#### **Contribution**

This project was mainly conducted by Sandra Rieger, I participated in the expression analysis (Figure 3) and the recording of additional movies followed by data analysis (shown in Figure 4) for the revision process of this paper.



# Polysialyltransferase Expression Is Linked to Neuronal Migration in the Developing and Adult Zebrafish

Sandra Rieger, Katrin Volkmann, and Reinhard W. Köster\*

Modulation of cell–cell adhesion is crucial for regulating neuronal migration and maintenance of structural plasticity in the embryonic and mature brain. Such modulation can be obtained by the enzymatic attachment of polysialic acid (PSA) to the neural cell adhesion molecule (NCAM) by means of the polysialyltransferases STX and PST. Thus, differential expression of STX and PST is likely to be responsible for varying functions of PSA-NCAM during neuronal differentiation, maintenance, plasticity, and regeneration. We have isolated the zebrafish homologues of STX (St8sia2) and PST (St8sia4) and demonstrate that their expression in the embryonic and adult nervous system is often confined to regions of neuronal migration. Moreover, in the adult cerebellum, the complementary expression pattern of both polysialyltransferases suggests a function in regulating cerebellar neuronal plasticity. Enzymatic removal of PSA in the embryonic cerebellum results in impaired neuronal migration, suggesting that PSA-NCAM is a key regulator of motility for cerebellar neuronal progenitors. *Developmental Dynamics* 237:276–285, 2008. © 2007 Wiley-Liss, Inc.

**Key words:** polysialyltransferase; PSA-NCAM; cell adhesion; zebrafish; cerebellum; neuronal migration; bio-imaging

Accepted 11 November 2007

## INTRODUCTION

The neural cell adhesion molecule (NCAM) plays multiple roles during the development of the central nervous system (CNS). It has been shown to be involved in regulating embryonic neurogenesis (Ponti et al., 2006), neuronal migration (Ono et al., 1994; Wang et al., 1994; Hu et al., 1996), axonal pathfinding (Tang et al., 1992; Daston et al., 1996; Cremer et al., 1997; Marx et al., 2001), as well as synaptogenesis (Seki and Rutishauser, 1998). Furthermore, in the mature brain, NCAM has been impli-

cated in regulating adult neurogenesis (Vutskits et al., 2006), neuronal migration (Cremer et al., 1994), survival of neural stem cell derived neuronal progenitors (Gascon et al., 2007), synaptic plasticity, and learning (Becker et al., 1996; Muller et al., 1996). During these processes the properties of NCAM are modulated by the reversible attachment of polysialic acid (PSA) to its extracellular domain. For example, PSA weakens the adhesive properties of NCAM by steric hindrance and thus promotes migration of neuronal progenitors in the rostral

migratory stream of the vertebrate olfactory system (Ono et al., 1994; Rutishauser and Landmesser, 1996; Rutishauser, 1998). In addition, PSA-bearing NCAM regulates the expression of the low-affinity neurotrophin receptor p75 and thereby promotes survival of these migrating neuronal progenitors (Gascon et al., 2007). PSA attached to NCAM has also been involved in binding and presenting growth factors thereby regulating long-term potentiation (Becker et al., 1996; Muller et al., 2000). Therefore, reversible PSA attachment

The Supplementary Material referred to in this article can be found at <http://www.interscience.wiley.com/jpages/1058-8388/suppmat>  
 GSF- National Research Center for Environment and Health, Institute of Developmental Genetics, Neuherberg-Munich, Germany  
 Grant sponsor: the German Ministry of Education and Research (BMBF); Grant number: 0311889; Grant sponsor: the Helmholtz-Association (HGF).

\*Correspondence to: Reinhard W. Köster, GSF- National Research Center for Environment and Health, Institute of Developmental Genetics, Ingolstädter Landstrasse 1, 85764 Neuherberg-Munich, Germany. E-mail: reinhard.koester@gsf.de

DOI 10.1002/dvdy.21410

Published online 18 December 2007 in Wiley InterScience (www.interscience.wiley.com).

and removal is crucial for modulating NCAM-activity and, thus, CNS development and function.

PSA synthesis on NCAM is specifically mediated by two polysialyltransferases, STX and PST, which act in a differential as well as synergistic manner (Ong et al., 1998; Angata et al., 1998; Nakayama et al., 1998; Angata and Fukuda, 2003; Angata et al., 2004; Weinhold et al., 2005). Based on their differential expression PSA synthesis during embryogenesis has mainly been attributed to STX, whereas adult PSA synthesis is thought to be mediated preferentially by PST (Becker et al., 1996; Hildebrandt et al., 1998; Ong et al., 1998). The expression and function of these polysialyltransferases has attracted increasing biomedical interest for several reasons: (1) high PSA levels as well as STX expression can serve as diagnostic markers for neuroblastomas with poor prognostic outcome (Cheung et al., 2006; Seidenfaden et al., 2003); (2) polysialyltransferase activity promotes metastasis formation and, thus, represents an interesting pharmaceutical target; (3) the migration promoting activity of either STX- or PST-mediated PSA synthesis in genetically engineered Schwann cells significantly supports regeneration by increasing axon outgrowth and Schwann cell-mediated remyelination (Lavdas et al., 2006; Zhang et al., 2007).

Due to their small size, transparency, and extracorporeal development, zebrafish embryos allow one to observe highly dynamic cell behaviors such as neuronal migration (Köster and Fraser, 2006), axon pathfinding (Fricke et al., 2001), or synaptogenesis (Niell et al., 2004; Mumm et al., 2006) directly in the living organism and are, thus, well suited to address PSA-NCAM and polysialyltransferase function in vivo. Moreover, in contrast to mammals, adult zebrafish show significant levels of neurogenesis in almost all regions of the adult brain and have a pronounced capability to regenerate CNS lesions (Becker et al., 2004; Zupanc et al., 2005; Zupanc and Zupanc, 2006; Adolf et al., 2006; Grandel et al., 2006). For example, stab wounds in the adult zebrafish cerebellum are repaired within several days by an up-regulation of neurogenesis in

the cerebellar molecular layer followed by directed migration of these neuronal progenitors toward the lesion site (Liu et al., 2004; Zupanc and Zupanc, 2006). Such adult neurogenesis, migration, and regeneration in zebrafish could likely involve PSA-NCAM function, but research on PSA-NCAM has only been initiated recently. In an elegant study, polysialylation of NCAM in zebrafish embryos has been demonstrated to play a crucial role in axon fasciculation, but also commissural axonal guidance during midline crossing (Marx et al., 2001). Recently, the cloning and expression of the highly conserved zebrafish STX- and PST-homologues were reported and both were shown to be capable of synthesizing PSA (Marx et al., 2007). Consistent with its predominant expression during embryogenesis, antisense-morpholino studies revealed that STX is likely to be solely responsible for PSA synthesis during zebrafish embryogenesis. This finding is in good agreement with mammalian STX and PST function (Eckhardt et al., 2000; Angata et al., 2004). Surprisingly though, in the adult zebrafish brain, only STX expression was found to correlate with PSA synthesis, while PST expression was either weak or absent, suggesting that STX may be the sole PSA-synthesizing enzyme relevant in the developing and adult zebrafish CNS (Marx et al., 2007).

In addition to axonal fasciculation and guidance, additional functional roles for PSA-NCAM during zebrafish embryogenesis remained unclear so far. To address whether PSA-NCAM in zebrafish is involved in regulating neuronal migration, we have independently isolated zebrafish homologues of the polysialyltransferases STX and PST and compared their expression to NCAM and PSA. Intriguingly, in the developing cerebellum, where extensive neuronal migration from the cerebellar rhombic lip has been shown (Köster and Fraser, 2001a), NCAM is broadly expressed, while STX and PSA expression delineate the anteroventral pathway of cerebellar rhombic lip derived neuronal progenitors during early migration. Furthermore, in vivo time-lapse analysis reveals that neuronal migration from the cerebellar rhombic lip is inhibited after enzy-

matic removal of PSA, suggesting a migration-promoting function for the polysialylation of NCAM. Moreover, in contrast to the previous report, we find extensive expression for PST in numerous regions throughout the adult CNS. In particular in the adult cerebellum, PST and STX show an overlapping but complementary expression pattern. While STX is strongly expressed in the Purkinje cell layer, PST shows stronger expression in the granule cell layer. This finding suggests that, in the adult zebrafish cerebellum, cell type specific regulation of PSA synthesis is mediated by cooperative and differential polysialyltransferase expression in differentiated neurons and, thus, may serve additional functions such as regulating the plasticity of cerebellar neuronal circuitries. Thus, our study suggests that PST and STX functions are much more conserved between teleosts and mammals than previously thought and lay the ground for PSA-NCAM functional studies on adult CNS regeneration in vertebrates.

## RESULTS

### Polysialyltransferase Expression in the Developing Zebrafish CNS

Polysialylated NCAM has been implicated in the control of neuronal migration during mammalian nervous system development (Murakami et al., 2000; Marx et al., 2001; Ulfig and Chan, 2004). The two polysialyltransferases STX and PST are key enzymes in the synthesis of polysialic acid on NCAM in vertebrates (Angata and Fukuda, 2003). Zebrafish homologues of *pst* and *stx* were initially identified by sequence similarity searches in the zebrafish genome (Harduin-Lepers et al., 2005). Recently, the cloning of these homologues by reverse transcriptase-polymerase chain reaction (RT-PCR) and their first functional characterization in axon pathfinding has been reported (Marx et al., 2007). To address a possible role for polysialyltransferase activity during neuronal migration in the developing and mature zebrafish nervous system, we have independently cloned both polysialyltransferases from cDNA of 54 hpf zebrafish embryos. The sequences

of both genes correspond to those reported previously (Harduin-Lepers et al., 2005; Marx et al., 2007). The onset of *stx* expression had been determined to occur at approximately 13 hours postfertilization (hpf) and to remain relatively ubiquitously in the nervous system until approximately 40 hpf, when expression was found to decline in most regions (Marx et al., 2007). We focused our analyses on differentiation stages of CNS development and found, consistent with Marx et al., that continued high *stx* expression at 48 hpf remains along the dorsal hindbrain brain ventricle (Fig. 1A, black arrowhead), in the differentiating cerebellum (Fig. 1A), and in some cranial motor neurons coexpressing GFP in embryos of the transgenic islet1:GFP line (Fig. 1G–J, white asterisks; Higashijima et al., 2000), all are domains of pronounced neuronal migration. Low *stx* expression levels were detected in the telencephalon, diencephalon, tectum, and the anterior spinal cord. At 96 hpf when migration ceases in the zebrafish nervous system, *stx* expression levels declined in these regions and only faint expression remained in the cerebellum (Fig. 1B) and along the ventricles (not shown). At 7 dpf, weak *stx* staining was retained in a dorsomedial domain of the anterior hindbrain (Fig. 1C dashed box and inset), while *stx* expression was not evident in other brain regions anymore.

Expression of the polysialyltransferase *pst* was generally weaker in the CNS throughout development when compared with *stx* (Fig. 1D–F). At 48 hpf, *pst* expression was detected in ventral regions of the fore-, mid-, and anterior hindbrain (Fig. 1D) and around the ventricles (not shown). *pst* expression was most prominent in dorsoventral stripes in the hindbrain (Fig. 1D inset, black asterisks), delineating the central domains of individual rhombomeres. Similarly to the decline in *stx* expression also *pst* levels diminished with progression of organogenesis and low expression remained in patches in the hindbrain at 96 hpf (Fig. 1E). At 1 week postfertilization, *pst* expression could not be detected further in the nervous system (Fig. 1F compare inset with Fig. 1C showing *stx* expression in this domain). These findings reveal that the

spatiotemporal expression pattern of *stx* in the developing zebrafish is similar to that of mouse, where STX is the major polysialyltransferase during CNS development, but its expression declines at postnatal stages (Ong et al., 1998). In contrast, mouse PST expression is continuous and lasts at moderate levels from embryogenesis to adulthood, whereas in zebrafish PST expression is lost during juvenile stages.

### STX and PST Are Both Expressed in Common and Differential Domains in the Adult Zebrafish Brain

STX and PST polysialyltransferases show moderate expression levels in varying brain regions of the adult mammalian nervous system (Angata et al., 1997; Hildebrandt et al., 1998). To compare the expression patterns of both enzymes in the adult zebrafish brain, we analyzed paraffin sections by in situ hybridization. Our results reveal that, despite the decline in the expression levels of *stx* and *pst* at 1 week post fertilization (Fig. 1C,F), expression of both enzymes reappears in the mature brain (Fig. 2A–F). Recently, PST expression was reported to be absent in the adult zebrafish nervous system, suggesting an exclusive role for STX in modulating NCAM activity in the mature brain (Marx et al., 2007). In contrast, our in situ hybridization analyses revealed a clear cell type and tissue-specific expression of *pst* in the adult brain (Fig. 2D–F).

On sagittal sections, expression of both enzyme-encoding genes were detected in the outermost glomerular layer (GL), the adjacent external cellular layer (ECL) and the internal cellular layer (ICL) of the olfactory bulb (OB; Wullmann et al., 1996), in the pallium, and in stripes of the subpallium in the telencephalon (Fig. 2B,E), which has been considered an equivalent of the rostral migratory stream (RMS) in rodents (Adolf et al., 2006). The expression domains of *stx* and *pst* in the subpallial stripe correlate well with the presence of PSA-NCAM in migrating proliferative neuroblasts (Adolf et al., 2006). Expression of both enzymes was, furthermore, detected in the periventricular gray zone of the midbrain, the optic tectum (Fig.

2A,D), and along the lateral diencephalic ventricles of the hypothalamus (Fig. 2C,F). *stx* and *pst* expression was, furthermore, found in the molecular (ML), Purkinje (PCL), and granule cell layers (GCL, white asterisks) of the corpus cerebelli and the valvula cerebelli (Fig. 2H–K), as well as in the crista cerebellaris (*pst* in Fig. 2D, not shown for *stx*). Of interest, the cells in the PCL expressed high *stx* but low *pst* levels. In contrast, cells in the GCL strongly expressed *pst* but showed weak *stx* expression (Fig. 2H–K). In addition, pronounced but unique expression of *stx* was found in the pre-optic nucleus, the thalamic region (Fig. 2A), in the caudal lobe of the cerebellum (Fig. 2H, black asterisk), in the vagal lobe of the hindbrain, and in several regions of the medulla extending into the spinal cord (Fig. 2A).

Our expression analysis of *stx* and *pst* in the adult brain shows that both are not ubiquitously expressed, but that *stx* as well as *pst* expression is confined to distinct brain regions. It is noteworthy that these tissues also show expression of NCAM (e.g., corpus cerebelli shown in Fig. 2G) and PSA (not shown). These findings suggest a function for STX and PST in regulating adult neurogenesis, neuronal migration, and plasticity by means of modulation of NCAM polysialylation.

### NCAM, STX, and PSA Are Coexpressed in Domains of Neuronal Migration in the Developing Zebrafish Cerebellum

Modulation of NCAM by means of PSA addition has been shown to be important for neuronal migration (Cremer et al., 1994; Ono et al., 1994; Murakami et al., 2000), but in zebrafish, such a function for PSA-NCAM remained elusive. We, therefore, compared the expression of NCAM, STX, and PSA in the differentiating cerebellum during stages of intense neuronal migration (note that *pst* is not expressed in the cerebellum during embryonic stages), when neuronal progenitors migrate from the upper rhombic lip (URL) toward and along the midbrain–hindbrain bound-

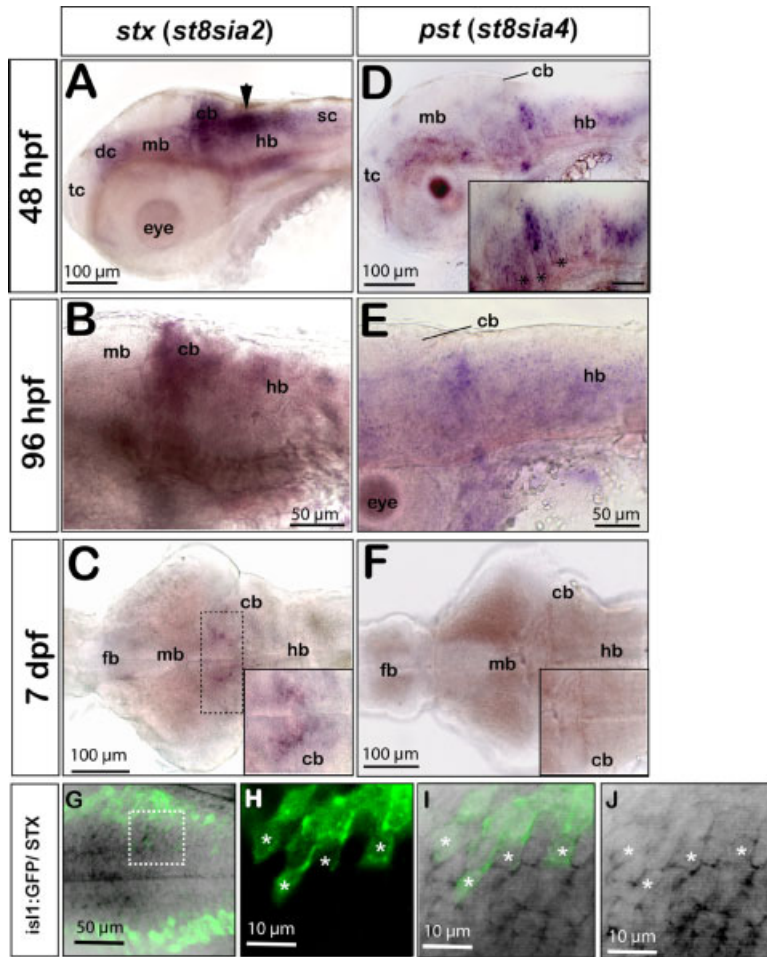


Fig. 1.

**Fig. 1.** *stx* and *pst* expression in the differentiating zebrafish central nervous system. Panels A,B,D,E show lateral and C,F dorsal views, anterior is to the left. **A:** At 48 hours postfertilization (hpf) *stx* expression is weakly present in the ventral telencephalon, in the diencephalon, midbrain, in the floorplate, and in the spinal cord. Strong expression is found in dorsal regions of the caudal hindbrain along the fourth ventricle (black arrow) and in the differentiating cerebellum. **B:** *stx* expression remains weakly detectable in the differentiating cerebellum and in ventral regions of the mid- and hindbrain at 96 hpf. **C:** At 7 days postfertilization (dpf), only the dorsomedial domain of the hindbrain retains low levels of *stx* (dashed box and inset showing high magnification of the dorsomedial domain in the anterior hindbrain with remaining *stx* expression). **D:** At 48 hpf, *pst* is expressed in the ventral domains of the fore- and midbrain. A striped expression pattern can be observed in the hindbrain, being confined to the central domains of individual rhombomeres (inset, asterisks). **E:** Only some patches in the hindbrain retain low *pst* expression levels at 96 hpf. **F:** *pst* expression is no longer detectable in the brain at 7 dpf (compare inset in F with inset in C). G–J: Expression of *stx* in a subset of cranial motoneurons as revealed by colabeling of *stx* and green fluorescent protein (GFP) in embryos of the *islet1*:GFP transgenic line. **G:** Maximum intensity projection of a 30- $\mu$ m stack of optical sections showing *stx* expression in medial domains of the hindbrain (black) and more laterally positioned GFP-expressing cranial motoneurons (green). **H–J:** A subset of cranial motoneurons (H, white asterisks) expresses *stx* (J, white asterisks), which can be identified in 1- $\mu$ m single optical sections at high magnification. **I:** Overlay of GFP and *stx* expression. cb, cerebellum; dc, diencephalon; fb, forebrain; hb, hindbrain; mb, midbrain; sc, spinal cord; tc, telencephalon

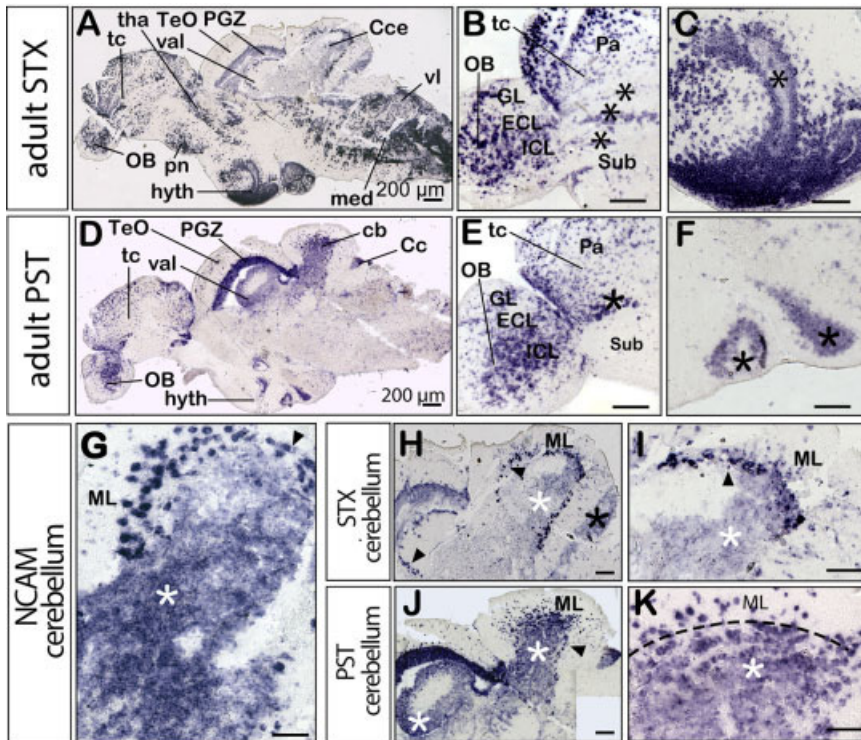


Fig. 2.

**Fig. 2.** Comparison of *stx* and *pst* expression in the adult zebrafish brain. All panels show medial sagittal sections, anterior is to the left. A–C,H,I show *stx* expression and D–F,J,K show *pst* expression. **A:** Overview of *stx* expression. **D:** Overview of *pst* expression. **B,E:** Cells in the pallial migratory domains of the telencephalon and olfactory bulb are marked by asterisks. **C,F:** Ventricular staining in the hypothalamic region. **G:** *ncam* expression in the molecular layer (ML), Purkinje cell layer (PCL, black arrowhead), and granule cell layer (GCL, white asterisk) of the cerebellum. **H:** Higher magnification of the cerebellum showing *stx* expression in some cells of the ML and strong expression in cells of the PCL, extending from the corpus into the valvula cerebelli (black arrowheads). Weak expression levels are present in the caudal lobe (black asterisk) and in the GCL (white asterisk). **I:** A higher magnification of *stx* expression in the adult cerebellum. **J:** Strong *pst* expression in the GCL of the corpus cerebelli and in the valvula cerebelli being more pronounced than *stx* expression (H, white asterisk). **K:** A higher magnification of *pst* expression in the adult cerebellum, being detected in the ML and GCL, separated by a dashed line. Cc, crista cerebellaris; Cce, corpus cerebelli; ECL, external cellular layer; GL, glomerular layer; hyth, hypothalamus; IL, internal cellular layer; med, medulla; ML, molecular layer; OB, olfactory bulb; Pa, pallium; PGZ, periventricular gray zone of the optic tectum; pn, preoptic nucleus; Sub, subpallium; tc, telencephalon; tha, thalamus; val, valvula cerebelli; vl, vagial lobe. Scale bars = 200  $\mu$ m.

ary (MHB) to ventral brain regions (Köster and Fraser, 2001a).

Consistent with a potential role in regulating migration, uniform but strong expression of *ncam* (Fig. 3A,D) and *stx* (Fig. 3B,E) was detectable in the cerebellum (black dashed circle) in sagittal (Fig. 3A,B) and transverse sections (Fig. 3D,E) during stages of onset of migration at 30 hpf. Furthermore, using the mAb735 antibody (Marx et al., 2001), PSA immunoreactivity was confined to *ncam*- and *stx*-expression domains, along the migratory route of cerebellar rhombic lip derived neuronal progenitors (Fig. 3C, arrows, F). These findings suggest that STX mediates NCAM polysialylation during migration of URL-derived neuronal progenitors.

Of interest, sagittal (Fig. 3G–I) and transverse (Fig. 3J–L) sections revealed that *ncam* expression remained broad throughout the cerebellum at 48 hpf (Fig. 3G,J), while the expression of *stx* declined close to the URL (Fig. 3H, red dashed circle) and became restricted to the rostral cerebellum (Fig. 3K, blacked dashed circle). Similarly, PSA immunoreactivity was found at this stage to delineate the anteroventral migratory pathway of neuronal progenitor cells in the dorso-rostral cerebellum (Fig. 3L, black dashed circle), while PSA levels close to the URL diminished (Fig. 3I, red dashed circle).

### PSA Removal Impairs Migration of URL-Derived Cerebellar Neuronal Progenitors

Given that PSA-NCAM is capable of regulating neuronal migration in mouse (Cremer et al., 1994; Ono et al., 1994) together with our findings that NCAM, STX, and PSA are coexpressed along the major neuronal migratory pathway in the differentiating cerebellum, we set out to investigate whether PSA-NCAM is capable of regulating URL-derived migration in the zebrafish cerebellum.

PSA is broadly expressed throughout the zebrafish nervous system already at 17 hpf and, thus, significantly earlier than the onset of URL-derived neuronal migration. We thus decided against a morpholino-mediated knockdown of polysialyltrans-

ferase expression as it lacks temporal control and does not allow discriminating between direct and indirect effects of PSA removal on neuronal migration in the developing cerebellum. In addition, injections of MO-STX1 (Marx et al., 2007) resulted only at very high concentrations (16 ng, approximately 2 nl of undiluted 1 mM stock) in a reduction but not complete absence of PSA together with malformations of embryos occurring before neuronal migration in the cerebellum. This finding suggests a weak functionality of the respective morpholino and requires careful controls in future functional studies to demonstrate the efficiency of anti-*stx*-morpholinos.

Therefore, recombinant EndoN enzyme, which selectively degrades poly-Sia residues from NCAM (Rut-

ishauser et al., 1985; Marx et al., 2001; Franz et al., 2005), was used to specifically remove PSA from the differentiating brain at 33 hpf, shortly after the onset of PSA-NCAM expression in the cerebellum (Marx et al., 2001). The efficiency of PSA removal in EndoN- and phosphate buffered saline (PBS)-treated control embryos was monitored by immunohistochemistry using the mAb735 anti-PSA antibody at 2 and 24 hr after injection. While control embryos displayed no obvious reduction in the levels of PSA at both time points (Fig. 4A,B, note that endogenous PSA levels decline at approximately 60 hpf), PSA was completely absent in the CNS of EndoN-injected embryos (Fig. 4C,D). This finding demonstrates that EndoN is capable to sufficiently degrade PSA

**Fig. 3.** Comparison of *ncam*, *stx* and polysialic acid (PSA) expression in the differentiating cerebellum during stages of neuronal migration. **A–L:** High magnification of lateral (A–C,G–I) and transverse (D–F,J–L) sections of the anterior hindbrain are shown at 30 hpf (A–F) and 48 hpf (G–L). The anterior cerebellar border at the midbrain–hindbrain boundary (MHB) and the posterior edge of the cerebellum are marked with a dashed and solid line, respectively. The mRNA in situ analysis was performed for *ncam* (A,D,G,J) and *stx* expression (B,E,H,K), while PSA immunoreactivity was detected using the mAb735 antibody (C,F,I,L). At 30 hours postfertilization (hpf), *ncam* expression was found to be strong and uniform in the cerebellum (A,D) similar to *stx* expression showing strongest expression at the ventricle (B,E). Moderate PSA levels can also be detected in this domain (C,F) during onset of rhombic lip derived neuronal migration (compare areas of dashed oval circles demarcating one cerebellar half). G,J: At 48 hpf, *ncam* expression is still uniform in the cerebellum. H,I: In contrast, *stx* and PSA expression have become restricted to the rostral cerebellar region along the MHB and are not longer detectable along the ventricle (red dashed circle). K,L: Transverse views of *stx* and PSA expression in the anterior cerebellum delineating the anteroventral migration route of neuronal progenitors. Scale bars = 50  $\mu$ m.

**Fig. 4.** Polysialic acid (PSA) degradation in the central nervous system of EndoN-treated embryos impairs migration from the cerebellar rhombic lip. All panels show lateral views, anterior is to the left. Panels A–D show PSA expression in cerebellar primordia after phosphate buffered saline (PBS) and EndoN treatment at 33 hours postfertilization (hpf). **A,B:** Control embryos injected with PBS show PSA immunoreactivity after 2 hr (A) and 24 hr (B). Note the weaker expression levels at 57 hpf are due to endogenous down-regulation of PSA. **C,D:** EndoN injection at 33 hpf completely abolished PSA expression already after 2 hr (C), lasting up to 24 hr (D). Panels E–J are maximum intensity projections (50- $\mu$ m stacks recorded every 12 min) showing migrating neuronal progenitors in the differentiating cerebellum after PBS (E–G) and EndoN treatment (H–J), recorded by in vivo time-lapse confocal microscopy. **E:** A group of neuronal progenitor cells at the upper rhombic lip (URL) in the control embryo is marked by a white arrowhead 2 hr post-injection. **F:** These cells migrated approximately halfway between URL and midbrain–hindbrain boundary (MHB) after 6 hr, while others have reached the MHB (white arrowhead). **G:** After 11 hr, cells in the ventral cerebellar region become stationary and form a cluster (white arrowhead, see Supplementary Movie S1). **H:** After injection of EndoN into the hindbrain ventricle, neuronal progenitors marked by an arrowhead are positioned at the URL or are polarized and span across the cerebellum between the URL and MHB (white arrowheads). **I,J:** Eight hours later (I), these neuronal progenitor cells are stalled at the URL and remain in this position (J) for up to 17 hr of time-lapse recording (see Supplementary Movie S2). K,L: The migratory routes of five individual uncGFP-expressing neuronal progenitor cells in PBS (K) and EndoN (L)-treated embryos were traced using the manual tracking tool plug-in of ImageJ1.34, the migratory direction is marked by an arrowhead. **K:** Anteroventral migration of cells in a PBS-injected embryo. **L:** Reduced migration of cells in EndoN-injected embryo. **M:** Quantification of neuronal progenitor migration from the cerebellar rhombic lip in PBS- and EndoN-treated embryos. While 84% of neuronal progenitors ( $n = 5$  movies, 37 cells analyzed) in PBS-treated embryos were migratory, covering an average distance of almost 30  $\mu$ m during a 4-hr period, only 23% of neuronal progenitors ( $n = 5$  movies, 47 cells analyzed) in EndoN-treated embryos were migratory and covered a similar average migration distance. Cells were classified as nonmigratory when they moved less than one cell diameter (approximately 10  $\mu$ m) during the observation period.

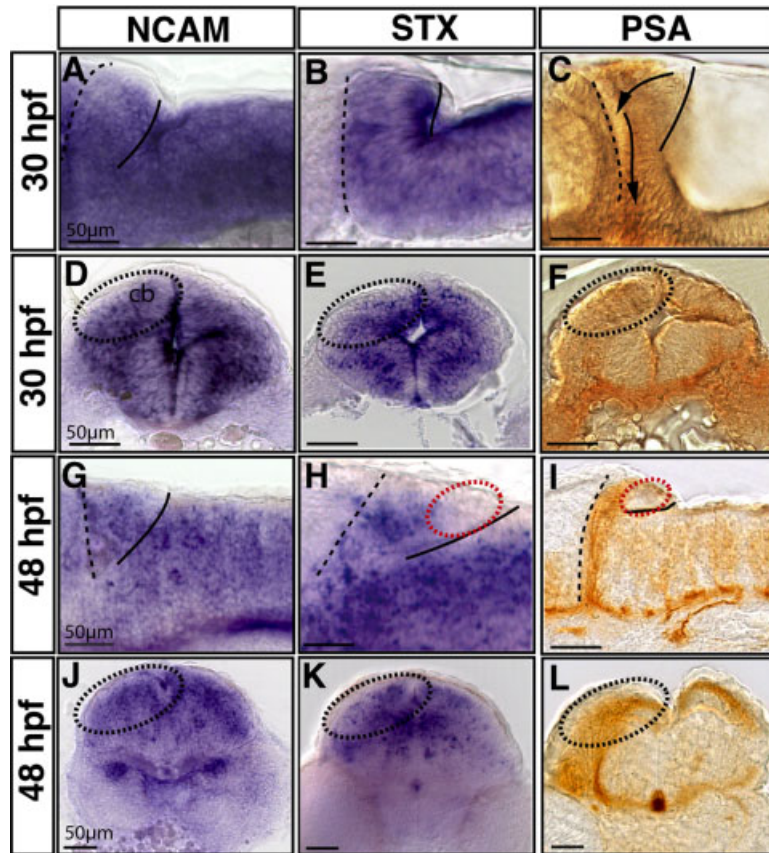


Fig. 3.

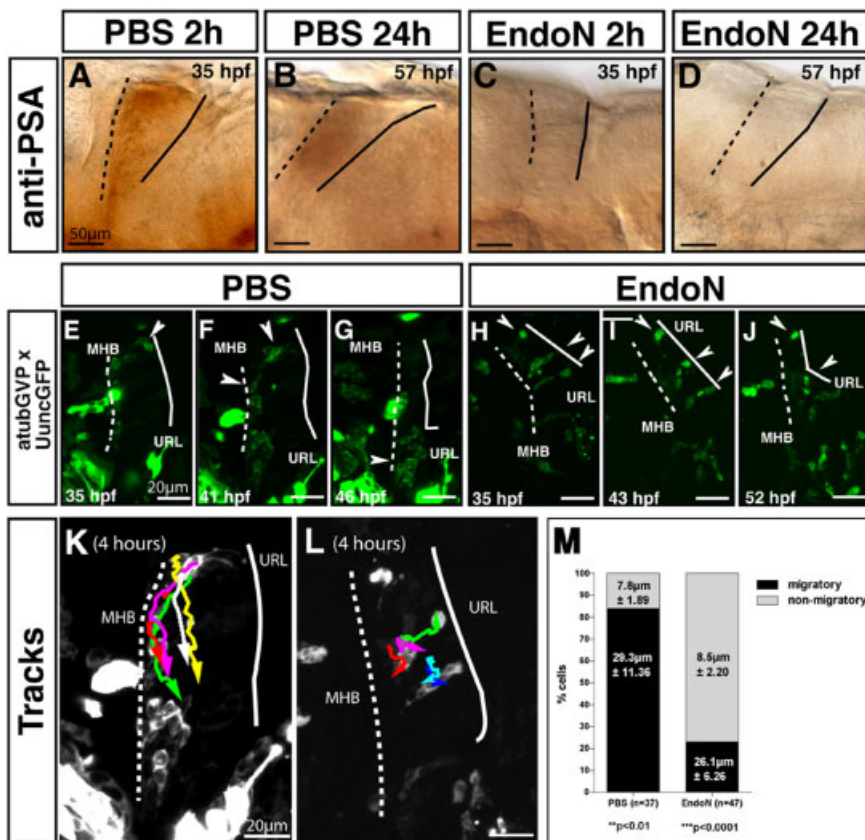


Fig. 4.

from neuronal progenitors in the differentiating cerebellum for at least a 24-hr period.

Altered levels of PSA in the differentiating CNS after EndoN injection were not expected to result in any gross morphological changes. Thus, we used time-lapse confocal microscopy to investigate cerebellar migration on a single-cell level. Neuronal progenitors were labeled in a mosaic manner through co-injection of atubGFP and UuncGFP expression vectors (25 pg each) into one-cell stage embryos as previously described (Köster and Fraser, 2001a,b). At 33 hpf, either 3–4 nl of PBS or 100 ng/μl EndoN/PBS was injected into the hind-brain ventricle of these green fluorescent protein (GFP)-expressing embryos and time-lapse imaging was performed starting 2 hr after injection (see Supplementary Movies S1 and S2, which can be viewed at <http://www.interscience.wiley.com/jpages/1058-8388/suppmat>).

In control embryos, clusters of labeled neuronal progenitor cells initiated migration by becoming polarized and extending leading processes into the direction of the MHB (Fig. 4E, white arrowhead). These progenitors then followed the characterized anteroventral pathway toward and along the MHB (Fig. 4F) to ventral regions of the anterior hindbrain (Fig. 4G, see also Supplementary Movie S1, n = 5 movies, 37 cells analyzed). Additional tracing of individual cells over a time period of 4 hr using the manual tracking tool plug-in of the ImageJ software (plug-in: Farbrice Cordeliers, Inst. Curie, Orsay, France; Abramoff et al., 2004) further demonstrated the proper anteroventral migration pathway of these cells from the URL toward and along the MHB (Fig. 4K, arrows point in the direction of migration). In contrast, URL-derived neuronal progenitors in EndoN-injected embryos exhibited dramatic migration defects after PSA degradation (see Supplementary Movie S2, n = 5 movies, 47 cells analyzed). Already 2 hr after EndoN-injection, URL-positioned neuronal progenitors failed to form a stable leading process, despite filopodial activity (Fig. 4H, white arrowheads). Consequently, such progenitors, although being polarized at the beginning, never initiated migration and ceased leading

process formation after 8 hr (Fig. 4I, white arrowheads). These cells never pursued anteroventral migration and remained stalled at a position close to the URL during the entire period of time-lapse recordings (Fig. 4I,J white arrowheads). This reduced or complete lack of migration became further evident by individual cell tracing during a 4-hr period (Fig. 4L), showing that neuronal progenitors in EndoN-injected embryos remained in close proximity to their original position.

Additional quantification revealed that, in PBS-injected embryos, approximately 84% of neuronal progenitors (31/37) migrated significant distances during a 4-hr period covering an average distance of  $29.3\mu\text{m}$  ( $\text{SD} \pm 11.4\mu\text{m}$ ), while 16% (6/37) of the cells remained at the URL or in close proximity, moving an average of  $7.8\mu\text{m}$  ( $\text{SD} \pm 1.9\mu\text{m}$ ) and, thus, less than a cell diameter (Fig. 4M left column;  $P < 0.01$ ). In contrast, only 23% of URL-derived neuronal progenitors (11/47) in EndoN-injected embryos were clearly migratory (average migratory distance:  $26.1\mu\text{m}$   $\text{SD} \pm 6.3\mu\text{m}$ ), while the majority of these neuronal progenitors (77%, 36/47) were nonmigratory (average migratory distance:  $8.5\mu\text{m}$   $\text{SD} \pm 2.2\mu\text{m}$ ) and remained stalled close to the URL (Fig. 4M right column;  $P < 0.001$ ). Thus, our *in vivo* time-lapse analyses and quantifications of cell migration reveal that PSA is essential for regulating cellular motility of migratory neurons emanating from the zebrafish cerebellar rhombic lip.

## DISCUSSION

In this report, we have addressed the spatiotemporal polysialylation of the adhesion factor NCAM in zebrafish by means of cloning zebrafish homologues of the highly conserved polysialyltransferases STX and PST and characterizing their expression patterns. We expand recent findings by characterizing their expression during stages of CNS differentiation, when migration and terminal differentiation of many neuronal populations occur.

Consistent with previous findings, STX remains the predominant polysialyltransferase expressed during brain differentiation (Marx et al.,

2007). Interestingly, in addition to ventral diencephalic and tegmental brain regions, *stx* expression is mostly confined to dorsal hindbrain structures including the rhombic lip, from where neuronal progenitors have been shown to initiate long-distance migration. In particular, in the cerebellum, neuronal migration initiated from the cerebellar rhombic lip occurs toward and along the MHB (Köster and Fraser, 2006). The *stx* expression together with expression of *ncam* and PSA was found to delineate this migratory pathway.

In contrast to a very remote or lack of *pst* expression reported for embryonic stages (Marx et al., 2007), we find expression of *pst* in the differentiating zebrafish brain in ventral regions, but generally weaker when compared with *stx*. The *pst* expression is found in the hindbrain reaching from the dorsally positioned lower rhombic lip, which also expresses high levels of *stx*, toward the floorplate along the central domains of each rhombomere, where neuronal differentiation occurs (Cheng et al., 2004). At 4 days of embryonic development, expression of both polysialyltransferases has declined to minute amounts. During these embryonic stages, the peak of neuronal migration in the hindbrain and particular in the cerebellum has passed and terminal differentiation of neuronal populations is well under way (K. Volkman et al., *in press*). These findings show that in addition to axonal pathfinding (Marx et al., 2001), polysialylation of NCAM could well play a role in regulating neuronal migration in zebrafish, such as in higher vertebrates (Murakami et al., 2000).

Based on the partially overlapping expression of *stx* and *pst* in the zebrafish brain, both enzymes could well play a synergistic or redundant function in modulating NCAM adhesion. Thus, rather than interfering with polysialyltransferase activity, the removal of PSA is a more robust assay to address a potential PSA-NCAM function during zebrafish neuronal migration. We have imaged rhombic lip-derived migration in the differentiating cerebellum, revealing that lack of PSA results in impaired cell migration. The observation that neuronal progenitors remained stalled in the vicinity of the URL after PSA removal suggests that

polysialylated NCAM is required for mediating cellular motility. These findings are in good agreement with results from migrating neuronal progenitors in the rostral migratory stream in mammals. Here, tangential migration in mice lacking PSA-NCAM is severely decreased mainly in a cell-autonomous manner, leading to a significant size reduction of the olfactory bulb (Cremer et al., 1994; Chazal et al., 2000). However, a role for PSA in regulating early migration in the developing mouse cerebellum has remained elusive so far.

Recently, the cerebellar rhombic lip in mice has been shown to produce different neuronal cell populations over time (Wang et al., 2005; Machold and Fishell, 2005). Similarly, in the zebrafish, cerebellum rhombic lip derived migration starts at approximately 28 hpf, but granule progenitor cells do not initiate migration from the URL before 50 hpf, reaching its peak of migration between 60 and 80 hpf (K. Volkman et al., *in press*). Thus, high expression levels of *ncam*, *stx*, and PSA in the zebrafish cerebellum, and successively declining levels of *stx* and PSA after 48 hpf, are consistent with PSA-NCAM specifically regulating early phases of rhombic lip derived migration. Intriguingly, the later arising granule progenitor cells rely on a cadherin-mediated adhesion system for proper migration (S. Rieger et al., unpublished results). This finding suggests that different adhesion systems and their specific spatiotemporal regulation may discriminate between different neuronal populations within the cerebellum to regulate their migratory behavior.

Our expression analysis in the adult zebrafish brain contrasts previous results, in which *pst* expression was reported to be absent (Marx et al., 2007). Similarly to the embryonic situation, we observed many cooperative expression domains of PST and STX throughout the mature brain such as in the RMS and olfactory bulb, the cerebellum or in the hypothalamus. Within these tissues the polysialyltransferases show both unique cell-type specific expression, such as in the caudal lobe of the cerebellum (*stx* only), and coexpression, such as in the hypothalamic lateral ventricles (*pst* and *stx*). These findings suggest that

PST and STX activity could act in an individual or synergistic manner in the adult CNS. Their expression is confined to many regions of adult neurogenesis and neuronal migration, which occurs more widespread in zebrafish than in higher vertebrates (Zupanc et al., 2005; Adolf et al., 2006; Grandel et al., 2006). For example, *pst* and *stx* expression is found in the subpallial stripe, the zebrafish equivalent of the mammalian RMS (Adolf et al., 2006) and in other ventricular regions such as in the periventricular gray zone of the optic tectum or the hypothalamus. Notably, in the cerebellum, complementary *stx* and *pst* expression is found in adjacent neuronal layers of synaptic partners. In the Purkinje cell layer, high expression levels of *stx* and low levels of *pst* could be detected, whereas low *stx* and high *pst* expression levels were found in the granule cell layer. Of interest, PSA is restricted to the axons (parallel fibers) and dendrites of the cerebellar granule cells but excluded from the soma (not shown). Therefore, based on the differential polysialyltransferase expression pattern in the mature cerebellum variances in polysialylation could play a role in mediating synaptic plasticity as it has been shown in mice, where PSA and polysialyltransferases can influence synaptic plasticity and long-term potentiation (Becker et al., 1996; Muller et al., 1996; Eckhardt et al., 2000). Furthermore, mice lacking polysialylated NCAM display deficits in spatial learning (Cremer et al., 1994; Becker et al., 1996).

Thus, as in higher vertebrates and mammals, spatiotemporal NCAM polysialylation is highly regulated during development and adulthood. While we have shown that PSA-NCAM is required for proper cell migration in the differentiating cerebellum, the dynamic expression of the polysialyltransferases suggests further functions during neurogenesis, axon pathfinding (Marx et al., 2001), synaptogenesis, and synaptic plasticity in memory and learning. This finding shows that polysialyltransferase activity in zebrafish may be more conserved to mammals than has been previously thought (Marx et al., 2007). Many of these functions when disrupted are not likely to result in gross

morphological changes and will require more sophisticated phenotype analysis such as time-lapse imaging, electrophysiology, or behavioral studies. Given the accessibility of zebrafish for genetics, in vivo imaging and behavioral tests, analyzing PSA-NCAM function in zebrafish will be a rewarding research area. In particular, when addressed in the context of the high regenerative capacity of the zebrafish adult CNS, the regeneration-promoting activities of polysialyltransferases may reveal valuable insights for neuroregenerative approaches (Lavdas et al., 2006; Zhang et al., 2007).

## EXPERIMENTAL PROCEDURES

### Fish Strains and Maintenance

Raising, spawning, and maintaining of zebrafish lines were performed as described previously (Kimmel et al., 1995; Westerfield, 1995). For embryonic in situ hybridization, immunohistochemical analyses, and confocal time-lapse microscopy fish of the brass strain were used. The transgenic line *islet1:GFP* has been described (Higashijima et al., 2000). For adult paraffin sections, 9-month-old fish of the wild-type AB strain were used.

### Cloning of Polysialyltransferases *pst* and *stx*

The zebrafish homologues of the polysialyltransferases STX and PST were isolated by RT-PCR using cDNA from 54 hpf embryos. The following primers were used: PST<sup>up</sup>: TCTCGAGATGCGGCTTTCACG; PST<sup>low</sup>: TAGATAAGTTGATGTGCATTTAGATGTC; STX<sup>up</sup>: TACTCGAGATGTCTTTTGAATCCGAATACTGA; and STX<sup>low</sup>: TATCTAGATCATGTAGGAGGTTTCATGGTCCC. Amplified fragments of expected size (PST: ~1,070 bp; STX: ~1,150 bp) were subcloned into pC-RII-vector (Invitrogen, San Diego, CA). Sequences were identical to those recently published NM 153662 (STX), NM 001099416 (PST; Harduin-Lepers et al., 2005; Marx et al., 2007).

## RNA Expression Analysis

Both zebrafish polysialyltransferases and NCAM expression was analyzed by in situ hybridization on embryonic whole-mounts and adult paraffin sections. Zebrafish NCAM cDNA was obtained from (Mizuno et al., 2001). Digoxigenin-labeled antisense RNA (Roche, Germany) of *stx*, *pst*, and NCAM were hybridized on whole-mounts at 57°C and on paraffin sections at 68°C. For sagittal and transverse sections, whole-mount stained embryos were embedded in 5% agarose/1× PBS and 30- to 50- $\mu$ m sections were cut on a Vibratome HM650V (MICROM, Germany). Paraffin-embedded adult brains were sectioned in 8- $\mu$ m steps on a microtome 355S (MICROM, Germany). During incubations, sections were kept in a humidity chamber. Tween20 was omitted from all buffers except for the hybridization buffer. All stainings were photographed using an Axio-plan2 microscope and AxioCam HRC camera (Zeiss, Germany) and processed with Adobe Photoshop7.0.

## Immunohistochemistry

For PSA immunohistochemistry, embryos were acetone re-hydrated and blocked in 10% normal goat serum (NGS)/PBS-Tween20. DAB staining was performed after mAb735 anti-PSA (1:750) (Marx et al., 2001) and anti-mouse IgG-HRP antibody incubation (1:300; Jackson ImmunoResearch, West Grove, PA). Immunohistochemistry on *islet1:GFP* transgenic embryos at 48 hpf was performed after in situ hybridization for *stx*. Embryos were blocked in 10% NGS/PBS-Tween20 for 1 hr and incubated in a 1:500 dilution of rabbit anti-GFP antibody (Torrey Pines Biolabs, Houston, TX) overnight at 4°C. Secondary antibody incubation was performed using a 1:1,000 dilution of Cy2-conjugated anti-rabbit IgG antibody (Dianova, Germany).

## Microinjection

For vital labeling of migrating neuronal progenitors, 25  $\mu$ g each of the vectors atub-GFP and UuncGFP (Köster and Fraser, 2001b) in 0.02% Phenol Red/H<sub>2</sub>O were co-injected into one-cell stage embryos. Embryos at 33 hpf ex-



pressing GFP in cells of the cerebellar rhombic lip were further injected into the fourth ventricle with 3–4 nl of 1× PBS or EndoN/PBS at 100 ng/μl. Time-lapse recordings were started 2 hr after injection.

### Intravital Imaging

Mounting and image recording for three-dimensional time-lapse confocal microscopy was performed as described (Köster and Fraser, 2004) using a LSM510 Meta laser-scanning microscope (Zeiss, Germany). Image data were analyzed and processed with the Zeiss LSM-Software version 4.5 and Adobe Photoshop7.0.

### Quantification of Migration

Tracing of UuncGFP-labeled cerebellar neuronal progenitors was performed over a 4-hr period using the manual tracking tool plug-in of the open source software ImageJ1.34s (plug-in: Farbrice Cordelieres, Inst. Curie, Orsay, France; Abramoff et al., 2004). Statistical analyses were performed using the GraphPad software Prism4.

### ACKNOWLEDGMENTS

We thank Enrico Kühn, Petra Hammerl, and Andrea Kneutinger for excellent technical assistance and animal care. We also thank Yoshihiro Yoshihara for sending us the zebrafish NCAM cDNA, Rita Gerardy-Schahn for providing us with recombinant EndoN, and Monika Marx and Martin Bastmeyer for providing the anti-PSA antibody. We thank all members of the Institute of Developmental Genetics for helpful suggestions and discussions. This work was supported by a BioFuture-Award Grant from the German Ministry of Education and Research.

### REFERENCES

Abramoff MD, Magelhaes PJ, Ram SJ. 2004. Image processing with ImageJ. *Biophoton Int* 11:36–42.

Adolf B, Chapouton P, Lam CS, Topp S, Tannhauser B, Strähle U, Götz M, Bally-Cuif L. 2006. Conserved and acquired features of adult neurogenesis in the zebrafish telencephalon. *Dev Biol* 295:278–293.

Angata K, Fukuda M. 2003. Polysialyltransferases: major players in polysialic

acid synthesis on the neural cell adhesion molecule. *Biochimie* 85:195–206.

Angata K, Nakayama J, Fredette B, Chong K, Ranscht B, Fukuda M. 1997. Human STX polysialyltransferase forms the embryonic form of the neural cell adhesion molecule. Tissue-specific expression, neurite outgrowth, and chromosomal localization in comparison with another polysialyltransferase, PST. *J Biol Chem* 272:7182–7190.

Angata K, Suzuki M, Fukuda M. 1998. Differential and cooperative polysialylation of the neural cell adhesion molecule by two polysialyltransferases, PAS and STX. *J Biol Chem* 273:28524–28532.

Angata K, Chan D, Thibault J, Fukuda M. 2004. Molecular dissection of the ST8Sia IV polysialyltransferase. Distinct domains are required for neural cell adhesion molecule recognition and polysialylation. *J Biol Chem* 279:25883–25890.

Becker CG, Artola A, Gerardy-Schahn R, Decker T, Welzl H, Schachner M. 1996. The polysialic acid modification of the neural cell adhesion molecule is involved in spatial learning and hippocampal long-term potentiation. *J Neurosci Res* 45:143–152.

Becker CG, Lieberoth BC, Morellini F, Feldner J, Becker T, Schachner M. 2004. L1.1 is involved in spinal cord regeneration in adult zebrafish. *J Neurosci* 24:7837–7842.

Chazal G, Durbec P, Jankovski A, Rougon G, Cremer H. 2000. Consequences of neural cell adhesion molecule deficiency on cell migration in the rostral migratory stream of the mouse. *J Neurosci* 20:1446–1457.

Cheng YC, Amoyel M, Qiu X, Jiang YJ, Xu Q, Wilkinson DG. 2004. Notch activation regulates the segregation and differentiation of rhombomere boundary cells in the zebrafish hindbrain. *Dev Cell* 6:539–550.

Cheung IY, Vickers A, Cheung NK. 2006. Sialyltransferase STX (ST8SiaII): a novel molecular marker of metastatic neuroblastoma. *Int J Cancer* 119:152–156.

Cremer H, Lange R, Christoph A, Plomann M, Vopper G, Roes J, Brown R, Baldwin S, Kraemer P, Scheff S, et al. 1994. Inactivation of the N-CAM gene in mice results in size reduction of the olfactory bulb and deficits in spatial learning. *Nature* 367:455–459.

Cremer H, Chazal G, Goridis C, Represa A. 1997. NCAM is essential for axonal growth and fasciculation in the hippocampus. *Mol Cell Neurosci* 8:323–335.

Daston MM, Bastmeyer M, Rutishauser U, O'Leary DDM. 1996. Spatially restricted increase in polysialic acid enhances corticospinal axon branching related to target recognition and innervation. *J Neurosci* 16:5488–5497.

Eckhardt M, Bukalo O, Chazal G, Wang L, Goridis C, Schachner M, Gerardy-Schahn R, Cremer H, Dityatev A. 2000. Mice deficient in the polysialyltransferase ST8SiaIV/PST-1 allow discrimination of the roles of neural cell adhesion

molecule protein and polysialic acid in neural development and synaptic plasticity. *J Neurosci* 20:5234–5244.

Franz CK, Rutishauser U, Rafuse VF. 2005. Polysialylated neural cell adhesion molecule is necessary for selective targeting of regenerating motor neurons. *J Neurosci* 25:2081–2091.

Fricke C, Lee JS, Geiger-Rudolph S, Bonhoeffer F, Chien CB. 2001. A zebrafish roundabout homolog required for retinal axon guidance. *Science* 292:507–510.

Gascon E, Vutskits L, Jenny B, Durbec P, Kiss JZ. 2007. PSA-NCAM in postnatally generated immature neurons of the olfactory bulb: a crucial role in regulating p75 expression and cell survival. *Development* 134:1181–1190.

Grandel H, Kaslin J, Ganz J, Wenzel I, Brand M. 2006. Neural stem cells and neurogenesis in the adult zebrafish brain: origin, proliferation dynamics, migration and cell fate. *Dev Biol* 295:263–277.

Harduin-Lepers A, Mollicone R, Delannoy P, Oriol R. 2005. The animal sialyltransferase-related genes: a phylogenetic approach. *Glycobiology* 15:805–817.

Higashijima S, Hotta Y, Okamoto H. 2000. Visualization of cranial motor neurons in live transgenic zebrafish expressing green fluorescent protein under the control of the islet-1 promoter/enhancer. *J Neurosci* 20:206–218.

Hildebrandt H, Becker C, Murau M, Gerardy-Schahn R, Rahmann H. 1998. Heterogeneous expression of the polysialyltransferases ST8Sia II and ST8Sia IV during postnatal rat brain development. *J Neurochem* 71:2339–2348.

Hu HY, Tomasiewicz H, Magnuson T, Rutishauser U. 1996. The role of polysialic acid in migration of olfactory bulb interneuron precursors in the subventricular zone. *Neuron* 16:735–743.

Kimmel CB, Ballard WW, Kimmel SR, Uhlmann B, Schilling TF. 1995. Stages of embryonic development of the zebrafish. *Dev Dyn* 203:235–310.

Köster RW, Fraser SE. 2001a. Direct imaging of in vivo neuronal migration in the developing cerebellum. *Curr Biol* 11:1858–1863.

Köster RW, Fraser SE. 2001b. Tracing transgene expression in living zebrafish embryos. *Dev Biol* 233:329–346.

Köster RW, Fraser SE. 2004. Time-lapse microscopy of brain development. In: Detrich HW, Leonard MW, Zon I, editors. *The zebrafish: cellular and developmental biology*. San Diego: Academic Press. p 205–233.

Köster RW, Fraser SE. 2006. FGF signaling mediates regeneration of the differentiating cerebellum through repatterning of the anterior hindbrain and reinitiation of neuronal migration. *J Neurosci* 26:7293–7304.

Lavdas AA, Franceschini I, Dubois-Dalcq M, Matsas R. 2006. Schwann cells genetically engineered to express PSA show enhanced migratory potential without

- impairment of their myelinating ability in vitro. *Glia* 53:868–878.
- Liu Q, Azodi E, Kerstetter AE, Wilson AL. 2004. Cadherin-2 and cadherin-4 in developing, adult and regenerating zebrafish cerebellum. *Dev Brain Res* 150:63–71.
- Machold R, Fishell G. 2005. Math1 is expressed in temporally discrete pools of cerebellar rhombic-lip neural progenitors. *Neuron* 48:17–24.
- Marx M, Rutishauser U, Bastmeyer M. 2001. Dual function of polysialic acid during zebrafish central nervous system development. *Development* 128:4949–4958.
- Marx M, Rivera-Milla E, Stummeyer K, Gerardy-Schahn R, Bastmeyer M. 2007. Divergent evolution of the vertebrate polysialyltransferases Stx and Pst genes revealed by fish-to-mammal comparison. *Dev Biol* 306:560–571.
- Mizuno T, Kawasaki M, Nakahira M, Kagamiyama H, Kikuchi Y, Okamoto H, Mori K, Yoshihara Y. 2001. Molecular diversity in zebrafish NCAM family: three members with different VASE usage and distinct localization. *Mol Cell Neurosci* 18:119–130.
- Muller D, Wang C, Skibo G, Toni N, Cremer H, Calaora V, Rougon G, Kiss JZ. 1996. PSA-NCAM is required for activity-induced synaptic plasticity. *Neuron* 17:413–422.
- Muller D, Djebbara-Hannas Z, Jourdain P, Vutskits L, Durbec P, Rougon G, Kiss JZ. 2000. Brain-derived neurotrophic factor restores long-term potentiation in polysialic acid-neural cell adhesion molecule-deficient hippocampus. *Proc Natl Acad Sci U S A* 97:4315–4320.
- Mumm JS, Williams PR, Godinho L, Koerber A, Pittman AJ, Roeser T, Chien CB, Baier H, Wong RO. 2006. In vivo imaging reveals dendritic targeting of laminated afferents by zebrafish retinal ganglion cells. *Neuron* 52:609–621.
- Murakami S, Seki T, Rutishauser U, Arai Y. 2000. Enzymatic removal of polysialic acid from neural cell adhesion molecule perturbs the migration route of luteinizing hormone-releasing hormone neurons in the developing chick forebrain. *J Comp Neurol* 420:171–181.
- Nakayama J, Anagata K, Ong E, Katsuyama T, Fukuda M. 1998. Polysialic acid, a unique glycan that is developmentally regulated by two polysialyltransferases: PST and STX, in the central nervous system: from biosynthesis to function. *Pathol Int* 48:665–677.
- Niell CM, Meyer MP, Smith SJ. 2004. In vivo imaging of synapse formation on a growing dendritic arbor. *Nat Neurosci* 7:254–260.
- Ong E, Nakayama J, Angata K, Reyes L, Katsuyama T, Arai Y, Fukuda M. 1998. Developmental regulation of polysialic acid synthesis in mouse directed by two polysialyltransferases, PST and STX. *Glycobiology* 8:415–424.
- Ono K, Tomaszewicz H, Magnuson T, Rutishauser U. 1994. N-CAM mutation inhibits tangential neuronal migration and is phenocopied by enzymatic removal of polysialic acid. *Neuron* 13:595–609.
- Ponti G, Peretto P, Bonfanti L. 2006. A subpial, transitory germinal zone forms chains of neuronal precursors in the rabbit cerebellum. *Dev Biol* 294:168–180.
- Rutishauser U. 1998. Polysialic acid at the cell surface: biophysics in service of cell interactions and tissue plasticity. *J Cell Biochem* 70:304–312.
- Rutishauser U, Landmesser L. 1996. Polysialic acid in the vertebrate nervous system: a promoter of plasticity in cell-cell interactions. *Trends Neurosci* 19:422–427.
- Rutishauser U, Watanabe M, Silver J, Troy FA, Vimr ER. 1985. Specific alteration of NCAM-mediated cell adhesion by an endoneuraminidase. *J Cell Biol* 101:1842–1849.
- Seidenfaden R, Krauter A, Schertzing F, Gerardy-Schahn R, Hildebrandt H. 2003. Polysialic acid directs tumor cell growth by controlling heterophilic neural cell adhesion molecule interactions. *Mol Cell Biol* 23:5908–5918.
- Seki T, Rutishauser U. 1998. Removal of polysialic acid neural cell adhesion molecule induces aberrant mossy fiber innervation and ectopic synaptogenesis in the hippocampus. *J Neurosci* 18:3757–3766.
- Tang J, Landmesser L, Rutishauser U. 1992. Polysialic acid influences specific pathfinding by avian motoneurons. *Neuron* 8:1031–1044.
- Ulfig N, Chan WY. 2004. Expression patterns of PSA-NCAM in the human ganglionic eminence and its vicinity: role of PSA-NCAM in neuronal migration and axonal growth? *Cells Tissues Organs* 177:229–236.
- Vutskits L, Gascon E, Zraggen E, Kiss JZ. 2006. The polysialylated neural cell adhesion molecule promotes neurogenesis in vitro. *Neurochem Res* 31:215–225.
- Wang C, Rougon G, Kiss JZ. 1994. Requirement of polysialic acid for the migration of the O-2A glial progenitor cell from neurohypophyseal explants. *J Neurosci* 14:4446–4457.
- Wang VY, Rose MF, Zoghbi HY. 2005. Math1 expression redefines the rhombic lip derivatives and reveals novel lineages within the brainstem and cerebellum. *Neuron* 48:31–43.
- Weinhold B, Seidenfaden R, Rockle I, Muhlendorff M, Schertzing F, Conzelmann S, Marth JD, Gerardy-Schahn R, Hildebrandt H. 2005. Genetic ablation of polysialic acid causes severe neurodevelopmental defects rescued by NCAM deletion. *J Biol Chem* 280:42971–42977.
- Westerfield M. 1995. The zebrafish book. A guide for the laboratory use of zebrafish (*Danio rerio*), 3rd ed. Eugene, OR: University of Oregon Press. 385 p.
- Wullimann MF, Rupp B, Reichert H. 1996. Neuroanatomy of the zebrafish brain. CH-4010 Basel, Switzerland: Birkhauser Verlag. 139 p.
- Zhang Y, Zhang X, Yeh J, Richardson P, Bo X. 2007. Engineered expression of polysialic acid enhances Purkinje cell axonal regeneration in L1/GAP-43 double transgenic mice. *Eur J Neurosci* 25:351–361.
- Zupanc GK, Zupanc MM. 2006. New neurons for the injured brain: mechanisms of neuronal regeneration in adult teleost fish. *Regen Med* 1:207–216.
- Zupanc GK, Hinsch K, Gage FH. 2005. Proliferation, migration, neuronal differentiation, and long-term survival of new cells in the adult zebrafish brain. *J Comp Neurol* 488:290–319.

## Appendix 3

Article in **The Journal of Cell Biology**

### **The centrosome neither persistently leads migration nor determines the site of axonogenesis in migrating neurons *in vivo***

Martin Distel, Jennifer C. Hocking, Katrin Volkmann, and Reinhard W. Köster

The Journal of Cell Biology 191: 875-890 (2010)

#### **Contribution**

For this study I generated the stable transgenic *atoh1a:KalTA4* strain and characterized it initially. I recorded the time-lapse movie shown in Figure 3.

# The centrosome neither persistently leads migration nor determines the site of axonogenesis in migrating neurons in vivo

Martin Distel, Jennifer C. Hocking, Katrin Volkmann, and Reinhard W. Köster

Helmholtz Zentrum München German Research Center for Environmental Health, Institute of Developmental Genetics, 85764 Munich-Neuherberg, Germany

**T**he position of the centrosome ahead of the nucleus has been considered crucial for coordinating neuronal migration in most developmental situations. The proximity of the centrosome has also been correlated with the site of axonogenesis in certain differentiating neurons. Despite these positive correlations, accumulating experimental findings appear to negate a universal role of the centrosome in determining where an axon forms, or in leading the migration of neurons. To further examine this controversy in an *in vivo* setting, we have generated cell type-specific multi-cistronic gene expression to monitor

subcellular dynamics in the developing zebrafish cerebellum. We show that migration of rhombic lip-derived neurons is characterized by a centrosome that does not persistently lead the nucleus, but which is instead regularly overtaken by the nucleus. In addition, axonogenesis is initiated during the onset of neuronal migration and occurs independently of centrosome proximity. These *in vivo* data reveal a new temporal orchestration of organelle dynamics and provide important insights into the variation in intracellular processes during vertebrate brain differentiation.

## Introduction

Neuronal progenitors undergo a variety of developmental steps to form a functional brain. After proliferation, they migrate, differentiate terminally, and generate dendrites and axons to establish neuronal circuits. Cell behavior at each step is coordinated by the subcellular organelle dynamics occurring within the developing neurons. The centrosome in particular, through its function as a microtubule-organizing center (MTOC), has been proposed to act as a main organizer of polarized cell behaviors such as directed migration and axonogenesis (Higginbotham and Gleeson, 2007).

Within cells in a proliferating neuroepithelium, the centrosome localizes strictly to the apical (ventricular) side to maintain apico-basal polarity (Hinds and Ruffet, 1971; Shoukimas and Hinds, 1978). During both radial and tangential migration, the apical process of the immature neuron becomes disconnected

from the proliferation zone and the cell body advances behind an extended membrane protrusion termed the leading process. Individual migratory steps of neurons are characterized by the forward movement of the nucleus—a process termed nucleokinesis—which can occur in a saltatory manner alternating with resting phases. In most analyzed neurons migrating by saltatory nucleokinesis, the centrosome is localized ahead of the nucleus to face toward the leading process, with the centrosome moving forward before the nucleus (Solecki et al., 2004; Tanaka et al., 2004; Bellion et al., 2005; Schaar and McConnell, 2005; Métin et al., 2006; Tsai et al., 2007). Due to these observations, a common model for saltatory nucleokinesis in migrating neurons—defined by the sequential subcellular events of a continuously leading centrosome followed by a trailing nucleus—attributes the centrosome with a permanently leading role in initiating and directing migration. (Tsai and Gleeson, 2005; Marín et al., 2006; Higginbotham and Gleeson, 2007; Métin et al., 2008).

Such an orientation of the centrosome in the direction of cell migration and ahead of the nucleus is not unique to neurons,

Correspondence to Reinhard W. Köster: Reinhard.Koester@helmholtz-muenchen.de  
M. Distel's present address is Natural Sciences Building, Room 6310, University of California, San Diego, 9500 Gilman Drive, La Jolla, CA 92093.

K. Volkmann's present address is The Wellcome Trust Sanger Institute, Wellcome Trust Genome Campus, Hinxton, Cambridge CB10 1SA, England, UK.

Abbreviations used in this paper: hpf, hours postfertilization; INM, interkinetic nuclear movement; MHB, midbrain–hindbrain boundary; MTOC, microtubule-organizing center; THN, tegmental hindbrain nuclei; UAS, upstream activating sequence; URL, upper rhombic lip.

© 2010 Distel et al. This article is distributed under the terms of an Attribution–Noncommercial–Share Alike–No Mirror Sites license for the first six months after the publication date (see <http://www.rupress.org/terms>). After six months it is available under a Creative Commons License (Attribution–Noncommercial–Share Alike 3.0 Unported license, as described at <http://creativecommons.org/licenses/by-nc-sa/3.0/>).

but has been observed in many other cell types during migration, such as endothelial cells (Gotlieb et al., 1981), macrophages (Nemere et al., 1985), and fibroblasts (Kupfer et al., 1982; Schliwa et al., 1999). In non-neuronal migrating cells though, a correlation between migration and a leading centrosome is less consistent. For example, in fibroblasts migrating on grooved substrates or in collagen gels, the centrosome position is randomized with respect to the nucleus and the cell front (Schütze et al., 1991), whereas the centrosome in PtK cells lags behind the nucleus during wound-healing migration (Yvon et al., 2002). Similarly, a centrosome trailing the nucleus has been observed in cells of the migrating lateral line primordium in zebrafish embryos (Pouthis et al., 2008).

Reorientation of the centrosome can be stimulated by molecular interactions or gradients (Nemere et al., 1985; Renaud et al., 2008), electrical stimulation (Pu and Zhao, 2005; Zhao et al., 2006), or shear stress (Coan et al., 1993; Lee et al., 2005). This suggests that centrosome position is strongly influenced by the local molecular composition of the environment, but also by physical and physiological parameters such as morphogenetic constraints and electrical activity. Centrosome orientation may thus vary depending on the cell type, the tissue, and the developmental stage. Strikingly, it was recently shown that in radially migrating granule neurons of the developing cerebellum, the centrosome does not strictly lead migration during saltatory nucleokinesis, but it is often overtaken by the nucleus (Umeshima et al., 2007). This centrosomal behavior conflicts with the commonly used model of neuronal nucleokinesis; however, it was suggested that bidirectional movements of the nucleus may be the reason for the unusual temporary trailing of the centrosome in migrating granule neurons (Vallee et al., 2009). Clearly, further *in vivo* investigations are required to address a potential cell-type dependency of centrosome dynamics during neuronal migration.

An equally important role attributed to the centrosome is the determination of the site of axon outgrowth, as the centrosome is found in close proximity to the neurite that becomes the axon (Zmuda and Rivas, 1998; de Anda et al., 2005). In support, centrosome duplication through inhibition of cytokinesis resulted in two axons emerging adjacent to the centrosomes, whereas laser inactivation of the centrosome in cultured *Drosophila* neurons impaired axon formation (de Anda et al., 2005). In contrast though, axonogenesis is unaffected in *DSas-4* mutant flies, which are unable to replicate centrioles and therefore lack functional centrosomes by the third instar larval stage (Basto et al., 2006). Additionally, it was recently reported that, at least after axon induction, continued axon outgrowth from hippocampal neurons occurs through centrosome-independent polymerization of microtubule fibers, and is in fact unaffected by laser ablation of the centrosome (Stiess et al., 2010). These controversial observations argue for differences between the cell culture and *in vivo* situation or suggest that organelle dynamics differ between neuronal cell types. Therefore, an *in vivo* investigation into the temporal relationship between centrosome dynamics and emerging axonogenesis is needed. Such an approach though, requires a cell type-specific multiple organelle labeling technology.

We have established efficient coactivation of multiple cell biological fluorescent reporter proteins expressed from Gal4-dependent multi-cistronic expression cassettes. In addition, we generated a stable transgenic zebrafish strain expressing the modified Gal4 transcriptional activator KalTA4 (Distel et al., 2009) under the control of regulatory elements from the zebrafish *aton11a* gene and thus specifically in neuronal progenitors of the hindbrain rhombic lip. These neurons of the tegmental hindbrain nuclei (THN) have been shown to undergo long-distance migration along characteristic pathways through the developing zebrafish cerebellum and into the hindbrain tegmentum in an evolutionarily conserved manner (Köster and Fraser, 2001a; Volkmann et al., 2010). Expression of the multi-cistronic constructs in this transgenic Gal4 activator strain therefore allows the dynamics of the nucleus, the centrosome, and the emerging axon to be monitored simultaneously during THN migration *in vivo*. We demonstrate that the centrosome in migrating THN neurons is regularly overtaken by the nucleus and apparently does not lead migration by continuously advancing ahead of the nucleus. In addition, we reveal the temporal sequence of subcellular dynamics during THN neuron axonogenesis, which exclude an *in vivo* function of the centrosome in determining the site of axon outgrowth based on proximity to the centrosome. Thus, multicolor *in vivo* time-lapse imaging at subcellular resolution provides important insights into the dynamics of cellular processes and promises that the large fields of developmental genetics and cell biology can be merged in transparent zebrafish embryos into a field of vertebrate *in vivo* cell biology.

## Results

### Simultaneous subcellular intravital labeling in zebrafish cells

To fluorescently label subcellular structures in zebrafish, we first tested available fusion proteins in zebrafish Pac2 fibroblasts (Senghaas and Köster, 2009). Although  $\beta$ 3-tubulin-GFP (mouse) was mostly localized to the cytoplasm (Fig. 1 A), GFP-tubulin (Fig. 1 B, mouse) and EB1-GFP (Fig. 1 C, mouse) each marked the microtubule network, although the specificity of labeling was dose dependent. In contrast, expression of GFP-DCX (Fig. 1 D, mouse) or Tau-GFP (Fig. 1 E, mouse) resulted in robust microtubule labeling, while EB3-GFP (Fig. 1 F, mouse) successfully marked microtubule plus-ends. These data indicate that subcellular labeling constructs cannot be easily transferred from one species to another, but require careful testing.

Subsequently, we used a similar approach to achieve mitochondrial targeting in zebrafish fibroblasts (mitochondrial targeting sequence from subunit VIII of human cytochrome *c* oxidase; Fig. 1 G), as well as labeling of the endoplasmic reticulum (ER targeting sequence from calreticulin and ER retention sequence KDEL), the Golgi apparatus (N-terminal 81 aa of human  $\beta$ 1-4 galactosyltransferase; Fig. 1 H), and the actin cytoskeleton (zebrafish cytoskeletal actin; Fig. 1 I). Finally, fluorescent protein fusions of the C terminus (Fig. 1 J) and the N terminus (Fig. 1 K) of a partial zebrafish centrin-2 cDNA were each used successfully to visualize the two centrioles of the centrosome at the hub of the microtubule network (Fig. 1 L, inset). To eventually allow

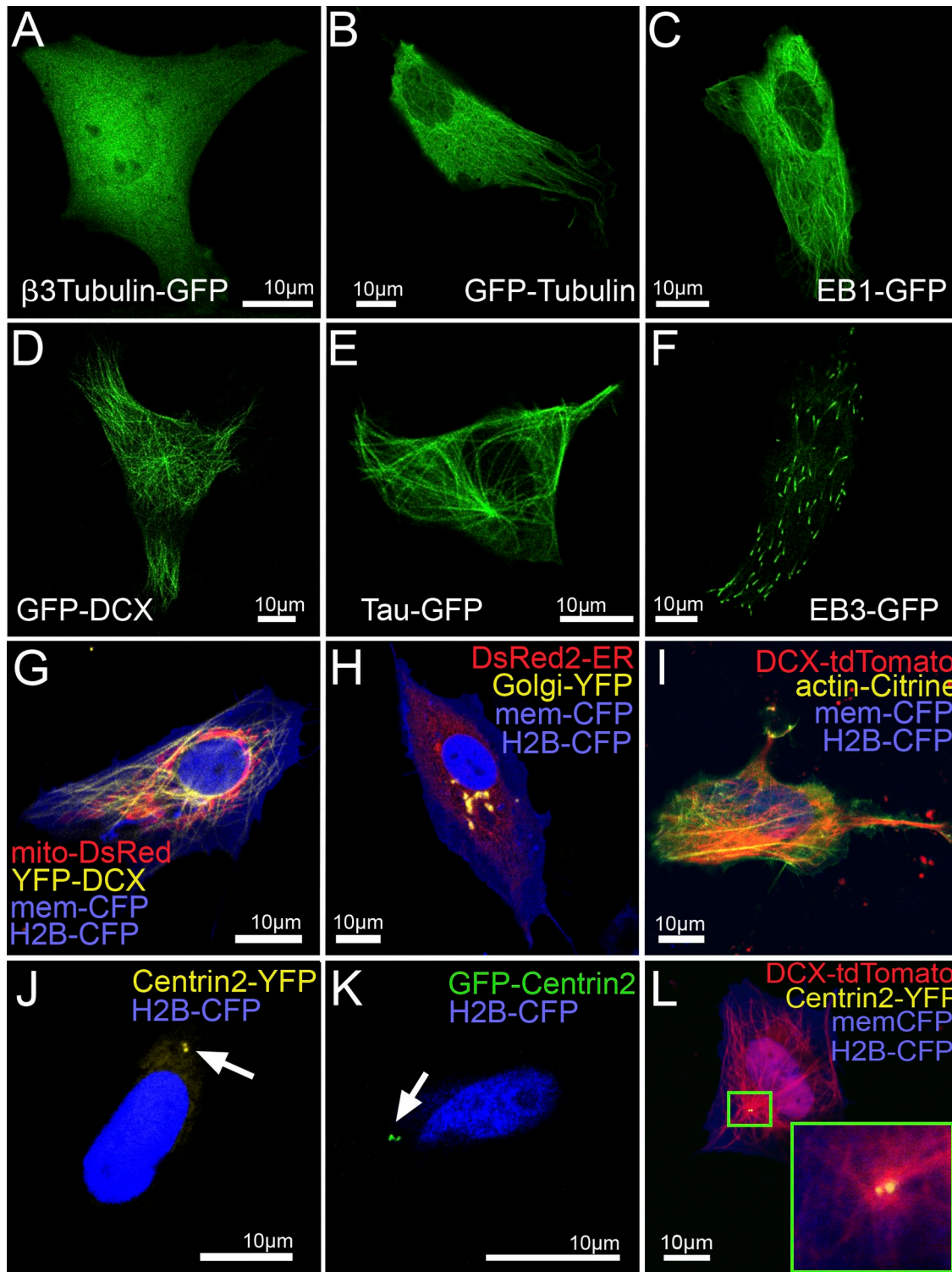


Figure 1. **Identification of subcellular markers for in vivo imaging of zebrafish cells.** Images of zebrafish Pac2 fibroblasts transfected with pCS2+ constructs encoding fluorescently tagged markers for subcellular labeling 24 h after transfection. (A)  $\beta$ 3-tubulin-GFP, (B) GFP-tubulin, (C) EB1-GFP, (D) GFP-DCX, (E) Tau-GFP, and (F) EB3-GFP. (G) mito-DsRed to label mitochondria in red, YFP-DCX to label microtubules in yellow, memCFP to label the cytoplasmic membrane in blue and H2B-CFP to label the nucleus in blue; (H) DsRed2-ER to label the ER in red, Golgi-YFP to label the Golgi apparatus in yellow, memCFP and H2B-CFP; (I) DCX-tdTomato to label microtubules in red, actin-Citrine to label the actin cytoskeleton in yellow, memCFP, H2B-CFP; (J) Centrin2-YFP to label the centrosome in yellow (arrow is indicating the two centrioles of the centrosome) and H2B-CFP; (K) GFP-Centrin2 to label the centrosome in green (arrow is indicating the two centrioles of the centrosome) and H2B-CFP; (L) DCX-tdTomato, Centrin2-YFP, memCFP, and H2B-CFP. The inset shows a higher magnification of the centrosome at the hub of the microtubule network. These data present a collection of subcellular-targeted fluorescent proteins tested for their specificity in zebrafish cells. “mem” represents a membrane localization signal, which consists of a palmitoylation and myristinylation sequence of the human Lck kinase.

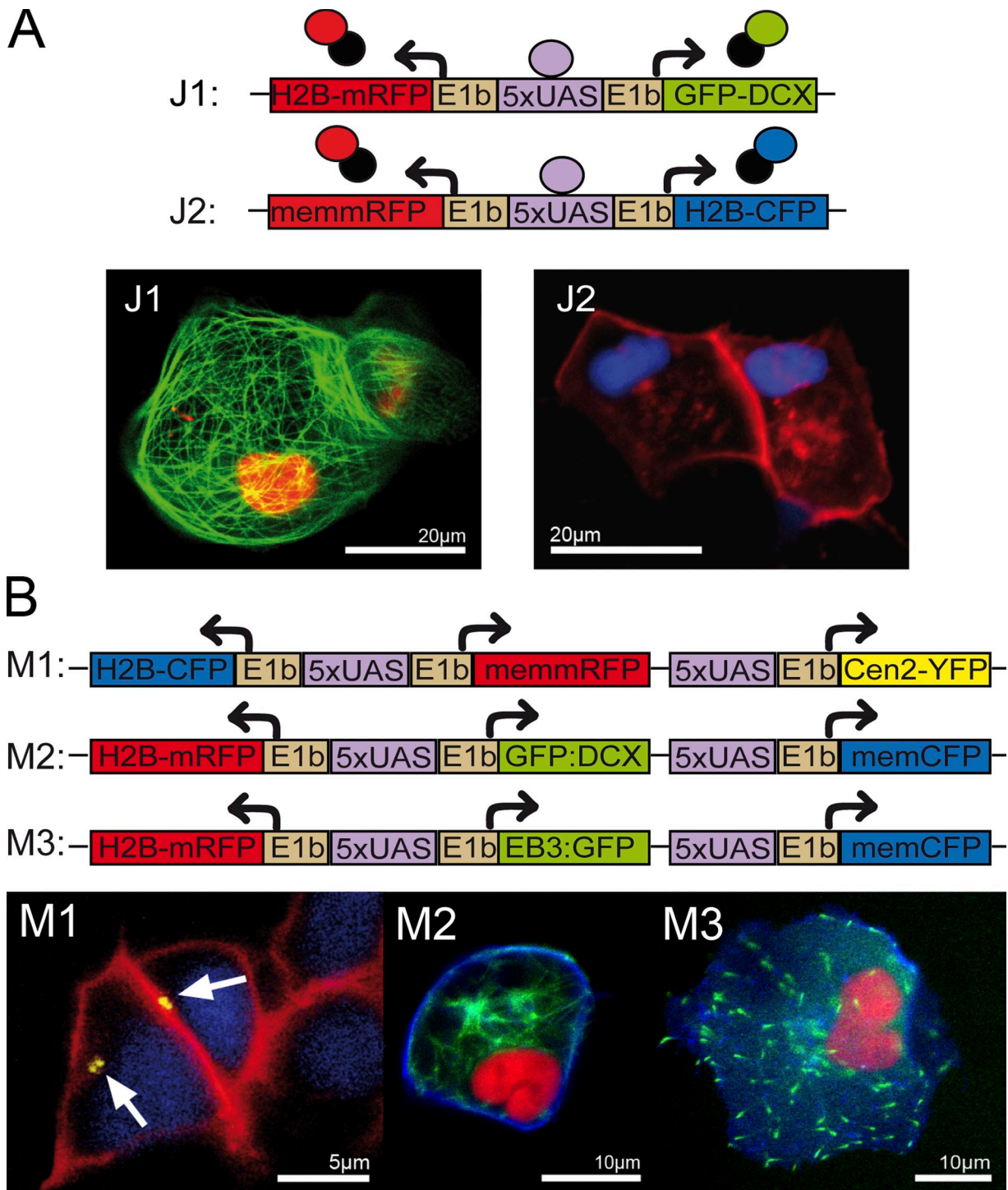


Figure 2. **Janus and Medusa Gal4 effector constructs for simultaneous expression of multiple subcellular labels.** (A) Schematic representation of bidirectional Janus vectors J1 and J2. Upon binding of Gal4, two subcellular markers are expressed simultaneously (J1: H2B-mRFP labels the nucleus in red and GFP-DCX the microtubules in green; J2: memmRFP labels the membrane in red and H2B-CFP the nucleus in blue). (B) Schematic representation of Medusa vectors M1, M2, and M3. From each vector, the expression of three subcellular markers is activated in the presence of Gal4. M1 encodes H2B-CFP to label the nucleus in blue, memmRFP to mark the membrane in red, and Centrin2-YFP to label the centrioles of the centrosome in yellow. M2: H2B-mRFP to label the nucleus in red, GFP-DCX to label microtubules in green, and memCFP to label the membrane in blue. M3 codes for the same nuclear and membrane markers as M2, but contains EB3-GFP to label the plus-ends of microtubules. These data demonstrate that reliable coexpression of various transgenes can be achieved from Gal4-mediated multicistronic expression vectors. Images were obtained from living zebrafish embryos (24 hpf) coinjected at the one-cell stage with the respective Janus or Medusa vectors and a vector coding for Gal4. “mem” represents a membrane localization signal, which consists of a plamitylation and myristinylation sequence of the human Lck kinase. Arrows in M1 indicate YFP-labeled centrosomes.

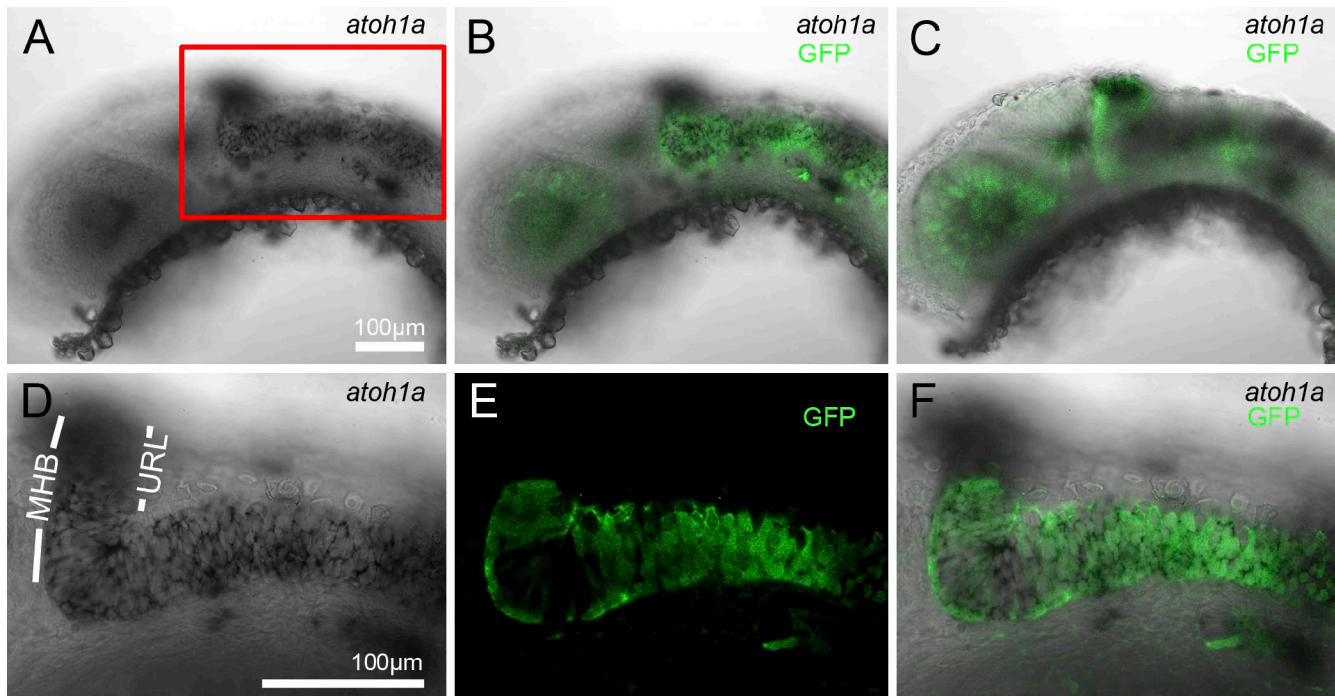


Figure 3. **Characterization of *Tg(atoh1a:Gal4TA4)<sup>hzm2</sup>* transgenic zebrafish.** Lateral view of an offspring of *Tg(atoh1a:Gal4TA4)<sup>hzm2</sup> x Tg(4xUAS:GFP)<sup>hzm3</sup>* transgenic fish at 24 hpf. (A) Endogenous *atoh1a* expression in the rhombic lip as revealed by in situ hybridization (black). (B) Immunostaining for GFP after in situ hybridization for *atoh1a* on *Tg(atoh1a:Gal4TA4)<sup>hzm2</sup>/Tg(4xUAS:GFP)<sup>hzm3</sup>* double-transgenic fish shows expression of GFP (green) in the rhombic lip in *atoh1a*-expressing cells (black). (C) In addition, some GFP-expressing cells can be found in the retina, the midbrain tegmentum, and the tectum of *Tg(atoh1a:Gal4TA4)<sup>hzm2</sup>/Tg(4xUAS:GFP)<sup>hzm3</sup>* double-transgenic fish. (D) Enlargement of boxed area in A showing in situ hybridization for *atoh1a* in the hindbrain. (E) Immunostaining for GFP. (F) Overlay of D and E. These data show that *KalTA4* expression in *Tg(atoh1a:Gal4TA4)<sup>hzm2</sup>* embryos faithfully recapitulates rhombic lip expression of endogenous *atoh1a*. MHB, midbrain–hindbrain boundary; URL, upper rhombic lip.

for multiple combinations of subcellular markers, we generated fusion proteins with spectrally different fluorescent proteins for most of these subcellular markers (Table S1).

### Simultaneous multicolor labeling

To mediate the simultaneous expression of two fluorescent subcellular markers by Gal4 transcriptional activators, we generated bidirectional Gal4-dependent effector constructs. These so-called Janus vectors carry a series of Gal4 binding sites (upstream activating sequences, UAS) flanked on both sides by E1b minimal promoters (Fig. 2 A; Paquet et al., 2009).

Two of these Janus vectors (Fig. 2 A; J1, J2) were used to evaluate the degree of coexpression of the two markers in vitro by cotransfection with a *KalTA4*-encoding expression vector (pCS-*KalTA4GI*) into Pac2 fibroblasts (not depicted) and in vivo by coinjection with pCS-*KalTA4GI* at the one-cell stage. Coexpression was found to be reliable, both in Pac2 cells and in embryos (ranging between 97–99%), indicating that bound *KalTA4* is able to activate gene expression upstream and downstream, even when only a single UAS site is used (Fig. S1). Currently though, we cannot distinguish whether bidirectional activation occurs after *KalTA4* is bound to UAS or whether bidirectional activation requires off and on events of *KalTA4* binding to UAS.

To further evaluate if the position upstream or downstream of the UAS sites is favored by *KalTA4* for activating transgene expression, we generated the Janus constructs mRFP:5xUAS:GFP and GFP:5xUAS:mRFP. Both vectors were cotransfected

with pCS-*KalTA4GI* into zebrafish Pac2 fibroblasts and protein levels of GFP and mRFP were determined by Western blot analysis ( $n = 3$ ). When the ratios of the expression levels were compared for both orientations, the position downstream of the UAS was found to be slightly more strongly activated ( $\sim 1.15$  fold) than the position upstream of the UAS sites (unpublished data). Although this differential activation does not represent a marked difference, this information may be valuable when the dose of the expressed transgenes is of importance.

Next, we established so-called Medusa vectors containing additional UAS sites or Janus units for triple or quadruple transgene expression. This, for example, allows the nucleus, the cytoplasmic membrane, and the centrosome (M1) to be labeled simultaneously from a single Medusa expression construct. In addition, Medusa vectors labeling microtubule fibers (M2) or microtubule plus-ends (M3) together with the nucleus and the cell membrane were successfully expressed in zebrafish embryos (Fig. 2 B) and allow one to clearly observe microtubule dynamics in nondividing (Video 1) or dividing cells (Videos 2 and 3) in living zebrafish embryos. Furthermore, two Janus cassettes can be combined to achieve quadruple subcellular labeling (not depicted).

### Generation of a rhombic lip-specific *KalTA4* activator line

To express transgenes specifically in cells derived from the rhombic lip, we identified regulatory elements of the zebrafish *atoh1a* homologue and flanked a *KalTA4* expression cassette



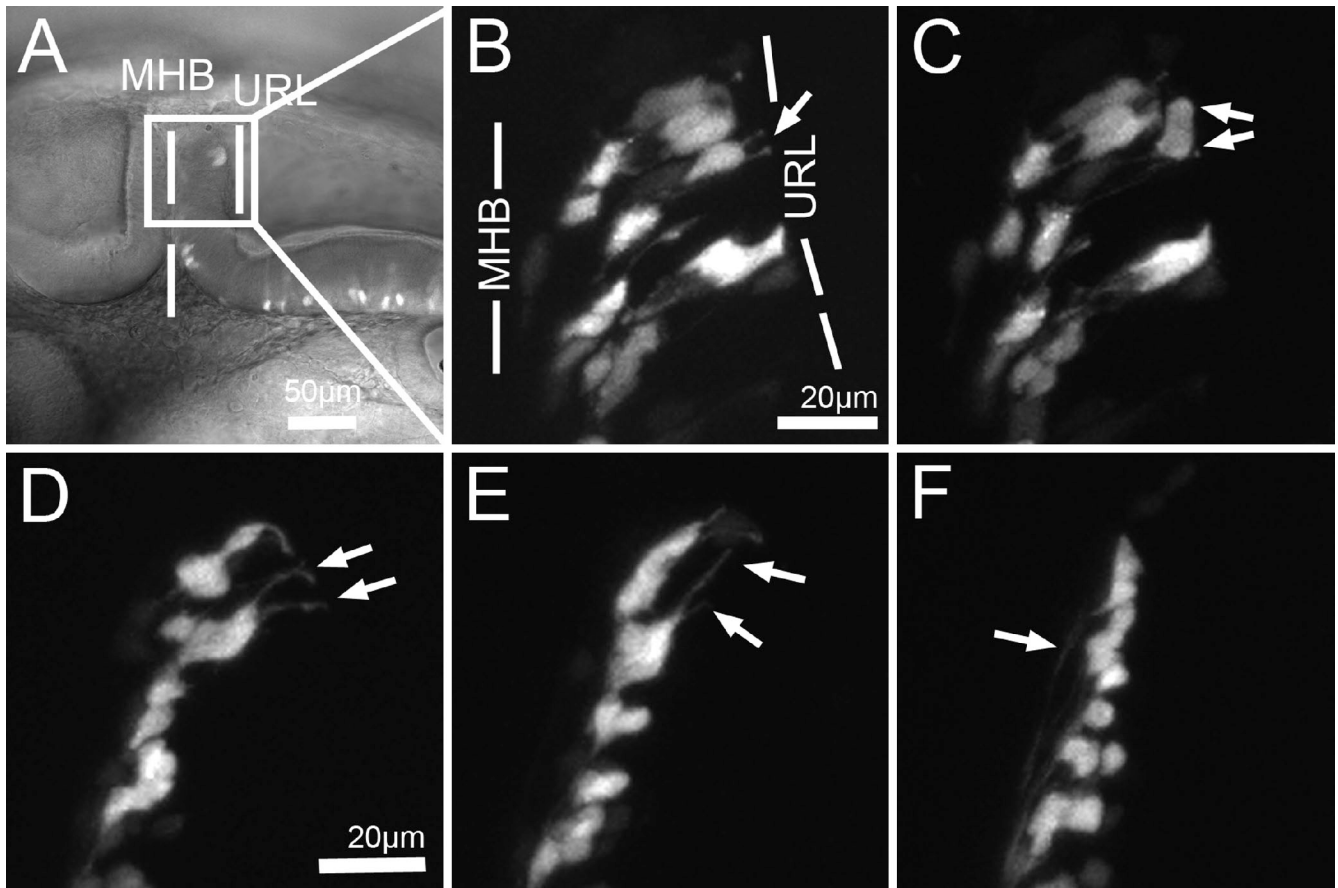


**Figure 4. Time-lapse analysis of THN progenitor behavior.** (A) Lateral view of the MHB region of a *Tg(ato1a:Gal4TA4)<sup>hzm2</sup> x Tg(shhb:Gal4TA4,5xUAS:mRFP)<sup>hzm4</sup>* embryo at 24 hpf. URL-derived THN progenitors are labeled by mRFP expression. The boxed area is enlarged in B–F. (B) mRFP-expressing THN progenitors are connected to the apical surface by thin processes (arrow). (C) THN progenitors divide at the apical side (arrows indicate dividing cell). (D) During radial migration these cells maintain apical processes (arrows) that are retracted (E) once the nuclei reach the MHB. (F) Around the same time, axon-like processes become visible (arrow). These time-lapse data show that transgene expression mediated by Gal4 in *Tg(ato1a:Gal4TA4)<sup>hzm2</sup>* embryos reveals cell behavior consistent with that previously observed for URL-derived THN neurons (Köster and Fraser, 2001a; Volkmann et al., 2010). Images were taken from Video 4. MHB, midbrain–hindbrain boundary; URL, upper rhombic lip.

(KalTA4GipA; Distel et al., 2009) with them. Subsequently, transgenic fish *Tg(ato1a:Gal4TA4)<sup>hzm2</sup>* were generated using I-SceI-meganuclease mRNA coinjection (Babaryka et al., 2009). When crossed to *Tg(4xUAS:GFP)<sup>hzm3</sup>* carriers, the offspring showed the expected pattern of GFP expression throughout the rhombic lip (Fig. 3, B and C). Although some ectopic GFP expression domains in the retina and optic tectum (Fig. 3 C) could be observed, GFP fluorescence throughout the hindbrain and in sensory hair cells recapitulated the expression of endogenous *aton1a*, as confirmed by coexpression analysis against *aton1a* mRNA (Fig. 3, A and D) and anti-GFP immunohistochemistry (Fig. 3, B, E, and F).

Confocal time-lapse recording of fluorescent URL-derived cells in embryos from crosses of *Tg(ato1a:Gal4TA4)<sup>hzm2</sup> x Tg(shhb:Gal4TA4,5xUAS:mRFP)<sup>hzm4</sup>* (TG5xR; Distel et al., 2009), in which Gal4-expressing cells mosaically expressed mRFP, revealed that these cells divided at the URL starting at ~24 hours postfertilization (hpf; Fig. 4 C), and subsequently moved radially to the MHB while still connected to the URL by a long trailing process (Fig. 4 D). They eventually retracted this trailing process and migrated ventrally in a tangential manner along the MHB (Fig. 4, E and F). These early URL-emigrating

cells have recently been identified as neurons of tegmental hind-brain nuclei (Volkmann et al., 2010). Intriguingly, as has been described before (Köster and Fraser, 2001a), these THN neurons already begin to project axons along the MHB and into the mid-brain before and during ventral migration (Fig. 4 F, white arrow; see Video 4).

#### Subcellular analysis of THN neuronal progenitors during cell division

The establishment of subcellular markers and multi-cassette UAS-based vectors, in addition to the URL-specific KalTA4 expression in the transgenic strain *Tg(ato1a:Gal4TA4)<sup>hzm2</sup>*, set up the possibility of doing *in vivo* cell biological experiments in a defined neuronal population. *Tg(ato1a:Gal4TA4)<sup>hzm2</sup>* embryos injected at the one-cell stage with the Medusa M1 construct showed expression of the subcellular markers in THN neuron progenitors from at least 22 hpf onwards. THN neuronal progenitors were observed to span the entire cerebellar primordium, being connected by endfeet-like processes to the apically positioned URL and basally located MHB (Fig. 5 A). THN progenitors underwent interkinetic nuclear movements (INM) and divided strictly at or close to the apical side, along the ventricle

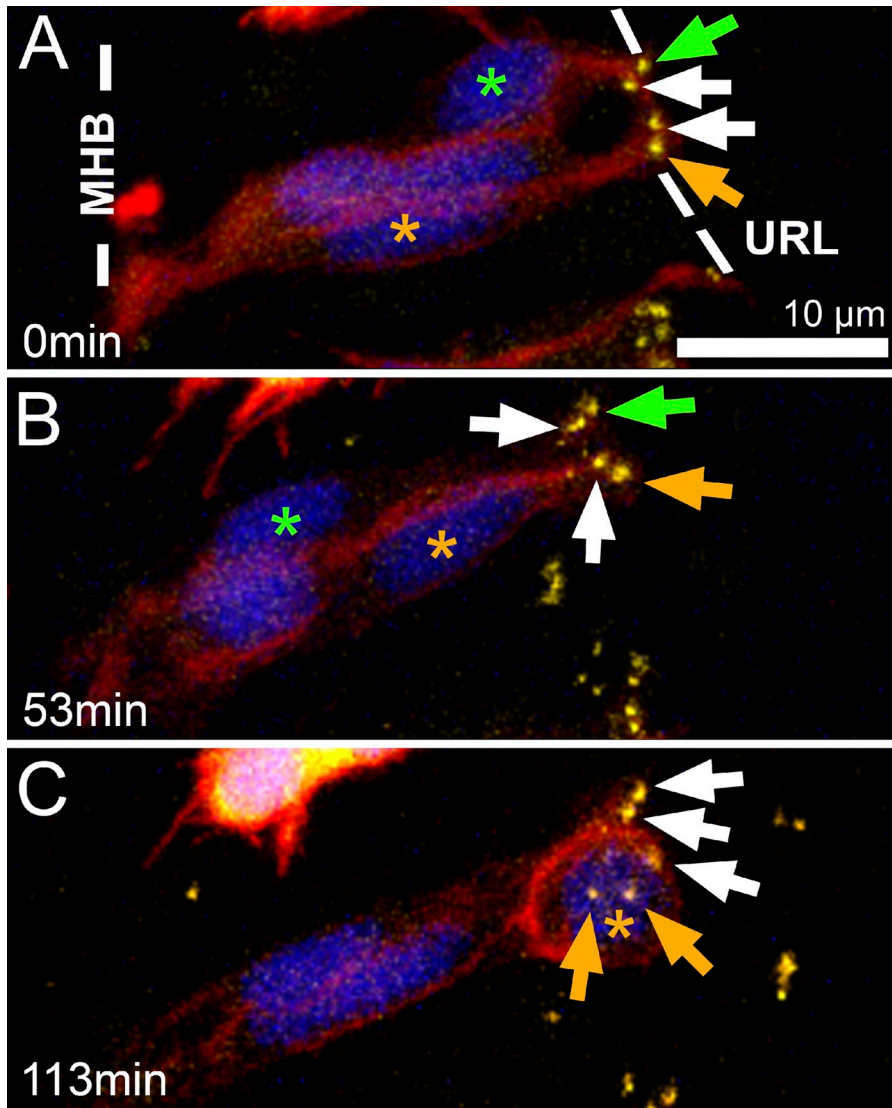


**Figure 5. In vivo subcellular imaging of INM and mitotic cleavages of THN progenitors.** Lateral view of THN progenitors in the cerebellum of an  $\sim 24$ -hpf *Tg(atoh1a:Gal4TA4)<sup>hzm2</sup>* transgenic embryo injected with Medusa vector M1. Centrosomes are shown in yellow, cell nuclei in blue, and cellular membranes in red. (A) Centrosomes (arrows) were found to line the fourth ventricle at the apical side of the four THN progenitors undergoing INM between the midbrain–hindbrain boundary (MHB) and the fourth ventricle. Throughout INM, the centrosomes did not change their positions. Green asterisk demarcates a nucleus moving from apical to basal (A and B), while the corresponding centrosome (green arrow) stays at the apical side. The orange asterisk demarcates a nucleus that moves from basal to apical (A–C) to undergo a mitotic cleavage at the apical side (C). The corresponding centrosome (orange arrow) stays at the apical side, replicating to build the two spindle poles of the spindle apparatus (C, orange arrows). Thus, THN progenitors along the URL show characteristic INM behavior. Images are taken from [Video 5](#). Note: some yellow-only labeling may suggest insufficient co-expression of transgenes from Medusa vectors. However, dependent on the z-level position of organelles and different intensities in expression levels, proper co-labeling can only be observed in cells of interest for which z-stacks were recorded. MHB, midbrain–hindbrain boundary; URL, upper rhombic lip.

(Fig. 4 C, white arrows, and Fig. 5 C, yellow asterisk;  $n = 31$  cells, 8 embryos). Mitotic events of these cells elsewhere in the cerebellar neuroepithelium were rarely observed, consistent with results from immunostainings against phosphorylated histone 3, an established M phase marker, which only labeled cells near the ventricle (Fig. S2). During INM phases, the centrosomes neither precede nor follow the movement of the nuclei, but remain stationary, being localized strictly to the apical membrane (Fig. 5, A–C, arrows; [Video 5](#);  $n = 17$ , 4 independent embryos), as reported previously for mitotically active neuronal progenitors in polarized dividing neuroepithelia (Hinds and Ruffet, 1971; Chenn et al., 1998; Xie et al., 2007).

#### **THN neuronal progenitors maintain a mitotic organization during preparation for migration**

When time-lapse recordings were performed over a prolonged period of time, we observed that THN progenitors appeared to change their behavior. THN progenitors are elongated and during INM the long axis of cells in the mid-cerebellum is oriented only  $\sim 32$  degrees off the apico-basal axis between the URL and MHB

(Fig. 6, A–C; [Fig. S3](#);  $32.5 \pm 4.6$ ,  $n = 5$  cells). As THN progenitors approach the MHB in preparation for ventral migration, however, the cells become more ventrally oriented, deviating now  $\sim 65$  degrees from the apico-basal axis of the cerebellum (Fig. 6 F; [Fig. S3](#);  $66.9 \pm 6.9$ ,  $n = 4$  cells). Medusa vector labeling of the centrosome, the membrane, and the nucleus revealed that THN progenitors initiating migration leave behind a long trailing process that remained connected with the apical membrane. The centrosome remained stationary in the apical process, near the ventricular surface (Fig. 6, B and C), until shortly before the apical process began to detach from the germinal zone. If neuronal migration is considered to be an event whereby a neuron follows a leading process and moves from its birth place to its terminal site of later function without being connected to either position, then the final forward movement of bipolar THN progenitors toward the MHB does not represent neuronal migration. Rather, the apically positioned centrosome within a trailing process still in contact with the germinal zone is characteristic of proliferating neuronal progenitors and argues that the nuclear translocation toward the MHB in conjunction with a ventral turn of the cell actually represents an extended final step of INM.

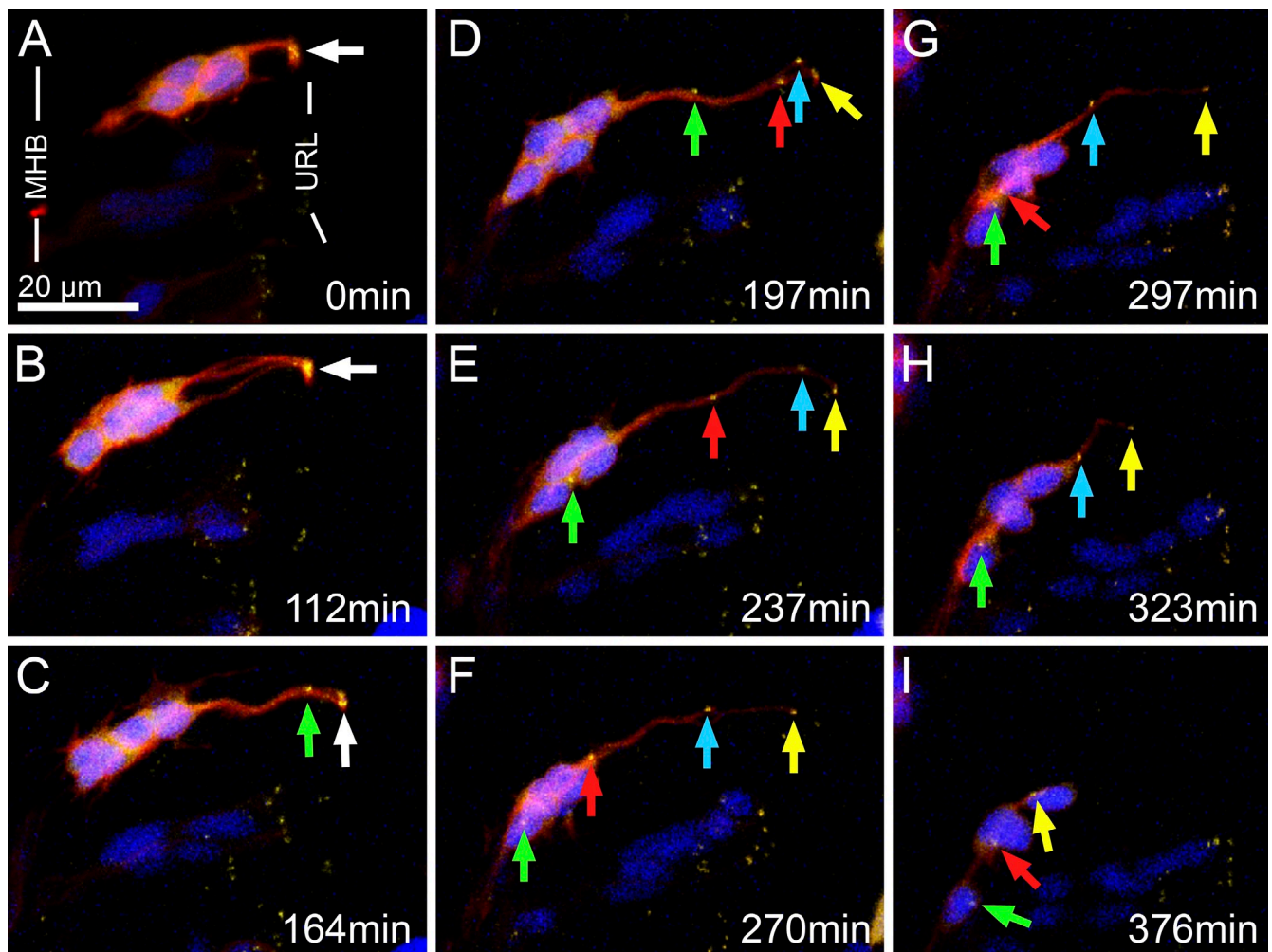


Figure 6. **In vivo subcellular imaging of centrosome dynamics in THN progenitors.** Lateral view of the cerebellar anlage of an  $\sim 36$ -hpf *Tg(atoh1a:Gal4TA4)<sup>hzm2</sup>* transgenic embryo injected with Medusa vector M1. Centrosomes (green arrow indicates the first centrosome, red arrow second, turquoise third, and yellow fourth; white arrows are shown when centrosomes are indistinguishable) are labeled in yellow, cell nuclei in blue, and cellular membranes in red. (A) Centrosomes (arrow) of the four THN progenitors were found to line the fourth ventricle. (B) Nuclei translocate basally toward the MHB, leaving behind a long trailing process containing the centrosome at its most apical part. This subcellular coordination argues that the final MHB-directed cell movement to initiate migration represents an extended final step of INM. (C–I) When nuclei reach the MHB, trailing processes containing the centrosomes at the most apical position are retracted, representing the initiation of THN neuron migration. Images are taken from [Video 6](#). MHB, midbrain–hindbrain boundary; URL, upper rhombic lip.

#### Initiation of migration by THN neurons is accompanied by saltatory nuclear movements

When the cell soma approached the MHB, THN progenitors started to retract their trailing process, with the centrosome homing toward the soma and reaching the nucleus ( $n = 27$  cells, 7 embryos) within  $\sim 1.5$  to 2 h (Fig. 6, C–I; [Videos 6](#) and [7](#)). Subsequently, THN neurons continued to migrate in a ventral direction to eventually reach their terminal positions in tegmental hindbrain areas.

To further quantify the subcellular processes during initiation of migration, we first performed a kymograph analysis of nuclear movements. THN progenitors connected with the URL via a trailing process showed a gradual pace of forward nuclear movement (see Fig. 8 A). In contrast, saltatory nucleokinesis alternating with resting phases was observed for nuclei of THN neurons migrating ventrally parallel to the MHB (see Fig. 8 B, white asterisk). When the distance of nuclear movement was plotted against time,

a similar average pace of nucleokinesis could be determined for gradual ( $0.22 \mu\text{m}/\text{min}$ ) and saltatory ( $0.21 \mu\text{m}/\text{min}$ ) nucleokinesis. During the latter though, the nucleus only moved on average  $1.17 \mu\text{m}$  ( $\pm 0.7 \mu\text{m}$ ) during resting phases, while suddenly progressing  $7.54 \mu\text{m}$  ( $\pm 1.43 \mu\text{m}$ ) during saltatory steps ( $n = 8$  saltatory steps, 3 independent videos), which is more than a nuclear diameter ( $6.63 \pm 0.67 \mu\text{m}$ , 10 nuclei measured). Thus, migration of THN neurons disconnected from the URL is marked by a switch from gradual to saltatory nucleokinesis.

#### The nucleus repeatedly surpasses the centrosome during nucleokinesis of THN neurons

A current model of saltatory nucleokinesis proposes that the centrosome permanently advances ahead of the nucleus, and that this organization is crucial for forward nuclear movement (Tsai and Gleeson, 2005; Métin et al., 2008). Indeed, during THN migration along the MHB, Medusa labeling revealed that

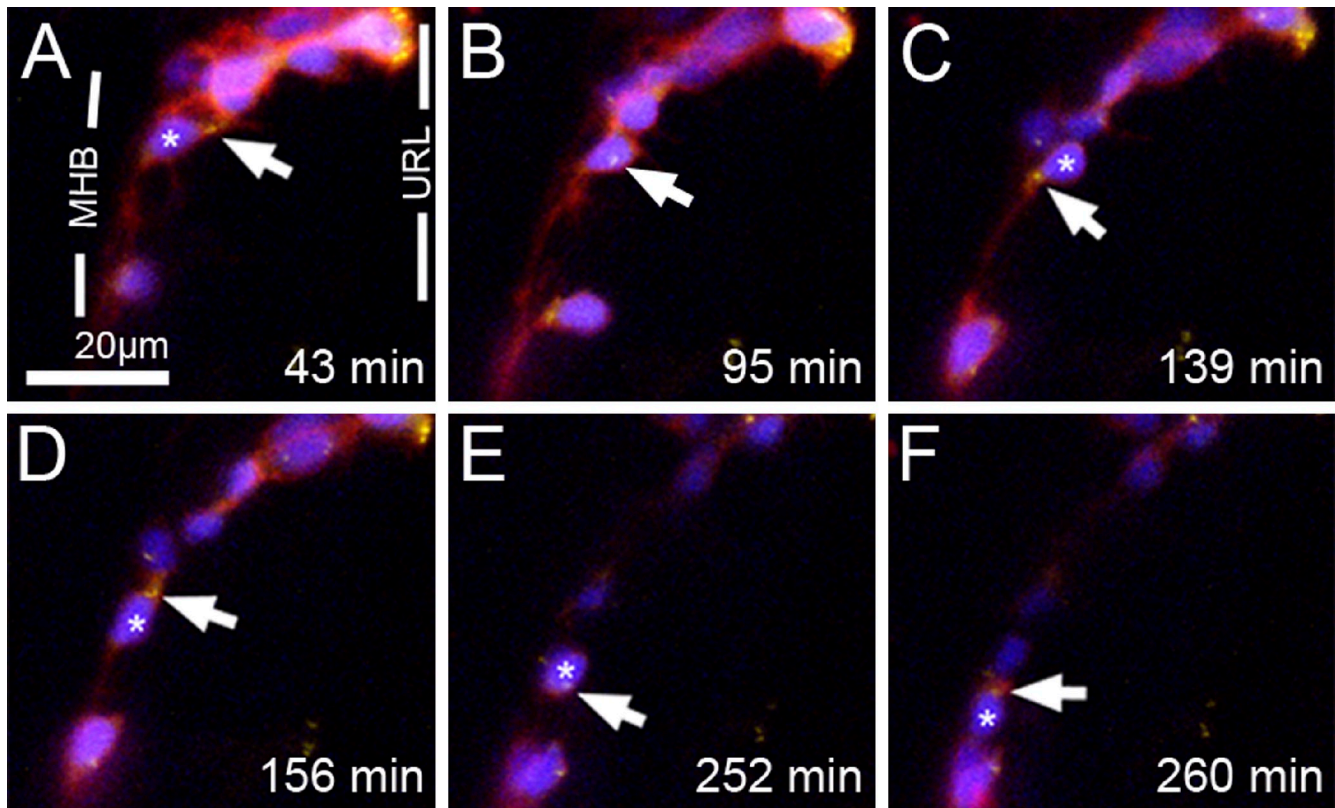


**Figure 7. Subcellular imaging of saltatory nuclear movements in migrating THN progenitors.** Lateral views of a region of the cerebellum of a 36-hpf *Tg(ato1a:Gal4TA4)<sup>hzm2</sup>* transgenic zebrafish embryo injected with Medusa vector M1. (A–C) According to the direction of migration, the centrosome (arrow) translocates in front of the nucleus (asterisk). (C and D) The nucleus then overtakes the centrosome in a rapid saltatory movement such that the centrosome locates posterior to the nucleus (D). Subsequently, the centrosome translocates once again ahead of the nucleus (E). In a second saltatory movement, the nucleus again overtakes the centrosome (F). These time-lapse data show that during saltatory nucleokinetic migration, THN neurons display iterative cycles of a centrosome leading and trailing the nucleus. Images are maximum projections of z-stacks. The time between images taken from [Video 8](#) is indicated in the bottom right of each panel. MHB, midbrain–hindbrain boundary; URL, upper rhombic lip.

the centrosome moved ahead of the nucleus (Fig. 6, F and G, red arrow; G–I, yellow arrowhead). Intriguingly, our time-lapse recordings showed that the centrosome did not remain strictly in front of the nucleus. Instead, with each forward migratory step, the nucleus passes the centrosome (Fig. 7, C–F; Fig. 8 B, white asterisks). Plotting of distance over time showed that the centrosome moved at a nearly constant pace, whereas the nucleus alternated between resting and sudden advances (Fig. 8 D). Quantification revealed that the centrosome most often trailed the nucleus and is ahead of it for only ~35% of the time (Fig. 8 E). However, the centrosome repeatedly passed the nucleus during the preparatory phase of nuclear movement (Fig. 7, A–C, D, and E), when the centrosome seemed to indicate the direction of the next forward migratory step ( $n = 16$  cells, 6 embryos; [Video 8](#)). Thus, when the nucleus is not stationary ( $72.22\% \pm 14.40\%$  of time), the centrosome and the nucleus move in the same direction ( $70.9\% \pm 9.9$ ) and rarely opposite ( $8.4\% \pm 4.5\%$ ) to one another ( $n = 4$  ventrally migrating cells, 3 embryos), indicating the same directionality of their movements (for a detailed analysis of the direction of movements of the centrosome and the nuclear centroid in the ventrally migrating cell shown in Fig. 8 B, see Fig. 8 F).

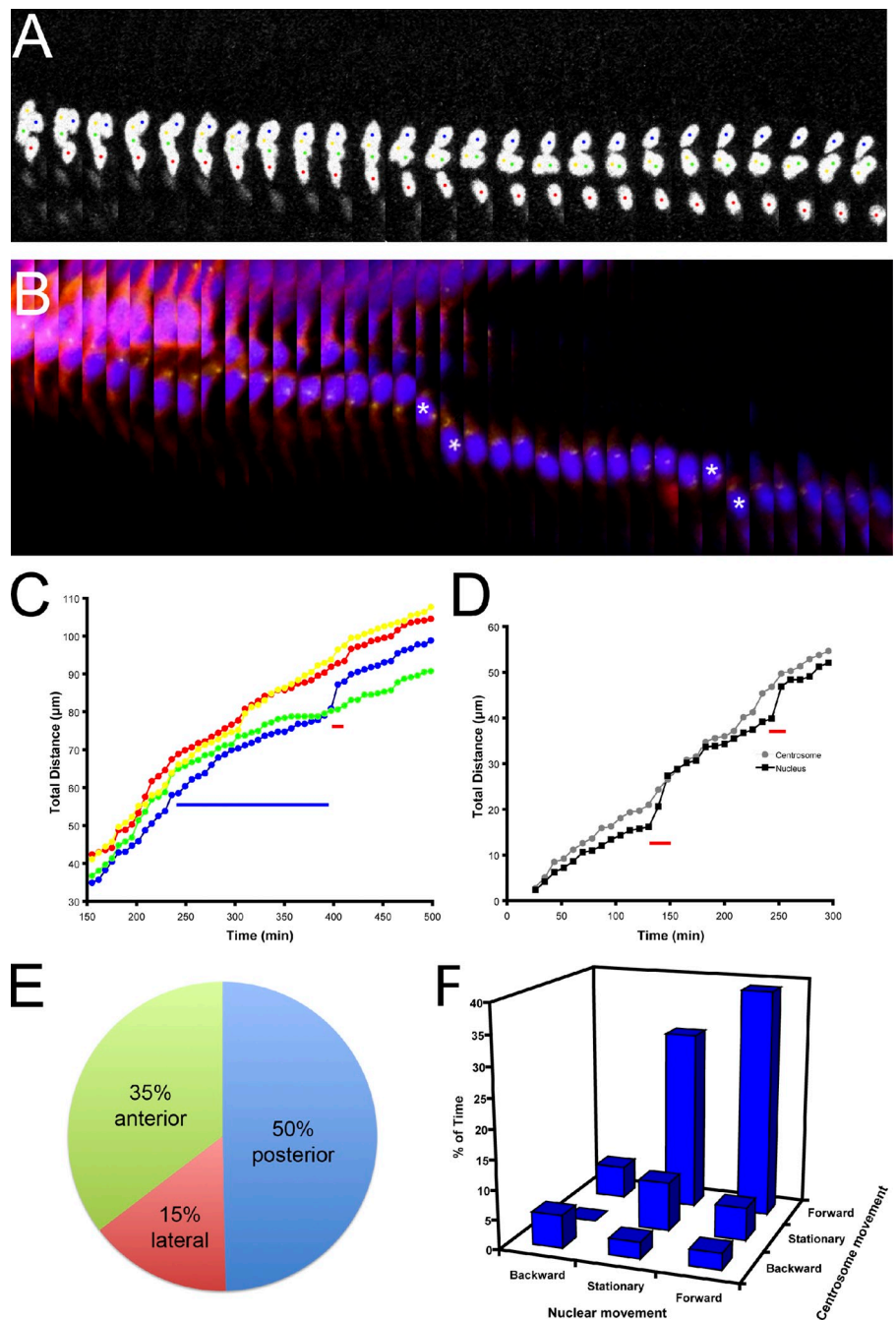
This iterative change in relative position of the nucleus and the centrosome to one another and the mostly trailing centrosome differ from the commonly used saltatory nucleokinetic

model of a permanently leading centrosome during all steps of neuronal migration. Thus, either zebrafish THN neurons follow a different, cell population–specific form of saltatory nucleokinetic migration or saltatory nucleokinesis is less strictly orchestrated than previously thought, perhaps requiring a forward position of the centrosome only during a certain time window just before nuclear movement.

#### Axonogenesis of THN neurons occurs at the MHB

THN neurons approaching the MHB begin to extend from their leading edge a longer axon-like cellular process (Fig. 9 A, white asterisk; for axon projection into the midbrain see also final image sequence of [Video 4](#)). To verify the axonal identity of these emerging leading process structures, we performed immunohistochemistry against the axonal-specific marker acetylated tubulin. Acetylation of lysine40 of the  $\alpha$ -tubulin subunit to stabilize microtubules is a key characteristic of the proximal axon and is important for axon outgrowth (Hammond et al., 2008; Witte and Bradke, 2008; Conde and Cáceres, 2009). Double-transgenic *Tg(ato1a:Gal4TA4)<sup>hzm2</sup> x Tg(4xUAS:GFP)<sup>hzm3</sup>* embryos were raised until 40–42 hpf, by which time many GFP-expressing THN neurons had reached the MHB (Fig. 9 B). Subsequent fluorescent immunohistochemistry against GFP and acetylated  $\alpha$ -tubulin

**Figure 8. Analysis of THN migratory movements.** (A) Kymograph of a portion of [Video 6](#) (229–390 min) showing the gradual movement of cell nuclei toward the MHB. Images have been rotated 45° and only the blue channel is shown in order to better visualize the nuclei. Each nucleus is labeled with a colored dot. Time between frames is 404.2 s. (B) Kymograph created from [Video 8](#), showing two saltatory movements of the nucleus (asterisks) and the comparatively smooth forward migration of the centrosome during ventral migration. Images were rotated 45° and the time between frames is 522.6 s. The centrosome is ahead of the nucleus immediately before a nucleokinetic movement, but is overtaken when the nucleus jumps forward. (C) Graph of the cumulative migration distance (in any direction) for each nucleus in [Video 6](#). Colors match the dots used for labeling nuclei in A. Tracking was done on 2D maximum projections with the Manual Tracking tool of ImageJ. The nuclei move at a gradual pace until they reach the MHB, at which point one nucleus undergoes a saltatory movement (red bar). The blue bar represents the region of the video shown in the kymograph in A. (D) Graph of the cumulative migration distance (in all directions) of the centrosome and nucleus in [Video 8](#). During ventral migration, the cells undergo obvious nucleokinetic movements (red bars). The centrosome moves at a more consistent and gradual pace. (E) Pie chart showing the amount of time that the centrosome spends ahead of, lateral to, or behind the centroid of the nucleus ( $n = 4$  cells, 3 embryos). (F) 3D graph showing the portion of time during which the centrosome and nucleus in [Video 8](#) are each stationary, move in the direction of migration (forward), or move opposite to the direction of migration (backward). The movement of both organelles is predominantly in the direction of migration, but much of the forward centrosomal movement occurs while the nucleus is stationary.



showed that indeed GFP-expressing THN neurons at the MHB already possessed acetylated  $\alpha$ -tubulin-positive processes (Fig. 9 C, white arrows), which likely emerged from the leading processes observed in Medusa-labeled cells (Fig. 9 A, white asterisk). These data strongly suggest that THN neurons initiate axon formation at the beginning of migration.

Interestingly, time-lapse imaging of subcellular Medusa-labeled THN neurons revealed the emergence of the axon-like protrusion, which subsequently developed a clear growth cone structure (Fig. 9, D–F; red arrow), at the time when trailing process retraction and centrosome repositioning from the apical germinal zone toward the cell soma were still occurring ( $n = 9$  cells, 8 embryos; Fig. 9, D–F, white arrow; [Video 9](#)). This suggests

that axonogenesis in THN neurons occurs in parallel to, or shortly after, proliferative INM is terminated.

#### **Axonogenesis in THN neurons is not induced by proximity to the centrosome**

Our subcellular *in vivo* time-lapse studies of centrosome dynamics, together with the immunohistochemical analysis of axon formation, argue that axonogenesis in zebrafish THN neurons is initiated by a membrane protrusion far away from the microtubule-organizing centrosome. To directly resolve the temporal sequence of axonogenesis and centrosome dynamics in THN neurons *in vivo*, we made use of the reporter Kif5C<sup>560</sup>-YFP, which accumulates selectively in the forming axon very soon after axon

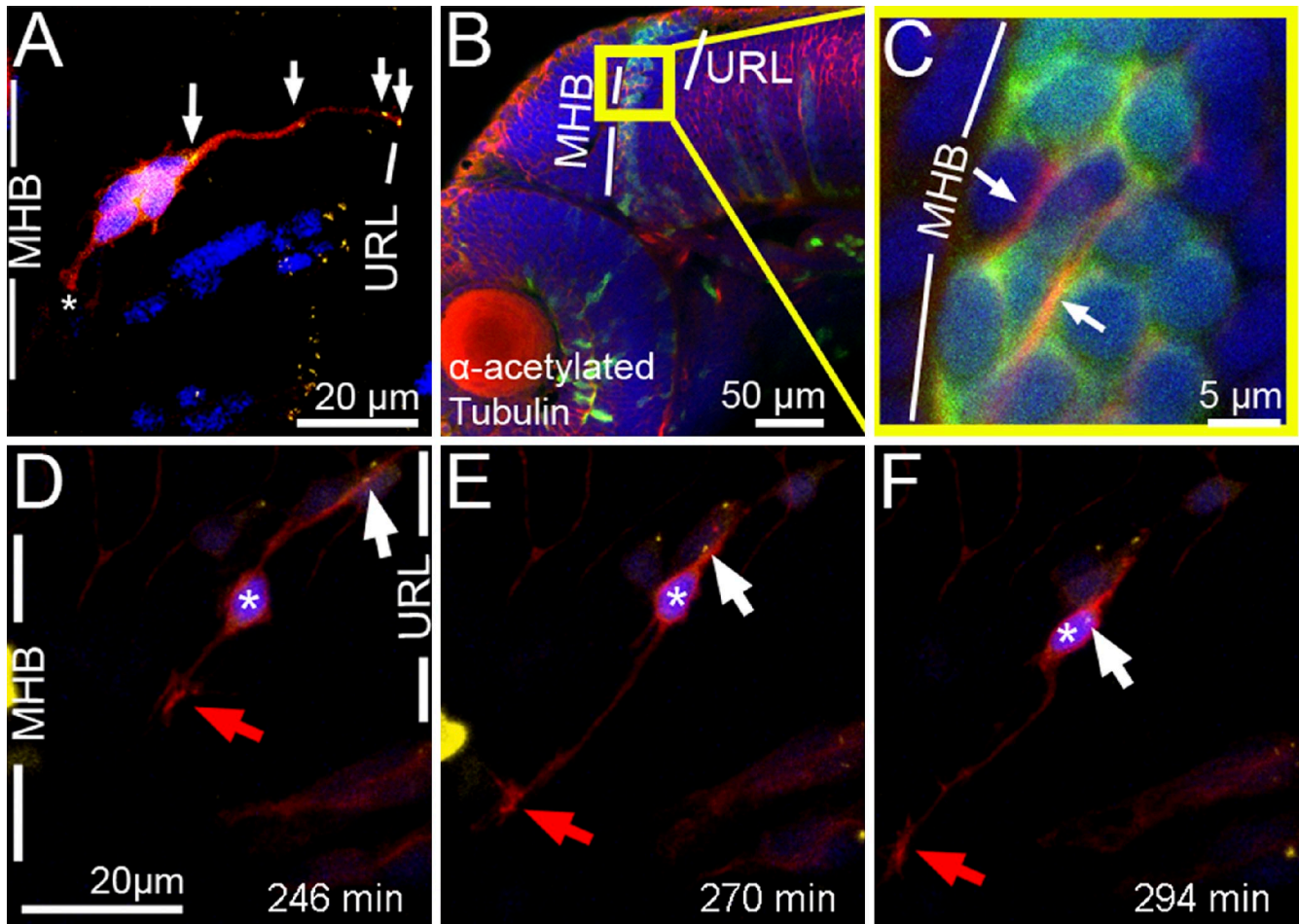


**Figure 9. THN progenitors initiate axonogenesis from their leading process independent of centrosome proximity.** (A) Lateral view of the cerebellar anlage of an ~42-hpf *Tg(ato1a:Gal4TA4)<sup>hzm2</sup>* transgenic zebrafish embryo injected with Medusa vector M1. An axon-like protrusion (white asterisk) has formed at the time when the centrosome (white arrow) is still homing toward the soma. (B) Lateral view of a *Tg(ato1a:Gal4TA4)<sup>hzm2</sup> × Tg(4xUAS:GFP)<sup>hzm3</sup>* transgenic zebrafish embryo at 42 hpf. GFP-expressing cells are visualized by anti-GFP immunostaining (green) and acetylated microtubules by anti-acetylated tubulin immunostaining (red). (C) Enlargement of boxed area in B. Arrows indicate acetylated microtubules present in GFP-expressing THN progenitors, indicating the presence of axons by 42 hpf. (D–F) Lateral view of the cerebellum of a 40-hpf *Tg(ato1a:Gal4TA4)<sup>hzm2</sup>* transgenic zebrafish embryo injected with Medusa vector M1. (D) A THN progenitor (white asterisk) extends a process, the presumptive axon with a growth cone-like structure (red arrow), while the centrosome (white arrow) starts to translocate toward the soma. (E and F) The axon-like process elongates while the centrosome is moving toward the soma and is still far removed from the site of axonogenesis. These findings suggest that the site of axon formation in THN neurons is independent of a proximally positioned centrosome. Images in D–F are taken from [Video 9](#). MHB, midbrain–hindbrain boundary; URL, upper rhombic lip.

specification (Jacobson et al., 2006; Reed et al., 2006). The Kif5C<sup>560</sup>-YFP axon reporter was expressed under UAS control in *Tg(ato1a:Gal4TA4)<sup>hzm2</sup>* embryos together with the Janus construct J8, demarcating the nucleus by blue and the centrosome by red fluorescence (see Table S1). Therefore, the emergence of THN axons could be visualized in real time relative to the position and movement of the centrosome within the same THN neuron. We purposely chose a coexpression strategy of two different vectors for this experiment, rather than generating a triple-cistron Medusa construct, in order to yield a high degree of mosaicism of transgene expression, allowing for observation of Kif5C<sup>560</sup>-YFP localization in a single cell of a Janus-labeled group or cluster of THN neurons. We confirmed by immunohistochemistry that such single Kif5C<sup>560</sup>-YFP-positive processes coexpressed axon-specific acetylated tubulin (unpublished data).

Time-lapse sequences starting at 36 hpf were recorded from THN neurons that had reached the MHB, but showed a

fluctuating cytoplasmic distribution of Kif5C<sup>560</sup>-YFP (Fig. 10 A, green arrow) and had their centrosomes (Fig. 10 A, red arrows) still positioned in the apical URL, indicating that these THN neurons had not yet initiated axonogenesis. Strikingly, Kif5C<sup>560</sup>-YFP fluorescence soon accumulated in front of the nucleus and close to the MHB (Fig. 10, B and C; green arrow), while the centrosome remained stationary in the URL and far away from the emerging axon (Fig. 10 B, red arrows). Only when axonogenesis was well under way and the outgrowing axon extended ventrally along the MHB did the centrosome begin to detach from the proliferation zone and move toward the nucleus (Fig. 10, D–F; see also [Video 10](#)). This temporal sequence of axonogenesis occurring significantly before centrosome movements toward the cell soma and leading edge demonstrates that in vivo proximity to the centrosome is not relevant for axon determination from the leading process of THN neurons. Interestingly, reorientation of the THN neuron from an apico-basal to a dorso-ventral orientation

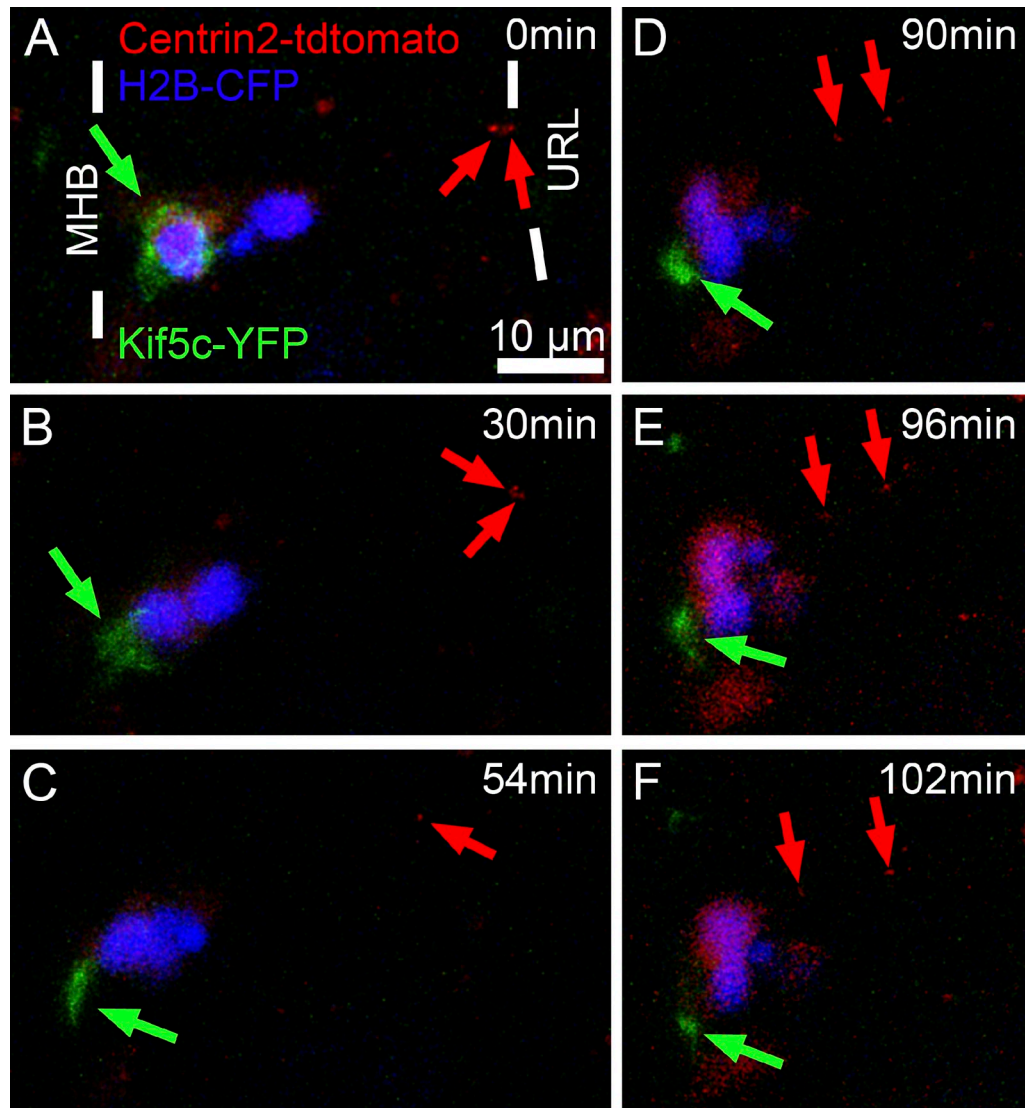


Figure 10. **In vivo imaging of axonogenesis.** Lateral view of the cerebellar anlage of a 36-hpf *Tg(ato1a:Gal4TA4)<sup>hzm2</sup>* transgenic zebrafish embryo coinjected with Janus vector J8 (marking nucleus in blue and centrosome in red, red arrows) and *5xUAS:Kif5c-YFP* (emerging axons labeled with yellow fluorescence, here shown in green). (A) Due to coinjection of two vectors, only the more anteriorly located cell expresses the *Kif5c-YFP* fusion protein. *Kif5c-YFP* is initially distributed throughout the soma of the cell (green arrow), while the centrosomes of both cells are localized at the apical side (red arrows). (B–D) *Kif5c-YFP* localizes to a protrusion, the later axon, in the front of the cell, at the time when the centrosome is homing toward the soma. (E and F) *Kif5c-YFP* localizes to a growth cone-like structure of the emerging axon, while the centrosome has not reached the soma. This temporal sequence of axonogenesis and centrosome dynamics reveals that a proximal position of the centrosome is not required for selecting the site of axon formation in THN neurons in vivo. Images are taken from [Video 10](#). MHB, midbrain-hindbrain boundary; URL, upper rhombic lip.

(compare position of nuclei in Fig. 10, C and F) also preceded the arrival of the centrosome in the cell soma (Fig. 10, C–F). This strongly suggests that repolarization during turning behavior of THN neurons is similarly not mediated by repositioning of the centrosome.

## Discussion

In this study, we have expanded the use of Gal4 combinatorial genetics in zebrafish for cell biological characterization by establishing simultaneous expression of multiple subcellular markers in a cell type-specific manner. Enhancer and gene trap screens have already generated a multitude of zebrafish Gal4 activator strains (Davison et al., 2007; Scott et al., 2007; Asakawa et al., 2008;

Distel et al., 2009) that could be used for cell type-specific cell biological analysis. The presented collection of subcellular fluorescent reporters and their cassette-like assembly in Janus or Medusa vectors will facilitate Gal4-mediated in vivo cell biology in zebrafish, but also in other vertebrates such as chick embryos (Fig. S4). It has to be noted though, that obtaining high contrast for specific subcellular structures sometimes requires the careful adjustment of the expression levels. For example, strong expression levels for centrosome labeling will lead to saturation effects, with excess fluorescent protein accumulating in the cytoplasm. Low expression levels instead will only sparsely label the centrosome, making it too dim for fast image acquisition. The Gal4 system allows one to fine-tune expression levels by either adjusting the number of UAS sites or by selecting a

Gal4 activator with the appropriate transactivation potential (Distel et al., 2009). By this means, optimal labeling results can be achieved.

Medusa labeling showed that once THN neurons have become postmitotic, expressing markers such as PSA-NCAM or acetylated tubulin, and have initiated axonogenesis (Rieger et al., 2008), the apical centrosome-containing process detaches from the germinal URL and moves together with the centrosome toward the MHB-positioned cell somata to initiate neuronal migration. In a common model for tangentially migrating neurons, the centrosome typically moves significantly ahead of the nucleus, establishes an axonal swelling, and organizes the microtubule skeleton. This is followed by the saltatory translocation of the nucleus toward the displaced centrosome (Bellion et al., 2005; Schaar and McConnell, 2005; Métin et al., 2008). Also in zebrafish, tangentially migrating facial branchiomotor neurons display such a leading centrosome, which reorients during migratory turns. Failure to maintain the proper apico-basal positioning of the centrosome is accompanied by migration in ectopic directions, suggesting a role for the centrosome in regulating directional migration (Grant and Moens, 2010). In this respect the ventral migration of THN neurons along the MHB displays an unexpected subcellular orchestration. Only during the preparation for nucleokinesis is the centrosome positioned ahead of the nucleus, being then overtaken during the saltatory forward translocation of the nucleus. For most of the time, the centrosome trailed the nucleus, although it moved at a constant pace even during resting periods of the nucleus. Thereby an iterative cycle of centrosome–nucleus leapfrogging is created.

Interestingly, the role of the centrosome in permanently leading the nucleus of radially migrating neurons has also been called into question recently. In radially migrating cerebellar granule neurons, it was shown that the centrosome is similarly overtaken by the nucleus during nucleokinetic forward movements (Umeshima et al., 2007). In these neurons though, the centrosome advances ahead of the nucleus less regularly than in THN neurons and only during long resting phases. Notably, radial migration occurs along oriented glia fibers, which provide additional cues for the directionality of migration, whereas tangential migration of neurons occurs independently of a guiding glial meshwork. Therefore, tangential THN neuron migration may depend more strongly on a leading centrosome preparing forward migration during each migratory step, whereas radially migrating neurons may not need this consistent directional information from the centrosome. On the other hand, the centrosome in radially migrating cortical neurons does remain strictly ahead of the nucleus (Tsai et al., 2007). Taken together, these findings argue that, like in non-neuronal cells, the exact subcellular orchestration of saltatory nucleokinetic migration is strongly context dependent, varying with the neuronal cell type, local environment, and morphogenetic constraints.

A key role for the centrosome, and in particular its positioning, has been postulated for the induction of axonogenesis in several neuronal populations (Lefcort and Bentley, 1989; Zmuda and Rivas, 1998; Arimura and Kaibuchi, 2007). Findings in cultured hippocampal neurons and cortical neurons *in vivo* have established that the neurite nearest to the centrosome is selected

to become the axon (de Anda et al., 2005, 2010). Subsequent axon extension though, does not require a functional centrosome (Stiess et al., 2010). Our *in vivo* time-lapse studies show that axonogenesis in THN neurons is initiated during the onset of migration and occurs clearly distant from the centrosome. These observations thus differ from hippocampal and cortical neurons, and THN neurons instead behave like retinal ganglion cells in the zebrafish retina, which initiate an axon from the basal process while retraction of the centrosome-containing apical process is still underway (Zolessi et al., 2006). Thus, in retinal ganglion cells and migratory THN neurons, the position of the centrosome does not predict the site of axonogenesis. Our findings argue that the cellular mechanisms of axonogenesis cannot be generalized and are, similar to migration, dependent on the cell type, morphogenetic constraints, and the makeup of the extracellular environment. For example, a strong influence on cerebellar granule neuron axonogenesis and centrosome positioning is exerted by the composition of the ECM and associated signaling molecules (Gupta et al., 2010), which can vary significantly among neuronal tissues. In THN neurons, cellular and molecular events occurring in the leading process itself may predispose the leading process to later axon formation. These events are probably initiated already during the extended interkinetic nuclear movement step of THN progenitors toward the MHB. Thus, the different molecular and cellular dynamics in the apical and leading processes, as well as their temporal orchestration, need to be further characterized *in vivo* in different cell types in order to better understand the course of neuronal development from birth to terminal differentiation. The cell type–specific multicolor labeling of individual neuronal cells, as established here, is a promising step in this direction.

## Materials and methods

### Maintenance of fish

Zebrafish strains were raised and maintained at 27°C in a manufactured fish facility (Aqua Schwarz GmbH, Göttingen, Germany) with circulating and constantly filtered water at 800–1,000 µS salinity (Kimmel et al., 1995; Westerfield, 1995). In the *Tg(shhb:Gal4TA4,5xUAS:mRFP)<sup>hzm4</sup>* strain (TG5xR), the notochord-specific *shhb* (formerly *twhh*) promoter element drives the expression of GalTA4, which in turn activates expression of the red fluorescent protein mRFP under control of five UAS sites and the Elb basal promoter (Babaryka et al., 2009; Distel et al., 2009).

### Construction of vectors

**S14: #801 pCS GFP-DCX.** The ORF encoding GFP-DCX was isolated from the pEGFP-C2DCX vector (a kind gift of Fiona Francis, Institut Cochin, Université Paris Descartes, Paris, France) by Eco47III–Sall digest and cloned into StuI–XhoI-digested pCS2+ (Rupp et al., 1994).

**U15: #699 pSK14xUAS:H2B-mRFP.** The ORF encoding H2B-mRFP was isolated from pCSH2B-mRFP (a kind gift of Sean Megason, Harvard Medical School, Boston, MA) by Asp718 (Klenow blunted)–NsiI digest and cloned behind the E1b promoter of the XhoI (Klenow blunted)–NsiI-digested pSK14xUASE1b vector (Köster and Fraser, 2001b).

**U16: #709 pSKH2B-mRFP:5xUASE1b.** The E1b minimal promoter and the ORF encoding H2B-mRFP were isolated from U15 by XbaI–NotI (Klenow blunted) digest and inserted into the SmaI site of the pSK5xUASE1b vector (Distel et al., 2009).

**J1: #828 pSK-H2B-RFP:5xUAS:GFP-DCX.** The ORF encoding GFP-DCX was isolated from S14 by ClaI–Asp718 digest and cloned into ClaI–Asp718-digested U16.

**U17: #627 pSK14xUAS:H2B-GFP.** H2B-GFP was isolated from pCSH2B-GFP Sall (Klenow blunted)–ApaI digest and cloned behind the E1b promoter



of the XhoI (Klenow blunted)–ApaI-digested pSK14xUASE1b vector (Köster and Fraser, 2001b).

**U18: #665 pSKH2B-GFP:5xUASE1b.** The E1b minimal promoter and the ORF encoding H2B-GFP were isolated from U17 by XbaI–NotI (Klenow blunted) digest and inserted into the SmaI site of the pSK5xUASE1b vector (Distel et al., 2009).

**J11: #700 pSKH2B-GFP:5xUAS:memmRFP.** The ORF encoding memmRFP was isolated from pCSmemmRFP (a kind gift of Sean Megason) by XhoI (Klenow blunted)–ApaI digest and inserted into EcoRV–ApaI-digested U18. “mem” represents a membrane localization signal, which consists of a palmitoylation and myristinylation sequence of the human Lck kinase.

**U2: #860 memmRFP:5xUAS.** The E1b minimal promoter and the ORF encoding memmRFP were isolated from J11 by XbaI–NotI (Klenow blunted) digest and inserted into the SmaI site of the pSK5xUASE1b vector (Distel et al., 2009). “mem” represents a membrane localization signal, which consists of a palmitoylation and myristinylation sequence of the human Lck kinase.

**#878 pH2B-CFP.** The ORF encoding H2B was isolated from pCSH2B-mRFP (a kind gift of Sean Megason) by XhoI–AgeI digest and inserted into XhoI–AgeI-digested pECFP-C1 (Takara Bio Inc.).

**S5: #895 pCSH2B-CFP.** The ORF encoding H2B-CFP was isolated from pH2B-CFP by NotI (Klenow blunted)–XhoI digest and cloned into XbaI (Klenow blunted)–XhoI-digested pCS2+.

**J2: #939 pSKmemmRFP:5xUAS:H2B-CFP.** The ORF encoding H2B-CFP was isolated from S5 by XhoI–NotI (Klenow blunted) digest and inserted into Asp718-digested (Klenow blunted) U2.

**#766 pCRIICentrin2.** The ORF of zebrafish *centrin2* (acc. nr.: EU183505) was cloned by RT-PCR to generate C-terminal fusions using total RNA from adult brain and the following primers: HindIII *centrin2*-up: 5'-TTAAGCTTATGGCGTCCGGCTTCAGGAA-3'; *centrin2*-low BamHI: 5'-TAGGATCCCCGTACAGATTGGTTTCTTCA-3'. The fragment was subcloned into the pCRII-Topo vector (Invitrogen) and sequenced.

**#767 pCRIICentrin2STOP.** The ORF of zebrafish *centrin2* (acc. nr.: EU183505) was amplified by RT-PCR to generate N-terminal fusions using total RNA from adult brain and the following primers: BamHI *centrin2*-up: 5'-TTGGATCCATGGCGTCCGGCTTCAGGAA-3'; *centrin2*-low XbaI: 5'-TTTC-TAGATCAGTACAGATTGGTTTCTTCA-3'. The fragment was subcloned into the pCRII-Topo vector (Invitrogen) and sequenced.

**#769 pCentrin2-YFP.** The ORF encoding Centrin2 was isolated by BamHI–HindIII digest from pCRII-Centrin2 and cloned into BamHI–HindIII-digested pEYFP-N1 (Takara Bio Inc.).

**S3: #783 pEGFP-Centrin2.** The ORF encoding Centrin2 was isolated by BamHI–EcoRI digest from pCRII-Centrin2Stop and cloned into BglII–EcoRI-digested pEGFP-C1 (Takara Bio Inc.).

**S2: #848 pCSCentrin2-YFP.** The ORF encoding Centrin2-YFP was isolated from pCentrin2-YFP by NotI (Klenow blunted)–XhoI digest and inserted into SmaI–XhoI-digested pCS2+.

**U5: #996 pSK5xUAS:Centrin2-YFP.** The ORF encoding Centrin2-YFP was isolated from pCSCentrin2-YFP by EcoRI–ApaI digest and inserted into EcoRI–ApaI-digested pSK5xUAS (Distel et al., 2009).

**M1: #1595 pSKmemmRFP:5xUAS:H2B-CFP:5xUAS:Centrin2-YFP.** The 5xUAS:Centrin2-YFP cassette was isolated from U5 by SpeI–Asp718 digest (Klenow blunted) and inserted into SpeI-digested (Klenow blunted) J2.

**S6: #938 pCSmemmRFP.** mRFP of pCSmemmRFP (a kind gift of Sean Megason) was removed by SmaI–AgeI digest and replaced with CFP from NotI (Klenow blunted)–AgeI-digested pECFP-1 (Takara Bio Inc.). “mem” represents a membrane localization signal, which consists of a palmitoylation and myristinylation sequence of the human Lck kinase.

**U6: #997 pSK5xUAS:memCFP.** The ORF encoding memCFP was isolated from S6 by ClaI–ApaI digest and inserted into ClaI–ApaI-digested pSK5xUAS.

**M2: #998 pSKH2B-mRFP:5xUAS:GFP-DCX-5xUAS:memCFP.** The 5xUAS:memCFP cassette was isolated from U6 by NotI (Klenow blunted) and inserted into Asp718-digested (Klenow blunted) J1.

**S10: #771 pCSEB3-GFP.** The ORF encoding EB3-GFP was isolated from pEB3-GFP (a kind gift of Anna Akhmanova, Erasmus Medical Center, Rotterdam, Netherlands) by NotI (Klenow blunted)–SalI digest and inserted into XbaI (Klenow blunted)–XhoI-digested pCS2+.

**J4: #780 pSKH2B-mRFP:5xUAS:EB3-GFP.** The ORF encoding EB3-GFP was isolated from S10 by StuI–Asp718 digest and inserted into EcoRV–Asp718-digested U16.

**M3: #999 pSKH2B-mRFP:5xUAS:EB3-GFP-5xUAS:memCFP.** The 5xUAS:memCFP cassette was isolated from U6 by NotI (Klenow blunted) and inserted into Asp718-digested (Klenow blunted) J4.

**#868 pCStdTomato.** The ORF encoding tdTomato was isolated from pRSETtdTomato (a kind gift of Roger Tsien, University of California, San Diego, La Jolla, CA) by BamHI–EcoRI digest and inserted into BamHI–EcoRI-digested pCS2+.

**S1: #879 pCSCentrin2-tdtomato.** The ORF encoding Centrin2 was isolated from pCRII-Centrin2 by BamHI–HindIII digest and inserted into BamHI–HindIII-digested pCStdTomato.

**#1532 pSKE1B5xUASE1b.** The E1b5xUASE1b cassette was isolated from U2 by EcoRI digest and inserted into EcoRI-digested pBSK.

**U9: #2022 pSKH2B-CFP:5xUASE1b.** The ORF encoding H2B-CFP was isolated from pCSH2B-CFP by Asp718 digest and inserted into SmaI-digested pSKE1b5xUASE1b.

**J8: #2146 pSKH2B-CFP:5xUAS:Centrin2-tdTomato.** The ORF encoding Centrin2-tdTomato was isolated from S1 by HindIII–Asp718 digest and inserted into HindIII–Asp718-digested U9.

**pSC-BKif5c-YFP.** Kif5c-YFP was PCR amplified from Kif5c-YFP (a kind gift of Gary Banker, Oregon Health and Science University, Portland, OR) and a kozak sequence was added using primers Kif5cEcoHinfKoz: 5'-AAAGAATCAAGCTTCCACCATGGCAGATCCAGCCGAATGCAG-CATC-3'; and Venus4: 5'-TACTCGAGTACTGTGACAGCTCGTCCAT-3' and subcloned into pSC-B (Agilent Technologies).

**S20: #2328pCSKif5c-YFP.** The ORF encoding Kif5c-YFP was isolated from pSC-BKif5c-YFP by EcoRI (Klenow blunted)–HindIII digest and inserted into HindIII–SnaBI-digested pCS2+.

**U14: #2329 pSK5xUAS:Kif5c-YFP.** The ORF encoding Kif5c-YFP was isolated from pCSKif5c-YFP by HindIII–Asp718 digest and inserted into HindIII–Asp718-digested pSK5xUAS

Further cloning strategies are available upon request.

#### Generation of *atoh1a:KalTA4G1* transgenic zebrafish

To express transgenes in rhombic lip–derived cells, KalTA4 was placed between up- and downstream regulatory elements of zebrafish *atoh1a*. A 2950-bp fragment upstream of *atoh1a* was amplified from a BAC (RZPD, CH211-247L22) using primers #394: 5'-GCGGTCGACAAATGGGACTGTATGGATGTTTCCC-3' and #396: 5'-TGCGGATCCTCTGTTGGTTGTGCTTTTGGGAG-3'. Likewise, a 5900-bp fragment downstream of *atoh1a* was amplified by using primers #395: 5'-ATAGCGGCGCTTCTCGCCTCACTCGCACTTCA-3' and #397: 5'-GCGCCGCGGAGCTTTGGGTTTGGTTAGTTCGTAAGACTG-3' for 1–3250 bp and #398: 5'-GACGGAGACCGCAGGTTTATTCTCACAGAAG-3' and #399: 5'-ATACCGCGGGTATCTTGTTACATTGATATGC-3' for 3250–5900 bp and joining these fragments after subcloning by SacI digest. KalTA4G1pA (Distel et al., 2009) was inserted between the 5' and 3' fragments. This construct was flanked with I-SceI recognition sites and injected into one-cell stage zebrafish embryos together with mRNA coding for I-SceI at the one-cell stage (Babaryka et al., 2009). Injected zebrafish embryos were raised to adulthood and tested for successful integration by mating to *Tg(shhb:Gal4TA4,5xUAS:mRFP)<sup>hzm4</sup>* or *Tg(4xUAS:GFP)<sup>hzm3</sup>* transgenic fish (Babaryka et al., 2009; Distel et al., 2009). *Tg(atoh1a:Gal4TA4)<sup>hzm2</sup>* carriers showing fluorescence expression in the rhombic lip were maintained up to the F4 generation.

#### Microinjection

Zebrafish embryos were injected with expression plasmids (25 ng/μl each, 1.5 nL) at the one-cell stage. Raised embryos were screened for expression right before microscopy analysis.

#### Microscopy

For image recording, embryos were dechorionated and embedded in 1.2% ultra low melting agarose/30% Danieau (Distel and Köster, 2007). Images of living embryos and of transfected cells were recorded using a confocal microscope (LSM 510; Carl Zeiss, Inc.) and LSM software (Carl Zeiss, Inc.). Images of *in situ* hybridizations were recorded using an Axioplan2 microscope equipped with an AxioCam HRc and Axiovision 4.5 software (all from Carl Zeiss, Inc.). Images in Fig. 1 and Fig. 2 B (M2, M3) were recorded using a 63x Plan-Apochromat oil immersion objective (NA 1.4); in Fig. 2, A and B (M1), Fig. 3, D–F, Figs. 5, 6, 7, 9, and 10 using a 40x C-Apochromat water immersion objective (NA 1.2); and in Fig. 3, A–C and Fig. 4 A using a 20x EC Plan-Neofluar objective (NA 0.5). Images in Figs. 4–7, Fig. 9, D–F, and Fig. 10 represent maximum intensity projections taken from respective videos of time-lapse analysis.

#### Quantification of subcellular dynamics

**Migration angle analysis.** In a lateral view of the cerebellum, the apico-basal axis was determined by drawing a horizontal line from the URL to the MHB, perpendicular to the MHB. The nuclear centroids of THN progenitors

were tracked using the Manual Tracking tool of ImageJ software (NIH, Bethesda, MD). The angle between the migration path of the respective cell and the apico-basal axis of the cerebellum was determined in THN progenitors undergoing INM and neurons initiating ventral migration using Adobe Photoshop CS3.

**Centrosome and nuclear centroid tracking.** Centrosome and nuclear centroid tracking over time and measurements of migration distances and migration velocities of the respective organelles were performed on maximum projections of the respective z-stacks using the Manual Tracking tool of ImageJ software.

**Generation of kymographs.** The kymographs in Fig. 8, A and B were generated manually using Adobe Photoshop CS4. 2D maximum projections shown in Videos 6 and 8 were rotated 45 degrees counterclockwise and regions containing the nuclei (Video 6, Fig. 8 A) or containing the nucleus and the centrosome (Video 8, Fig. 8 B) were extracted for each time point. Cropped regions were assembled in one image starting with the earliest time point on the left.

**Determination of the position of the centrosome with respect to the nuclear centroid and migration direction.** A 0.4- $\mu\text{m}$ -thick line was drawn through the nuclear centroid and orthogonal to the direction of cell migration, dividing the cell into two halves. The position of the centrosome was then scored manually to be either in the anterior half (anterior to the nuclear centroid), in the posterior half (posterior to the nuclear centroid), or on the line (scored as lateral to the nuclear centroid). Cells were analyzed during ventral migration, starting at the time point when the centrosome had reached the soma of the cell and ending when the cell no longer showed apparent migration. The pie chart in Fig. 8 was generated in Microsoft Excel.

**Determination of directions of centrosomal and nuclear movements.** To determine the direction of centrosomal and nuclear movements during ventral migration, images were rotated where necessary so that cells migrated approximately along the y axis. Afterward, the y position of the respective cell organelle was determined using ImageJ (Measure tool or Manual Tracking plug-in). Subsequent y positions were subtracted (and corrected for tissue growth if necessary) to yield the net movement. Movements less than 0.5  $\mu\text{m}$  were scored as stationary. Greater movements were scored as in the direction of migration (forward) or as opposite to the direction of migration (backward). The 3D bar graph of the respective movement combinations was generated in Microsoft Excel.

### Transfection

Zebrafish Pac2 fibroblasts were maintained in Leibovitz L15 medium supplemented with 1x L-glutamine (Invitrogen) and 10% fetal bovine serum. Pac2 cells were transfected using the Effectene transfection kit (QIAGEN) or the Nanofectin transfection kit (PAA; Senghaas and Köster, 2009).

### Immunohistochemistry

GFP-expressing offspring of *Tg(ato1a:Gal4TA4)<sup>hzm2</sup>* and *Tg(4xUAS:GFP)<sup>hzm3</sup>* transgenic carriers (Distel et al., 2009) were fixed in 4% PFA at 36 and 42 hpf for 12 h and transferred into 100% MeOH. Embryos were then transferred to acetone ( $-20^{\circ}\text{C}$ ), incubated at  $-20^{\circ}\text{C}$  for 7 min, and then incubated in  $\text{H}_2\text{O}$  at room temperature for 1 h. Subsequently, embryos were washed with PBS/0.1% Tween (PTW) twice for 5 min each, after which embryos were incubated in 10 mM sodium citrate, pH 6.0/0.1% Tween for 15 min at  $100^{\circ}\text{C}$  for antigen retrieval. Subsequently, embryos were washed twice in PTW for 5 min each and blocked in 10% goat serum in PTW for 1 h at room temperature. Embryos were incubated with the primary antibodies chicken anti-GFP (1:500; Aves, catalog no. 1020) and mouse anti-acetylated tubulin (1:500; Sigma-Aldrich, catalog no. T6793) at  $4^{\circ}\text{C}$  overnight. After several washes in PTW, embryos were incubated with the secondary antibodies anti-mouse Alexa546 (1:100; Invitrogen) and anti-chicken FITC (1:100; Jackson ImmunoResearch Laboratories, Inc., catalog no. 703 095 155) overnight at  $4^{\circ}\text{C}$ . Nuclei were stained using DAPI (1  $\mu\text{g}/\mu\text{l}$ ; Roche, catalog no. 10236276001).

### Online supplemental material

Online supplemental material is provided with this manuscript, including a table of expression constructs and their identifier numbers, which should be used for construct ordering. In addition, figures showing expression from a Janus construct using a single UAS-site (Fig. S1), anti-PH3 immunohistochemistry for detecting proliferating cells in the developing cerebellum (Fig. S2), a quantification of the ventral turning angle of migrating THN neurons (Fig. S3), and triple-cistronic Medusa vector expression in the developing chick tegmentum (Fig. S4) are provided. Finally, the supplemental material contains all of the videos and their respective legends referred to in this manuscript. Video 1 visualizes MT dynamics in a zebrafish keratinocyte, Videos 2 and 3

visualize MT dynamics in cells of a gastrulating zebrafish embryo, Video 4 shows a time-lapse recording of THN neuron migration, Video 5 shows nucleus and centrosome dynamics during interkinetic nuclear movements of THN progenitors, Videos 6 and 7 show trailing process retraction and centrosome dynamics in THN neurons preparing to migrate ventrally, Video 8 shows centrosome dynamics in a ventrally migrating THN neuron, Video 9 shows a time-lapse recording of an emerging axon of a THN neuron, and Video 10 shows the localization of the axon specific marker Kif5c-YFP and the centrosome during THN axonogenesis.

We are grateful for excellent fish husbandry and technical assistance by Petra Hammerl, Enrico Kühn, and Christiane Lach. We thank Karsten Boldt for help with Western blot quantification and Damian Refajo for carefully reading and commenting on the manuscript. We thank Fiona Francis, Alexander Reugels, Jürgen Wehland, Anna Akhmanova, Sean Megason, Timm Schroeder, and Roger Tsien for generously providing us with different expression vectors.

M. Distel, J.C. Hocking, K. Volkman, and R.W. Köster designed the experiments and performed the data analysis; M. Distel, J.C. Hocking, and K. Volkman performed the experiments; M. Distel, J.C. Hocking, and R.W. Köster wrote the manuscript.

This work was generously supported by a BioFuture Award Grant of the German Ministry of Education and Research (BMBF 03 1 1889), the German Research Association (DFG, KO1949/3-1), a Fellowship of the Studienstiftung des deutschen Volkes (M. Distel), and a postdoctoral fellowship from the Natural Sciences and Engineering Research Council (NSERC) of Canada (J.C. Hocking).

Submitted: 29 April 2010

Accepted: 14 October 2010

## References

- Arimura, N., and K. Kaibuchi. 2007. Neuronal polarity: from extracellular signals to intracellular mechanisms. *Nat. Rev. Neurosci.* 8:194–205. doi:10.1038/nrn2056
- Asakawa, K., M.L. Suster, K. Mizusawa, S. Nagayoshi, T. Kotani, A. Urasaki, Y. Kishimoto, M. Hibi, and K. Kawakami. 2008. Genetic dissection of neural circuits by Tol2 transposon-mediated Gal4 gene and enhancer trapping in zebrafish. *Proc. Natl. Acad. Sci. USA.* 105:1255–1260. doi:10.1073/pnas.0704963105
- Babaryka, A., E. Kühn, and R.W. Köster. 2009. In vivo synthesis of meganuclease for generating transgenic zebrafish *Danio rerio*. *J. Fish Biol.* 74:452–457. doi:10.1111/j.1095-8649.2008.02075.x
- Basto, R., J. Lau, T. Vinogradova, A. Gardiol, C.G. Woods, A. Khodjakov, and J.W. Raff. 2006. Flies without centrioles. *Cell.* 125:1375–1386. doi:10.1016/j.cell.2006.05.025
- Bellion, A., J.P. Baudoin, C. Alvarez, M. Bornens, and C. Métin. 2005. Nucleokinesis in tangentially migrating neurons comprises two alternating phases: forward migration of the Golgi/centrosome associated with centrosome splitting and myosin contraction at the rear. *J. Neurosci.* 25:5691–5699. doi:10.1523/JNEUROSCI.1030-05.2005
- Chenn, A., Y.A. Zhang, B.T. Chang, and S.K. McConnell. 1998. Intrinsic polarity of mammalian neuroepithelial cells. *Mol. Cell. Neurosci.* 11:183–193. doi:10.1006/mcne.1998.0680
- Coan, D.E., A.R. Wechezak, R.F. Viggers, and L.R. Sauvage. 1993. Effect of shear stress upon localization of the Golgi apparatus and microtubule organizing center in isolated cultured endothelial cells. *J. Cell Sci.* 104:1145–1153.
- Conde, C., and A. Cáceres. 2009. Microtubule assembly, organization and dynamics in axons and dendrites. *Nat. Rev. Neurosci.* 10:319–332. doi:10.1038/nrn2631
- Davison, J.M., C.M. Akitake, M.G. Goll, J.M. Rhee, N. Gosse, H. Baier, M.E. Halpern, S.D. Leach, and M.J. Parsons. 2007. Transactivation from Gal4-VP16 transgenic insertions for tissue-specific cell labeling and ablation in zebrafish. *Dev. Biol.* 304:811–824. doi:10.1016/j.ydbio.2007.01.033
- de Anda, F.C., G. Pollarolo, J.S. Da Silva, P.G. Camoletto, F. Feiguin, and C.G. Dotti. 2005. Centrosome localization determines neuronal polarity. *Nature.* 436:704–708. doi:10.1038/nature03811
- de Anda, F.C., K. Meletis, X. Ge, D. Rei, and L.-H. Tsai. 2010. Centrosome motility is essential for initial axon formation in the neocortex. *J. Neurosci.* 30:10391–10406. doi:10.1523/JNEUROSCI.0381-10.2010
- Distel, M., and R.W. Köster. 2007. In vivo time-lapse imaging of zebrafish embryonic development. *Cold Spring Harbor Protocols.* doi:10.1101/pdb.prot4816
- Distel, M., M.F. Wullmann, and R.W. Köster. 2009. Optimized Gal4 genetics for permanent gene expression mapping in zebrafish. *Proc. Natl. Acad. Sci. USA.* 106:13365–13370. doi:10.1073/pnas.0903060106

- Gotlieb, A.I., L.M. May, L. Subrahmanyam, and V.I. Kalnins. 1981. Distribution of microtubule organizing centers in migrating sheets of endothelial cells. *J. Cell Biol.* 91:589–594. doi:10.1083/jcb.91.2.589
- Grant, P.K., and C.B. Moens. 2010. The neuroepithelial basement membrane serves as a boundary and a substrate for neuron migration in the zebrafish hindbrain. *Neural Dev.* 5:9. doi:10.1186/1749-8104-5-9
- Gupta, S.K., K.F. Meiri, K. Mahfooz, U. Bharti, and S. Mani. 2010. Coordination between extrinsic extracellular matrix cues and intrinsic responses to orient the centrosome in polarizing cerebellar granule neurons. *J. Neurosci.* 30:2755–2766. doi:10.1523/JNEUROSCI.4218-09.2010
- Hammond, J.W., D. Cai, and K.J. Verhey. 2008. Tubulin modifications and their cellular functions. *Curr. Opin. Cell Biol.* 20:71–76. doi:10.1016/j.ccb.2007.11.010
- Higginbotham, H.R., and J.G. Gleeson. 2007. The centrosome in neuronal development. *Trends Neurosci.* 30:276–283. doi:10.1016/j.tins.2007.04.001
- Hinds, J.W., and T.L. Ruffet. 1971. Cell proliferation in the neural tube: an electron microscopic and Golgi analysis in the mouse cerebral vesicle. *Zeitschrift für Zellforschung.* 115:226–264. doi:10.1007/BF00391127
- Jacobson, C., B. Schnapp, and G.A. Banker. 2006. A change in the selective translocation of the Kinesin-1 motor domain marks the initial specification of the axon. *Neuron.* 49:797–804. doi:10.1016/j.neuron.2006.02.005
- Kimmel, C.B., W.W. Ballard, S.R. Kimmel, B. Ullmann, and T.F. Schilling. 1995. Stages of embryonic development of the zebrafish. *Dev. Dyn.* 203:253–310.
- Köster, R.W., and S.E. Fraser. 2001a. Direct imaging of in vivo neuronal migration in the developing cerebellum. *Curr. Biol.* 11:1858–1863. doi:10.1016/S0960-9822(01)00585-1
- Köster, R.W., and S.E. Fraser. 2001b. Tracing transgene expression in living zebrafish embryos. *Dev. Biol.* 233:329–346. doi:10.1006/dbio.2001.0242
- Kupfer, A., D. Louvard, and S.J. Singer. 1982. Polarization of the Golgi apparatus and the microtubule-organizing center in cultured fibroblasts at the edge of an experimental wound. *Proc. Natl. Acad. Sci. USA.* 79:2603–2607. doi:10.1073/pnas.79.8.2603
- Lee, J.S., M.I. Chang, Y. Tseng, and D. Wirtz. 2005. Cdc42 mediates nucleus movement and MTOC polarization in Swiss 3T3 fibroblasts under mechanical shear stress. *Mol. Biol. Cell.* 16:871–880. doi:10.1091/mbc.E03-12-0910
- Lefcort, F., and D. Bentley. 1989. Organization of cytoskeletal elements and organelles preceding growth cone emergence from an identified neuron in situ. *J. Cell Biol.* 108:1737–1749. doi:10.1083/jcb.108.5.1737
- Marín, O., M. Valdeolillos, and F. Moya. 2006. Neurons in motion: same principles for different shapes? *Trends Neurosci.* 29:655–661. doi:10.1016/j.tins.2006.10.001
- Métin, C., J.P. Baudoin, S. Rakić, and J.G. Parnavelas. 2006. Cell and molecular mechanisms involved in the migration of cortical interneurons. *Eur. J. Neurosci.* 23:894–900. doi:10.1111/j.1460-9568.2006.04630.x
- Métin, C., R.B. Vallee, P. Rakic, and P.G. Bhide. 2008. Modes and mishaps of neuronal migration in the mammalian brain. *J. Neurosci.* 28:11746–11752. doi:10.1523/JNEUROSCI.3860-08.2008
- Nemere, I., A. Kupfer, and S.J. Singer. 1985. Reorientation of the Golgi apparatus and the microtubule-organizing center inside macrophages subjected to a chemotactic gradient. *Cell Motil.* 5:17–29. doi:10.1002/cm.970050103
- Paquet, D., R. Bhat, A. Sydow, E.M. Mandelkow, S. Berg, S. Hellberg, J. Fäلتing, M. Distel, R.W. Köster, B. Schmid, and C. Haass. 2009. A zebrafish model of tauopathy allows in vivo imaging of neuronal cell death and drug evaluation. *J. Clin. Invest.* 119:1382–1395. doi:10.1172/JCI37537
- Pouthas, F., P. Girard, V. Lecaudey, T.B. Ly, D. Gilmour, C. Boulin, R. Pepperkok, and E.G. Reynaud. 2008. In migrating cells, the Golgi complex and the position of the centrosome depend on geometrical constraints of the substratum. *J. Cell Sci.* 121:2406–2414. doi:10.1242/jcs.026849
- Pu, J., and M. Zhao. 2005. Golgi polarization in a strong electric field. *J. Cell Sci.* 118:1117–1128. doi:10.1242/jcs.01646
- Reed, N.A., D. Cai, T.L. Blasius, G.T. Jih, E. Meyhofer, J. Gaertig, and K.J. Verhey. 2006. Microtubule acetylation promotes kinesin-1 binding and transport. *Curr. Biol.* 16:2166–2172. doi:10.1016/j.cub.2006.09.014
- Renaud, J., G. Kerjan, I. Sumita, Y. Zagar, V. Georget, D. Kim, C. Fouquet, K. Suda, M. Sanbo, F. Suto, et al. 2008. Plexin-A2 and its ligand, Sema6A, control nucleus-centrosome coupling in migrating granule cells. *Nat. Neurosci.* 11:440–449. doi:10.1038/nn2064
- Rieger, S., K. Volkmann, and R.W. Köster. 2008. Polysialyltransferase expression is linked to neuronal migration in the developing and adult zebrafish. *Dev. Dyn.* 237:276–285. doi:10.1002/dvdy.21410
- Rupp, R.A.W., L. Snider, and H. Weintraub. 1994. *Xenopus* embryos regulate the nuclear localization of XMyoD. *Genes Dev.* 8:1311–1323. doi:10.1101/gad.8.11.1311
- Schaar, B.T., and S.K. McConnell. 2005. Cytoskeletal coordination during neuronal migration. *Proc. Natl. Acad. Sci. USA.* 102:13652–13657. doi:10.1073/pnas.0506008102
- Schliwa, M., U. Euteneuer, R. Gräf, and M. Ueda. 1999. Centrosomes, microtubules and cell migration. *Biochem. Soc. Symp.* 65:223–231.
- Schütze, K., A. Maniotis, and M. Schliwa. 1991. The position of the microtubule-organizing center in directionally migrating fibroblasts depends on the nature of the substratum. *Proc. Natl. Acad. Sci. USA.* 88:8367–8371. doi:10.1073/pnas.88.19.8367
- Scott, E.K., L. Mason, A.B. Arrenberg, L. Ziv, N.J. Gosse, T. Xiao, N.C. Chi, K. Asakawa, K. Kawakami, and H. Baier. 2007. Targeting neural circuitry in zebrafish using GAL4 enhancer trapping. *Nat. Methods.* 4:323–326.
- Senghaas, N., and R.W. Köster. 2009. Culturing and transfecting Pac2 zebrafish fibroblast cells. *Cold Spring Harbor Protocols.* doi:10.1101/pdb.prot5235
- Shoukimas, G.M., and J.W. Hinds. 1978. The development of the cerebral cortex in the embryonic mouse: an electron microscopic serial section analysis. *J. Comp. Neurol.* 179:795–830. doi:10.1002/cne.901790407
- Solecki, D.J., L. Model, J. Gaetz, T.M. Kapoor, and M.E. Hatten. 2004. Par6alpha signaling controls glial-guided neuronal migration. *Nat. Neurosci.* 7:1195–1203. doi:10.1038/nn1332
- Stiess, M., N. Maghelli, L.C. Kapitein, S. Gomis-Rüth, M. Wilsch-Bräuninger, C.C. Hoogenraad, I.M. Tolić-Nørrelykke, and F. Bradke. 2010. Axon extension occurs independently of centrosomal microtubule nucleation. *Science.* 327:704–707. doi:10.1126/science.1182179
- Tanaka, T., F.F. Serneo, C. Higgins, M.J. Gambello, A. Wynshaw-Boris, and J.G. Gleeson. 2004. Lis1 and doublecortin function with dynein to mediate coupling of the nucleus to the centrosome in neuronal migration. *J. Cell Biol.* 165:709–721. doi:10.1083/jcb.200309025
- Tsai, L.H., and J.G. Gleeson. 2005. Nucleokinesis in neuronal migration. *Neuron.* 46:383–388. doi:10.1016/j.neuron.2005.04.013
- Tsai, J.W., K.H. Bremner, and R.B. Vallee. 2007. Dual subcellular roles for LIS1 and dynein in radial neuronal migration in live brain tissue. *Nat. Neurosci.* 10:970–979. doi:10.1038/nn1934
- Umeshima, H., T. Hirano, and M. Kengaku. 2007. Microtubule-based nuclear movement occurs independently of centrosome positioning in migrating neurons. *Proc. Natl. Acad. Sci. USA.* 104:16182–16187. doi:10.1073/pnas.0708047104
- Vallee, R.B., G.E. Seale, and J.W. Tsai. 2009. Emerging roles for myosin II and cytoplasmic dynein in migrating neurons and growth cones. *Trends Cell Biol.* 19:347–355. doi:10.1016/j.tcb.2009.03.009
- Volkmann, K., Y.-Y. Chen, M.P. Harris, M.F. Wullimann, and R.W. Köster. 2010. The zebrafish cerebellar upper rhombic lip generates tegmental hindbrain nuclei by long-distance migration in an evolutionary conserved manner. *J. Comp. Neurol.* 518:2794–2817.
- Westerfield, M. 1995. *The Zebrafish Book*. University of Oregon Press, Eugene, OR. 385 pp.
- Witte, H., and F. Bradke. 2008. The role of the cytoskeleton during neuronal polarization. *Curr. Opin. Neurobiol.* 18:479–487. doi:10.1016/j.conb.2008.09.019
- Xie, Z., L.Y. Moy, K. Sanada, Y. Zhou, J.J. Buchman, and L.H. Tsai. 2007. Cep120 and TACCs control interkinetic nuclear migration and the neural progenitor pool. *Neuron.* 56:79–93. doi:10.1016/j.neuron.2007.08.026
- Yvon, A.-M.C., J.W. Walker, B. Danowski, C. Fagerstrom, A. Khodjakov, and P. Wadsworth. 2002. Centrosome reorientation in wound-edge cells is cell type specific. *Mol. Biol. Cell.* 13:1871–1880. doi:10.1091/mbc.01-11-0539
- Zhao, M., B. Song, J. Pu, T. Wada, B. Reid, G. Tai, F. Wang, A. Guo, P. Walczysko, Y. Gu, et al. 2006. Electrical signals control wound healing through phosphatidylinositol-3-OH kinase-gamma and PTEN. *Nature.* 442:457–460. doi:10.1038/nature04925
- Zmuda, J.F., and R.J. Rivas. 1998. The Golgi apparatus and the centrosome are localized to the sites of newly emerging axons in cerebellar granule neurons in vitro. *Cell Motil. Cytoskeleton.* 41:18–38. doi:10.1002/(SICI)1097-0169(1998)41:1<18::AID-CM2>3.0.CO;2-B
- Zolessi, F.R., L. Poggi, C.J. Wilkinson, C.B. Chien, and W.A. Harris. 2006. Polarization and orientation of retinal ganglion cells in vivo. *Neural Dev.* 1:2. doi:10.1186/1749-8104-1-2

## **Appendix 4**

Article in **Developmental Biology**

### **The zebrafish cerebellar rhombic lip is spatially patterned in producing granule cell populations of different functional compartments**

Katrin Volkmann, Sandra Rieger, Andreas Babaryka, Reinhard W. Köster

Developmental Biology 313: 167–180 (2008)

#### **Contribution**

For this study I conducted most of the experiments, recorded the images and analyzed the data with the exception of Figure 2A-B`, Figure 3A, Figure 4A-I, Figure 5A-C, Figure 6C-K and Movie 1). I collected data from published articles, discussed our data and the literature with my co-authors and contributed to the writing process of the manuscript. I wrote the methods part and reviewed the manuscript together with my co-authors.

# The zebrafish cerebellar rhombic lip is spatially patterned in producing granule cell populations of different functional compartments

Katrin Volkmann, Sandra Rieger, Andreas Babaryka, Reinhard W. Köster\*

*GSF—National Research Center for Environment and Health, Institute of Developmental Genetics,  
Ingolstädter Landstrasse 1, 85764 Neuherberg-Munich, Germany*

Received for publication 24 April 2007; revised 18 September 2007; accepted 15 October 2007  
Available online 24 October 2007

## Abstract

The upper rhombic lip, a prominent germinal zone of the cerebellum, was recently demonstrated to generate different neuronal cell types over time from spatial subdomains. We have characterized the differentiation of the upper rhombic lip derived granule cell population in stable GFP-transgenic zebrafish in the context of zebrafish cerebellar morphogenesis. Time-lapse analysis followed by individual granule cell tracing demonstrates that the zebrafish upper rhombic lip is spatially patterned along its mediolateral axis producing different granule cell populations simultaneously. Time-lapse recordings of parallel fiber projections and retrograde labeling reveal that spatial patterning within the rhombic lip corresponds to granule cells of two different functional compartments of the mature cerebellum: the eminentia granularis and the corpus cerebelli. These cerebellar compartments in teleosts correspond to the mammalian vestibulocerebellar and non-vestibulocerebellar system serving balance and locomotion control, respectively. Given the high conservation of cerebellar development in vertebrates, spatial partitioning of the mammalian granule cell population and their corresponding earlier-produced deep nuclei by patterning within the rhombic lip may also delineate distinct functional compartments of the cerebellum. Thus, our findings offer an explanation for how specific functional cerebellar circuitries are laid down by spatio-temporal patterning of cerebellar germinal zones during early brain development.

© 2007 Elsevier Inc. All rights reserved.

*Keywords:* Zebrafish; Cerebellum; Granule cell; Neuronal migration; Bioimaging; Cell tracing; Fate mapping

## Introduction

Many developmental, histological and functional properties of the cerebellum are highly conserved among vertebrates ranging from teleost fish to mammals. This evolutionary conservation includes the position and patterning of the cerebellum under control of the organizer activity of cells at the midbrain–hindbrain boundary (MHB) (Voogd and Glickstein, 1998; Middleton and Strick, 1998; Martinez et al., 1999; Wurst and Bally-Cuif, 2001; Wang and Zoghbi, 2001), its laminar organization comprised by few neuronal cell types of distinct morphology (Nieuwenhuys, 1967; Lannoo et al., 1991; Altman and Bayer, 1997), the characteristic cerebellar feedback circuitry (Wullimann and Northcutt, 1988; Wullimann, 1998; Bengtsson and Hesslow, 2006; Ito, 2006) and, lastly, the role of

the cerebellum in coordinating locomotion and contributing to motor learning (Elbert et al., 1983; Roberts et al., 1992; Fiez, 1996; Gao et al., 1996; Boyden et al., 2004; Morton and Bastian, 2004; Rodriguez et al., 2005). Thus, the cerebellum represents one of the highest conserved compartments of the vertebrate brain.

Migration of neuronal precursors is a key step in cerebellar differentiation (Goldowitz and Hamre, 1998; Sotelo, 2004). The precursors of the most common cerebellar interneurons, the granule cells, migrate over long distances. Several fate mapping studies in mouse and chick embryos have revealed their detailed migratory pathways (Miale and Sidman, 1961; Hatten and Heintz, 1995; Lin et al., 2001; Gilthorpe et al., 2002). Granule cells arise from the cerebellar part of a specific germinal zone, called the rhombic lip, which runs along the dorsal aspect of the entire hindbrain ventricle (4th ventricle) (Ben-Arie et al., 1997; Alder et al., 1996). This cerebellar rhombic lip, termed upper rhombic lip (URL), undergoes a reorientation caused by the

\* Corresponding author. Fax: +49 89 3187 3192.

E-mail address: [Reinhard.Koester@gsf.de](mailto:Reinhard.Koester@gsf.de) (R.W. Köster).

rotation of the cerebellar primordium during opening of the hindbrain ventricle (Sgaier et al., 2005; Distel et al., 2006). Thus, the URL displays a mediolateral orientation, while the remaining rhombic lip of the hindbrain posterior to the cerebellum, the lower rhombic lip (LRL), displays an anterior–posterior orientation.

Recent fate mapping studies demonstrated that the upper rhombic lip successively produces different neuronal cell types during embryogenesis including neurons of various mesencephalic and hindbrain nuclei, followed by cerebellar deep nuclei and finally granule cells (Machold and Fishell, 2005; Wang et al., 2005; Wingate, 2005; Wilson and Wingate, 2006). Furthermore, lineage tracing of clonally related clusters of URL cells in chick and mouse embryos have shown that the URL gives rise to parasagittal domains of granule cells (Ryder and Cepko, 1994; Mathis and Nicolas, 2003). This suggests that the URL is also spatially patterned along its mediolateral axis. Elegant evidence for such URL subdomains was provided by genetic fate mapping in mouse embryos, where the differential mediolateral extent of expression driven by the promoters from the *engrailed1* and *engrailed2* genes within the cerebellar primordium was exploited (Sgaier et al., 2005). This study showed that granule cell progenitors maintain their mediolateral coordinates after emigration from the URL until the initiation of cerebellar foliation. At this time, granule cell progenitors derived from lateral positions within the URL migrate medially to preferentially populate the posterior-most folia of the mouse cerebellum (Sgaier et al., 2005). Recent genetic experiments suggest that different cerebellar subdomains are generated by a differential sensitivity to *engrailed* gene function (Sgaier et al., 2007). Similar genetic fate mapping studies in mouse for the lower rhombic lip have shown that it is subdivided as well, along its anteroposterior axis (Farago et al., 2006). Such spatio-temporal partitioning of germinal zones provides a powerful means of specifying distinct functional compartments in the mature brain at embryonic stages (Landsberg et al., 2005; Farago et al., 2006).

The zebrafish has become an important model organism to characterize the genetic mechanisms underlying vertebrate brain development. The largely transparent zebrafish embryos are particularly suited for intravital time-lapse studies. In this fashion, molecular mechanisms of neuronal migration (Köster and Fraser, 2001; Haas and Gilmour, 2006; Kirby et al., 2006) and axon pathfinding (Dynes and Ngai, 1998; Hutson and Chien, 2002; Bak and Fraser, 2003) can be studied in the context of brain morphogenesis. Although some genetic studies on the induction of the cerebellar primordium have been performed in the zebrafish (Reifers et al., 1998; Jaszai et al., 2003; Tallafuss and Bally-Cuif, 2003; Foucher et al., 2006), cerebellar morphogenesis, circuitry formation and function remain poorly characterized. In addition, with the exception of Purkinje cells (Lannoo et al., 1991), none of the other cerebellar neuronal cell types, including the cerebellar granule cells, nor patterning within the rhombic lip have been characterized in zebrafish.

In this study we identify the granule cell population of the zebrafish cerebellum. By combining expression analysis with

single cell tracing via time-lapse imaging and retrograde labeling, we characterize granule cell differentiation in the context of cerebellar morphogenesis. We also show that the zebrafish cerebellar rhombic lip is spatially patterned similar to mammals. Moreover, we determine that depending on their mediolateral positions within the URL, granule cell progenitors contribute to different functional domains of the mature zebrafish cerebellum. These findings provide an explanation for how zebrafish cerebellar circuitries of different function may be laid down by spatial patterning of germinal zones during embryonic cerebellar development.

## Materials and methods

### Maintenance of fish

Raising, spawning, and maintaining of zebrafish lines were performed as described previously (Kimmel et al., 1995; Westerfield, 1995). For simplicity, stable transgenic *gata1*:GFP embryos and adult fish of the strain 781 (Long et al., 1997) will be referred to as *gata1*:GFP throughout the manuscript.

### RT-PCR

Cloning of a partial cDNA of the zebrafish Gaba<sub>A</sub>-receptor alpha 6 subunit was performed by degenerate RT-PCR using cDNA from adult brains. The following primers were used: Gaba-up: ATGGAATTCACIATIGAYGITITTYTYMG and Gaba-low: GACGCATGCRWARCAIACIGCIATRAACCA to amplify an approximately 560-bp fragment, which was cloned into the pCRII-vector (Invitrogen, San Diego, CA). From this vector, a fragment containing a partial cDNA fragment of 423 bp of the zebrafish GabaR $\alpha$ 6 subunit (accession number: EF364095) was amplified using the specific primers *gabaRa6up*: CAACGTGGATAGATGACCGGCTGAA and *gabaRa6lo*: ACCTGTGTTTGACTTCAACCTTTCCTAGAC followed by subcloning into the pSC-B vector (Stratagene, La Jolla, CA).

### Morphological stainings

In order to visualize neuropil and the cellular organization of the cerebellum, vital embryo staining and counterstaining of tissue sections were performed by soaking overnight in 0.001% green-fluorescent Bodipy FL C<sub>5</sub>-ceramide (D-3521, Invitrogen) or red-fluorescent Bodipy 630/650-X (D-10000, Invitrogen), respectively. For nuclear counterstaining of fixed tissue, DAPI was used at 0.1  $\mu$ g/ml (Roche, Indianapolis, IN). To remove excess dye, stained specimens were rinsed in PBS/0.1% Tween-20 before images were acquired.

### Expression analysis

mRNA in situ hybridization was performed as described (Köster and Fraser, 2006) with the following additions: juvenile and adult brains were dissected after sacrificing zebrafish by an overdose of MS22 (3-aminobenzoic acid ethylester, Sigma, St. Louis, MO) followed by fixation overnight in 4% paraformaldehyde/PBS/0.1% Tween-20. After hybridization, brains were embedded in 4% agarose/PBS. Vibratome sections (Microm HM 650 V, Walldorf, Germany) were cut at 100  $\mu$ m thickness and mounted on SuperFrostPlus slides (Menzel, Braunschweig, Germany) prior to probe detection.

For immunohistochemical detection the following antibodies were used: polyclonal rabbit anti-GFP (TP401, 1:500, Torrey Pines Biolabs, Houston, TX), mouse anti-GFP (1:500, Molecular Probes, Eugene, OR), polyclonal rabbit anti-phosphohistone H3, PH3, (1:200, Upstate Biotechnology, Lake Placid, NY), mouse anti-human HuC/D (1:500, Molecular Probes), polyclonal rabbit anti-zebrafish Tag-1 (1:1000, received from C. Stürmer), chicken anti-mouse IgG AlexaFluor488-conjugated (1:200, Molecular Probes), goat anti-rabbit IgG Cy2- or Cy5-conjugated (1:200, Jackson ImmunoResearch West Grove, PA) and

goat anti-mouse IgG Cy3-conjugated (1:200, Jackson ImmunoResearch). Stained sections were photographed using an Axioplan2 microscope equipped with an Axiocam HRc camera. Alternatively, confocal images were acquired using an LSM510 laser-scanning microscope (all from Zeiss, Oberkochen, Germany).

#### *Intravital imaging*

Recording of still images and time-lapse microscopy of live zebrafish embryos were performed as described in detail (Köster and Fraser, 2004; Köster and Fraser, 2006). GFP-expressing cells were tracked using the NIH ImageJ software (1.34 S; <http://rsb.info.nih.gov/ij/>) together with the Manual Tracking plug-in.

#### *Retrograde neuronal labeling*

Transgenic *gatal*:GFP zebrafish larvae were anesthetized at 6 dpf with 0.01% MS22 (3-aminobenzoic acid ethylester, Sigma) in 30% Danieau/0.75 mM phenylthiourea (PTU) followed by embedding in a drop of 1.2% ultra-low gelling agarose (Sigma) with the dorsal side facing up. 6% tetramethylrhodamine-dextran, 3000 MW (Invitrogen) dissolved in PBS/0.4% Triton X-100 was microinjected into the GFP-fluorescent crista cerebellaris of the right larval hindbrain. After dye application, the agarose was removed and the larvae were maintained at 28 °C for 1 day prior to re-embedding and image recording as described previously (Köster and Fraser, 2004; Volkmann and Köster, 2007).

## Results

### *gatal*:GFP cells are of rhombic lip origin

We have recently shown that in embryos of the transgenic *gatal*:GFP 781-strain (Long et al., 1997) (for simplification *gatal*:GFP from hereon) GFP expressing neuronal precursors migrate from the dorsoposterior region of the cerebellum, likely the upper rhombic lip, toward and along the midbrain–hindbrain boundary (Köster and Fraser, 2006). The identity of this cerebellar neuronal cell type, however, remained unclear. Recent genetic fate mapping studies in the mouse embryo have defined the rhombic lip molecularly by its expression of the bHLH transcription factor *Atonal1* (*Math1*) (Machold and Fishell, 2005; Wang et al., 2005). In contrast, cells derived from the remainder of the cerebellar ventricular zone of the cerebellum express the bHLH transcription factor *Ptf1a* (Hoshino et al., 2005; Wingate, 2005). This mutually exclusive expression of *atonal1* and *ptf1a* has been conserved in zebrafish (A. Babaryka & R. W. Köster, unpublished). To molecularly confirm that GFP-expressing cells in the cerebellum of the *gatal*:GFP zebrafish strain are derived from the rhombic lip, we characterized the mRNA expression patterns of *atonal1a* (Kim et al., 1997) and *ptf1a* (Zecchin et al., 2004) using in situ hybridization.

Shortly after the first GFP-expressing cells were detectable in the developing cerebellum, *gatal*:GFP embryos were fixed and processed for mRNA in situ hybridization followed by immunohistochemistry against GFP (Chapouton et al., 2006). Expression analysis by confocal microscopy revealed that GFP-expressing cells express the rhombic lip marker *atonal1a* (Figs. 1A–D). In addition, GFP-expressing cells were found to be positioned in areas spared by *ptf1a*-expression (Figs. 1E–H). This confirms that GFP-expressing cells in the developing

cerebellum of *gatal*:GFP embryos are derived from the rhombic lip.

GFP-expressing cells were found to be distributed within the *atonal1a* expression domain in a mosaic manner and were mostly positioned at some distance to the posterior edge of the upper rhombic lip (Figs. 1A, C), where proliferation occurs. To address whether cerebellar GFP-expressing neuronal precursors still proliferate, we analyzed the co-expression of the M-phase marker phosphorylated histone 3 (PH3) and GFP by immunohistochemistry at 68 hpf, when migration of GFP-expressing neuronal precursors is predominant in the differentiating zebrafish cerebellum. Only a small number of GFP-expressing neuronal precursors co-localized with PH3-expression (Figs. 1I, J, yellow arrowhead). This is consistent with very few cell divisions of GFP-fluorescent neuronal precursors that were observed in our time-lapse studies, with dividing cells leaving the rhombic lip region soon afterwards. Instead, most of the GFP-expressing cells (Fig. 1K, yellow arrowhead) co-expressed the postmitotic neuronal marker HuC/D (Figs. 1L, M, note HuC is excluded from nucleus unlike GFP), which is expressed anterior to the rhombic lip region all the way to the MHB. This spatio-temporal relation of GFP-expression and mitotic markers suggests that GFP expression in the neuronal precursors is activated when cells are about to leave the proliferative rhombic lip to follow their migratory route.

### *gatal*:GFP cells are glutamatergic and express granule cell marker genes

The mouse cerebellar rhombic lip sequentially generates different migratory neuronal cell types, all of which acquire a glutamatergic fate. Granule neurons are the last of the cell types to be produced (Machold and Fishell, 2005; Wang et al., 2005; Wingate, 2005; Wilson and Wingate, 2006). Neuronal migration from the zebrafish rhombic lip is initiated at around 28 hpf (Köster and Fraser, 2001). In contrast, GFP-expression and onset of rhombic lip-derived migration in *gatal*:GFP embryos is not observed prior to 48 hpf (Köster and Fraser, 2006). This suggests that the *gatal*:GFP population arises late from the zebrafish rhombic lip. We therefore analyzed *gatal*:GFP cells for expression of genes expressed in cerebellar granule cell progenitors.

The transcription factor *NeuroD* and the adhesion molecule *Tag1* are expressed in differentiating migratory cerebellar granule cell precursors in the mouse embryo (Miyata et al., 1999; Schüller et al., 2006; Hatten et al., 1997). When 3-day-old *gatal*:GFP embryos were analyzed for the expression of these genes, both of them were found to co-localize with GFP-expressing cells along their migratory pathway from the rhombic lip towards and along the MHB (Figs. 2A–A", B–B"). Furthermore, at 4 dpf the GFP-expressing cells express the vesicular glutamate transporter 1, *vglut1*, indicative of a glutamatergic neurotransmitter identity (Figs. 2C–C").

At 4 days post-fertilization, zebrafish larvae stand upright and begin to show directed swimming behavior coordinating balance, body posture and locomotion. Thus, beginning at

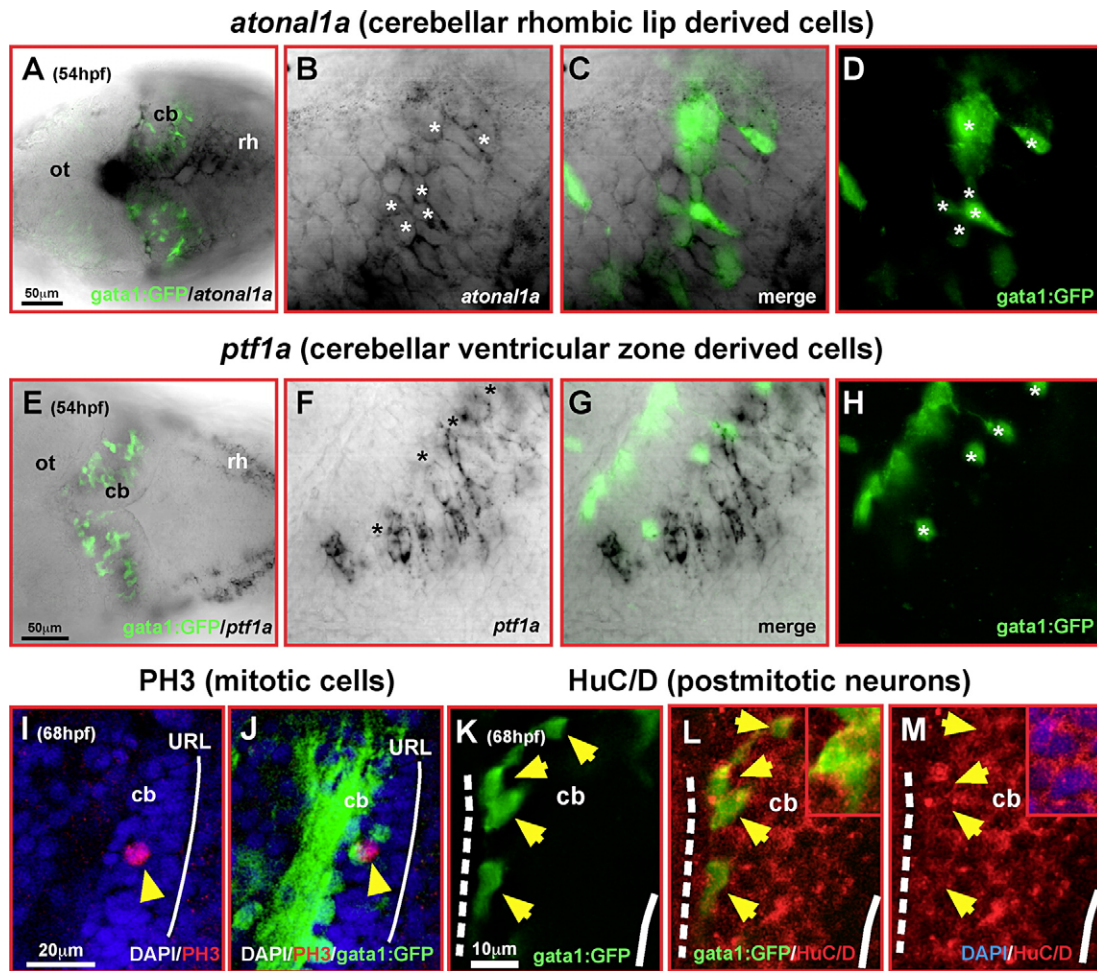


Fig. 1. Differentiating GFP-expressing cells in the cerebellum of transgenic *gata1:GFP* embryos are derived from the rhombic lip. Dorsal views of cerebella (A, E) or single optical section taken by confocal microscopy of one magnified cerebellar half (B–D, F–H) analyzed by immunohistochemistry against GFP-expression and mRNA in situ hybridization for zebrafish *atonal1a* (A–D) or *ptf1a*-expression (E–H), respectively. Whereas GFP-expressing cells (D, H, white asterisk) are co-expressing *atonal1a* (B), they are spared by *ptf1a*-expression and are positioned in gaps of the *ptf1a*-expression pattern (F). (I–M) Single optical section of the lateral view of the cerebellum recorded by confocal microscopy at 68 hpf. Although only few GFP-expressing cells (I, J, yellow arrowhead) co-express the mitotic M-phase marker PH3 close to the upper rhombic lip (white solid line), most GFP-expressing neuronal precursors (K–M, yellow arrowheads) co-express the neuronal postmitotic marker HuC/D (L, see also inset) close to the MHB (white dashed line; note that GFP is localized throughout the cell, while HuC is confined to the cytoplasm as shown by the DAPI nuclear counterstain in the inset of panel M). Abbr.: cb, cerebellum; MHB, midbrain–hindbrain boundary; ot, optic tectum; rh, rhombencephalon; URL, upper rhombic lip.

4 days post-fertilization zebrafish larvae likely possess functional cerebellar circuitries. During these late differentiation stages, granule cells express the transcription factor Pax6 and throughout their life the extracellular matrix molecule Reelin (Costagli et al., 2002; Schüller et al., 2006; Foucher et al., 2006). The expression of both zebrafish homologs *pax6a* (Figs. 2D–D'') and *reelin* (Figs. 2E–E'') largely co-localized with GFP-expressing cells in the cerebellum of 6 dpf *gata1:GFP* larvae. This developmental expression profile suggests an identity for cerebellar *gata1:GFP*-expressing cells as zebrafish granule cell progenitors.

*GFP-expression in the gata1:GFP larval cerebellum is confined to cerebellar granule cells*

Cerebellar rhombic lip-derived neuronal progenitors share many genes in their expression profile, such as *neuroD* or

*reelin*, which are expressed by precursors of both granule neurons as well as deep nuclei neurons (D'Arcangelo et al., 1995; Schüller et al., 2006). In contrast, the evolutionary conserved GABA<sub>A</sub> receptor  $\alpha 6$  subunit (GABA<sub>A</sub>R $\alpha 6$ ) is exclusively expressed in the cerebellum by granule cells in all vertebrates, allowing cerebellar granule cells to be identified unambiguously (Jones et al., 1996; Bahn et al., 1996; Fünfschilling and Reichardt, 2002; Aller et al., 2003).

Using primers targeted against conserved domains of goldfish GABA<sub>A</sub>R $\alpha 6$ , we amplified a 423 bp cDNA fragment from zebrafish adult brain by degenerate RT–PCR. The deduced amino acid sequence of this zebrafish cDNA fragment (Fig. 3A) shows a 99.3% sequence identity to the goldfish GABA<sub>A</sub>R $\alpha 6$  homolog, also containing the characteristic  $\alpha 6$ -subunit specific Arginine-residue (Fig. 3A, red box) that determines the specific pharmacology of this GABA<sub>A</sub> receptor subunit (Lüddens et al., 1990; Bahn et al., 1996).



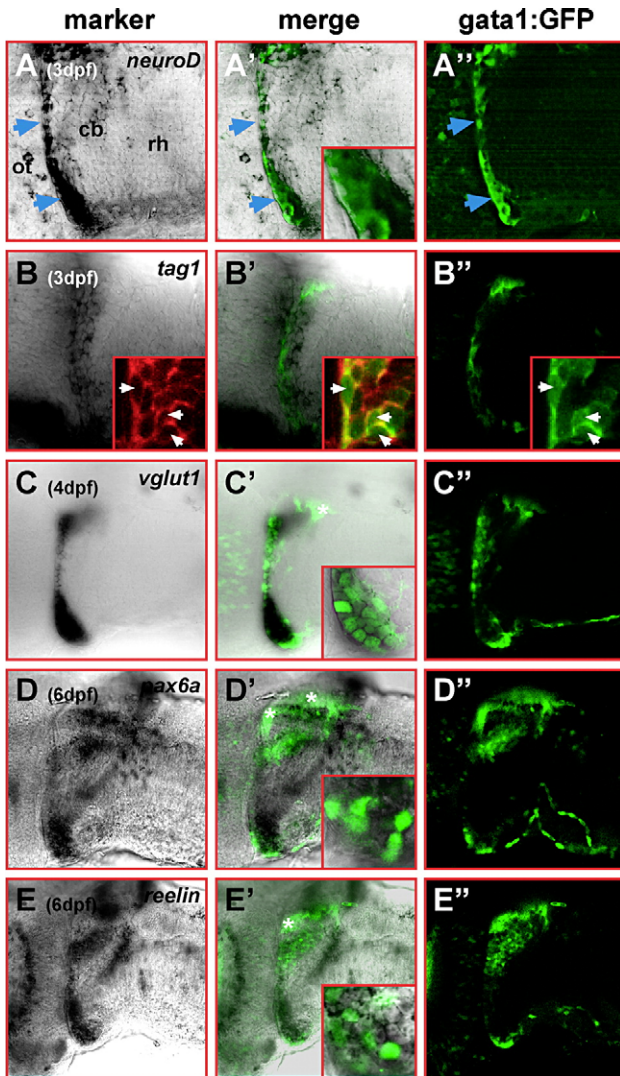


Fig. 2. Cerebellar *gata1:GFP* cells show a granule cell expression profile. Single optical sections of lateral views of cerebella at 3 dpf (A–A'', B–B''), 4 dpf (C–C'') and dorsolateral views at 6 dpf (D–D'', E–E''), respectively, recorded by laser scanning confocal microscopy. In the left column, the cerebellar expression pattern of (A) *neuroD*, (B) *tag1*, (C) *vglut1*, (D) *pax6a* and (E) *reelin* is displayed. In the right column, cerebellar GFP-expression of the same optical section is displayed, while the overlap of both expression patterns is shown in the column in the middle with insets demonstrating the co-expression of GFP and the respective marker gene. Insets in panels B–B'' display Tag-1 expression detected by immunohistochemistry (B) co-localizing to GFP-expressing *gata1:GFP* cells (B', B'' white arrowheads). GFP-expression in the dorsal-most cerebellum (white asterisks) is confined to parallel fibers (see Fig. 6), and thus, shows no co-localization with the analyzed marker gene expression. Abbr.: cb, cerebellum; ot, optic tectum; rh, rhombencephalon.

Expression analysis of zebrafish *gaba<sub>A</sub>R $\alpha$ 6* in 7-day-old *gata1:GFP* larvae showed a close overlap of both expression patterns in all cerebellar areas (Fig. 3B, a–i, note panels d–f and g–i represent magnifications of orange and blue boxed areas in picture a). Migration of granule cell progenitors in the zebrafish cerebellum along the MHB still occurs at day 7 and beyond (see Movie 2 and Movie 3 in supplementary data). This could explain why a few GFP-positive cells along the MHB may not have activated expression of *gaba<sub>A</sub>R $\alpha$ 6* yet (Fig. 3B, g, white arrowheads). In sagittal brain sections of 1-, 2-, and 4-

week-old zebrafish, expression of *gaba<sub>A</sub>R $\alpha$ 6* was confined to the internal granule cell layer of the zebrafish corpus cerebelli (Suppl. Fig. 1A, D, G), the granule cell-containing caudal lobe (Suppl. Fig. 1E, H) and the eminentia granularis (not shown) co-localizing with *gata1:GFP* cells. In addition, parallel fibers from GFP-expressing *gata1:GFP* cells within the internal granule cell layer could be observed that project to the molecular layer (Suppl. Fig. 1C, F, I, yellow arrowhead). Expression of *gaba<sub>A</sub>R $\alpha$ 6* in these different granule cell populations could still be found in the adult cerebellum (Suppl. Fig. 1J–M). Taken together, these data identify the GFP-expressing cells in the cerebellum of *gata1:GFP* embryos as cerebellar granule neurons.

#### *The cerebellar rhombic lip is spatially patterned producing different granule cell clusters*

Time-lapse studies of neuronal migration in zebrafish embryos of the stable transgenic *gata1:GFP* strain have suggested that the rhombic lip of the zebrafish cerebellum is patterned along its mediolateral axis (Köster and Fraser, 2006). As observations from these studies suggested that several neuronal clusters appeared to originate from different regions of the rhombic lip, we aimed to corroborate this finding by tracing individually migrating granule precursor cells in time-lapse recordings at higher magnification ( $n=3$  movies).

Starting at about 48 hpf GFP-expressing granule precursor cells appear along the entire cerebellar rhombic lip (Fig. 4A) and set out to migrate soon afterwards anteriorly towards the MHB (Figs. 4A–C). About 10 hours later, the initial formation of GFP-expressing granule cell clusters can be observed at the MHB (Fig. 4C). These clusters are positioned dorsomedially (Figs. 4F, J, orange dashed circle) and ventrolaterally (Figs. 4F, J, blue dashed circle), remain stationary but grow further in size due to continued neuronal migration (see Movie 1 in supplementary material and additional movies in supplementary material of Köster and Fraser, 2006). Furthermore, continued time-lapse imaging up to 7 dpf demonstrated that GFP-expressing granule cells stayed within their clusters (see Movie 2 and Movie 3 in supplementary material covering a developmental period from 100–113 hpf and 144–162 hpf, respectively). Neither exchange of granule cells between these brightly labeled clusters nor emigration out of these clusters in different directions was apparent. This indicates that granule precursor cells cease migration upon reaching the forming clusters and become stationary.

When individual GFP-fluorescent cells were manually traced, it became evident that migrating granule precursor cells contributing to the dorsomedial cluster (marked orange) originate in the medial third of the cerebellar rhombic lip adjacent to the dorsal midline. In contrast, migrating cells contributing to the ventrolateral cluster (marked blue) originate in the lateral two thirds of the URL (Figs. 4A–C, F, J). Interestingly, we identified a third almost stationary GFP-expressing population that remained positioned along the URL (Figs. 4D–F, J, marked yellow). Due to the large number of GFP-expressing cells situated within the URL at earlier time-

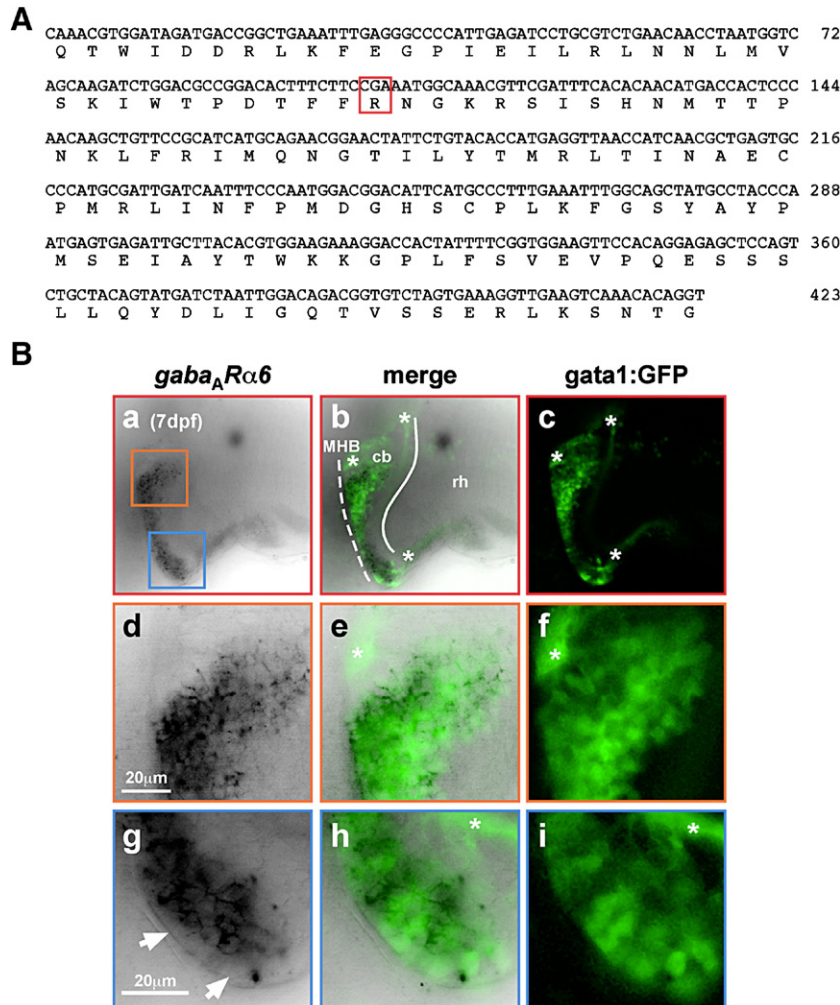


Fig. 3. *gata1:GFP* cells in the cerebellum are granule neurons. (A) Nucleotide and deduced amino acid sequence of isolated zebrafish *gaba<sub>A</sub>Rα6*-cDNA fragment. The characteristic subunit-specific Arginine-residue conserved throughout vertebrates is demarcated by a red box. (B) mRNA in situ hybridization to analyze *gaba<sub>A</sub>Rα6*-expression in zebrafish larvae at 7 dpf. In single optical sections recorded by confocal microscopy, 7 dpf larvae of the *gata1:GFP* strain display a close overlap of *gaba<sub>A</sub>Rα6*- and GFP-expression in the cerebellum [a–c, dorsolateral view to simultaneously show GFP-expressing cells in the dorsal (orange box) and the ventrolateral (blue box) cerebellum, respectively]. Magnifications of the developing dorsal cerebellum (d–f) and the ventrolateral cerebellum (g–i) demonstrate an almost complete overlap of *gaba<sub>A</sub>Rα6*- and GFP-expression. Few GFP-positive cells along the MHB (g, white arrowhead), which do not co-express *gaba<sub>A</sub>Rα6*-mRNA, may represent not yet terminally differentiated granule cells arriving after migration along the MHB. GFP-expression in zebrafish granule cells is also confined to parallel fibers (marked by white asterisk in panels b, c, e, f, h, i; see also Fig. 6), and thus, shows no co-localization with *gaba<sub>A</sub>Rα6*-mRNA expression. Abbr.: cb, cerebellum; MHB, midbrain–hindbrain boundary; rh, rhombencephalon.

points, these cells could only be discerned clearly at about 68 hpf (Fig. 4D), leaving their time-point of activation of GFP-expression unclear.

To further support our manual tracing results, we independently traced GFP-expressing cells via software-assisted visualization (ImageJ 1.34 S, Manual Tracking plug-in) of migratory routes. This software-assisted tracing confirmed our results demonstrating the different migratory routes and final positions of URL-derived cells (Figs. 4G, H, J, orange, blue) depending on their origin within the URL. In addition, the existence of a third stationary population remaining at the dorsoposterior edge of the differentiating cerebellum was confirmed (Figs. 4I, J, yellow). From dorsal projections of the time-lapse data, it may appear as if granule precursor cells from the medial and lateral subdomains of the rhombic lip simply migrate parallel to one another. Lateral projection of the end-

point of the time-lapse data though reveals that granule precursor cells from the medial subdomain of the rhombic lip remain in dorsal positions in the cerebellum close to the MHB (Fig. 4J, orange dashed circle). In contrast, granule precursor cells from the lateral subdomain of the rhombic lip not only migrate in an anterior direction but also follow a ventrally oriented migratory route (Fig. 4J, blue dashed circle). Depth-coding of the time-lapse data demonstrates that the dorsomedial and the ventrolateral granule cell clusters are located about 30 to 50 μm apart (Fig. 4K) along the dorsoventral axis of the cerebellum at 3 dpf. This distance increases until 7 dpf to 50–100 μm (Fig. 4L) due to continued growth of the cerebellum. From these cell-tracing experiments it is evident that granule cells follow divergent migratory routes (dorsal versus lateral-ventral) and settle in different parts of the cerebellum depending on their place of origin.

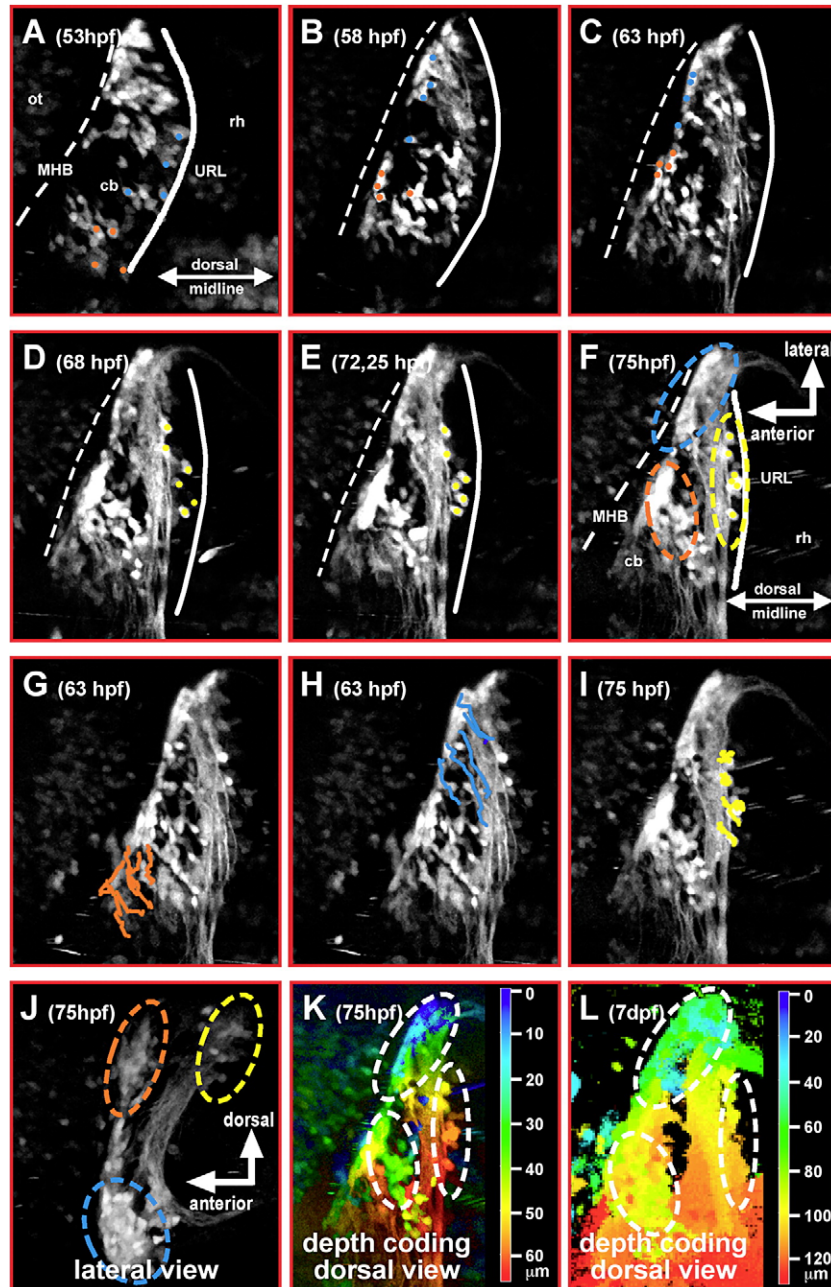


Fig. 4. Tracing of migrating GFP-expressing granule precursor cells in *gata1:GFP* transgenic embryos reveals a spatial pattern of the cerebellar rhombic lip. (A–F) Dorsal view of one cerebellar half; maximum brightness projections from individual time-points of a time-lapse microscopy study of a transgenic *gata1:GFP* embryo are shown. Manually traced granule precursor cells contributing to the dorsomedial cluster have been marked by an orange dot, cells contributing to the ventrolateral cluster are marked by a blue dot (A–C). A smaller stationary population of GFP-expressing granule precursor cells (yellow dots) remains at the dorsoposterior edge of the differentiating cerebellum (D–F). (G–I) Independently, migratory routes were visualized by ImageJ supported cell tracing. Routes have been overlaid onto pictures of individual time-points (G, H, 63 hpf; I, 75 hpf) at which tracing has been finished. (J) Lateral view of the cerebellum, maximum intensity projection (stack of 21 images each 3  $\mu\text{m}$  apart) showing that the medial and lateral granule cell clusters marked in dorsal view projections (F) are positioned apart from one another along the dorsoventral axis of the cerebellum. While granule precursor cells migrating towards the medial cluster (orange) remain in dorsal positions, migration of granule precursor cells heading towards the lateral cluster involves a strong ventral component. Depth coding of granule cell positions indicates that the medial and lateral granule cell clusters are about 30 to 50  $\mu\text{m}$  apart along the dorsoventral axis of the cerebellum at 3 dpf (K), increasing to values of 50 to 100  $\mu\text{m}$  at 7 dpf (L) due to continued growth of the cerebellum. Abbr.: cb, cerebellum; MHB, midbrain–hindbrain boundary; ot, optic tectum; rh, rhombencephalon; URL, upper rhombic lip.

*gata1:GFP* cells in the cerebellum represent all the cerebellar granule cell populations in teleosts

The co-expression of *gaba<sub>A</sub>R $\alpha$ 6* in GFP-expressing cells in the cerebellum of *gata1:GFP* larvae suggested that the spatial

patterning of the zebrafish cerebellar rhombic lip during early embryonic stages corresponds to the different granule cell populations present in the mature teleost cerebellum. We therefore addressed the final localization of the forming granule cell clusters in larval and juvenile *gata1:GFP* zebrafish brains.

First, we aimed to reveal when layer formation in the cerebellum occurs. We reasoned that layer formation would represent a developmental period when granule progenitor cells settle in their final location and can be attributed to distinct granule cell populations. Towards this end, we performed *in vivo* Bodipy Ceramide stainings to label the neuropil of the developing molecular layer. Such membrane staining demonstrated that at 60 hpf the zebrafish cerebellum is not yet subdivided in different recognizable cellular domains (Fig. 5A). At 3 dpf the first patches of neuropil on the dorsal side of both cerebellar halves appear (Fig. 5B, blue arrowheads), indicating that cerebellar layer formation has been initiated.

This is further supported by our observations that around 3 dpf migration of neuronal precursors diminishes and that zebrafish Purkinje cells initiate the expression of the terminal differentiation marker *ZebrinII* (not shown). Finally, at 6 dpf intense Bodipy Ceramide staining demarcates a prominent and continuous molecular layer covering the entire zebrafish cerebellum (Fig. 5C, blue asterisk). Thus, cerebellar lamination must be well under way after 1 week of zebrafish embryonic development.

To address the final localization of the GFP-expressing granule cells, *gata1:GFP* larvae and juvenile fish were sectioned, processed for immunohistochemistry against GFP

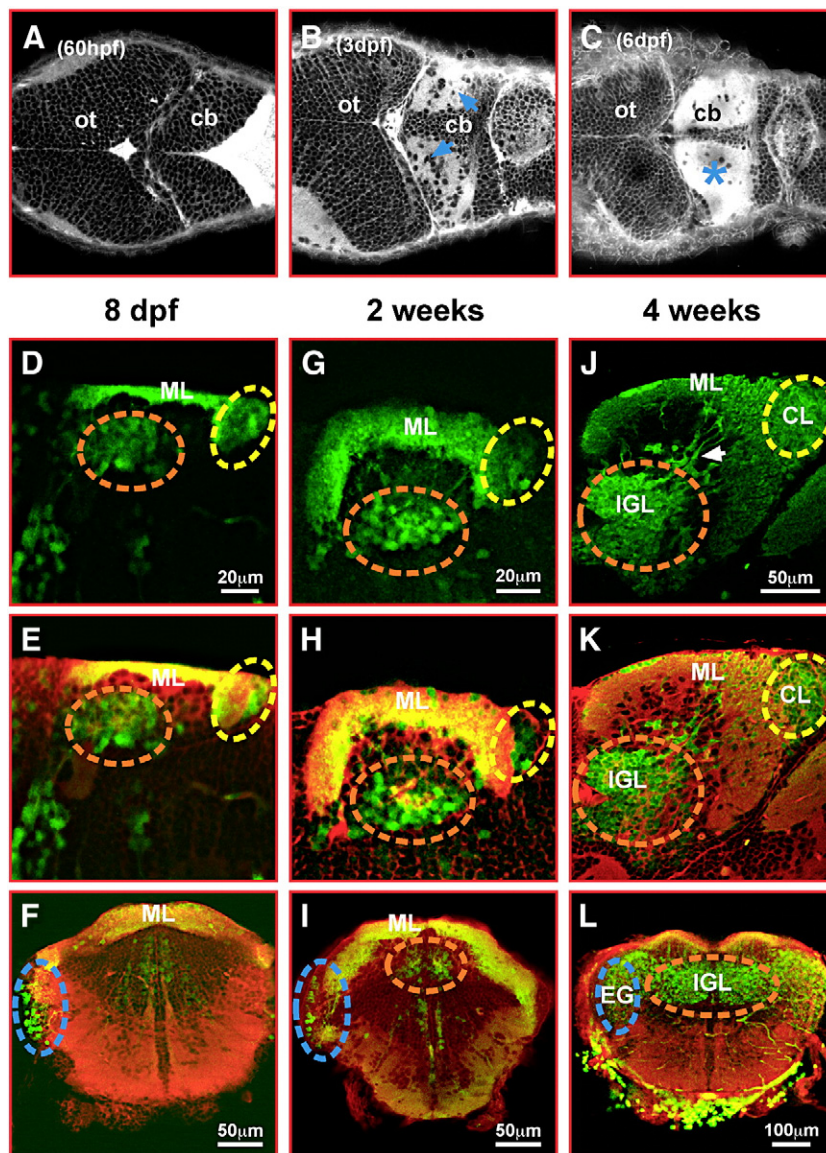


Fig. 5. *gata1:GFP* granule cells contribute to the corpus cerebelli, the eminentia granularis and the cerebellar caudal lobe. (A–C) Dorsal views of the embryonic and larval zebrafish cerebellum stained with Bodipy FL  $C_5$ -ceramide. Staining of cellular membranes, intense in neuropil (blue arrows and asterisk), was recorded by optical sectioning using laser scanning microscopy. (D, E, G, H, J, K) sagittal sections and (F, I, L) transverse sections through the cerebellum of 8 dpf (D–F), 2 weeks (G–I) and 4 weeks (J–L) old *gata1:GFP* larval and juvenile fish. GFP-expression (D, G, J) was visualized by immunohistochemistry followed by red fluorescent counterstaining with Bodipy 630/650-X (E, F, H, I, K, L) and image recording using laser scanning confocal microscopy. A dashed circle marks the forming IGL of the corpus cerebelli (orange), the eminentia granularis (blue) and the caudal lobe (yellow), respectively. Note GFP-expressing granule cells still appearing to migrate into the IGL of the corpus cerebelli at 4 weeks (J, white arrow). Abbr.: cb, cerebellum; CL, caudal lobe; EG, eminentia granularis; IGL, internal granule cell layer; ML, molecular layer; ot, optic tectum.

and subsequently counterstained with Bodipy 630/650-X to outline the cellular organization of the cerebellum. At 8 dpf sagittal sectioning of the cerebellum through the position of the embryonic dorsomedial granule cell cluster (marked orange in Fig. 4) indicated a GFP-expressing granule cell population at the medial base of the cerebellum (Figs. 5D, E, orange dashed circle). Cerebellar sections after 2 and 4 weeks of zebrafish development identified this population as the internal granule cell layer of the forming corpus cerebelli (Figs. 5G, H, J, K, orange dashed circle). Thus, the embryonic dorsomedial *gata1*:GFP cluster, which arises from the medial rhombic lip, likely represents the later granule cell population of the corpus cerebelli.

Transverse sections of the cerebellum at 8 dpf targeting the ventrolateral *gata1*:GFP cell cluster (marked blue in Fig. 4) revealed in addition to the medial corpus a granule cell population at the lateral ventral edge of the larval cerebellum (Fig. 5F, blue dashed circle). Sectioning after 2 and 4 weeks of development identified this population as the granule cells of the eminentia granularis in the mature zebrafish cerebellum (Figs. 5I, L, blue dashed circle). Thus, granule cell precursors arising in the lateral rhombic lip (Fig. 4) are likely to represent the later granule cell population of the eminentia granularis.

Finally, sagittal sections at 8 dpf through the position of the embryonic dorsoposterior *gata1*:GFP cell cluster (marked yellow in Fig. 4) revealed a third granule cell population at the dorsoposterior edge of the larval cerebellum (Fig. 5D, E, yellow dashed circle). Sectioning after 2 and 4 weeks of larval development identified this structure as the granule cell population of the caudal lobe of the mature cerebellum (Figs. 5G, H, J, K, yellow dashed circle). The granule precursor cells found to remain almost stationary within the dorsoposterior rhombic lip in our time-lapse recordings (Fig. 4, yellow marked cells, see Movie 1) are thus likely to correspond to the later granule cell population of the zebrafish cerebellar caudal lobe.

#### *gata1*:GFP granule cells project commissural axons into the crista cerebellaris

Teleost cerebellar granule cells from the eminentia granularis and the caudal lobe but not the corpus cerebelli project axons, called parallel fibers, posteriorly into the crista cerebellaris (Caird, 1978; Montgomery, 1981; Puzdrowski, 1989). Consistent with being granule neurons, GFP-expressing cells in the cerebellum of transgenic *gata1*:GFP embryos display prominent axonal projections posteriorly into dorso-anterior regions of the hindbrain at 8 dpf (Fig. 6A, blue arrowheads). Furthermore, these projections were found to be positioned within the crista cerebellaris when cerebella of 4 weeks old juvenile *gata1*:GFP fish were sagittally sectioned and stained for GFP-expression by immunohistochemistry (Figs. 6B–B'', blue arrowhead).

To further characterize these GFP-labeled granule neuron axons, their projections were followed by intravital time-lapse analysis ( $n=3$  movies) using confocal scanning microscopy (see Movie 1 in supplementary material). The first parallel fibers were recognizable at about 58 hpf, 10 hours after the

onset of granule cell migration, predominantly projecting from the ventrolateral granule cell cluster (Fig. 6D, blue dashed circle) along the posterior region of the developing cerebellum (Fig. 6D, blue arrows). These parallel fibers extended towards the cerebellar dorsal midline where they crossed to continue their projection into the contralateral half of the cerebellum (Figs. 6E–F, blue arrows). Occasionally, contacts between axon terminals from both cerebellar halves meeting close to the dorsal midline were observed (Fig. 6E, F, yellow circle), followed by a quick avoidance and continuation of commissural axon extension (Figs. 6D–H, blue and red arrows). After formation of the dorsal commissure, parallel fibers turned at the lateral edge of the cerebellum at about 65 hpf finally extending into the dorsoposterior crista cerebellaris (Figs. 6I–K, green arrow).

#### *Retrograde labeling in the crista cerebellaris discriminates the granule cells of the vestibulocerebellar system in zebrafish*

In our initial time-lapse and cell-tracing analysis, diverse populations of granule precursor cells emanating from different regions along the cerebellar rhombic lip and settling in different clusters had been distinguished (Fig. 4 and Fig. 5). Only parallel fibers of the vestibulocerebellar system (composed of eminentia granularis and caudal lobe), but not of the corpus cerebelli, project into the crista cerebellaris (Figs. 7D, H) (Puzdrowski, 1989; Wullmann, 1998). This offers a means of discriminating between granule cells of the vestibulocerebellar and non-vestibulocerebellar system by retrograde labeling.

Rhodamine-dextran was focally injected into one half of the forming crista cerebellaris of 6 dpf *gata1*:GFP transgenic larvae (Fig. 7, white asterisk) (Volkman and Köster, 2007). This dye is actively transported in a retrograde manner only within injured axons. One day after rhodamine-dextran application, maximum intensity projections of recorded image stacks revealed many labeled cells in areas of the cerebellum where the *gata1*:GFP expressing granule cells of the ventrolateral (blue dashed circle) and the dorsoposterior cluster (yellow dashed circle) are positioned (Figs. 7A–C). Further analysis of single optical sections indeed revealed individual GFP-expressing granule cells of these two populations marked by rhodamine-dextran (Figs. 7E–G). Independent retrograde labeling experiments using DiI-crystals confirmed that these two granule cell populations project axons into the crista cerebellaris (not shown). Granule cells of the forming eminentia were labeled in both cerebellar halves, indicating that the granule cell projections from the eminentia granularis into the crista cerebellaris are of dual composition containing ipsilateral and commissural contralateral axons. This is consistent with parallel fibers of the bifurcating granule cell axons projecting into both halves of the vertebrate cerebellum (Altman and Bayer, 1997). In contrast, projections of the caudal lobe granule cell population into the crista cerebellaris occur predominantly ipsilaterally (Fig. 7E) and only a few contralateral projections were observed (Fig. 7F). Currently, we have no explanation for this discrepancy in the projection of granule cells of the

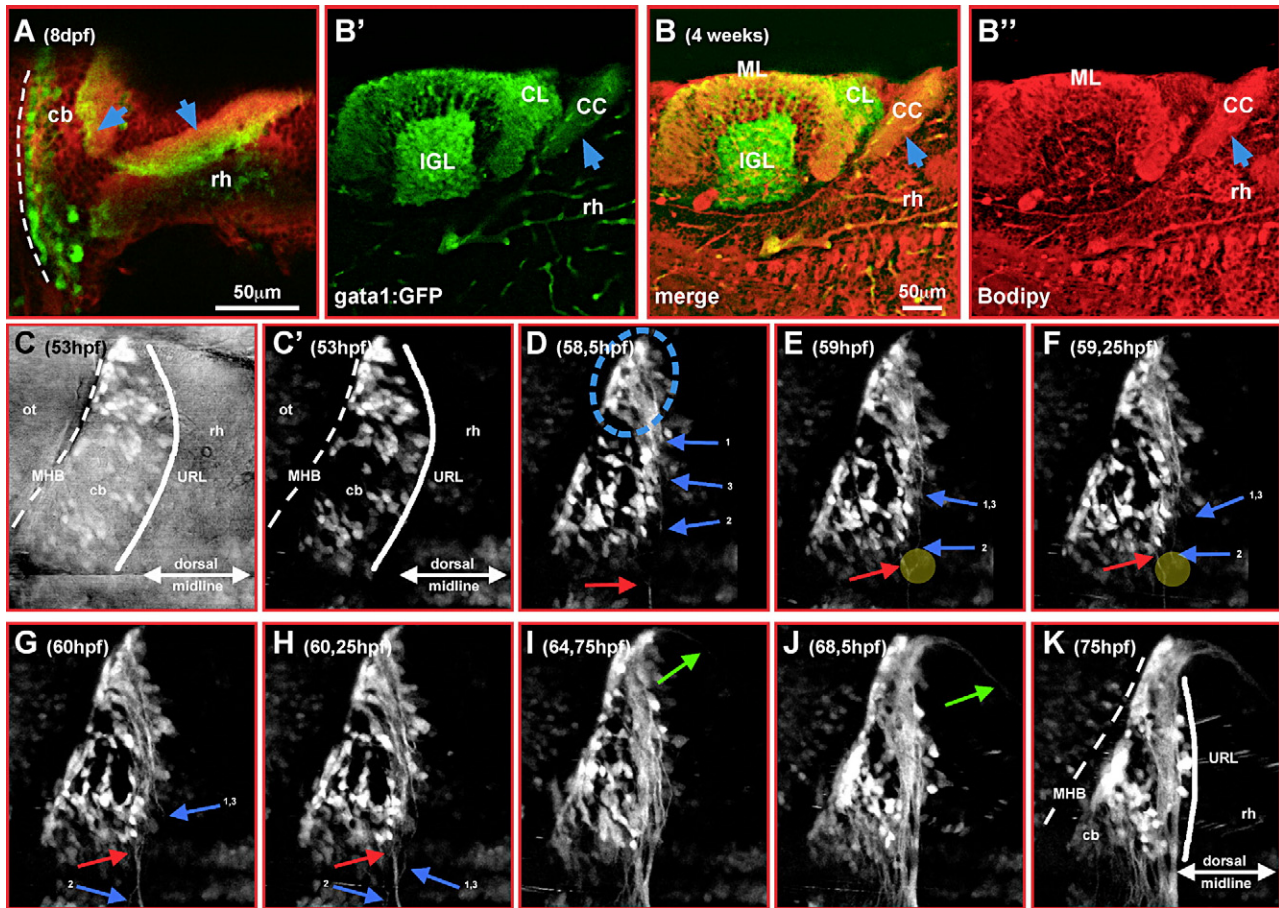


Fig. 6. *gata1:GFP* granule cells project commissural axons into the crista cerebellaris. (A) Optical section of the cerebellum of 8 dpf *gata1:GFP* transgenic larvae. Note the dorsoposterior projection out of the cerebellum (blue arrow). Sagittal sectioning of 4-week-old *gata1:GFP* cerebella, immunohistochemistry against GFP-expression (B') and counterstaining with Bodipy 630/650-X (B'') reveal positioning of these projections within the crista cerebellaris (B–B'', blue arrow). (C–K) 3-D time-lapse analysis (dorsal view) to characterize axonal projections into the crista cerebellaris (60  $\mu$ m stacks of 21 individual images spaced 3  $\mu$ m were recorded every 12 min). Brightest point projections of images of individual time-points are displayed. Individual axons are marked with arrows; note the contact and avoidance of growing axons from opposite cerebellar halves close to the dorsal midline (E, F, yellow circle; see slow motion sequence at the end of Movie 1). Around 65 hpf first projections into the forming crista cerebellaris can be observed (see green arrows in Movie 1 in supplementary material). Abbr.: cb, cerebellum; CC, crista cerebellaris; CL, caudal lobe; IGL, internal granule cell layer; MHB, midbrain–hindbrain boundary; ML, molecular layer; ot, optic tectum; rh, rhombencephalon; URL, upper rhombic lip.

zebrafish vestibular cerebellum. Further electrophysiological and behavioral experiments are required to unravel the functional consequence of this projection pattern of the zebrafish vestibular system.

Nevertheless, these retrograde labeling results support our findings from the GFP-expression analysis in the larval and juvenile cerebellum of *gata1:GFP* zebrafish. Taken together, our studies identify the ventrolateral *gata1:GFP* cell cluster in the embryonic cerebellum as the granule cell population of the future eminentia granularis, while the embryonic dorsoposterior cell cluster represents the granule cells of the future caudal lobe (Figs. 7D, H). Both granule cell populations together form the vestibulocerebellar system of the zebrafish cerebellum. In contrast, retrograde labeling either with rhodamine-dextran (Figs. 7A–C, orange dashed circle) or by using DiI revealed that granule cells of the dorsomedial cluster never project axons into the crista cerebellaris. This identifies the embryonic dorsomedial *gata1:GFP* cell cluster as the future granule cell population of the corpus cerebelli (Figs.

7D, H), representing the non-vestibulocerebellar system in zebrafish. Based on our tracing of individual granule cell progenitors, the embryonic zebrafish rhombic lip is spatially patterned, with the lateral rhombic lip generating granule cells of the vestibulocerebellum, while granule cells of the zebrafish non-vestibulocerebellar system originate from the medial rhombic lip.

We have shown that migration from the zebrafish URL initiates at about 28 hpf (Köster and Fraser, 2001), whereas zebrafish granule cell progenitors begin to emigrate from the URL at about 48 hpf. This suggests that in common with mammals, the zebrafish URL generates different cerebellar neuronal cell types over time (Machold and Fishell, 2005; Wang et al., 2005; Wingate, 2005; Wilson and Wingate, 2006). In addition, our data revealed that the zebrafish cerebellar rhombic lip is spatially patterned along its mediolateral axis such that different subpopulations of cerebellar granule cells are generated with different positions, connectivities and functions. Thus, rather than being a simple proliferative zone, the zebrafish

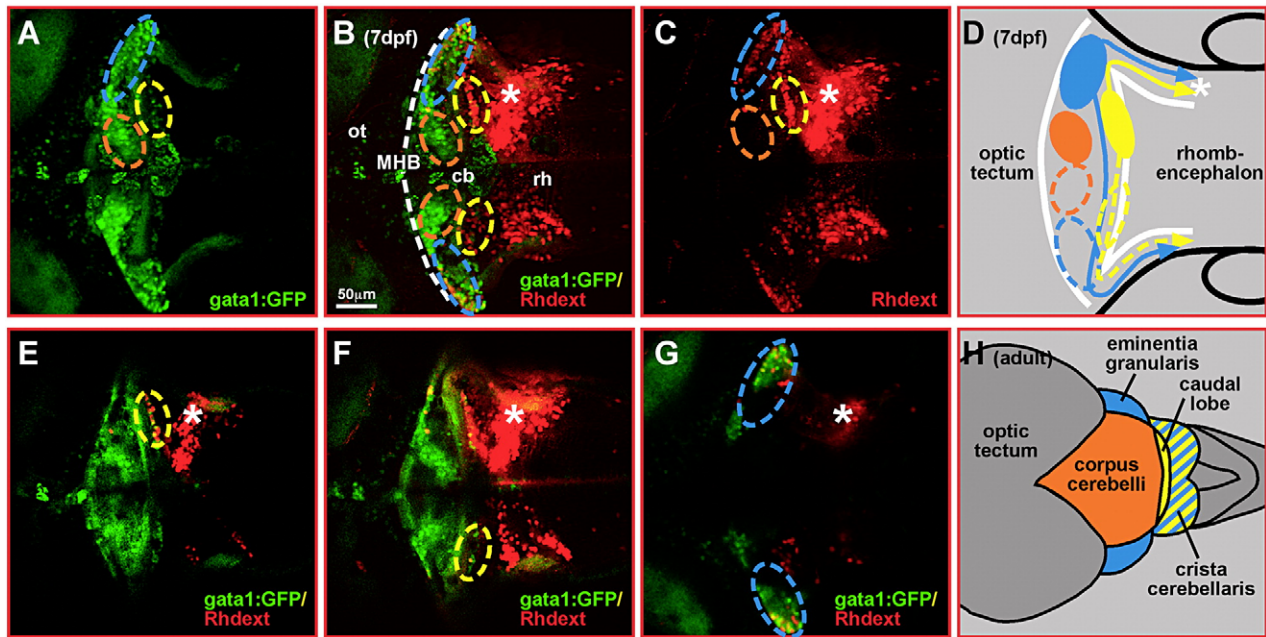


Fig. 7. Rhodamine-dextran retrograde labeling of crista cerebellaris projections discriminates between granule cells of the vestibulo- and non-vestibulocerebellar system. Rhodamine-dextran was microinjected into one half of the GFP-fluorescent crista cerebellaris (white asterisk) in transgenic *gata1:GFP* embryos at 6 dpf. (A–C) Maximum intensity projections of 3-D image stack (148  $\mu\text{m}$ , 75 images at 2  $\mu\text{m}$  distance) recorded by laser scanning confocal microscopy at 7 dpf reveal many rhodamine-dextran labeled cells in areas of the ventrolateral (blue dashed circle) and dorsoposterior (yellow dashed circle) *gata1:GFP* granule cell clusters. (E–G) Single optical sections indeed revealed co-labeling of GFP-cells with rhodamine-dextran in these granule cell populations. In contrast, rhodamine-dextran labeled cells were never found in the area or to co-localize with cells of the dorsomedial granule cell cluster (orange dashed circle). (D, H) Schematic drawing of granule cell projections deduced from rhodamine-dextran retrograde labeling; note that granule cells of the dorsomedial cluster (marked orange) do not project into the crista. These studies identify the embryonic ventrolateral (D, blue dashed circle) and dorsoposterior (D, yellow dashed circle) *gata1:GFP* granule cell clusters as granule cells of the adult vestibulocerebellar system in zebrafish (H, schematic drawing of dorsal view) formed by the eminentia granularis (blue) and the caudal lobe (yellow), respectively. Abbr.: cb, cerebellum; MHB, midbrain–hindbrain boundary; ot, optic tectum; rh, rhombencephalon.

cerebellar rhombic lip is a complex germinal structure with distinct characteristics in time and space.

## Discussion

The identification of individual neuronal cell types and the analysis of their specific developmental differentiation program is a key step towards understanding the morphogenesis of the vertebrate nervous system. In particular, comparison of neuronal differentiation in different vertebrate species allows one to distinguish evolutionary conserved and divergent processes of brain development and to exploit the specific advantages of each individual model organism for an overall comprehensive insight into the mechanisms of neuronal circuitry formation. Zebrafish have become one of the favorite model organisms to tackle the characterization and conservation of basic genetic and cell biological mechanisms underlying central nervous system development in vertebrates. Despite numerous studies addressing cellular and molecular mechanisms of fore-, mid- and hindbrain development, the cerebellum has been largely neglected. For example, zebrafish cerebellar neuronal cell types are poorly characterized if at all; molecular markers are barely established and the time-course of cerebellar differentiation is almost unknown. This is particularly surprising as the cerebellum represents one of the most conserved brain compartments in vertebrates promising that cerebellar research

in zebrafish will be directly meaningful for higher vertebrates and mammals including humans.

We have narrowed this knowledge gap by characterizing the differentiation program of zebrafish cerebellar granule cells, the most numerous neuronal cell population of the cerebellum. Combining expression analysis with *in vivo* time-lapse imaging, we have shown that zebrafish granule cell precursors start to differentiate at about 48 hpf. At this developmental stage, granule cell precursors leave the germinal zone, the cerebellar rhombic lip; become postmitotic; and initiate migration over long distances towards and along the MHB (Köster and Fraser, 2006). Consistent with the onset of granule cell cluster formation at about 60 hpf and their growth due to the continued arrival of additional granule cell precursors, subsequent initiation of layer formation in the zebrafish cerebellum begins at 72 hpf. While the peak of migration occurs from 48 hpf until about 84 hpf, granule cells continue to be added over the following days (see Movie 2 and Movie 3 in supplementary data); and it appears that even in juvenile zebrafish, granule cell migration still contributes at a low rate into the internal granule cell layer (IGL) of the corpus cerebelli (Fig. 5J, white arrow; note few individual GFP-expressing cells appearing to move from the dorsoposterior region of the cerebellum into the IGL of the corpus cerebelli). Prominent expression of the terminal differentiation marker *gaba<sub>A</sub>R $\alpha$ 6* in cerebellar granule cells can already be found at 4 dpf in the

zebrafish cerebellum. Thus, cerebellar differentiation in zebrafish occurs within 2 days. This is much faster when compared to mice, in which granule precursor cells become induced at about embryonic day 13 with migration from the external to the internal granule cell layer peaking well after birth and first *gaba<sub>A</sub>R $\alpha$ 6* expression being observed about 2 weeks after birth (Hatten et al., 1997; Machold and Fishell, 2005; Wang et al., 2005). Thus, cerebellar development in zebrafish is temporally far more condensed than in other vertebrate model organisms, making zebrafish especially suited for intravital time-lapse studies, in which relative short periods of image recording cover almost the entire cerebellar differentiation program. Our characterization of cerebellar morphogenesis and granule cell development in zebrafish, the establishment of molecular markers and the identification of a transgenic line displaying GFP-expression throughout the granule cell population will largely facilitate such in vivo imaging studies.

We have used an intravital time-lapse approach to follow granule cell migration emanating from the cerebellar rhombic lip. This specific proliferation zone in the dorsoposterior cerebellum was initially thought to exclusively give rise to cerebellar granule cells (Alder et al., 1996), making this germinal zone unique in providing a source for isolating and culturing a single neuronal cell type. Recently though, it has become evident by genetic fate mapping and time-lapse analysis that the cerebellar rhombic lip produces different neuronal populations in a temporal sequence, with granule cells being generated last (Lin et al., 2001; Köster and Fraser, 2001; Machold and Fishell, 2005; Wang et al., 2005; Wilson and Wingate, 2006). Additionally, spatial patterning within the mouse cerebellar rhombic lip was demonstrated by genetic fate mapping approaches (Mathis and Nicolas, 2003; Sgaier et al., 2005, 2007). Our in vivo time-lapse studies and individual cell-tracing analysis suggest that such a spatial patterning also occurs in the zebrafish cerebellar rhombic lip. Beyond this, we found that the mediolateral pattern of the embryonic cerebellar rhombic lip corresponds to different functional domains in the mature cerebellum. While granule progenitor cells of the zebrafish corpus cerebelli arise close to the dorsal midline, granule cell precursors populating the future eminentia granularis originate in lateral positions of the rhombic lip. Thus, the mediolateral positioning of granule cells in the mature cerebellum is already reflected in the embryonic germinal zone prior to neuronal migration. Continued time-lapse imaging showed that this spatial organization of the cerebellar rhombic lip is maintained over several days well beyond the peak of granule cell migration (see Movie 2 and Movie 3 in supplementary data).

Our observations cannot resolve whether fate specification of granule precursor cells towards a corpus cerebelli or an eminentia granularis identity occurs within the rhombic lip. Alternatively, granule precursor cells may learn during migration after having left the rhombic lip which granule cell cluster to join. Based on our data we favor that granule cell specification occurs already inside the rhombic lip. Migratory routes of granule cells emanating from the rhombic lip and heading towards the different clusters are very directional, do

not cross or intermingle even close to the rhombic lip, which we would expect if granule precursor cells learn about their destination only after having left the rhombic lip. This directional migratory behavior can again be found at 4 dpf and 6 dpf, respectively. Here, granule precursor cells in more lateral positions do not leave the rhombic lip in an anterior direction but initially migrate laterally within the rhombic lip until they migrate ventrally to join the ventrolateral granule cell cluster (see cells marked with blue dot in Movie 2 and Movie 3 in supplementary data). Granule cells migrating within the rhombic lip towards the dorsal midline were never observed. Heterotopic transplantations of granule cell precursors to different positions inside the rhombic lip could help to answer this open question of when granule precursor cell specification and determination to a vestibular or non-vestibular fate occurs.

Granule cells of the eminentia granularis and the corpus cerebelli clearly represent two different types of granule cells with different functions in teleosts. Granule cells of the eminentia and the caudal lobe (also termed auricles) receive neuronal input mainly from the vestibular system and the lateral line system (Puzdrowski, 1989; Wullimann, 1998). These cerebellar domains in zebrafish resemble most closely the vestibulocerebellum in mammals mainly serving balance control of the organism. In contrast, granule cells of the zebrafish corpus cerebelli receive input from spinocerebellar and tectocerebellar fibers transmitting proprioceptive and other sensory inputs (Nieuwenhuys, 1967; Wullimann and Northcutt, 1988; Wullimann, 1998). The zebrafish corpus cerebelli is mostly homologous to the non-vestibular cerebellar system, the diencephalo-, mesencephalo- and spinocerebellum in mammals serving coordination of locomotion and higher motor functions. Our in vivo cell-tracing studies combined with retrograde labeling reveal that in zebrafish, granule cells of the vestibular and the non-vestibular cerebellar system arise in spatially distinct regions along the mediolateral axis of the cerebellar rhombic lip. Thus, over the last years, it has become evident that the cerebellar rhombic lip is much more than just a granule cell producer being very dynamic in generating divergent cell types through temporally and spatially changing differentiation programs. Knowing the precise origin of different granule precursor cells within the cerebellar rhombic lip offers a powerful means to more specifically target distinct granule cell populations of the mature cerebellum. This will allow genetic manipulations, for instance, via electroporation or viral infection, to specifically target granule cells of the vestibular or non-vestibular cerebellar system in zebrafish, thereby improving the specificity of cerebellar research.

Given the high evolutionary conservation of the cerebellum, our findings of spatial patterning within the cerebellar rhombic lip representing functional domains of the mature cerebellum could well hold true for higher vertebrates. Here, spatial subdivisions of the rhombic lip could give rise to granule cells of the later vermis, paravermis and hemispheres, respectively. These cerebellar subdivisions also receive different neuronal input and serve different functions in controlling body posture and locomotion (vermis), coordination of extremity movements



(paravermis) and higher motor skills needed for example for speech control (hemispheres).

Prior to granule cell progenitors, the rhombic lip in mice has been shown to produce neurons of the later deep nuclei, the only output structures of the cerebellum (Machold and Fishell, 2005; Wang et al., 2005; Wilson and Wingate, 2006). Interestingly, the different cerebellar subdivisions in mice release their neuronal output via different deep nuclei, which are positioned at the base of the mammalian cerebellum in a mediolateral organization. For example, the medially positioned cerebellar vermis connects to the fastigial nucleus at the medial base of the cerebellum, the paravermis to the nucleus interpositus, whereas the lateral hemispheres project to the dentate nucleus, the most laterally positioned deep nucleus at the cerebellar base. Thus, the spatial pattern of the cerebellar rhombic lip could not only hold true for granule cells but also for the earlier generated deep nuclei neurons. This offers the exciting possibility that the spatial pattern of the embryonic rhombic lip already manifests the different positional and functional subdivisions of the mature cerebellum. Thus, individual rhombic lip precursors could be dedicated due to their spatial position to produce deep nuclei neurons and their corresponding cerebellar interneurons (granule cells) of the same cerebellar circuitry over time. This offers a means of how cerebellar subdivisions and their highly regular circuitries are being laid down by temporal and spatial patterning during early embryonic development.

## Acknowledgments

We thank Enrico Kühn and Petra Hammerl for excellent technical assistance and animal care. We thank Andrea Huber and Andrea Wizenman for advice and support with retrograde backfilling. We thank Claudia Stürmer for the antibody against zebrafish Tag-1. We are grateful to Laure Bally-Cuif, Corinne Houart, Francesco Argenton, John Kuwada, Shin-ichi Higashijima and Marina Mione for kindly providing zebrafish cDNA constructs. We thank Lianne Godinho, Peter Saunders, Kazuhiko Namikawa, Niklas Senghaas and Martin Distel for helpful suggestions and critical reading of the manuscript. This work was generously supported by the Ministry for Education and Research through a BioFuture Award 0311889 and the Helmholtz Association.

## Appendix A. Supplementary data

Supplementary data associated with this article can be found, in the online version, at doi:10.1016/j.ydbio.2007.10.024.

## References

- Alder, J., et al., 1996. Embryonic precursor cells from the rhombic lip are specified to a cerebellar granule neuron identity. *Neuron* 17, 389–399.
- Aller, M.I., et al., 2003. Cerebellar granule cell Cre recombinase expression. *Genesis* 36, 97–103.
- Altman, J., Bayer, S.A., 1997. In: Petralia, P. (Ed.), *Development of the Cerebellar System in Relation to its Evolution, Structure, and Functions*. CRC Press, Inc., Boca Raton, FL.
- Bahn, S., et al., 1996. Conservation of gamma-aminobutyric acid type A receptor alpha 6 subunit gene expression in cerebellar granule cells. *Journal of Neurochemistry* 66, 1810–1818.
- Bak, M., Fraser, S.E., 2003. Axon fasciculation and differences in midline kinetics between pioneer and follower axons within commissural fascicles. *Development* 130, 4999–5008.
- Ben-Arie, N., et al., 1997. Math1 is essential for genesis of cerebellar granule neurons. *Nature* 390, 169–172.
- Bengtsson, F., Hesslow, G., 2006. Cerebellar control of the inferior olive. *Cerebellum* 5, 7–14.
- Boyden, E.S., et al., 2004. Cerebellum-dependent learning: the role of multiple plasticity mechanisms. *Annual Review of Neuroscience* 27, 581–609.
- Caird, D.M., 1978. A simple cerebellar system: the lateral line lobe of the goldfish. *Journal of Comparative Physiology* 127, 61–74.
- Chapouton, P., et al., 2006. her5 expression reveals a pool of neural stem cells in the adult zebrafish midbrain. *Development* 133, 4293–4303.
- Costagli, A., et al., 2002. Conserved and divergent patterns of reelin expression in the zebrafish central nervous system. *Journal of Comparative Neurology* 450, 73–93.
- D’Arcangelo, G., et al., 1995. A protein related to extracellular-matrix proteins deleted in the mouse mutant reeler. *Nature* 374, 719–723.
- Distel, M., et al., 2006. Multicolor in vivo time-lapse imaging at cellular resolution by stereomicroscopy. *Developmental Dynamics* 235, 843–845.
- Dynes, J.L., Ngai, J., 1998. Pathfinding of olfactory neuron axons to stereotyped glomerular targets revealed by dynamic imaging in living zebrafish embryos. *Neuron* 20, 1081–1091.
- Elbert, O.E., et al., 1983. Spastic mutant axolotl—Identification of a phenocopy pathway with implications for the control of axolotl swimming by the vestibulocerebellum. *Journal of Comparative Neurology* 220, 97–105.
- Farago, A.F., et al., 2006. Assembly of the brainstem cochlear nuclear complex is revealed by intersectional and subtractive genetic fate maps. *Neuron* 50, 205–218.
- Fiez, J.A., 1996. Cerebellar contributions to cognition. *Neuron* 16, 13–15.
- Foucher, I., et al., 2006. Differentiation of cerebellar cell identities in absence of Fgf signalling in zebrafish Otx morphants. *Development* 133, 1891–1900.
- Fünfschilling, U., Reichardt, L.F., 2002. Cre-mediated recombination in rhombic lip derivatives. *Genesis* 33, 160–169.
- Gao, J.-H., et al., 1996. Cerebellum implicated in sensory acquisition and discrimination rather than motor control. *Science* 272, 545–547.
- Gilthorpe, J.D., et al., 2002. The migration of cerebellar rhombic lip derivatives. *Development* 129, 4719–4728.
- Goldowitz, D., Hamre, K., 1998. The cells and molecules that make a cerebellum. *Trends in Neurosciences* 21, 375–382.
- Haas, P., Gilmour, D., 2006. Chemokine signaling mediates self-organizing tissue migration in the zebrafish lateral line. *Developmental Cell* 10, 673–680.
- Hatten, M.E., Heintz, N., 1995. Mechanisms of neural patterning and specification in the developing cerebellum. *Annual Review of Neuroscience* 18, 385–408.
- Hatten, M.E., et al., 1997. Genes involved in cerebellar cell specification and differentiation. *Current Opinion in Neurobiology* 7, 40–47.
- Hoshino, M., et al., 2005. Ptf1a, a bHLH transcriptional gene, defines the GABAergic neuronal fates in cerebellum. *Neuron* 47, 201–213.
- Hutson, L.D., Chien, C.B., 2002. Pathfinding and error correction by retinal axons: the role of astray/robo2. *Neuron* 33, 205–217.
- Ito, M., 2006. Cerebellar circuitry as a neuronal machine. *Progress in Neurobiology* 78, 272–303.
- Jaszai, J., et al., 2003. Isthmus-to-midbrain transformation in the absence of midbrain–hindbrain organizer activity. *Development* 130, 6611–6623.
- Jones, A., et al., 1996. Characterization of a cerebellar granule cell-specific gene encoding the gamma-aminobutyric acid type A receptor alpha6 subunit. *Journal of Neurochemistry* 67, 907–916.
- Kim, C.H., et al., 1997. Overexpression of neurogenin induces ectopic expression of HuC in zebrafish. *Neuroscience Letters* 239, 113–116.
- Kimmel, C.B., et al., 1995. Stages of embryonic development of the zebrafish. *Developmental Dynamics* 203, 235–310.
- Kirby, B.B., et al., 2006. In vivo time-lapse imaging shows dynamic oligodendrocyte progenitor behavior during zebrafish development. *Nature Neuroscience* 9, 1506–1511.

- Köster, R.W., Fraser, S.E., 2001. Direct imaging of *in vivo* neuronal migration in the developing cerebellum. *Current Biology* 11, 1858–1863.
- Köster, R.W., Fraser, S.E., 2004. Time-lapse microscopy of brain development. In: Westerfield, M., Detrich, H. William, Zon, Leonard I. (Eds.), *The Zebrafish: Cellular and Developmental Biology*, vol. 76. Academic Press, San Diego, pp. 205–233.
- Köster, R.W., Fraser, S.E., 2006. FGF signaling mediates regeneration of the differentiating cerebellum through repatterning of the anterior hindbrain and reinitiation of neuronal migration. *Journal of Neuroscience* 26, 7293–7304.
- Landsberg, R.L., et al., 2005. Hindbrain rhombic lip is comprised of discrete progenitor cell populations allocated by Pax6. *Neuron* 48, 933–947.
- Lannoo, M.J., et al., 1991. Development of the cerebellum and its extracerebellar purkinje—cell projection in teleost fishes as determined by Zebrin-II immunocytochemistry. *Progress in Neurobiology* 37, 329–363.
- Lin, J.C., et al., 2001. The external granule layer of the developing chick cerebellum generates granule cells and cells of the isthmus and rostral hindbrain. *Journal of Neuroscience* 21, 159–168.
- Long, Q.M., et al., 1997. GATA-1 expression pattern can be recapitulated in living transgenic zebrafish using GFP reporter gene. *Development* 124, 4105–4111.
- Lüddens, H., et al., 1990. Cerebellar GABAA receptor selective for a behavioural antagonist. *Nature* 346, 648–651.
- Machold, R., Fishell, G., 2005. Math1 is expressed in temporally discrete pools of cerebellar rhombic-lip neural progenitors. *Neuron* 48, 17–24.
- Martinez, S., et al., 1999. FGF8 induces formation of an ectopic isthmocerebellar organizer and isthmocerebellar development via a repressive effect on Otx2 expression. *Development* 126, 1189–1200.
- Mathis, L., Nicolas, J.-F., 2003. Progressive restriction of cell fates in relation to neuroepithelial cell mingling in the mouse cerebellum. *Developmental Biology* 258, 20–31.
- Miale, I.L., Sidman, R.L., 1961. An autoradiographic analysis of histogenesis in the mouse cerebellum. *Experimental Neurology* 4, 277–296.
- Middleton, F.A., Strick, P.L., 1998. The cerebellum: an overview—Introduction. *Trends in Neurosciences* 21, 367–369.
- Miyata, T., et al., 1999. NeuroD is required for differentiation of the granule cells in the cerebellum and hippocampus. *Genes & Development* 13, 1647–1652.
- Montgomery, J.C., 1981. Origin of the parallel fibers in the cerebellar crest overlying the intermediate nucleus of the elasmobranch hindbrain. *Journal of Comparative Neurology* 202, 185–191.
- Morton, S.E., Bastian, A.J., 2004. Cerebellar control of balance and locomotion. *The Neuroscientist* 10, 247–259.
- Nieuwenhuys, R., 1967. Comparative anatomy of the cerebellum. *Progress in Brain Research* 25, 1–93.
- Puzdrowski, R.L., 1989. Peripheral distribution and central projections of the lateral-line nerves in goldfish. *Brain, Behavior and Evolution* 34, 110–131.
- Reifers, F., et al., 1998. Fgf8 is mutated in zebrafish acerebellar mutants and is required for maintenance of midbrain–hindbrain boundary development and somitogenesis. *Development* 125, 2381–2395.
- Roberts, B.L., et al., 1992. The influence of cerebellar lesions on the swimming performance of the trout. *Journal of Experimental Biology* 167, 171–178.
- Rodriguez, F., et al., 2005. Cognitive and emotional functions of the teleost fish cerebellum. *Brain Research Bulletin* 66, 365–370.
- Ryder, E.F., Cepko, C.L., 1994. Migration patterns of clonally related granule cells and their progenitors in the developing chick cerebellum. *Neuron* 12, 1011–1028.
- Schüller, U., et al., 2006. Cerebellar ‘transcriptome’ reveals cell-type and stage-specific expression during postnatal development and tumorigenesis. *Molecular and Cellular Neuroscience* 33, 247–259.
- Sgaier, S.K., et al., 2005. Morphogenetic and cellular movements that shape the mouse cerebellum: insights from genetic fate mapping. *Neuron* 45, 27–40.
- Sgaier, S.K., et al., 2007. Genetic subdivision of the tectum and cerebellum into functionally related regions based on differential sensitivity to engrailed proteins. *Development* 134, 2325–2335.
- Sotelo, C., 2004. Cellular and genetic regulation of the development of the cerebellar system. *Progress in Neurobiology* 72, 295–449.
- Tallafuss, A., Bally-Cuif, L., 2003. Tracing of her5 progeny in zebrafish transgenics reveals the dynamics of midbrain–hindbrain neurogenesis and maintenance. *Development* 130, 4307–4323.
- Volkman, K., Köster, R.W., 2007. *In vivo* retrograde labeling of neurons in the zebrafish embryo or larva with rhodamine dextran. *Cold Spring Harbor Protocols* 2 (doi: 10.1101/pdb.prot4832).
- Voogd, J., Glickstein, M., 1998. The anatomy of the cerebellum. *Trends in Neurosciences* 21, 370–375.
- Wang, V.Y., Zoghbi, H.Y., 2001. Genetic regulation of cerebellar development. *Nature Reviews. Neuroscience* 2, 484–491.
- Wang, V.Y., et al., 2005. Math1 expression redefines the rhombic lip derivatives and reveals novel lineages within the brainstem and cerebellum. *Neuron* 48, 31–48.
- Westerfield, M., 1995. *The Zebrafish Book*. University of Oregon Press, Eugene, OR.
- Wilson, L.J., Wingate, R.J.T., 2006. Temporal identity transition in the avian cerebellar rhombic lip. *Developmental Biology* 297, 508–521.
- Wingate, R.J.T., 2005. Math-Map(ic)s. *Neuron* 48, 1–7.
- Wullmann, M.F., Northcutt, R.G., 1988. Connections of the corpus cerebelli in the green sunfish and the common goldfish—a comparison of perciform and cypriniform teleosts. *Brain, Behavior and Evolution* 32, 293–316.
- Wullmann, M.F., 1998. The central nervous system. In: Evans, D.H. (Ed.), *The Physiology of Fishes*. CRC Press, Boca Raton, New York, pp. 245–282.
- Wurst, W., Bally-Cuif, L., 2001. Neural plate patterning: upstream and downstream of the isthmocerebellar organizer. *Nature Reviews. Neuroscience* 2, 99–108.
- Zecchin, E., et al., 2004. Evolutionary conserved role of ptf1a in the specification of exocrine pancreatic fates. *Developmental Biology* 268, 174–184.

## **Appendix 5**

Protocol in **Cold Spring Harbor Protocols**

### ***In Vivo* Retrograde Labeling of Neurons in the Zebrafish Embryo or Larva with Rhodamine Dextran**

Katrin Volkmann and Reinhard W. Köster

CSH Protocols: doi:10.1101/pdb.prot4832 (2007)

#### **Contribution**

This manuscript was written by me, I conducted all described experiments, recorded the images shown and designed the figures. Reinhard W. Köster reviewed the manuscript.

Please cite as: CSH Protocols; 2007; doi:10.1101/pdb.prot4832



**Protocol**

# **In Vivo Retrograde Labeling of Neurons in the Zebrafish Embryo or Larva with Rhodamine Dextran**

**Katrin Volkmann and Reinhard W. Köster<sup>1</sup>**

GSF--National Research Center for Environment and Health, Institute of Developmental Genetics, 85764 Munich-Neuherberg, Germany

<sup>1</sup>Corresponding author (reinhard.koester{at}gsf.de)

## **INTRODUCTION**

Application of a fluorescent dye to a target area of axons or dendrites allows the identification of individual neurons projecting to the area and reconstruction of the tract of the neurite by retrograde labeling. For the red fluorescent dye tetramethylrhodamine dextran, the labeling occurs by active retrograde transport inside the cell. This protocol describes a method for applying tetramethylrhodamine dextran to living zebrafish embryos and larvae (2-7 dpf [days post-fertilization]) via microinjection. It may be adapted for use with green or yellow fluorescent dextran conjugates.

## **RELATED INFORMATION**


A protocol for [In Vivo Time-Lapse Imaging of Zebrafish Embryonic Development](#) (Distel and Köster 2007) is available. Visualization of neurons in the zebrafish is also described by [Fetcho and O'Malley \(1995\)](#).

## **MATERIALS**



### **Reagents**


Agarose with ultra-low gelling temperature (Sigma)

*To prepare the agarose (1.2%, w/v), boil it in embryo medium, and then keep the solution in an incubator at 28°C to prevent it from gelling.*

  Embryo medium

Tetramethylrhodamine dextran (3000 or 10000 MW, anionic, lysine-fixable) (Invitrogen)

  *Prepare a 6% tetramethylrhodamine dextran solution in 1X PBS containing 0.4% Triton X-100 (Sigma). Store the solution at -20°C; avoid repeated thawing and freezing; and protect it from light.*

 Tricaine (Sigma)

Zebrafish larvae or embryos (2-7 dpf, dechorionated)

## Equipment

Dissection needle (see Step 5)

Ice

Incubator

Joystick micromanipulator (Narishige, MN-151)

Microinjection needle (borosilicate glass capillaries with filament, 1.0 mm O.D. x 0.58 mm I.D.) (Harvard Apparatus, 30-0019)

Microinjector, FemtoJet express (Eppendorf)

Microloader (Eppendorf)

Micropipette puller, dual-stage glass (Narishige, PC-10)

*Set Heater 2 to 55°C and apply a single pull (see the product manual).*

Petri dishes (6 cm x 1.5 cm) (Nunc)

Stereomicroscope (Zeiss, Stemi SV11)

## METHOD

1. Anesthetize the zebrafish embryos/larvae with 0.01% (w/v) tricaine in embryo medium.
2. Under a stereomicroscope, embed embryos/larva in a drop of 1.2% ultra-low-gelling-temperature agarose (in embryo medium, 28°C) in the bottom of a Petri dish. Orient the samples with the injection side facing up. Place the Petri dish on ice and let the agarose solidify for up to 5 min.
3. Fill a microinjection needle with tetramethylrhodamine dextran solution using a microloader tip and place the needle into a micromanipulator. Carefully break the needle tip.  
*The diameter of the needle opening should be ~1-3  $\mu\text{m}$ .*
4. Under a stereomicroscope, pressure-inject the dye solution (100 pL-2 nL) into the area of interest using a FemtoJet express microinjector with low injection pressure (100-300 hPa, with a pulse duration of 0.5-1 sec) (see [Fig. 1](#)).

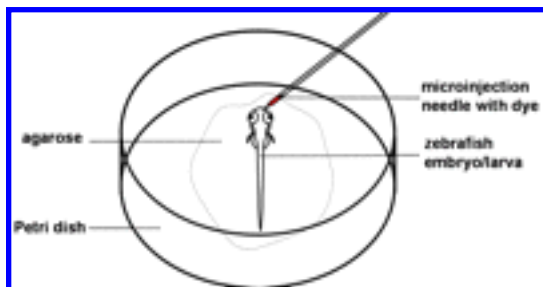


**Figure 1.** Injection of an agarose-embedded anesthetized zebrafish embryo/larva with tetramethylrhodamine-dextran. The microinjection needle is placed in a micromanipulator and connected to a FemtoJet express microinjector.

**View larger version (13K):**

[\[in this window\]](#)

[\[in a new window\]](#)

*It is not necessary to target the injection to single neurons, as the dye is taken up by the cells surrounding the injection site as well as the neuronal processes innervating or passing through the injection area.*

5. Add embryo medium and carefully remove the agarose (e.g., with a dissection needle). Maintain the embryos or larvae at 28°C in the dark for 5 h to 1 d.  
*Tetramethylrhodamine dextran is lysine-fixable (in 4% paraformaldehyde in 1X PBS containing 0.1% Tween 20, overnight at 4°C), so injected specimens can be processed for immunohistochemistry or tissue sectioning after fixation.*

6. Re-embed the embryos/larvae and record the images as described by [Köster and Fraser \(2004\)](#),

and in [In Vivo Time-Lapse Imaging of Zebrafish Embryonic Development](#) (Distel and Köster 2007).

Cell bodies are labeled brightly, while neurites show rather weak fluorescence (see [Fig. 2](#)). Note that neurons with processes (axons or dendrites) terminating in or passing through the injection site are likely to be labeled if damaged by the injection or the needle track.

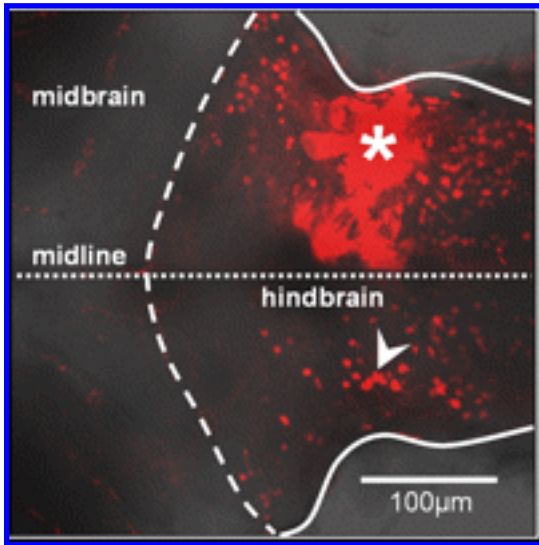


**Figure 2.** Maximum projection of an image stack of a living 7 dpf zebrafish larva injected with tetramethylrhodamine dextran, taken by laser scanning confocal microscopy. The injection was made into one-half of the hindbrain at 6 dpf (injection site is marked with an *asterisk*). Images were taken from a dorsal view (anterior at *left*). Note the cell bodies of commissural hindbrain neurons retrogradely labeled with the red fluorescent dye (*arrowhead*).

**View larger version** (102K):

[\[in this window\]](#)

[\[in a new window\]](#)

## TROUBLESHOOTING

**Problem:** If a vessel is hit during microinjection, the tetramethylrhodamine dextran is distributed rapidly over the whole body of the embryo/larva via blood flow.

**[Step 4]**

**Solution:** Wait (up to several hours); eventually, the dye will move out of the embryo into the surrounding medium by pronephric excretion.

**Problem:** There is too much dye in the tissue.

**[Step 4]**

**Solution:** Reduce the injection pressure.

## ACKNOWLEDGMENTS

The authors thank Andrea Wizenmann and Andrea Huber-Brösamle for advice and support. This work was supported by the Ministry for Education and Research through a BioFuture Award (0311889) and by the Helmholtz Association.

## REFERENCES

Distel, M. and Köster, R.W. 2007. In vivo time-lapse imaging of zebrafish embryonic development. *CSH Protocols* doi: 10.1101/pdb.prot4816. [[Abstract/Free Full Text](#)]

Fetcho, J.R. and O'Malley, D.M. 1995. Visualization of active neural circuitry in the spinal cord of intact zebrafish. *J. Neurophysiol.* **73**: 399–406. [[Abstract/Free Full Text](#)]

Köster, R.W. and Fraser, S.E. 2004. Time-lapse microscopy of brain development. *Methods Cell. Biol.* **76**: 207–235. [[Medline](#)]



**Caution**

## General warning

This material contains hazardous components. Please see recipe for full details.



**Caution**

## Tricaine

 See tricaine methanesulfonate.





## Caution

# Triton X-100

Triton X-100 causes severe eye irritation and burns. It may be harmful by inhalation, ingestion, or skin absorption. Wear appropriate gloves and safety goggles.

---



## Recipe

# Embryo medium

 30% Danieau solution

 0.75 mM *N*-phenylthiourea (PTU) (Sigma)


---





## Recipe


# Phosphate-buffered saline (PBS)

Reagent	Amount to add (for 1X solution)	Final concentration (1X)	Amount to add (for 10X stock)	Final concentration (10X)
---------	------------------------------------	-----------------------------	----------------------------------	------------------------------

NaCl	8 g	137 mM	80 g	1.37 M
 KCl	0.2 g	2.7 mM	2 g	27 mM
Na <sub>2</sub> HPO <sub>4</sub>	1.44 g	10 mM	14.4 g	100 mM
KH <sub>2</sub> PO <sub>4</sub>	0.24 g	1.8 mM	2.4 g	18 mM

If necessary, PBS may be supplemented with the following:

 CaCl <sub>2</sub> •2H <sub>2</sub> O	0.133 g	1 mM	1.33 g	10 mM
 MgCl <sub>2</sub> •6H <sub>2</sub> O	0.10 g	0.5 mM	1.0 g	5 mM

 PBS can be made as a 1X solution or as a 10X stock. To prepare 1 L of either 1X or 10X PBS, dissolve the reagents listed above in 800 mL of H<sub>2</sub>O. Adjust the pH to 7.4 (or 7.2, if required) with HCl, and then add H<sub>2</sub>O to 1 L. Dispense the solution into aliquots and sterilize them by autoclaving for 20 min at 15 psi (1.05 kg/cm<sup>2</sup>) on liquid cycle or by filter sterilization. Store PBS at room temperature.

[Copyright © 2007 by Cold Spring Harbor Laboratory Press.](#) Online ISSN: 1559-6095 [Terms of Service](#)

All rights reserved. Anyone using the procedures outlined in these protocols does so at their own risk. Cold Spring Harbor Laboratory makes no representations or warranties with respect to the material set forth in these protocols and has no liability in connection with their use. All materials used in these protocols, but not limited to those highlighted with the Warning icon, may be considered hazardous and should be used with caution. For a full listing of cautions, [click here](#).

All rights reserved. No part of these pages, either text or images, may be used for any reason other than personal use. Reproduction, modification, storage in a retrieval system or retransmission, in any form or by any means-electronic, mechanical, or otherwise-for reasons other than personal use is strictly prohibited without prior written permission.

 CiteULike  Connotea  Del.icio.us  Digg  Reddit  Technorati [What's this?](#)

## Appendix 6

Article in **Brain**

### **Complex I deficiency and dopaminergic neuronal cell loss in *parkin*-deficient zebrafish (*Danio rerio*)**

Laura Flinn, Heather Mortiboys, Katrin Volkmann, Reinhard W.  
Köster, Phillip W. Ingham and Oliver Bandmann

Brain 132: 1613-23 (2009)

#### **Contribution**

For this study I recorded the TEM images in the EM facility of the Helmholtz-Centre Munich (Figure 6 and 7) and contributed to the design of these figures and the figure legends.

# Complex I deficiency and dopaminergic neuronal cell loss in *parkin*-deficient zebrafish (*Danio rerio*)

Laura Flinn,<sup>1,2</sup> Heather Mortiboys,<sup>2</sup> Katrin Volkmann,<sup>3</sup> Reinhard W. Köster,<sup>3</sup> Phillip W. Ingham<sup>1</sup> and Oliver Bandmann<sup>1,2</sup>

1 MRC Centre for Biomedical and Developmental Genetics, University of Sheffield, Sheffield, UK

2 Academic Neurology Unit, Medical School, University of Sheffield, Sheffield, UK

3 Helmholtz-Centre Munich, Institute of Developmental Genetics, Ingolstädter Landstrasse 1, 85764 Neuherberg-Munich, Germany

Correspondence to: O. Bandmann,  
Academic Neurology Unit,  
Medical School, University of Sheffield,  
Beech Hill Road,  
Sheffield S10 2RX, UK.  
E-mail: o.bandmann@sheffield.ac.uk

Currently, only symptomatic therapy is available for Parkinson's disease. The zebrafish is a vertebrate animal model ideally suited for high throughput compound screening to identify disease-modifying compounds for Parkinson's disease. We have developed a zebrafish model for *Parkin* deficiency, the most commonly mutated gene in early onset Parkinson's disease. The zebrafish *Parkin* protein is 62% identical to its human counterpart with 78% identity in functionally relevant regions. The *parkin* gene is expressed throughout zebrafish development and ubiquitously in adult zebrafish tissue. Abrogation of *Parkin* activity leads to a significant decrease in the number of ascending dopaminergic neurons in the posterior tuberculum (homologous to the substantia nigra in humans), an effect enhanced by exposure to MPP+. Both light microscopic analysis and staining with the pan-neuronal marker HuC confirmed that this loss of dopaminergic neurons is not due to general impairment of brain development. Neither serotonergic nor motor neurons were affected, further emphasizing that the effect of *parkin* knockdown appears to be specific for dopaminergic neurons. Notably, *parkin* knockdown zebrafish embryos also develop specific reduction in the activity of the mitochondrial respiratory chain complex I, making this the first vertebrate model to share both important pathogenic mechanisms (i.e. complex I deficiency) and the pathological hallmark (i.e. dopaminergic cell loss) with human *parkin*-mutant patients. The zebrafish model is thus ideally suited for future drug screens and other studies investigating the functional mechanisms underlying neuronal cell death in early onset Parkinson's Disease. Additional electron microscopy studies revealed electron dense material in the t-tubules within the muscle tissue of *parkin* knockdown zebrafish. T-tubules are rich in L-type calcium channels, therefore our work might also provide a tentative link between genetically determined early onset Parkinson's disease and recent studies attributing an important role to these L-type calcium channels in late onset sporadic Parkinson's disease.

**Keywords:** Parkinson's disease; mitochondria

**Abbreviations:** Dpf = day post-fertilization; Hpf = hour post-fertilization; MO = morpholino; MPP+ = 1-methyl-4-phenylpyridinium; SNP = single nucleotide polymorphisms

## Introduction

Autosomal recessively inherited, homozygous or compound heterozygous mutations in the *parkin* gene on chromosome 6q25–27 are the most common identifiable genetic cause for early onset parkinsonism (Kitada *et al.*, 1998). There is also an ongoing debate whether a single heterozygote *parkin* mutation may be a susceptibility factor for late onset Parkinson's disease (Kay *et al.*, 2007; Klein *et al.*, 2007; Langston *et al.*, 2007). The *parkin* gene (PARK2) encodes a ubiquitin E3 ligase (Shimura *et al.*, 2000). Impaired mitochondrial function is currently seen as an important mechanism leading to neuronal cell loss in both genetically determined forms of early onset Parkinson's Disease and late onset, apparently sporadic Parkinson's disease (Schapira, 2008). Data on mitochondrial function in post-mortem brain tissue of patients with two *parkin* mutations are not available yet, but we and others have identified isolated complex I deficiency in peripheral tissue of *parkin*-mutant patients (Muftuoglu *et al.*, 2004; Mortiboys *et al.*, 2008). The results from the different post-mortem studies of *parkin*-mutant brains are somewhat variable, but share the core histopathological feature of neuronal cell death in the ascending nigrostriatal dopaminergic system with sporadic Parkinson's disease (Cookson *et al.*, 2008).

Zebrafish (*Danio rerio*) are vertebrates and therefore more closely related to humans than other model organisms such as *Drosophila* or *Caenorhabditis elegans*. They have a short generation time (3 months) and breed prodigiously (hundreds of offspring per female per week). Embryos develop externally, can readily be manipulated genetically and are transparent. Micro-injection of morpholino (MO) antisense oligonucleotides into zebrafish embryos at the single cell stage can be used to suppress the translation of a particular gene transiently (Ekker and Larson, 2001). The dopaminergic (DA) system is well characterized in both embryos and the adult zebrafish. Dopaminergic neurons are first detected at ~19-h post-fertilization (hpf) in a cluster of cells in the posterior tuberculum of the ventral diencephalon. These neurons represent the dopaminergic system ascending to the striatum, comparable to the nigrostriatal system in humans (Holzschuh *et al.*, 2001; Rink and Wullimann, 2001, 2002b). Zebrafish homologues with typically widespread expression pattern already at early stages of embryonic development have been identified for several firmly established Parkinson's disease genes, namely *alpha-synuclein*, *PINK1* and *DJ-1* (Bretaud *et al.*, 2007; Anichtchik *et al.*, 2008; Flinn *et al.*, 2008; Sun and Gilter, 2008).

We have identified a zebrafish orthologue of the human *parkin* gene, analysed its expression and used the MO antisense strategy to determine the effect of Parkin deficiency in zebrafish embryos. *parkin* knockdown (k/d) results in impaired mitochondrial function without concomitant abnormal mitochondrial morphology. *parkin* knockdown also leads to selective loss of dopaminergic neurons with increased susceptibility to the Parkinson's disease neurotoxin 1-methyl-4-phenylpyridinium (MPP<sup>+</sup>, the active metabolite of 1-methyl-4-phenyl-1,2,3,6-tetrahydropyridine, MPTP) without impairment of overall brain development and sparing of other neuronal sub-populations such as motor neurons which are also unaffected in human Parkinson's disease patients. Intriguingly,

EM analysis of muscle tissue in *parkin* knockdown zebrafish suggests protein aggregation in transverse (t)-tubules. T-tubules are invaginations of the surface membrane which are of crucial relevance for the calcium (Ca<sup>2+</sup>) homeostasis of the muscle tissue (Brette and Orchard, 2007). Of note, they are particularly rich in L-type Ca<sup>2+</sup> channels. Our data therefore suggest a tentative link between mechanisms leading to early onset Parkinson's Disease and impaired Ca channel function which has recently been implicated in late onset, sporadic Parkinson's disease (Chan *et al.*, 2007).

## Materials and Methods

### Fish strains and maintenance

The London wild-type (LWT) strain of zebrafish was used for all experiments. Embryos were collected after natural spawning, staged according to standard criteria, and synchronously raised at 28.5°C. All zebrafish husbandry and experimental procedures were performed in accordance with the UK Animals (Scientific Procedures) Act.

### Isolation and sequencing of zebrafish *parkin*

Human Parkin protein sequence (accession number NP\_004553) was blasted to the zebrafish genome using Ensembl ([http://www.ensembl.org/Danio\\_rerio/blastview](http://www.ensembl.org/Danio_rerio/blastview)). The conceptual translation product of a single annotated transcript (ENS DARG00000021555, zgc:112390; accession number NP\_001017635) was identified as the top match. The predicted zebrafish protein sequence was aligned with the human protein using ClustalX ([www.clustal.org](http://www.clustal.org)), and the predicted transcript aligned with the zebrafish genome in order to determine exon–intron boundaries and splice site locations. To confirm the *in silico* data, the coding sequence of *parkin* was amplified from reverse-transcribed zebrafish cDNA, using overlapping *parkin*-specific primer sets and experimental sequences aligned with *in silico* predictions.

### RT–PCR analysis of *parkin* mRNA expression

Total RNA was extracted from whole embryos at different stages of development and from various adult zebrafish organs, using Trizol reagent (Invitrogen, Paisley, UK). Up to 3 µg of total RNA per sample was used to synthesize first-strand cDNA using reverse transcriptase (Superscript II kit; Invitrogen). The resulting cDNA (2 µl) was amplified using primers for *parkin*, 5'-GCGAGTGTCTGAGCTGAA-3' (forward) and 5'-CACACTGGAACACCAGCACT-3' (reverse); for *β-actin*, 5'-AAGCAGGAGTACGA-TGAGTCTG-3' (forward) and 5'-GGTAAACGCTTCTGGAATGAC-3' (reverse) were used as a positive control to confirm consistent quality and quantity of cDNA.

### MO-mediated knockdown of Parkin

Anti-sense oligonucleotides (MO, GeneTools LLC, Philomath, OR, USA) were designed by GeneTools to target the splice donor site of exon 9 and splice acceptor site of exon 10 of the zebrafish *parkin* transcript. The MO sequences were: e9i9 5'-TGATTTGTTCTCTTACCCACAGC-3' and i9e10 5'-ACACAACTGACA-CAAACAGCAAAT-3'. Control MOs with five mismatches were used in order to distinguish phenotypic effects specific to the knockdown of *parkin*

from the effects of non-specific MO toxicity. MOs were re-suspended in sterile water at 2 mM stock concentration. Immediately prior to injection, e9i9 and i9e10 MOs were diluted to 0.75 mM and 1% phenol red (Sigma, Poole, UK) added to monitor injection efficiency. MOs were injected into the yolk of one- to two-cell stage embryos. Both *parkin* and control MOs were injected at 1.5  $\mu$ M final concentration. To confirm efficacy of the splice-blocking MOs, 2  $\mu$ l of cDNA were used in PCR amplifications using primers 5'-ATCGCCTGCACAGACATCAT-3' (forward) and 5'-GAGCCGCTTCTCATCTACAA-3', spanning exons 6–11 of the *parkin* mRNA.

## Mitochondrial respiratory chain function assays

Embryos harvested at 72 hpf (15–30 per sample) were homogenized in 200  $\mu$ l buffer (250 mM sucrose, 20 mM HEPES, 3 mM EDTA, pH 7.5), then stored at  $-80^{\circ}\text{C}$  until ready for use. All spectrophotometric assays were performed at  $30^{\circ}\text{C}$  in 200  $\mu$ l final volume using a Fluostar Omega spectrophotometer/plate reader, samples were diluted to 0.7 mg protein/ml and subjected to three cycles of liquid  $\text{N}_2$  freeze thawing. Complex I activity was determined by following the oxidation of nicotinamide adenine dinucleotide reduced disodium salt (NADH) at 340 nm with a reference wavelength of 425 nm ( $\epsilon = 6.22 \text{ mM}^{-1} \text{ cm}^{-1}$ ). The assay buffer contained 25 mM  $\text{KH}_2\text{PO}_4$ , 5 mM  $\text{MgCl}_2$ , (pH 7.2), 3 mM KCN, 2.5 mg/ml BSA, 50  $\mu$ M ubiquinone Q1, 2  $\mu$ g/ml antimycin A and zebrafish homogenate, the reaction was started with 125  $\mu$ M NADH and inhibited with 3  $\mu$ g/ml rotenone. Complex II activity was measured by following the reduction of 2,6-dichlorobenzenone-indophenol sodium salt (2,6-DCPIP) at 600 nm ( $\epsilon = 19.2 \text{ mM}^{-1} \text{ cm}^{-1}$ ). The assay buffer contained 25 mM  $\text{KH}_2\text{PO}_4$ , 5 mM  $\text{MgCl}_2$ , (pH 7.2), 3 mM KCN, 20 mM succinate and zebrafish homogenate and was incubated for 10 min before the addition of 50  $\mu$ M 2,6-DCPIP, 2  $\mu$ g/ml antimycin A and 3  $\mu$ g/ml rotenone, the reaction was started with 50  $\mu$ M ubiquinone Q1. The specific activity was normalized to that of citrate synthase.

Complex III was measured by following the reduction of cytochrome c at 550 nm with a reference wavelength of 580. The assay buffer contained 25 mM potassium phosphate, 5 mM  $\text{MgCl}_2$ , 3 mM KCN, 2.5 mg per ml BSA, 15  $\mu$ M cytochrome c, 3  $\mu$ g/ml rotenone and 50  $\mu$ M ubiquinol-2. The non-enzymatic reduction of cytochrome c by ubiquinol-2 was measured for 1 min, after which  $x \mu$ l zebrafish homogenate was added and the reaction followed for a further 4 min, finally a few grains of ascorbate were added to maximally reduce the cytochrome c. The rates were calculated as a first order constant and the results are expressed as K/min/citrate synthase activity. Complex IV activity was measured by following the oxidation of reduced cytochrome c at 550 nm, with a reference wavelength of 580 nm. The assay buffer contained 20 mM potassium phosphate, (pH 7.2), 150  $\mu$ g/ml *n*-dodecyl- $\beta$ -D-maltoside, 15  $\mu$ M reduced cytochrome c and mitochondrial extract. The reaction was followed for 3 min after which time a few grains of potassium ferricyanide were added to fully oxidize the cytochrome c. The rates were calculated as a first order constant and the results are expressed as K/min/citrate synthase activity.

## Toxin exposure using MPP+

WT (uninjected), control MO-injected and *parkin* knockdown embryos were raised for 48 hpf before exposure to toxins. At 24 hpf, embryos were transferred in groups of 20 to 12-well plates containing E3 embryo media. At 48 hpf, media was replaced in the treatment

groups with 3 mM MPP+ (Sigma, Poole, UK) in E3 embryo media. Propylthiouracil (Sigma) was used at 0.2 mM concentration to prevent the development of pigmentation in all experiments other than the behavioural analysis. Embryos were harvested at 72 hpf, fixed overnight at  $4^{\circ}\text{C}$  in 4% paraformaldehyde, then washed into 100% methanol and stored at  $-20^{\circ}\text{C}$ . All experiments were undertaken in triplicate.

## In situ hybridization for quantification of dopaminergic neurons

Whole-mount *in situ* hybridization was undertaken as previously described (Thisse and Thisse, 2008). Briefly, a digoxigenin-labelled antisense RNA probe was synthesized from pBS-tyrosine hydroxylase (TH) plasmid linearized by *Xho*I and transcribed using T3 RNA polymerase (Invitrogen, Paisley, UK). Embryos were fixed at 3-day post-fertilization (dpf) overnight in 4% paraformaldehyde in phosphate-buffered saline (PBS), then transferred to 100% methanol for storage at  $-20^{\circ}\text{C}$  for at least 24 h before undergoing hybridization. After the hybridization procedure was performed as described (Thisse and Thisse, 2008), embryos were washed extensively in 0.1% Tween 20 in PBS, re-fixed in 4% paraformaldehyde in PBS, then transferred to 80% glycerol. Embryos were mounted in glycerol and TH-positive diencephalic neurons counted under a Zeiss microscope. In order to avoid introducing unintended bias, all embryos were coded and scored blind. The results are expressed as percentage of neurons present in WT embryos (uninjected), which were staged and treated in parallel with *parkin* knockdown embryos.

## Combined in situ hybridization and antibody immunofluorescence

Digoxigenin-labelled antisense RNA probe was synthesized from pCR11topo-aromatic *amino acid decarboxylase* (AADC) plasmid, linearized by *Xho*I and transcribed using Sp6 RNA polymerase (Invitrogen). A modified *in situ* hybridization protocol was performed in which the anti-digoxigenin-POD antibody (Roche) was co-incubated with anti-tyrosine hydroxylase (TH) primary antibody (Millipore, UK) at 1:1000 final concentration overnight at  $4^{\circ}\text{C}$ . Embryos were extensively washed, stained with TSA-Cy3 (Perkin Elmer, Beaconsfield, UK) for AADC detection, again washed and then incubated with goat anti-rabbit AlexaFluor 488 antibody (Invitrogen, 1:500) for detection of TH. Whole-mount embryos were imaged using an Olympus laser scanning confocal microscope. Z-stack images were generated by scanning through the brain using a 20 $\times$  objective at an optimal image slice distance. All Z-stack images of control and *parkin* knockdown embryos were captured using identical settings, determined empirically for optimal imaging of control MO embryos.

## Whole-mount antibody immunofluorescence

For whole-mount antibody immunofluorescence detection of neuronal HuC/HuD proteins, embryos at 30 hpf were manually dechorionated, fixed at  $4^{\circ}\text{C}$  in 4% paraformaldehyde in PBS overnight, then stored at  $-20^{\circ}\text{C}$  in 100% methanol. Embryos were serially washed into water, acetone shocked for 7 min at  $-20^{\circ}\text{C}$ , then blocked for 2 h in 1% bovine serum albumin, 2% sheep serum in PBS containing 1% DMSO, 0.1% Tween 20 and 0.5% Triton X-100 (PBDDTT).

After blocking, embryos were incubated overnight at 4°C in blocking solution containing monoclonal 16A11 anti-Huc/D (Invitrogen) at 1:500 final concentration, followed by washing several times with PBDDT and incubation with secondary antibody (goat anti-mouse AlexaFluor 488, Invitrogen). Whole-mount embryos were imaged on an Olympus laser scanning confocal microscope as described. For visualization of Islet-1 positive motor neurons, primary anti-Islet1 antibodies (Developmental Studies Hybridoma Bank, IA, USA) were used in the same procedure (Higashijima *et al.*, 2000).

## Behaviour analysis of parkin knockdown embryos

Embryos were tested for behavioural consequences of *parkin* knockdown by measuring swimming behaviour at 5 dpf. WT and *parkin* knockdown embryos were raised in E3 and at 5 dpf screened for inflated swim bladder formation. Fully developed larvae were arrayed 1 per well in six-well plates containing 4.5 ml of E3 and placed on a light stage with both a transmitted and infrared light source. The larvae were allowed to acclimate to the dish for 5 min, and then recorded for 5 min using Ethovision Pro digital video recording to track movement (Tracksys, Nottingham, UK). All digital tracks were analysed for total distance moved, using an input filter of 0.06 cm as the minimum distance to be considered 'movement'. Each experiment was performed in triplicate, and the results expressed as mean total movement  $\pm$  SEM.

## Electron microscopic analysis

Larvae injected with *parkin* MO and WT larvae were fixed in 1 $\times$  PBS containing 2% paraformaldehyde and 2% glutaraldehyde at 5 dpf. Embedding, sectioning, and image acquisition were undertaken as previously described (Rieger and Koester, 2007).

## Statistical analysis

All experiments were undertaken in triplicate, each with  $n=10$  per treatment group. Data represent mean  $\pm$  SEM. Each treatment group was normalized to the appropriate WT, uninjected control group and results expressed as percentage of WT mean. One-way ANOVA and *t*-tests of significance were used when applicable as measures of significance (GraphPad Prism software).

# Results

## The zebrafish parkin orthologue is highly conserved

BLAST searching of the zebrafish genome identified a single gene homologous to human *parkin*, ENSDARG00000021555, on chromosome 13. This 1 455 base transcript encodes a peptide sequence of 458 amino acids, of which 62% are identical and 75% similar to the sequence of the human gene. Within the E3 ubiquitin ligase domain (residues 1–76 in human *parkin* protein sequence), the human and zebrafish amino acid sequences display 61% identity and 78% similarity, respectively. In the functionally relevant RING domain regions (residues 238–294 and 418–450),

the amino acid identity rises to 75–78% identity and 89–93% similarity. We confirmed the *in silico* results by amplifying reverse-transcribed zebrafish cDNA using *parkin*-specific primers and then sequencing the PCR products. Overlapping sequences were aligned and the consensus compared to *in silico* annotation. The genomic structure of zebrafish *parkin* is identical to the human gene, with a total of 12 translated exons. The sequence data we obtained from RT-PCR largely confirmed the annotated Ensembl sequence, with the exception of several single nucleotide polymorphisms (SNPs). Most of these single nucleotide polymorphisms were synonymous at the amino acid level (SNPs at positions 12, 27, 63, 69, 162, 210, 787, 1119, 1324 if the A in the ATG is +1). The only discrepancy between the *in silico* data and our own sequencing data resulting in a change of the protein sequence was a G substitution at position +112 in the highly conserved E3 ubiquitin ligase (UBL) domain, resulting in an alanine residue at codon 38. In contrast, the published Ensembl sequence at this position is a T, which would encode a serine. Of note, the corresponding residue in the human Parkin protein sequence is also an alanine.

## Parkin is expressed throughout zebrafish embryonic development and in adult tissues

We used RT-PCR to characterize the expression pattern of *parkin* in zebrafish embryos at various stages and in different adult tissues. *parkin* mRNA was detectable throughout embryogenesis, from ~5 hpf until 5 dpf (Fig. 1A). Similarly, *parkin* is expressed ubiquitously in adult zebrafish, with variable levels of transcript detectable in all organs tested (Fig. 1B).

## MO targeting of exon splice sites partially inactivates parkin in zebrafish embryos

Injection of the MOs e9i9 and i9e10 (see Materials and Methods section) resulted in complete (1 dpf) or partial (3 dpf) abolishment of full-length WT PCR product (Fig. 1C). Sequencing of the smaller band on the PCR gel revealed the primary product was indeed missing MO-targeted exon 9 from the mRNA, which results in deletion of 51 amino acids from the in-between ring (IBR) domain of Parkin. The amount of this product was greatly reduced in the knockdown embryos as compared to the WT, uninjected mRNA extracts, suggesting that nonsense-mediated decay may also affect the amount of mature *parkin* mRNA in MO-injected embryos.

## Complex I activity is reduced in parkin knockdown embryos

We next measured mitochondrial respiratory chain complex I activity to determine whether this abnormality of energy metabolism, currently considered to be of crucial relevance in the pathogenesis of human *parkin*-linked Parkinson's disease,



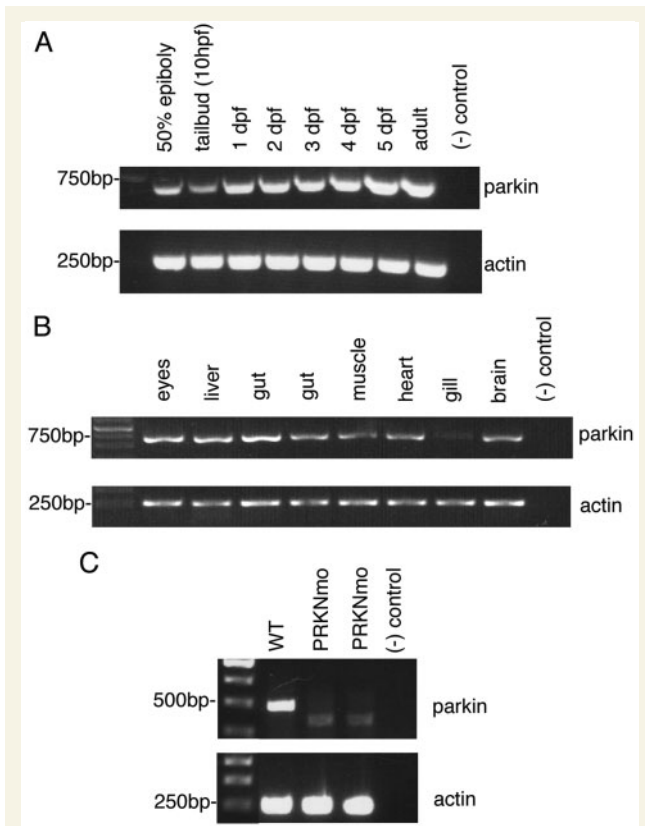


**Figure 1** *parkin* mRNA expression in developing embryos, adult tissues and *parkin* knockdown embryos. (A) RT-PCR from cDNA reverse transcribed from total embryo mRNA extracted at various time points, illustrating *parkin* expression at early developmental stages. (B) RT-PCR from cDNA reverse transcribed from total mRNA in various adult zebrafish tissues, indicating that *parkin* is ubiquitously expressed. (C) RT-PCR from WT (uninjected) and MO-injected embryos, at 3 dpf. RT-PCR for  $\beta$ -actin is shown as a positive control; the negative control is a sample lacking mRNA in reverse transcription.

is also manifest in *parkin* knockdown zebrafish embryos. Spectrophotometric assessment of complex I activity was lower by an average of 45% in *parkin* knockdown zebrafish compared to either WT embryos or control MO embryos (Fig. 2;  $P < 0.05$ ). In contrast, there was no significant difference in complex II activity in *parkin* knockdown embryos relative to both WT and control MO embryos (mean  $\pm$  SD, WT  $0.26 \pm 0.1$ , control MO  $0.31 \pm 0.09$ , *parkin* MO  $0.19 \pm 0.03$ ). Likewise measurement of complexes III and IV showed no significant difference in activity of either complex in the *parkin* knockdown embryos relative to both WT and control MO embryos, although there was a trend towards a reduction in complex IV activity (mean  $\pm$  SD, Complex III: WT  $85.75 \pm 19.7$ , control MO  $67.62 \pm 16.4$ , *parkin* MO  $74.7 \pm 5.7$ , Complex IV: WT  $9.32 \pm 3.7$ , control MO  $9.55 \pm 3.6$ , *parkin* MO  $5.87 \pm 1.5$ ). These findings are thus in good agreement with the current view that it is complex I which is specifically affected in *parkin*-related Parkinson's disease as well as in the more common, sporadic form of Parkinson's disease.

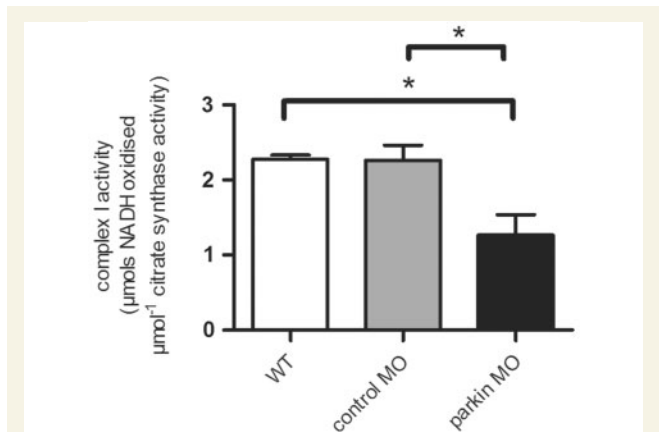


**Figure 2** *parkin* knockdown results in specific mitochondrial complex I deficiency. Mitochondrial complex I activity, measured relative to the mitochondrial marker enzyme citrate synthase, in extracts of WT, control MO and *parkin* MO-injected embryos at 3 dpf. Complex I activity in *parkin* MO embryo extracts is significantly reduced ( $*P < 0.05$ ).

## Knockdown of zebrafish parkin results in dopaminergic neuronal cell loss and increased susceptibility to MPP<sup>+</sup>

Using *in situ* hybridization with an antisense RNA probe for TH, we investigated the effect of *parkin* knockdown on the number of diencephalic dopaminergic neurons. Dopaminergic neurons ascending to the striatum (populations 1, 2, 4 and 5) according to terminology developed by Rink and Wullmann (2002a) were counted in WT uninjected embryos, control MO-injected embryos and *parkin* MO-injected embryos at 3 dpf. We calculated the mean number of these diencephalic dopaminergic neurons for WT embryos in each of three experiments and used this mean as the standard number of dopaminergic neurons, which was set to 100% in order to normalize the data. The number of ascending dopaminergic neurons present in each treatment group was then calculated as the percentage of the number of these dopaminergic neurons in WT zebrafish. *parkin* knockdown embryos showed a significant reduction in the number of diencephalic dopaminergic neurons by ~20% ( $P < 0.01$ ) already at 3 dpf. In contrast, the number of dopaminergic neurons in control MO-injected embryos did not differ significantly from WT uninjected embryos (Fig. 3A).

## Knockdown of zebrafish parkin results in increased susceptibility to MPP<sup>+</sup>

We next determined whether *parkin* knockdown results in an increased susceptibility to the mitochondrial neurotoxin MPP<sup>+</sup>. Treatment of *parkin* knockdown zebrafish embryos with MPP<sup>+</sup> resulted in a significantly greater reduction in the number of diencephalic dopaminergic ascending neurons by ~50% ( $P < 0.001$ ), suggesting a synergistic effect of *parkin* knockdown and MPP<sup>+</sup> treatment (Fig. 3B). In contrast, MPP<sup>+</sup> exposure of

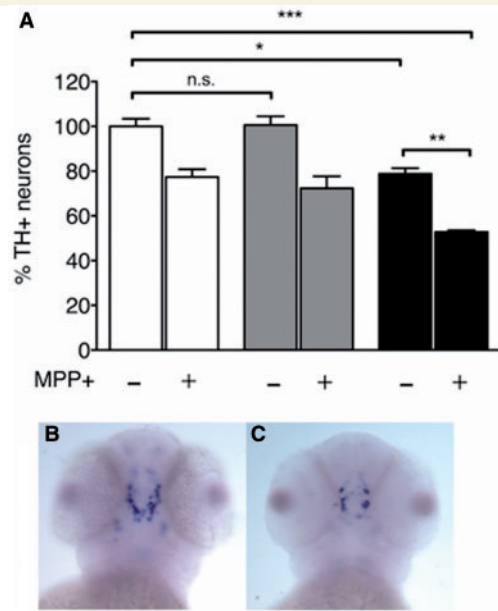


**Figure 3** Knockdown of *parkin* via MO injection decreases diencephalic dopaminergic neuron count. (A) Diencephalic dopaminergic neuron percentages counted by *in situ* hybridization using TH probe in WT (white bars), control MO-injected embryos (gray bars) and *parkin* MO-injected embryos (black bars) at 3 dpf. Concomitant treatment with MPP+ (indicated on x-axis) results in further decrease in dopaminergic neurons ( $*P < 0.05$ ;  $**P < 0.01$ ,  $***P < 0.001$ , one-way ANOVA). Error bars represent the SEM. (B) *In situ* hybridization with TH probe (blue staining) as a marker for dopaminergic neurons in 3 dpf zebrafish embryo injected with control MO. (C) Markedly reduced TH staining in 3 dpf zebrafish embryos injected with *parkin* MO and treated with MPP+.

WT and control MO-injected zebrafish embryos only resulted in a reduction by ~25% ( $P < 0.01$ ).

## The effect of *parkin* knockdown on dopaminergic neurons is specific

We next undertook double-staining with a TH antibody and an *in situ* probe for *aromatic amino acid decarboxylase* (AADC). This allowed us to discriminate between catecholaminergic and serotonergic neurons, respectively. While both neuronal sub-populations express AADC (red in Fig. 4), only catecholaminergic neurons express TH (green in Fig. 4) as well. Co-expression of both markers (yellow in Fig. 4) is thus specific for catecholaminergic neurons such as the ascending diencephalic dopaminergic neurons (Fig. 4A). These co-expression studies confirmed that the marked reduction of diencephalic neurons in *parkin* knockdown zebrafish embryos was specific for these dopaminergic neurons and further supported our assumption that the TH *in situ* based cell counting results were not simply reflecting down-regulation of TH transcription. In contrast, the (red) serotonergic neurons of the Raphe nuclei appeared similar in WT and *parkin* knockdown zebrafish embryos.

To exclude the possibility that the effect we observed was due to generalized impairment of brain development (either due to a specific effect of *parkin* knockdown or due to a non-specific toxic effect of the MO injections) rather than being specific to dopaminergic neurons we next undertook staining with anti-HuC/D antibody, an early pan-neuronal marker for post-mitotic neurons (Park *et al.*, 2000). The HuC staining resulted in a similar staining pattern and intensity in WT uninjected and *parkin* knockdown embryos at 30-hpf (Fig. 4B). To assess further the specificity of the *parkin* knockdown effect we also undertook staining of spinal motor neurons, using anti-Isl1 antibodies. The staining pattern was identical in WT uninjected and *parkin* knockdown embryos at 30 hpf (Fig. 4C). Overall, our morphological studies suggest that *parkin* knockdown has a largely selective effect on the number of ascending dopaminergic neurons rather than leading to gross morphological changes or widespread neuronal cell loss within the zebrafish brain.

## Parkin deficiency does not alter larval swimming behaviour

Because of the locomotor defects observed in Parkinson's disease patients, we next tested whether *parkin* knockdown results in changed swimming behaviour of 5 dpf larvae. We compared spontaneous swimming behaviour at 5 dpf in WT uninjected, control MO-injected, and *parkin* MO-injected larvae. The mean distance moved over three experiments for WT, control MO and *parkin* MO-injected larvae did not differ significantly (Fig. 5), suggesting no obvious differences in swimming ability between groups. We noted a trend towards reduced total distance moved in both control MO and *parkin* MO-injected larvae, but this result was not significant ( $P > 0.05$ ).

## Electron microscopy studies reveal morphologically normal mitochondria, but electron-dense material in the t-tubules in *parkin* knockdown zebrafish

*Drosophila parkin* mutants develop apoptotic muscle necrosis and swollen mitochondria with broken cristae (Greene *et al.*, 2003). In contrast, both muscle tissue as such and the mitochondria in particular are morphologically normal in *parkin* knockout mice (Palacino *et al.*, 2004). We therefore undertook TEM of fast muscle cells in the somites of the zebrafish trunk to determine whether abnormalities similar to those found in *Drosophila* are manifest in the absence of Parkin function. TEM did not reveal any obvious morphological abnormalities of the mitochondria in *parkin* knockdown zebrafish embryos. In particular, the mitochondria were not swollen and the cristae remained intact. Furthermore, there was no evidence for apoptotic muscle necrosis (Fig. 6A–D). Surprisingly, however, electron-dense material was observed in the t-tubules of the *parkin* MO-injected zebrafish (Fig. 7A–F). These invaginating tubules allow for fast depolarization of the interior of the cell and may thus play a role in  $Ca^{2+}$  mediated muscle contraction. In initial swimming tests *parkin* MO-injected larvae did not display obvious locomotive defects

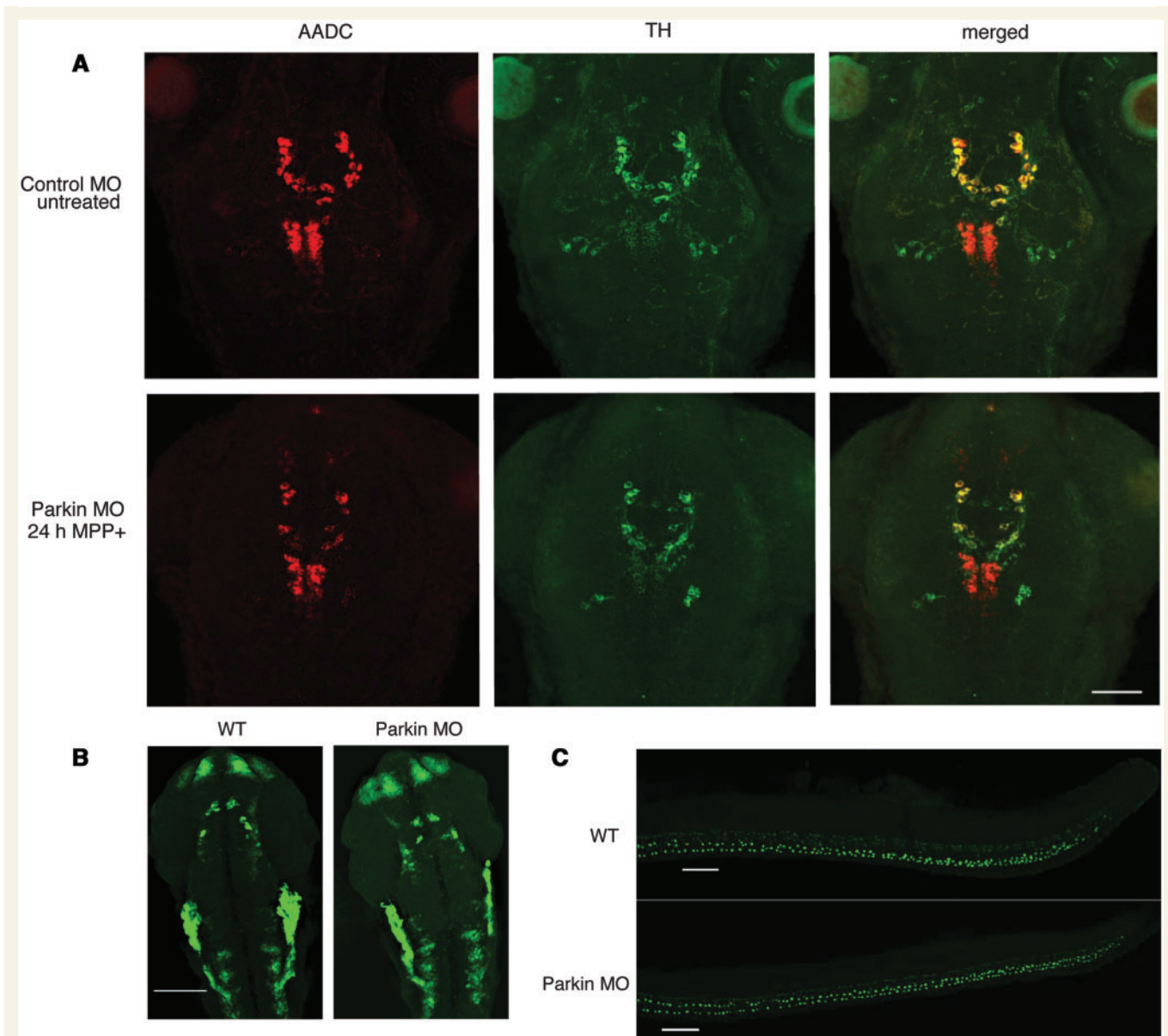


**Figure 4** Knockdown of *parkin* via MO injection is specific to dopaminergic neurons. (A) Whole-mount *in situ* hybridization for AADC (red) combined with immunohistochemical labelling using anti-TH antibody (green). Serotonergic neurons (red staining) are preserved in WT, untreated embryos and *parkin* knockdown embryos exposed to MPP+. Neurons positive for both AADC and TH (yellow staining) are reduced in *parkin* knockdown embryos treated with MPP+, indicating specific loss of dopaminergic cells in the posterior tuberculum. (B) Immunostaining with anti-HuC/D antibody labelling post-mitotic neurons shows similar morphology in 30 hpf WT and *parkin* knockdown embryos. (C) Immunostaining with anti-Islet-1 antibody indicates normal spinal cord motor neuron patterning in both 30 hpf WT and *parkin* knockdown embryos.

(see above). As the temporal activity of the MO is limited though this t-tubule alterations may be tolerated at larval stages but could become more severe in mutants with permanent Parkin depletion.

## Discussion

We have developed a new vertebrate model to study the biochemical and morphological consequences of Parkin deficiency

using MO-mediated knockdown of the zebrafish orthologue of the *parkin* gene. Comparison with embryos injected with a mismatch MO give us high confidence that the defects we observe are attributable specifically to the loss of Parkin activity rather than being caused by non-specific off target effects of the MO antisense oligonucleotide.

*parkin* knockdown zebrafish embryos share a lower activity of the mitochondrial respiratory chain complex I with *parkin*-mutant human patients (Muftuoglu *et al.*, 2004; Mortiboys *et al.*, 2008). Mitochondrial impairment is currently considered to be of crucial

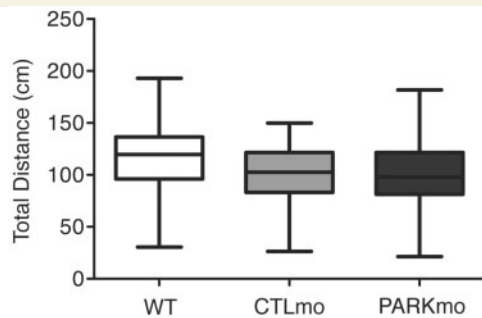


**Figure 5** Swimming behaviour is not altered by *parkin* knockdown in 5 dpf larvae. Larvae placed in 4.5 ml of E3 embryo media per well in a 12-well plate were monitored for 5 min. The swimming larvae were tracked and analysed for total distance moved. No significant difference was observed between WT, control MO or *parkin* MO-injected larvae. Data shown represent three experiments.

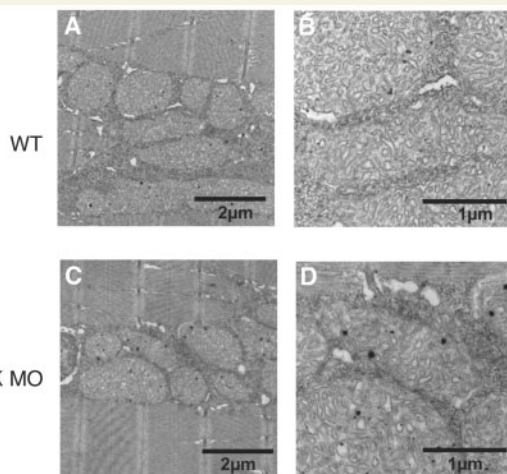


**Figure 6** Gross mitochondrial morphology is similar in WT and *parkin* knockdown embryos. Longitudinal TEM sections of fast muscle cells in the trunk somites of 5 dpf WT zebrafish larva (A and B) and larvae injected with *parkin* MO (C and D). The overview (A and C, 10 000 $\times$ ) shows normal mitochondria and myofibrils in both WT and *parkin* knockdown zebrafish embryos. (B and D) Higher magnification (25 000, B and D) reveals identical shape and structure of the mitochondrial cristae in WT and *parkin* knockdown zebrafish.

importance in the pathogenesis not only of *parkin*-related Parkinson's disease, but also in sporadic Parkinson's disease (Schapira, 2008). Furthermore, there is some evidence that Parkin itself may also be involved in the pathogenesis of sporadic Parkinson's disease: Parkin is clearly present in Lewy bodies and its transcription is upregulated in the substantia nigra of patients with sporadic Parkinson's disease (Schlossmacher *et al.*, 2002; Moran *et al.*, 2007). Parkin protects against the toxicity associated with mutant alpha-synuclein *in vitro* and *in vivo* (Lo Bianco *et al.*, 2002; Petrucelli *et al.*, 2002).

Post-mortem tissue of *parkin*-mutant patients has not as yet been assessed for morphological abnormalities of the mitochondria (Cookson *et al.*, 2008). The normal shape and integrity of mitochondrial cristae in the *parkin* knockdown zebrafish embryos that manifest impaired mitochondrial function could indicate that the latter leads to impaired mitochondrial morphology, but further studies are needed to clarify this issue. The MO antisense approach only causes transient loss of Parkin function. Other strategies such as targeted gene mutagenesis using zinc finger nucleases could be used to develop stable *parkin* knockout zebrafish lines which would then permit serial assessment of mitochondrial morphology at different ages (Woods and Schier, 2008). Similarly, t-tubule morphology and function could be assessed at different ages.

Morphological analysis revealed selective loss of dopaminergic neurons in *parkin* knockdown zebrafish embryos, a finding that contrasts both with the more widespread defects observed in *parkin* knockout *Drosophila*, and also with the absence of any robust morphological changes in *parkin* knockout mice (Greene *et al.*, 2003; Perez and Palmiter, 2005). Such selective dopaminergic neuronal cell loss together with lower complex I activity mirrors the human disease better than any other currently available animal model for *parkin* disease. The future development of stable *parkin* knockout zebrafish lines (see above) will help to determine whether the observed loss of dopaminergic neurons is progressive. The increased susceptibility to MPP+ observed in our *parkin* knockdown zebrafish model is in keeping with data from *in vitro* studies, but contrasts with the lack of increased susceptibility to this neurotoxin in *parkin* knockout mice (Hyun *et al.*, 2002; Thomas *et al.*, 2007). We had previously demonstrated increased susceptibility to a different mitochondrial toxin, rotenone, in *parkin*-mutant patient tissue (Mortiboys *et al.*, 2008).

In *Drosophila*, Parkin and PINK1 appear to act in the same mitochondrial pathway, resulting in the same phenotype when either (or both) of these genes is mutated (Clark *et al.*, 2006; Park *et al.*, 2006; Yang *et al.*, 2006). *PINK1* knockdown in zebrafish results in a severe developmental phenotype (Anichtchik *et al.*, 2008). In contrast, our morphological studies, in particular the normal staining pattern with the pan-neuronal marker HuC and the motor-neuron specific marker Islet-1, suggest a considerably more selective effect of *parkin* knockdown than *PINK1* knockdown. The MOs used in our study resulted in a 51 amino acid deletion within the in-between ring domain of *parkin*. The in-between ring domain augments binding of E2 proteins and the subsequent ubiquitination of proteins such as synphilin-1 (Beasley *et al.*, 2007). The resulting partially deleted Parkin protein in our study may thus have decreased enzymatic activity as a ubiquitin 3 ligase, but could nevertheless have some remaining functional activity since other crucial parts of the protein such as the ubiquitin ligase (UBL) domain and the two RING domains remained intact. In contrast, MOs directed against the ATG translation initiation site were used in the zebrafish *PINK1* knockdown studies (Anichtchik *et al.*, 2008). This might have led to a more complete suppression of PINK1 function. It is nevertheless difficult to understand why PINK1 deficiency results in such marked impairment of gross brain development in zebrafish embryos,

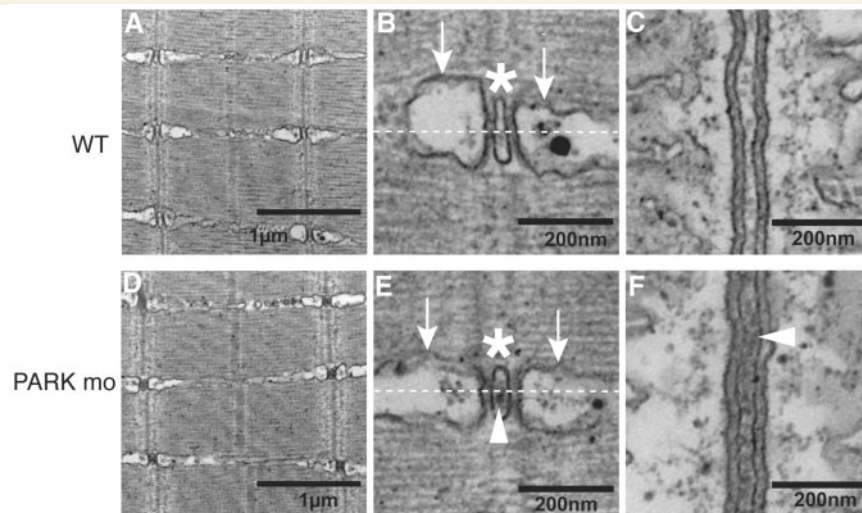


**Figure 7** Electron-dense staining in t-tubules of *parkin* knockdown embryos. Longitudinal TEM sections of fast muscle cells in the trunk somites of 5 dpf WT zebrafish larva (A–C) and larvae injected with *parkin* MO (D–F). The increase in electron dense material within the t-tubules in the *parkin* knockdown zebrafish embryos is already visible at lower magnification (25 000 $\times$  A and D). At higher magnification (60 000 $\times$ ) the triad, formed by the t-tubule (C and F, asterisk) and the terminal cisternae of the sarcoplasmic reticulum (SR, C and F, arrow) becomes more clearly visible and the increase in electron dense material thus more apparent. The dashed line depicts the plane of the sections shown in (B and E). In the *parkin* knockdown larvae the t-tubules contain electron dense material (E and F, arrowhead), the SR and the myofibrils appear normal.

but does not result in any morphological abnormalities in *PINK1* knockout mice (Zhou *et al.*, 2007; Gautier *et al.*, 2008). Post-mortem studies have not as yet been undertaken in human patients with *PINK1* mutations, but the clinical phenotype is obviously only suggestive of regionally selective neuronal cell loss rather than gross brain dysmorphology. Both the *PINK1*- and our *parkin* knockdown zebrafish studies nevertheless suggest that the encoded proteins may have a crucial role for the development and/or survival of neurons at early developmental stages. This may appear counter-intuitive for an adult-onset neurodegenerative condition, but is in keeping with recent observations describing abnormalities in key developmental mechanisms, namely microRNA signalling, in late-onset sporadic Parkinson's disease (Kim *et al.*, 2007).

*parkin* knockdown zebrafish embryos did not display an overt behavioural phenotype. It is currently thought that human patients have to lose at least two thirds of their dopaminergic neurons in the substantia nigra before they develop any motor symptoms of Parkinson's disease. The loss of dopaminergic neurons observed in our model system (~25%) may therefore not have been sufficient enough to result in a motor phenotype. Complete and longer lasting loss of Parkin function in stable *parkin* knockout lines will reveal whether dopaminergic neuron loss becomes more pronounced both during embryonic development and at later stages which may in turn lead to a more marked behavioural phenotype.

The observation of electron-dense material in the t-tubules of the *parkin* knockdown zebrafish embryos was a serendipitous finding. T-tubules are rich in L-type  $\text{Ca}^{2+}$  channels (Brette and Orchard, 2007). Dopaminergic neurons in the substantia nigra pars compacta (SNpc) rely on L-type  $\text{Ca}^{2+}$  channels for

pacemaking with a much larger  $\text{Ca}^{2+}$  influx in these neurons than in other cells (Surmeier, 2007). This increased  $\text{Ca}^{2+}$  load of the dopaminergic neurons could in turn lead to a considerably higher energy demand to transport  $\text{Ca}^{2+}$  back out of the cells, consuming ATP produced by oxidative phosphorylation in the mitochondria. Future studies are needed to determine whether the observed impairment of mitochondrial function in *parkin*-linked Parkinson's disease contributes to neuronal cell death not only due to its effect on overall energy production, but also because of the important role of mitochondria in the maintenance of intracellular  $\text{Ca}^{2+}$  homeostasis (Szabadkai and Duchon, 2008).

Zebrafish embryos are highly amenable to high throughput drug screening and might therefore be a useful new tool to work towards the identification of disease-modifying therapy for Parkinson's disease. We have already provided proof of principle data in our *DJ-1* knockdown studies that zebrafish embryos can be a useful tool to investigate compounds for their putative neuroprotective effect (Bretaud *et al.*, 2007). Similarly, we will now be able to use *parkin* knockdown zebrafish embryos to rapidly assess promising substances *in vivo* in this new vertebrate animal model of Parkin deficiency. The recent development of an enhancer trap transgenic zebrafish line, ETvmat2:GFP, with green fluorescent monoaminergic neurons will further facilitate the rapid assessment of drugs for a putative neuroprotective effect on dopaminergic neurons in high throughput compound screens (Wen *et al.*, 2008). It has been suggested that small molecules should be tested for their ability to induce *parkin* transcription to identify disease-modifying treatment for Parkinson's disease (Butcher, 2005). Genetically modified zebrafish embryos may also be an ideal tool to undertake such studies.

## Acknowledgements

We would like to acknowledge the contribution of Dr S. Breaud to the early stages of this project. We would also like to thank the aquarium staff at CDBG for zebrafish maintenance and Luise Jennen for excellent help with TEM recording.

## Funding

Parkinson's Disease Society (PDS, G-0608); Research into Ageing (RiA, 282 to O.B. and P.W.I.); Medical Research Council (MRC Centre Grant to P.W.I.); Bundesministerium fuer Bildung und Forschung (BMBF, BioFuture Grant 0311889 to K.V. and R.W.K.); Wellcome Trust (GR077544AIA) for the University of Sheffield Light Microscopy Facility.

## References

- Anichtchik O, Diekmann H, Fleming A, Roach A, Goldsmith P, Rubinsztein DC. Loss of PINK1 function affects development and results in neurodegeneration in zebrafish. *J Neurosci* 2008; 28: 8199–207.
- Beasley SA, Hristova VA, Shaw GS. Structure of the Parkin in-betweening domain provides insights for E3-ligase dysfunction in autosomal recessive Parkinson's disease. *Proc Natl Acad Sci USA* 2007; 104: 3095–100.
- Breaud S, Allen C, Ingham PW, Bandmann O. p53-dependent neuronal cell death in a DJ-1-deficient zebrafish model of Parkinson's disease. *J Neurochem* 2007; 100: 1626–35.
- Brette F, Orchard C. Resurgence of cardiac t-tubule research. *Physiology (Bethesda)* 2007; 22: 167–73.
- Butcher J. Parkin gene therapy could treat Parkinson's disease. *Lancet Neurol* 2005; 4: 82.
- Chan CS, Guzman JN, Ilijic E, Mercer JN, Rick C, Tkatch T, et al. 'Rejuvenation' protects neurons in mouse models of Parkinson's disease. *Nature* 2007; 447: 1081–6.
- Clark IE, Dodson MW, Jiang C, Cao JH, Huh JR, Seol JH, et al. Drosophila pink1 is required for mitochondrial function and interacts genetically with parkin. *Nature* 2006; 441: 1162–6.
- Cookson MR, Hardy J, Lewis PA. Genetic neuropathology of Parkinson's disease. *Int J Clin Exp Pathol* 2008; 1: 217–31.
- Ekker SC, Larson JD. K/d technology in model developmental systems. *Genesis* 2001; 30: 89–93.
- Flinn L, Breaud S, Lo C, Ingham PW, Bandmann O. Zebrafish as a new animal model for movement disorders. *J Neurochem* 2008; 106: 1991–7.
- Gautier CA, Kitada T, Shen J. Loss of PINK1 causes mitochondrial functional defects and increased sensitivity to oxidative stress. *Proc Natl Acad Sci USA* 2008; 105: 11364–9.
- Greene JC, Whitworth AJ, Kuo I, Andrews LA, Feany MB, Pallanck LJ. Mitochondrial pathology and apoptotic muscle degeneration in Drosophila parkin mutants. *Proc Natl Acad Sci USA* 2003; 100: 4078–83.
- Higashijima S, Hotta Y, Okamoto H. Visualization of cranial motor neurons in live transgenic zebrafish expressing green fluorescent protein under the control of the islet-1 promoter/enhancer. *J Neurosci* 2000; 20: 206–18.
- Holzschuh J, Ryu S, Aberger F, Driever W. Dopamine transporter expression distinguishes dopaminergic neurons from other catecholaminergic neurons in the developing zebrafish embryo. *Mech Dev* 2001; 101: 237–43.
- Hyun DH, Lee M, Hattori N, Kubo S, Mizuno Y, Halliwell B, et al. Effect of wild-type or mutant Parkin on oxidative damage, nitric oxide, antioxidant defenses, and the proteasome. *J Biol Chem* 2002; 277: 28572–7.
- Kay DM, Moran D, Moses L, Poorkaj P, Zabetian CP, Nutt J, et al. Heterozygous parkin point mutations are as common in control subjects as in Parkinson's patients. *Ann Neurol* 2007; 61: 47–54.
- Kim J, Inoue K, Ishii J, Vanti WB, Voronov SV, Murchison E, et al. A MicroRNA feedback circuit in midbrain dopamine neurons. *Science* 2007; 317: 1220–4.
- Kitada T, Asakawa S, Hattori N, Matsumine H, Yamamura Y, Minoshima S, et al. Mutations in the parkin gene cause autosomal recessive juvenile parkinsonism. *Nature* 1998; 392: 605–8.
- Klein C, Lohmann-Hedrich K, Rogaeva E, Schlossmacher MG, Lang AE. Deciphering the role of heterozygous mutations in genes associated with parkinsonism. *Lancet Neurol* 2007; 6: 652–62.
- Langston JW, Tanner CM, Schule B. Parkin gene variations and parkinsonism: association does not imply causation. *Ann Neurol* 2007; 61: 4–6.
- Lo Bianco C, Ridet JL, Schneider BL, Deglon N, Aebischer P. alpha-Synucleinopathy and selective dopaminergic neuron loss in a rat lentiviral-based model of Parkinson's disease. *Proc Natl Acad Sci USA* 2002; 99: 10813–8.
- Moran LB, Croisier E, Duke DC, Kalaitzakis ME, Roncaroli F, Deprez M, et al. Analysis of alpha-synuclein, dopamine and parkin pathways in neuropathologically confirmed parkinsonian nigra. *Acta Neuropathol* 2007; 113: 253–63.
- Mortiboys H, Thomas KJ, Koopman WJH, Klaffke S, Abou-Sleiman P, Olpin S, et al. Mitochondrial function and morphology are impaired in parkin-mutant fibroblasts. *Ann Neurol* 2008; 64: 555–65.
- Muftuoglu M, Elibol B, Dalmizrak O, Ercan A, Kulaksiz G, Ogues H, et al. Mitochondrial complex I and IV activities in leukocytes from patients with parkin mutations. *Mov Disord* 2004; 19: 544–8.
- Palacino JJ, Sagi D, Goldberg MS, Krauss S, Motz C, Wacker M, et al. Mitochondrial dysfunction and oxidative damage in parkin-deficient mice. *J Biol Chem* 2004; 279: 18614–22.
- Park HC, Hong SK, Kim HS, Kim SH, Yoon EJ, Kim CH, et al. Structural comparison of zebrafish Elav/Hu and their differential expressions during neurogenesis. *Neurosci Lett* 2000; 279: 81–4.
- Park J, Lee SB, Lee S, Kim Y, Song S, Kim S, et al. Mitochondrial dysfunction in Drosophila PINK1 mutants is complemented by parkin. *Nature* 2006; 441: 1157–61.
- Perez FA, Palmiter RD. Parkin-deficient mice are not a robust model of parkinsonism. *Proc Natl Acad Sci USA* 2005; 102: 2174–9.
- Petrucelli L, O'Farrell C, Lockhart PJ, Baptista M, Kehoe K, Vink L, et al. Parkin protects against the toxicity associated with mutant alpha-synuclein: proteasome dysfunction selectively affects catecholaminergic neurons. *Neuron* 2002; 36: 1007–19.
- Rieger S, Koester RW. Preparation of zebrafish embryos for transmission electron microscopy. *Cold Spring Harb Protoc* 2007; doi:10.1101/pdb.prot4772.
- Rink E, Wullmann MF. The teleostean (zebrafish) dopaminergic system ascending to the subpallium (striatum) is located in the basal diencephalon (posterior tuberculum). *Brain Res* 2001; 889: 316–30.
- Rink E, Wullmann MF. Connections of the ventral telencephalon and tyrosine hydroxylase distribution in the zebrafish brain (*Danio rerio*) lead to identification of an ascending dopaminergic system in a teleost. *Brain Res Bull* 2002a; 57: 385–7.
- Rink E, Wullmann MF. Development of the catecholaminergic system in the early zebrafish brain: an immunohistochemical study. *Brain Res Dev Brain Res* 2002b; 137: 89–100.
- Schapira AH. Mitochondria in the aetiology and pathogenesis of Parkinson's disease. *Lancet Neurol* 2008; 7: 97–109.
- Schlossmacher MG, Frosch MP, Gai WP, Medina M, Sharma N, Forno L, et al. Parkin localizes to the Lewy bodies of Parkinson disease and dementia with Lewy bodies. *Am J Pathol* 2002; 160: 1655–67.
- Shimura H, Hattori N, Kubo S, Mizuno Y, Asakawa S, Minoshima S, et al. Familial Parkinson disease gene product, parkin, is a ubiquitin-protein ligase. *Nat Genet* 2000; 25: 302–5.

- Sun Z, Gilter AD. Discovery and characterization of three novel synuclein genes in zebrafish. *Dev Dyn* 2008; 237: 2490–5.
- Surmeier DJ. Calcium, ageing, and neuronal vulnerability in Parkinson's disease. *Lancet Neurol* 2007; 6: 933–8.
- Szabadkai G, Duchon MR. Mitochondria: the hub of cellular Ca<sup>2+</sup> signaling. *Physiology (Bethesda)* 2008; 23: 84–94.
- Thisse C, Thisse B. High-resolution in situ hybridization to whole-mount zebrafish embryos. *Nat Protoc* 2008; 3: 59–69.
- Thomas B, von Coelln R, Mandir AS, Trinkaus DB, Farah MH, Leong Lim K, et al. MPTP and DSP-4 susceptibility of substantia nigra and locus coeruleus catecholaminergic neurons in mice is independent of parkin activity. *Neurobiol Dis* 2007; 26: 312–22.
- Wen L, Wei W, Gu W, Huang P, Ren X, Zhang Z, et al. Visualization of monoaminergic neurons and neurotoxicity of MPTP in live transgenic zebrafish. *Dev Biol* 2008; 314: 84–92.
- Woods IG, Schier AF. Targeted mutagenesis in zebrafish. *Nat Biotechnol* 2008; 26: 650–1.
- Yang Y, Gehrke S, Imai Y, Huang Z, Ouyang Y, Wang JW, et al. Mitochondrial pathology and muscle and dopaminergic neuron degeneration caused by inactivation of *Drosophila* Pink1 is rescued by Parkin. *Proc Natl Acad Sci USA* 2006; 103: 10793–8.
- Zhou H, Falkenburger BH, Schulz JB, Tieu K, Xu Z, Xia XG. Silencing of the Pink1 gene expression by conditional RNAi does not induce dopaminergic neuron death in mice. *Int J Biol Sci* 2007; 3: 242–50.





## **Eidesstattliche Erklärung**

Ich erkläre hiermit an Eides statt, daß ich die vorliegende Arbeit selbständig ohne unzulässige fremde Hilfe angefertigt habe. Die verwendeten Literaturquellen sind im Literaturverzeichnis vollständig zitiert.

Cambridge, 26.06.2011

---

(Katrin Volkmann)



## Danksagung

Danken möchte ich selbstverständlich all jenen, die mich durch vielfältige Unterstützung dem Ziel nähergebracht haben.

Mit größter Hochachtung möchte ich mich bei Prof. Dr. Reinhard Köster bedanken, dafür daß ich so viel von ihm lernen durfte, für seine stete Fairness und sein unermüdliches Engagement.

Prof. Dr. Wolfgang Wurst danke ich vor allem für das Schaffen der günstigen Forschungsbedingungen im IDG. Auch den übrigen Mitgliedern der Prüfungskommission Prof. Dr. Alfons Gierl und besonders Prof. Dr. Harald Luksch bin ich zu Dank verpflichtet.

Dr. Andreas Babaryka, Dr. Martin Distel und Dr. Jen Hocking möchte ich für so viel mehr danken als nur für das Korrekturlesen. Enrico Kühn, Dr. Sandra Rieger, Dr. Kazuhiko Namikawa, Dr. Niklas Senghaas und Anna-Lena Kerner sind mir so duft Kumpels gewesen, wie man sie sich nur wünschen kann. Sie alle haben mich wieder aufgerichtet als ich nicht mehr wußte wo oben und unten ist. Dr. Ruth Klafke, Helge und Annerose Kurz-Drexler – danke ich für die viele gute Laune. Petra Hammerl und den Fisch-Mädels, haben meinen Dank fürs Fische-Flüstern. Den vielen frischeren Blubb-Club Mitgliedern (Dr. Thomas Weber, Rosemarie Söllner, Christiane Lach, Changsheng Liu) gilt ein großes Dankeschön für die entgegengebrachte Sympathie ohne mich groß zu kennen. Keine Frage mit solchen duften Kollegen und einer solch entspannten Atmosphäre macht die Forschung Freude auch wens mal nich so hinhaut. Sehr gerne denke ich an die Zeit mit Euch allen zurück. Es war mir wahrlich ein Vergnügen.

Allen Kollaborateuren, besonders Danio danke ich für die wunderbare Zusammenarbeit.

Mama und Papa schulde ich tiefsten Dank für all die tausend kleinen und großen Hilfen. Meinem Bruder Stefan Volkmann danke ich besonders für die ermutigende Abwesenheit von Zweifeln. Meine Familie ist immer für mich dagewesen.

Michael Mrosek danke ich fürs Anspornen beim Endspurt.

